This meeting will be co-sponsored by The Electrochemical Society

BRNO UNIVERSITY OF TECHNOLOGY
FACULTY OF ELECTRICAL ENGINEERING AND COMMUNICATION

Institute of Inorganic Chemistry AS CR

9th ABA

BRNO 2008

Advanced Batteries and Accumulators

INTERNATIONAL CONFERENCE

June 29th - July 3rd 2008

Organised by:

Department of Electrotechnology,
Faculty of Electrical Engineering and Communication,
Brno University of Technology

Institute of Inorganic Chemistry,
Academy of Science of Czech Republic, Řež near Prague

Organizing committee:
Jiří Vondrák
Marie Sedlaříková

ISBN 978-80-214-3424-0

Conference is sponsored by:

This meeting will be co-sponsored
by The Electrochemical Society

We would like to express our thanks to the Brno University of Technology, Faculty of Electrical Engineering and Communication and to the Institute of Inorganic Chemistry AS CR for support and help with organising 8th ABA conference.

Honourary Scientific Committee:

John R. Owen
Raisa Apostolova
Petr Vanýsek
Libuše Trnková
Jana Bludská
Jiří Kazelle
Josef Jirák
Jiří Vondrák
Marie Sedlaříková

Organisation Committee:

Jiří Vondrák
Marie Sedlaříková
Vítězslav Novák
Peter Barath
Jiří Vognar
Jiří Vrbický
Tibor Jirák
Michal Macalík
Kristýna Jandová
Jaromír Makovička

Program Committee:

Jiří Vondrák
Marie Sedlaříková
Jiří Kazelle
Vítězslav Novák
Peter Barath
Petr Špičák
Jiří Špinka
Helena Polsterová
Zdenka Rozsívalová
Edita Hejátková

Contents

Nanosized or layered material

Solid and polymeric matherials

Fuel cells

Special electrochemical components

Accumulators

Methods

Sponsors

NOMINAL

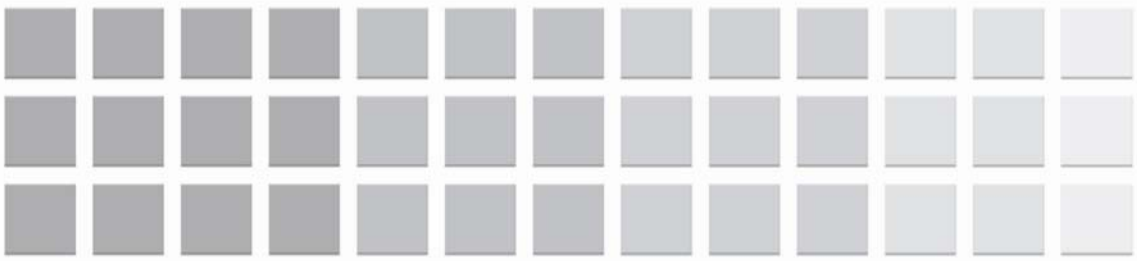

9th ABA

BRNO 2008

Advanced Batteries and Accumulators

Nanosized or layered materials

DUPLEX SURFACE TREATMENT OF TITANIUM BASED MATERIALS

Jaromir Kadlec[1], , Vojtech Hruby[1] and Milan Dvorak[2]

[1]Depth. of Mechanical Engineering, University of Defence, Kounicova 65, CZ-612 00, Brno, Czech Republic
[2]Depth. of Mechanical Technology, Faculty of Mechanical Engineering, Brno University of Technology, Technicka 2, CZ-616 69, Brno, Czech Republic

Corresponding author, kadlecjara@yahoo.com, phone +420 973442355

Introduction

Described technology of Ti_6Al_4V alloy plasma surface treatment is based on combination of both plasma nitriding of the component in micropulse plasma when nitridation atmosphere consisting nitrogen and hydrogen is used and subsequent deposition of thin TiOx film. The process is performed so that a layer of nitrides and other chemical components may be formed on the surface of nitrided components. The formed layer and subsequent deposited film are characterized by very good mechanical properties, e.g. an excellent adhesion and higher layer hardness.

Keywords: plasma nitriding, Ti_6Al_4V alloy, chemical composition, structure, properties

Experimental

Ti6Al4V alloy (3.7165, grade 5, DIN 17851) was used for experiment. Chemical composition according to DIN standard and measured by EDS method for selected chemical elements is presented in Table 1. Plasma nitriding process was carried out on the PN 60/60 equipment according to parameters in Table 2. For experiment two samples were used. Parameters of subsequent coating process are in Table 3.

Table 1 *Chemical composition of used Ti_6Al_4V alloy.*

Method	**Chemical composition (weight %)**							
	Ti	Fe	Ni	O	Al	C	V	**H**
DIN	rest	0.25	0.05	0.20	5.50 -	0.08	3.5 -	**max. 0.015**
EDS	rest	0.13	0.06	-	5.61	-	3.75	**-**

Parameters of EDS analysis: U = 30 kV, M = 100 x, I = 67 pA, WD = 20.50 mm, detector UltraDry

Chemical composition of substrate alloy was measured by EDS method (Noran system Six), depth profiles were evaluated by GDOES/QDP (SA2000 spectrometer). Calibration of nitrogen: JK41-1N and NSC4A standards. Microstructure and surface morphology

was evaluated by electron and light microscopy (Vega TS 5135 electron microscope and Olympus digital camera on the Neophot 32 light microscope), respectively. Surface structure was tested by 3D topography method (TALYSURF CLI 1000) with confocal gauge before and after treatment. Mechanical properties, such as layer thickness and microhardness were measured by indentation method (M400 microhardness tester). Other properties (adhesion, corrosion resistance) were evaluated, too. Relations among chemical composition, structure and diffusion layer properties were briefly discussed.

Table 2 *Parameters of plasma nitriding process.*

Sample 1 – two stage process (short time-higher temperature)			
Parameter	Plasma cleaning	Nitriding-stage 1	Nitriding-stage 2
Temperature (°C)	525	540	570
Time/Duration (min, h)	30 min	8 h	8 h
Flow H_2 ($l.min^{-1}$)	20	25	8
Flow N_2 ($l.min^{-1}$)	2	5	24
Voltage (V)	800	520	510
Pulse length (μs)	110	90	90
Pressure (Pa)	80	270	260
Sample 2 – one stage process (long time-lower temperature)			
Parameter	Plasma cleaning	Nitriding	
Temperature (°C)	510	520	
Time/Duration (min, h)	30 min	40 h	
Flow H_2 ($l.min^{-1}$)	20	24	
Flow N_2 ($l.min^{-1}$)	2	8	
Voltage (V)	800	510	
Pulse length (μs)	100	100	
Pressure (Pa)	80	280	

Table 3 *Parameters of subsequent coating process.*

Coating	Temperature (°C)/ Duration (min)	Current density ($mA.cm^{-2}$)	Washing (water)
TiO_x[1]	15-25/5-10	2-4	2 min

Results and Discussion

Depth profiles of plasma nitrided layers (Fig. 1 and Fig. 2) for both nitrogen and titanium are in good agreement with the proposed plasma treatment regimes. Nitrogen content decreases along the layer depth (from surface to substrate). As for nitrogen concentration, there is local maximum about one micrometer from the surface. Existence

[1] *Anodzing in H_2SO_4 based elektrolyte, (50-400 g/l water solution).*

of this maximum was verified by microstructure evaluation, too. Surface morphology for samle 1 and sample 2 is the same type, but with different roughness and other surface structure parameters (Fig. 3 and Fig. 4). This result is in conformity with metalographic measuring and next additional (e.g. 3D surface topography) evaluation. Qualitative and quantitative results of 3D surface topography measurements are in Fig. 5 and Fig. 6. The most important parameters of surface structure are presented at the same time.

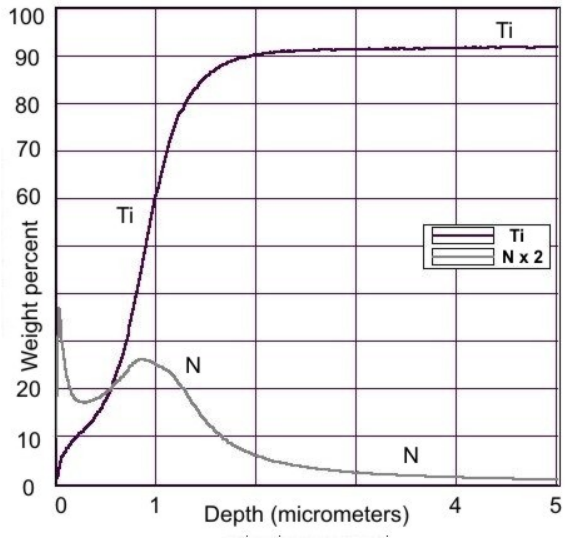

Fig. 1 *Depth profile after plasma nitriding, sample 1.*

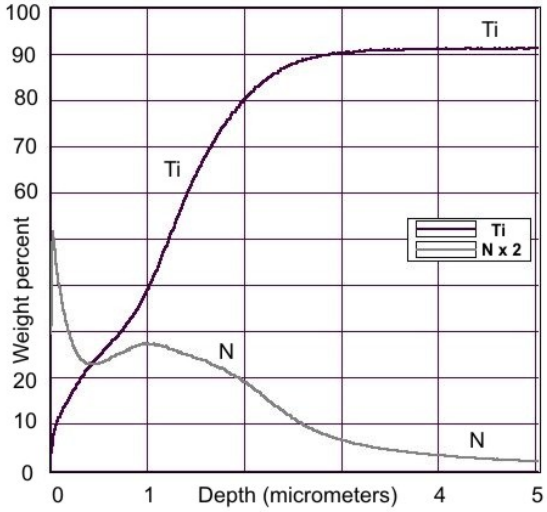

Fig. 2 *Depth profile after plasma nitriding, sample 2.*

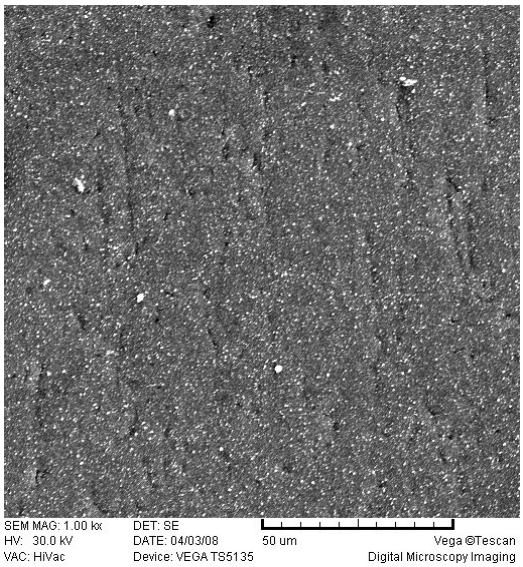

Fig. 3 *Surface morphology after plasma nitriding, sample 1.*

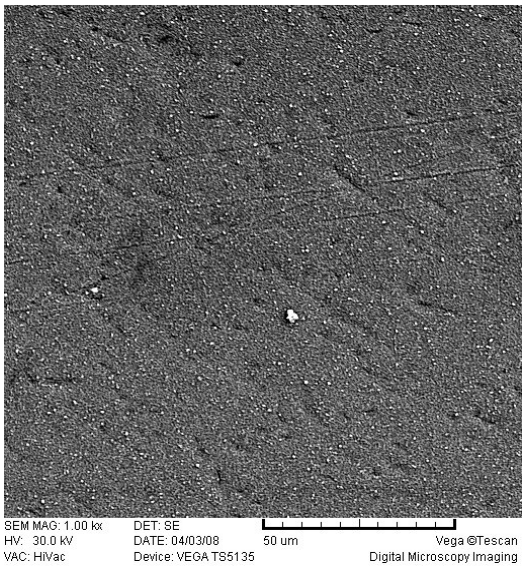

Fig. 4 *Surface morphology after plasma nitriding, sample 2.*

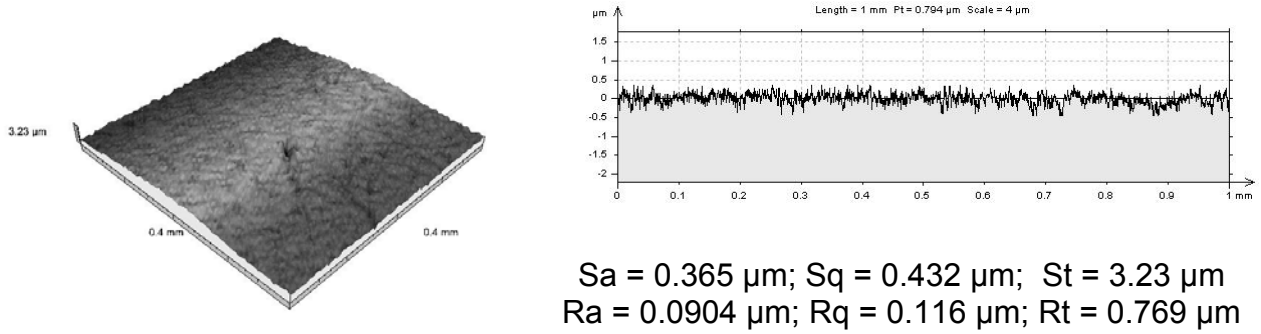

Sa = 0.365 µm; Sq = 0.432 µm; St = 3.23 µm
Ra = 0.0904 µm; Rq = 0.116 µm; Rt = 0.769 µm
Wa = 0.0289 µm; Wq = 0.0306 µm; Wt = 0.14 µm

Fig. 5 *3D surface topography after plasma nitriding, sample 1.*

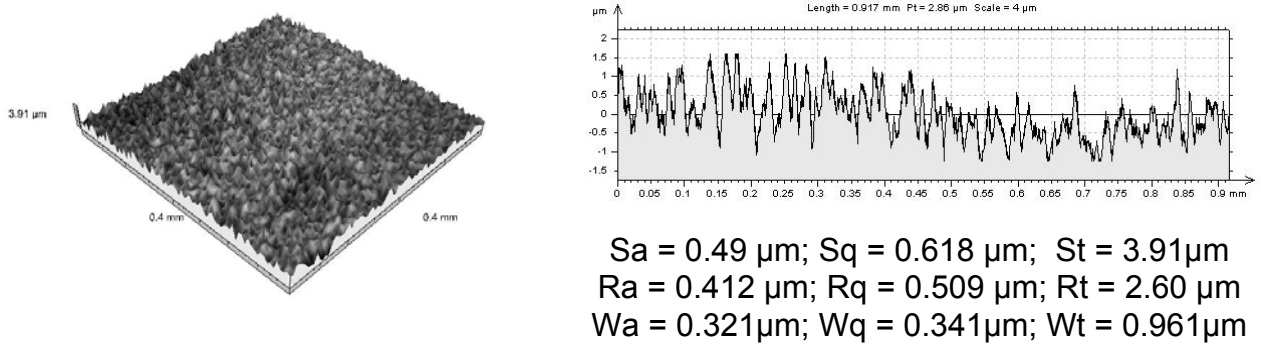

Sa = 0.49 µm; Sq = 0.618 µm; St = 3.91µm
Ra = 0.412 µm; Rq = 0.509 µm; Rt = 2.60 µm
Wa = 0.321µm; Wq = 0.341µm; Wt = 0.961µm

Fig. 6 *3D surface topography after plasma nitriding, sample 2.*

Conclusions

Plasma nitrided layer on the Ti6Al4V alloy surface created at two different regimes and subsequent anodized were carried out. The focus was on the relations among chemical composition, structure and properties of created duplex coating (layer/thin film). From GDOES measurements, it follows that a variable composition depth profile after plasma nitriding can be fabricated. To modify surface properties, TiOx type of very well adhesive thin film with thickness in units of micrometers was subsequently deposited. It can be used as a buffer layer for deposition of next coating, e.g. HAP type biocompatible ceramic films.

Acknowledgements

The work was supported by Grant Agency AS CR, project no. 106/08/1243 and by Ministry of Defence of the Czech Republic, project no. FVT 0000404.

References

[1] J. Kadlec, V. Hruby, M. Novak: Vacuum 41 (1990) 2226.
[2] J. Kadlec, M. Dvorak: Strength of Materials 40 (2008) 118.
[3] J. Kadlec, M. Dvorak: Problemy Prochnosti 1 (2008) 129.

ELECTROCHEMICAL FABRICATION OF SN-CO NANOWIRES IN ANODIC ALUMINA TEMPLATES

G. Ferrara, R. Inguanta, S. Piazza, C. Sunseri

Dipartimento di Ingegneria Chimica dei Processi e dei Materiali
Università degli Studi di Palermo, Viale delle Scienze Ed. 6, 90128 Palermo (Italy)

Corresponding author: Germano Ferrara
E-mail: g.ferrara@dicpm.unipa.it
Phone 00390916567230, Fax 00390916567280

Introduction

Ongoing developments in the field of micro-electronics have allowed realization of portable devices with high performances requiring sources of energy with high specific power. For these reasons, great attention has been placed on Lithium-ion batteries, which provide high capacity even after a high number of cycles of charging and discharging. This type of batteries has been widely studied in order to improve safety, increase electrical capacity and reduce costs to meet the needs of a quickly growing market. In particular, great attention has been devoted to the use of Sn instead of graphite as negative electrode, for the excellent performance of this metal in terms of gravimetrical capacity. Actually, it is possible to rise up from a theoretical value of about 370 mAh g-1 (for graphite) to 990 mAh g-1. Nevertheless, the electrochemical lithium insertion/extraction during the operating cycle of the battery has a deleterious effect on the structure of tin. Continuous swelling and relaxing of the crystalline lattice lead to its breakdown and subsequent deactivation of the battery. Extensive studies have investigated this issue, because a dimensionally stable tin-based negative electrode could be helpful for energy supply of small consumers. Literature proposes electrodes having a lot of structural shapes based on tin or tin oxides [1-4 and references therein], tin intermetallic compounds and other non-stoichiometric alloys [5-9 and references therein].

Sn-Co alloys, prepared by different methods, have been proposed as negative electrode for highly performing Li-ion batteries. These works highlighted that alloys giving the best performances must be amorphous [10-14]. In these alloys, the fundamental role of cobalt consists in improving the resistance of the negative electrode to mechanical stresses due to continuous volume changes during the electrochemical processes [15]. Further, it has been also shown that an increase in the specific capacity of Li-ion cell can be achieved by enlarging the exposed surface of the electrode [16-20]; for this purpose, use of nano-structured electrodes seems useful [4, 5, 11, 17-20].

In this work, we present some results relative to the preparation of amorphous Sn-Co nanowires (NWs) obtained by electrochemical deposition inside the channels of anodic

alumina membranes (AAM), used as template. We will show that it is possible to control the composition of the alloy and the length of the NWs by adjusting the deposition time.

Experimental

Sn-Co alloys were grown into the pores of commercially available AAM (Whatman, Anodisc 47), having average pore diameters of about 210 nm. Electrode preparation was detailed elsewhere [21-23]. Sn-Co potentiostatic deposition was performed from an aqueous solution containing Co2+ and Sn2+ ions, a supporting electrolyte and an organic chelating agent. The electrodeposition was carried out at -1.0 V(SCE) for different times (from 10 to 90 minutes). NWs were characterised by X-ray diffraction (XRD), scanning electron microscopy (SEM), and energy dispersive spectroscopy (EDS). The details of characterization methods were described in our previous works [21-25].

Results and Discussion

Fig. 1 shows the current density vs. time plot recorded during the electrodepositions. We can observe that current density is practically constant, with a value of about -1.0 mA cm-2, up to 60 min, then it increases slightly, probably owing to a small enhancement in the conductivity of the deposit due to the progressive enrichment in Co of the alloy (see below).

Fig. 2 shows the XRD patterns of deposits formed at different times. Up to 30 min, only peaks relative to gold metal sputtered on one side of AAM are present. The intensity of these peaks after 30 min of deposition is slightly lower than after 10 min. This finding can be due to the progressive growth, inside the channels of AAM, of an amorphous metallic deposit screening the underlying gold layer.

This interpretation is supported by the diffractogram recorded after 60 min of deposition. In this case, the peaks of gold practically disappeared while two new very weak peaks appeared at $2\theta = 43.70°$ and 30.65°. The small intensity of these peaks let us conclude so that also after 60 min of deposition nanostructure is practically amorphous. The identification of the peaks labelled with 2 and 3 in Fig. 2 is rather difficult after 60 min, because they are weak and without replicas. A tentative identification was performed analysing the XRD patterns after 90 min of deposition. Peaks 3 were assigned to Sn, whilst peaks 2 were attributed to CoSn2. After 90 min of deposition weak peaks, assigned to CoSn (peaks 4), were also present. In any case, all XRD patterns do not show any peak having significant intensity: therefore we can conclude that in the investigated interval of time deposits are practically amorphous. Morphology of deposits at different times is shown in Fig. 3. NWs are well evidenced in Fig. 3e, which is relative to NWs grown for 90 min, after AAM dissolution in 1M NaOH for 2 h. In the same figure, a typical EDS spectrum is reported, showing that NWs consist of Sn and Co. Taking into account the XRD analysis, we can conclude that NWs are constituted mainly of amorphous Sn-Co alloys. Deposited NWs appear parallel and their length increases with deposition time. Up to 30 min, NWs length was almost uniform, whilst for longer times of

deposition growth of the NWs was increasingly less even, as evident by comparing micrographs of Fig. 3. This behaviour could be ascribed to the hydrogen evolution reaction, occurring simultaneously with the Sn-Co alloys deposition. H+ ion reduction is accompanied by the formation of bubbles, partially entrapped inside the channels of AAM. Probably, the rate of bubbles evolution is not uniform: consequently, some channels are blocked for longer time while other ones are more active. We can conclude that the true distribution of active channels determines the distribution of NWs length observed in Fig. 3d. Of course, the effect of hydrogen bubbles is more significant at longer times of deposition, because they accumulate into the AAM pores. For this reason, evenness of NWs growth decreases with the deposition time.

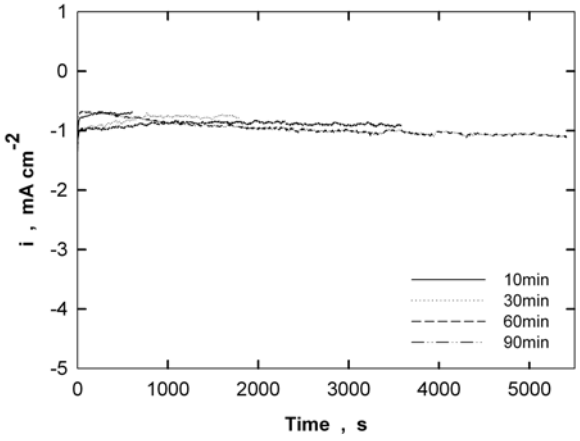

Fig. 1 *Current density vs. time plot for deposits obtained at constant potential of -1.0 V/SCE.*

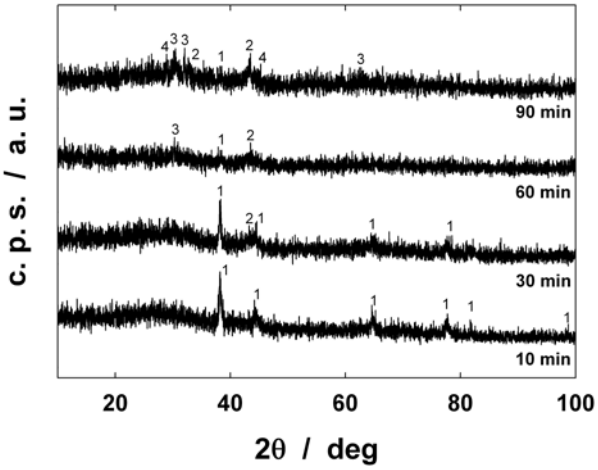

Fig. 2 *XRD patterns of deposits obtained at different times. 1: Au; 2: $CoSn_2$; 3: Sn; 4: CoSn [26].*

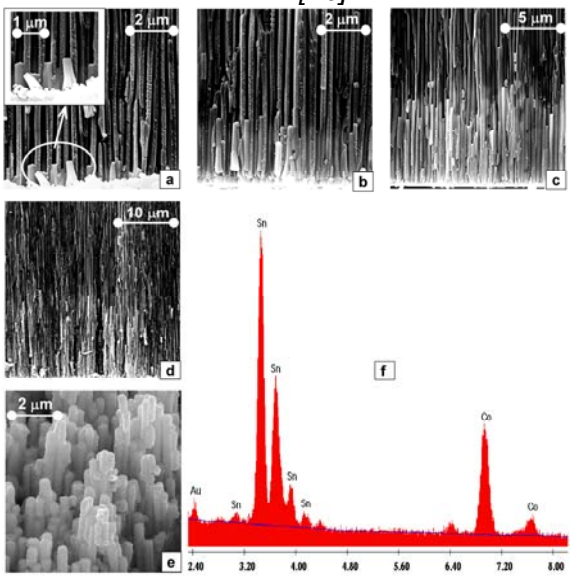

Fig. 3 *SEM images of deposits obtained after (a) 10 min, (b) 30 min, (c) 60 min, (d) 90 min, (e) 90 min and template dissolution. (f) A typical EDS spectrum of NWs.*

Fig. 4 shows the composition of the deposited NWs as function of time, as determined by EDS analysis. For comparison, composition of the deposition bath is also reported in

the same figure. We can observe that Co content is always higher in the deposit than in the bath, and that the difference increases with the deposition time. This finding can be attributed to a lower overpotential for Co deposition, since deposition of tin is thermodynamically favoured [27]. If current of Co deposition, is higher than that of Sn deposition, a progressive enrichment in Co of the alloy occurs (from 38% to 44% after 10 and 90 min, respectively).

The change in composition shown in Fig. 4 is accompanied by a change in the rate of deposition. This is shown in Fig. 5, where length of deposited NWs is plotted vs. time. We can observe that after 90 min of deposition NWs about 16 μm long were formed. Moreover, the rate of deposition changes from about 0.1 μm min-1, in the interval 0÷30 min, to 0.27 μm min-1, in the interval 60÷90 min. This finding indicates that deposition of the alloys is faster as its Co content increases.

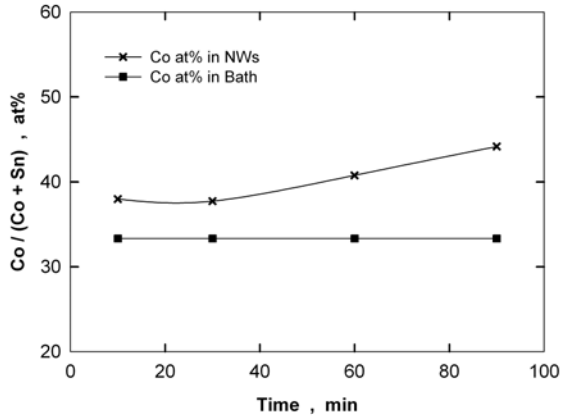

Fig. 4 *At% composition of deposited alloy vs. time plot. For comparison the composition of the electrolyte is also shown.*

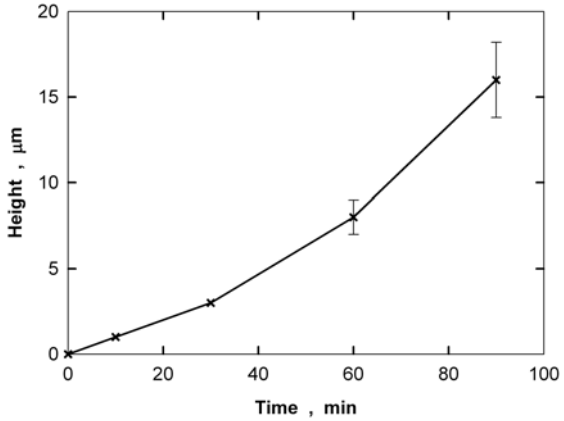

Fig. 5 *NWs length as function of deposition time.*

Conclusions

The fabrication of amorphous NWs of Sn-Co alloys discloses new perspective for future developments in the realisation of negative electrodes of Li-ion rechargeable batteries, because it is possible to increase greatly the active surface and to improve the dimensional stability. The new electrochemical route investigated in this work is a powerful tool in order to control the deposition process. The alloys deposited in the interval 15÷60 min were amorphous, whilst after 90 min some peaks appeared, but their intensity was so weak that we can consider almost amorphous also these last alloys. By adjusting the deposition time, NWs of different composition and length were formed. The content of Co in the alloy varied from less than 38 at%, after 10 min of deposition, to about 44 at%, after 90 min. The change in the NWs composition influences also the rate of deposition, which increases with the content of Co in the alloys. Length of the NWs changed from less than 2 μm, after 10 min, to about 16 μm, after 90 min. For short deposition time, length of the NWs is uniform in different channels, whilst after longer times (90 min) a lack of uniformity was observed. Further investigations are in progress

in order to find the best compromise between time of deposition and uniform length of the NWs.

Acknowledgements

This work is supported financially by Università di Palermo – APQ Ricerca della Regione Siciliana delibera CIPE no. 17/2003, “Laboratorio dell’innovazione nel settore dei beni culturali: Sperimentazione di Nanotecnologie e Nanomateriali.”

References

1. J. Hassoun, S. Panero, B. Scrosati: Electrochem. Comm. 9 (2007) 1239.
2. L. Balan , R. Schneider, P. William, D. Billaud: J. Power Sources 161 (2006) 587.
3. X. W. Lou, Y. Wang, C. Yuan, J. Y. Lee, L. A. Archer: Adv. Mater. 18 (2006) 2325.
4. F. Cheng, J. Chen: J. Mater. Res. 21 (2006) 2744.
5. J. Ren, X. He, L. Wang, W. Pu, C. Jiag, C. Wan: Electrochim. Acta 52 (2007) 2447.
6. T. Jiang, S. Zhang, X. Qiu, W. Zhu, L. Chen: J. Power Sources 166 (2007) 503.
7. Y. Kim, H. Hwang, C. S. Yoon, M. G. Kim, J. Cho: Adv. Mater 19 (2007) 92.
8. M-S. Park, S. A. Needham, G-X. Wang, Y-M. Kang, J-S. Park, S-X. Dou, H-K. Liu: Chem. Mater. 19 (2007) 2406.
9. X-Z. Liao, Z-F. Ma, J-H. Hu, Y-Z. Sun, X. Yuan: Electrochem. Comm. 5 (2003) 657.
10. J. Xie, X. B. Zhao, G. S. Cao, J. P. Tu: J. Power Sources 164 (2007) 386.
11. Y. Zheng, J. Yang, Y. NuLi, J. Wang: J. Power Sources 174 (2007) 624.
12. Q. Fan, P. J. Chupas, M. S. Whittingham: Electrochem. Solid-State Lett. 10 (2007) A274.
13. N. Tamura, Y Kato, A. Mikami, M. Kamino, S. Matsuta, S. Fujitani: J. Electrochem. Soc. 153 (2006) A1626.
14. J. R. Dahn, R. E. Mar, A. Abouzeid: J. Electrochem. Soc. 153 (2006) A361.
15. H. Guo, H. Zhao, X. Jia, X. Li, W. Qiu: Electrochim. Acta 52 (2007) 4853.
16. F. Cheng, Z. Tao, J. Liang, J. Chen: Chem. Mater. 20 (2008) 667.
17. F-S. Ke, L. Huang, H-B. Wei, J-S. Cai, X-Y. Fan, F-Z. Yang, S-G. Sun: J. Power Sources 170 (2007) 450.
18. S. Panero, B. Scrosati, M. Wachtler, F. Croce: J. Power Sources 129 (2004) 90.
19. C. R. Sides, N. Li, C. J. Patrissi, B. Scrosati, C. R. Martin: MRS Bull. 27 (2002) 604.
20. N. Li, C. R. Martin, B. Scrosati: J. Power Sources 97-98 (2001) 240.
21. R. Inguanta, C. Sunseri, S. Piazza: Electrochem. Solid-State Lett. 10 (2007) K63.
22. R. Inguanta, S. Piazza, C. Sunseri: Nanotechnology 18 (2007) 485605.
23. R. Inguanta, S. Piazza, C. Sunseri: Electrochim. Acta In press.
24. R. Inguanta, M. Butera, C. Sunseri, S. Piazza: Appl. Surf. Sci. 253 (2007) 5447.
25. R. Inguanta, S. Piazza, C. Sunseri: Electrochem. Comm. 10 (2008) 506.
26. International Centre for Diffraction Data, Power Diffraction file, (Au 4-784; CoSn2 65-2697; Sn 4-673; CoSn 65-3477) Pennsylvania, USA, 2001.
27. M. Pourbaix: Atlas of Electrochemical Equilibria in Aqueous Solutions. Pergamon Press, New York, 1966.

SYNTHESIS OF CARBON NANOSTRUCTURES BY PYROLYSIS OF ACETYLENE USING ALLOY AB_5

Katarzyna Lota[1], Grzegorz Lota[1,2], Agnieszka Sierczyńska[1]

[1]Institute of Non-ferrous Metals Department in Poznan,Central Laboratory of Batteries and Cells, 61-362 Poznan, Forteczna 12, Poland
[2]Poznan University of Technology, Institute of Chemistry and Technical Electrochemistry, 60-965 Poznan, Piotrowo 3, Poland

Introduction

Since carbon nanotubes were discovered in 1991 [1] by Iijima various methods are proposed for synthesize pure material. The carbon nanotubes have been reported to be very promising candidates for various application [2-8] because of their extraordinary physical and mechanical properties. They are excellent candidate for composite reinforcement e.g. as a actuators, sensors and biosensors in biological technologies, as a component of electrode materials or catalyst support.

Critical to the use of carbon nanotubes as a structural material, there is a need for development of nanotubes production techniques, on large scale and of course make it cost-effective. CCVD method is one of way to obtain on a large scale carbon nanotubes. Many parameters, such as size of catalyst, temperature, flow rate of the reaction gas have influence on the carbon nanotubes grown by CCVD. The possibility of controlling microscopic parameters, such as tube diameter, will allow to control the main material properties. The most effective catalysts for the CCVD growth of carbon nanotubes, as was investigated [9], are nickel (Ni) > cobalt (Co) > iron (Fe). The AB_5 type alloy was chosen as a catalyst, because of its big content of nickel and cobalt.

Experimental

Commercial AB5 type alloy – AUERSTORE® of overall formulas Mm(Ni-Co-Fe-Mn-Al)5 (Mm = La-rich mischmetal:33,1 wt.%, La: 53.3 wt.%; Ce: 33.7 wt.%; Nd: 9.8 wt.%; Pr: 3.2 wt.%; other rare earths: 66.9 wt.%, Ni: 47.8 wt.%; Co: 10.12 wt.%; Mn: 5.10 wt.%; Al: 1.86 wt.%; Fe: 0.055 wt.%) with average diameter 57,06 μm was used as a catalyst. About 250 mg of alloy was placed in a quartz boat and then placed in a flow furnace. First, nitrogen gas was introduced. When the furnace temperature raised to 700°C , nitrogen has been shut down and gas mixture of hydrogen and argon was introduced into the furnace for 0,5 hour or for 1hour. Next, acetylene was introduced. As comparison the carbon nanotubes were obtained with different ratio acetylene and hydrogen 2:1 and 4:1. When the furnace cooled down to the room temperature in a presence of nitrogen flow, carbon nanotubes were purified in concentrated hydrochloric acid. Scanning electron microscope LEO GEMINI 1525 with EDX was used to investigate the structure and composition of carbon nanostructures. Specific surface area measurements were performed using ASAP 2010 M.

Results and discussion

Previous experiments have shown that temperature of 600°C it is not enough to decompose acetylene over AB5 catalyst. The efficiency of such synthesis is negligible. All samples were prepared by decomposition of acetylene at 700°C. The sample designated as Ns 1 (nanostructure 1) was pretreated for 0,5 hour in hydrogen/argon mixture. The rest of samples were treated in such mixture for 1 hour. Catalyst is reduced from possible oxides to metallic form by these gases. Ns 1 has large specific surface area (Table 1) and more of amorphous carbon is produced. As comparison, the carbon nanostructures were also prepared in such conditions that the ratio of acetylene and hydrogen is set to 2:1 for Ns 1 I Ns 2 and 4:1 for Ns 3. Keeping the acetylene flow constant and decreasing flow rate of mixture of hydrogen and argon, more of amorphous carbon were seen to be deposited inside the quartz reactor.

Table 4 *BET specific surface area measurements*

BET of Ns 1 [m^2/g]	BET of Ns 2 [m^2/g]	BET of Ns 3 [m^2/g]
109	50	50

The ratio of acetylene and hydrogen in mixture has influence on impurity and defects. Increasing the content of hydrogen in the mixture of gases, the carbon nanostructures with less impurity content is obtained.

Conclusions

The efficiency of catalytic synthesis of carbon nanostructures by acetylene decomposition over Mm based multicomponent alloy of the AB5 type is discussed. Different parameters of the CCVD process has influence on the efficiency. Some of them were changed to obtain the highest amount of carbon material. Although the carbon nanotubes have been proven to posses superior properties, their relatively high cost restricts their practical use at the present time. Both catalyst and parameters of process (such as flow rate of acetylene) need further investigations. We have to continue our research into development of a cost-effective way of carbon nanotubes production.

References

1. T. Belin, F. Epron Mater. Sci. Eng. B 119 (2005) 105.
2. E. Thostenson, Z. Ren, T. Chou, Comp. Sci.Technol. 61 (2001)1899.
3. M. Trojanowicz Trends Anal. Chem. 25 (2006) 480.
4. S. Daniel, T. Rao, K. Rao, S. Rani, G. Naidu, H. Lee, T. Kawai, Sens. Actuators B, 122 (2007) 672.
5. G. Lota, K. Lota, E. Frąckowiak, Electrochem. Commun. 9 (2007) 1828.
6. E. Frąckowiak , G. Lota, T. Cacciaguerra, F. Beguin, Electrochem. Commun. 8 (2006) 129.
7. G. P. Rao, C. Lu, F. Su, Sep. Purif. Technol. 58 (2007) 224.
8. S. Demoustier, E. Minoux, M. Le Baillif, M. Charles, A. Ziaei, C. R. Physique 9 (2008) 53.
9. C.J. Lee, J. Park, J. A. Yu, Chem. Phys. Lett. 360 (2002) 250.

ABOUT THE FORMATION OF ANODIC NANOCOATINGS ON Nb IN POTASSIUM NITRATE MELT

Leonid Skatkov[1] and Valeriy Gomozov[2]

[1]PCB "Argo", 4/23 Shaul ha Melekh Str. 84797 Beer Sheva, Israel;
e-mail: sf_lskatkov@bezeqint.net
[2]National Technical Universitu "KhPI", 21 Frunze Str., 61002 Kharkov, Ukraine

This work is a further development of the investigations of the anodization of niobium in nitrate melts of salts at temperatures allowing recrystallization of oxide [1,2].
The anodic coatings ofnniobium formed in nitrate melt consists of sandwiches of phases of Nb_2O_5, NbO_2 and NbO (from the outer surface of the anodic oxide film toward the niobium substrate), and high anodization temperatures cause the intense dissolution of oxygen in the niobium substrate.

During the formation of an anodic film, it becomes saturated with the anionic and cationic components of the electrolyte. The uptake of the anions is most significant in the initial stages of growth of the oxide layer, while saturation with potassium occurs in the stages of anodization.

References

[1] L. Skatkov, V.Gomozov, Book of Abstract for CSSI 2002 (Hefei, China, 2002). – P. 28.
[2] L. Skatkov, V. Gomozov, S. Deribo, Proceedings 3rd Croatian Symp.Electrochemistry (Dubrovnic, Croatia, 2004). – P. 117.

NATURAL GRAPHITE AFTER OXIDATIVE TREATMENT FOR LI-ION BATTERIES

J. Makovička[1], M. Sedlaříková[1], J. Vondrák[2]

[1] Institute of Electrotechnology, Technical University of Brno, 602 00 Brno
[2] Institute of Inorganic Chemistry AS CR, 250 68 Řež near Prague

Corresponding author: Jaromír Makovička
E-mail: xmakov05@stud.feec.vutbr.cz

Introduction

In the last decades, many kinds of carbon materials have been investigated as anode materials for Li-ion batteries. Among them, natural graphite appears as a promising candidate due to its advantages such as high capacity at low electrode potential relative to lithium metal. However was found that raw natural graphite from mines cannot deliver satisfactory electrochemical performance. It was found that oxidative treatment can improve natural carbon electrochemical properties [1, 2].

In this paper is discussed the natural graphite which is treated in CO_2 atmosphere.

Experimental

Firstly natural graphite CR 5995 (Maziva s.r.o., Týn n. Vlt.) was annealed at 750 °C for an hour in CO2 atmosphere. The negative electrode was subsequently prepared in this way: The electrode material was prepared by mixing the natural graphite CR 5995 with PVdF at weight ratio of 95:5. A small amount of isopropanol was added to the mixture for making the proper paste. The resultant paste was coated on the nickel mesh. The coated mesh was pressed and dried at 150 °C for 1 h.

The three electrode cell was assembled in glove box to examine galvanostatic charge/discharge behaviors. A piece of lithium metal (purity 99.9 %) was used as a counter and reference electrode. The working (negative) electrode is described above. 1 M LiClO4 (purity 95 %) in EC-DEC [ethylene carbonate, diethyl carbonate (purity 99.9 %)] was used as electrolyte. The electrode was charged/discharged between 0 V and 1.5 V (vs.Li) at a constant current of 100 mA/g and 300mA/g. The AUTOLAB PGSTAT 30 was used for the measurement.

Results and Discussion

The results are shown in the table 1 and in the figures 1, 2. Both samples of natural graphite offer reversible capacity around 300 mAh/g, which is 80 % capacity

corresponds to structure LiC6. Natural graphite after oxidative treatment demonstrates higher capacity at a current density of 300 mAh/g than natural graphite without oxidative treatment which indicates a better electric contact between material pacticles.The cycling stability is also significantly improved after oxidative treatment.

Table 1 *Summarized properties of graphite CR 5995*

graphite	CR 5995	CR 5995 CO_2
Reversible capacity 1st cycle (100 mA/g)	305 mAh/g	289 mAh/g
Irreversible capacity 1st cycle	111 mAh/g	112 mAh/g
Irreversible capacity 1st cycle due to SEI formation	25 mAh/g	25 mAh/g
Coulombic efficiency 1st cycle	73 %	72 %
Coulombic efficiency 10th cycle	98 %	98 %
Reversible capacity 4th cycle (300 mA/g)	50 mAh/g	157 mAh/g
Reversible capacity 20th cycle	216 mAh/g	264 mAh/g

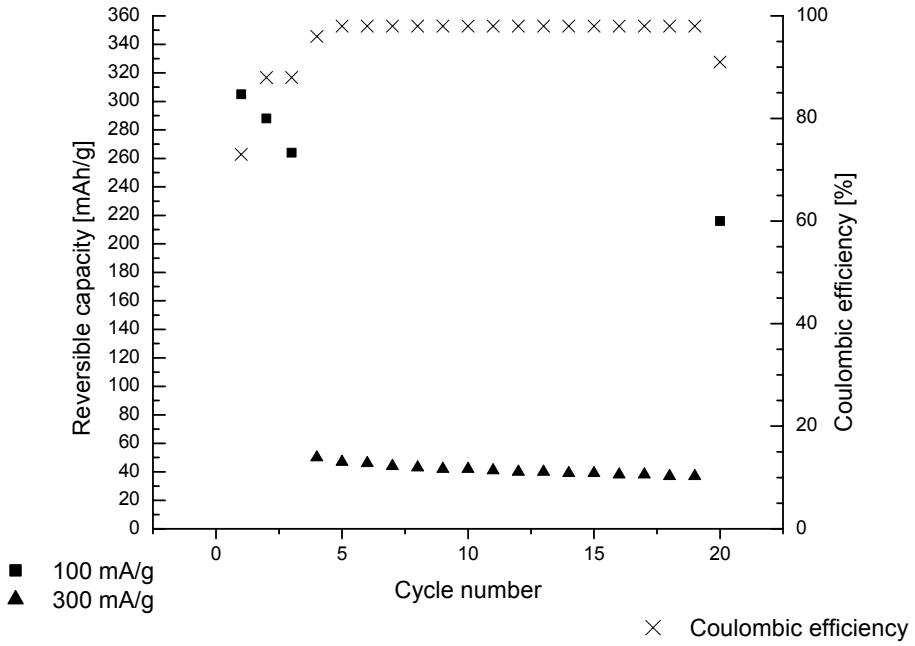

Fig. 1 *Summarized properties of graphite CR 5995, Crosses: coulombic efficiency, squares: current 100 mA/g, triangles: 300 mA/g*

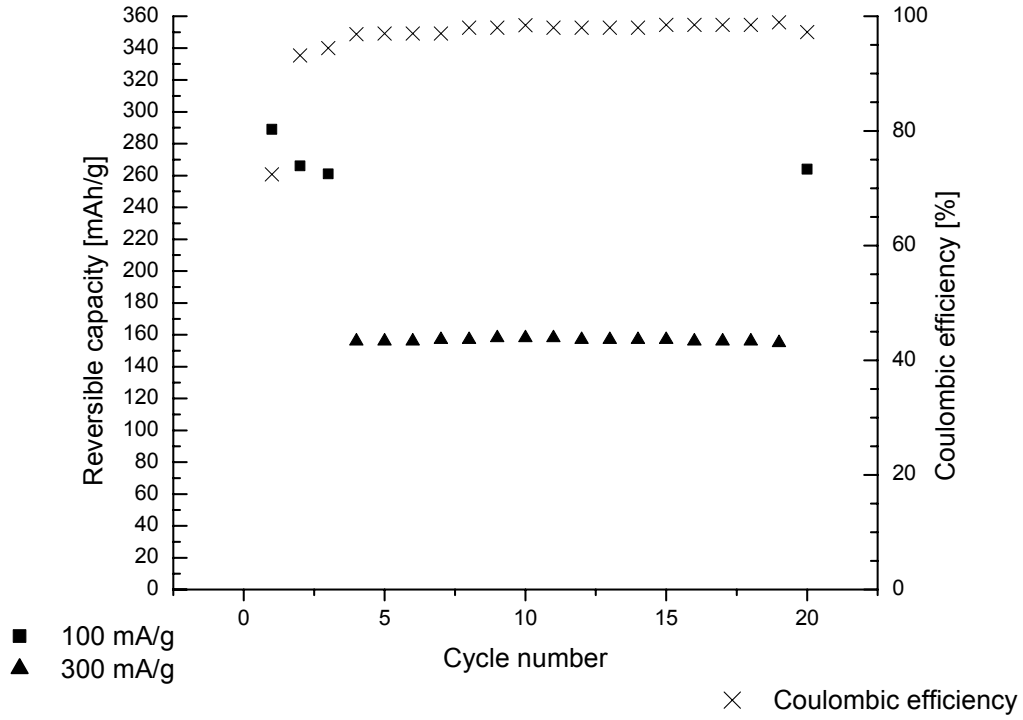

Fig. 2 *Summarized properties of graphite CR 5995 after CO_2 treatment, Crosses: coulombic efficiency, squares: current 100 mA/g, triangles: 300 mA/g*

Conclusion

The results illustrate that the natural graphite after oxidative treatment is suitable material for Li-ion batteries.

Acknowledgement

This work was supported by Ministry of Education (project MSM0021630516), Ministry of Environment (Grant No. VaVSN/3/171/05).

References

[1] C. Menachem a, Y. Wang b, J. Flowers c, E. Peled a, S.G. Greenbaum (1998) Characterization of lithiated natural graphite before and after mild oxidation, Journal of Power Sources 76 180-185

[2] Y.P.Wu a,b,*,C. Jiang,C.Wan,R. Holze (2003) Anode materials for lithium ion batteries by oxidative treatment of common natural graphite, Solid State ionics 156 283-290

HYBRID LASER-MAGNETRON DEPOSITION OF TIC AND TICN THIN FILMS

Jaromir Kadlec[1], , Miroslav Jelinek[2], Tomas Kocourek[2], Milan Dvorak[3] and Zdenek Joska[1]

[1]Depth. of Mechanical Engineering, University of Defence, Kounicova 65, 612 00, Brno, Czech Republic
[2] Institute of Physics, Na Slovance 2, 182 21 Prague 8, Czech Republic
[3]Depth. of Mechanical Technology, Faculty of Mechanical Engineering, Brno University of Technology, Technicka 2, 616 69, Brno, Czech Republic

Introduction

Hybrid laser-magnetron deposition system was developed and tested for study carbon based thin films. Films were fabricated in argon (TiC) and in argon/nitrogen (TiCN). Crystalline films were grown at room substrate temperature. Film properties were studied by SEM, XRD, XPS and GDOES.

Hybrid deposition systems are used to overcome some of the limitations of particular deposition techniques, to find new deposition possibilities, and to grow films with a new properties or under technologically acceptable conditions [1-2]. One group of hybrid systems is based on the combination of pulsed laser deposition and magnetron sputtering (PLDMS). The combination of high- energy laser plasma with low-energy magnetron plasma was used for producing hard, tough and low friction carbon based wear protective coatings, for the deposition of nanocomposite films as well as for fabrication of composite “chameleon” coatings with adaptation to dry/humid environments. The pioneering works in MSPLD were done by A. Voevodin [3-4]. The PLDMS technique allows growing of complicated multicompound and graded layers from two separate targets, at specific deposition conditions and to control film morphology, stoichiometry and crystal structure. In graded layers the fine, gradual change in composition and microstructure results in a corresponding change in the material properties.

Experimental

The experimental hybrid set-up consists of pulsed laser deposition and magnetron sputtering system. Laser and magnetron targets are placed in stainless steel deposition chamber. Both sputtering systems are running together and fluxes of material intersect on Si substrate. The focus was on creation of TiC and TiCN films. KrF excimer laser was used for deposition of carbon compounds and magnetron (2 inch K.J. Lesker) simultaneously sputtered Ti species. Basic arrangement of PLDMS deposition is in Fig. 1. Target-substrate distances X and Y, declination angle Z and eccentricity of substrate axis E were changed. Films were fabricated in argon (TiC) and argon-nitrogen (TiCN).

The substrates were cleaned in acetone and toluene. Each substrate was subsequently cleaned in the deposition chamber, before deposition, by RF discharge (100 W) in a mixture of argon and nitrogen. Substrate was rotated to ensure film thickness homogeneity over the surface of 3 cm x 3 cm.

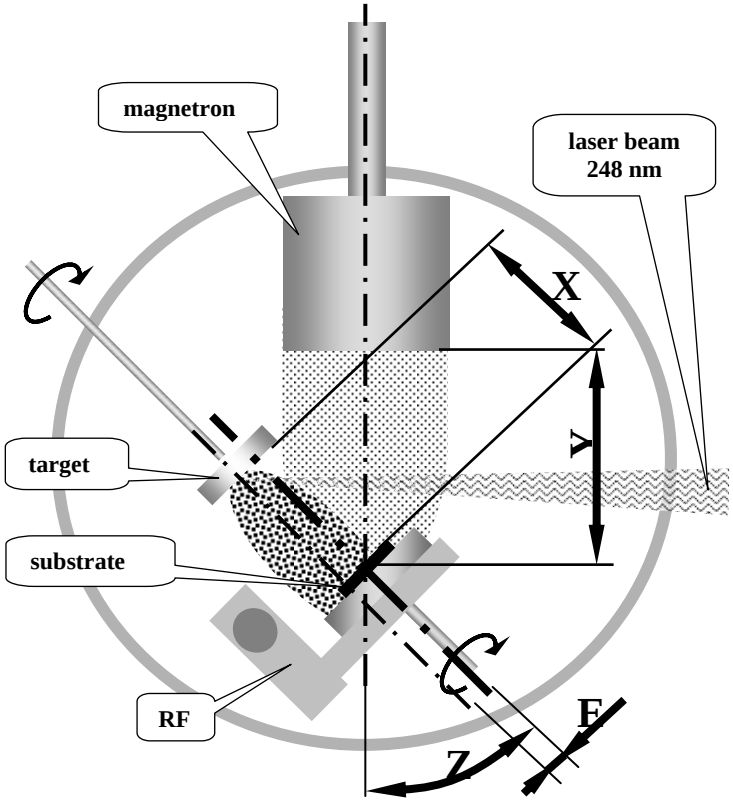

Fig. 1 *MSPLD arrangement*

The film properties was structurally characterized by XRD. A parallel beam optic geometry with a Huber two-circle diffractometer, powered by a rotating anode generator X-ray source (300 mA, 55 kV, Cu Kalpha radiation), RIGAKU Rotaflex RU 300 was used. The carbon, titanium, nitrogen and silicon concentrations along a film thickness profile were measured by the GDOES/QDP method (Glow Discharge Optical Emission Spectroscopy/ Quantitative Depth Profiling) using a LECO system type SA 2000. Information was taken from 4 mm diameter surface. XPS data were measured in a 2 x 10-8 Pa base pressure UHV chamber equipped with a Mg Kalpha radiation at 1253.6 eV X-ray source.

Results and discussion

The focus was on TiC and TiCN layers. Titanium carbide based materials exhibit an unique combination of physical properties such as high hardness, low friction coefficient, high thermal conductivity, and high thermal stability. TiCN thin films are used for improvement of adhesion of carbon based thin films as an interlayer prior to carbon based deposition [5-6].

TiC - magnetron was used for sputtering of titanium target and laser for ablation of carbon target. Films were grown at room substrate temperature (Ts) on Si substrates in nitrogen ambient of 0.3 Pa. Magnetron power was changed between 50 - 200 W. The following deposition configurations were tested - see Fig.1.

a) X = 45 mm, Y = 63 mm, angle Z = 23o, E = 5 – 10 mm,
b) X = 40 mm, Y = 85 mm, angle Z = 45o, E = 10 mm,
c) X = 45 mm, Y = 75 mm, angle Z = 45o, E = 0 mm.

The best film homogeneity was reached for configuration (b). In all three configu-rations a crystalline TiC was measured - see Fig. 2.

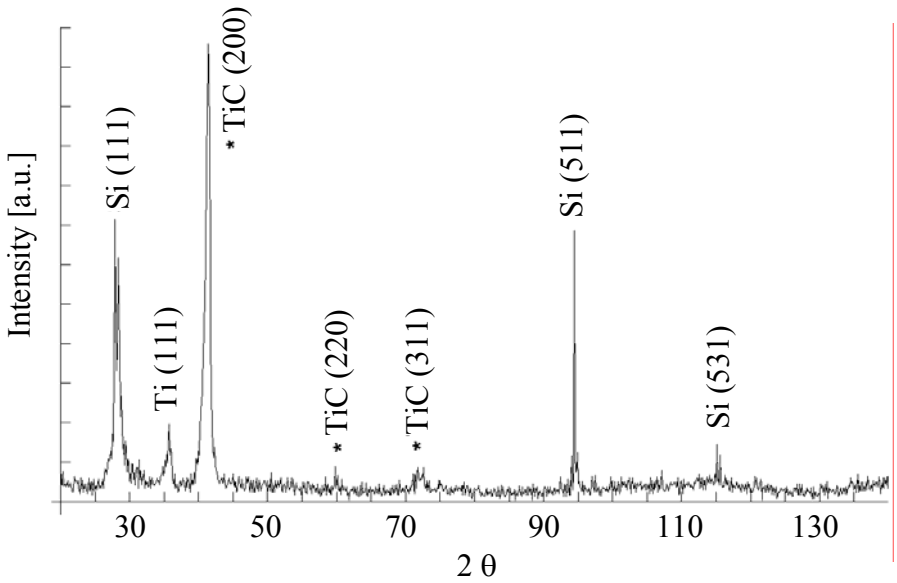

Fig. 2 *XRD spectrum of TiC sample prepared by PLDMS technology (magnetron power 50 W, laser energy density 11 J.cm-2, rep. rate 20 Hz, growth rate 14 nm/min).*

TiCN - for deposition the configuration (b) of magnetron and laser target was used. DC magnetron sputtered Ti and operated at 150 W. Laser fluence on the carbon target was 15 J.cm^{-2}. The stream of material was changed by laser repetition rate (4 - 14 Hz). Ambient argon-nitrogen pressure was adjusted in region from 1 Pa to 5 Pa. Substrate (111) Si was held at room temperature. Film growth rate was between 6 - 24 nm/min. Differently from crystalline TiC layers fabricated in vacuum at similar conditions all TiCN films were amorphous. Very smooth films on area as 3 cm x 3 cm were fabricated by adding RF discharge (13.56 MHz, held between substrate and chamber) into PLDMS process. The concentration of nitrogen in the films was in the region 17 - 26 at %, as confirmed by XPS measurement - see Table 1.

Table 1 *TiCN films - deposition conditions and XPS analysis (laser density 15 J.cm^{-2}, magnetron power 150 W)*

Sample	Laser rep. rate [Hz]	RF discharge [W]	Amb. Ar + N_2 [Pa]	Av. thick. [nm]	Concentration of elements in TiCN layers (at %) XPS			
					C	Ti	N	O
TD 22	7	-	1.5	710	63	17	17	3
TD 23	4	-	1.5	743	-	-	-	-
TD 26	4	-	5	635	40	30	18	12
TD 27	4	30	1.5	467	35	37	26	2
TD 28	4	10	1.5	643	39	34	24	3
TD 29	4	70	1.5	303	43	30	23	4

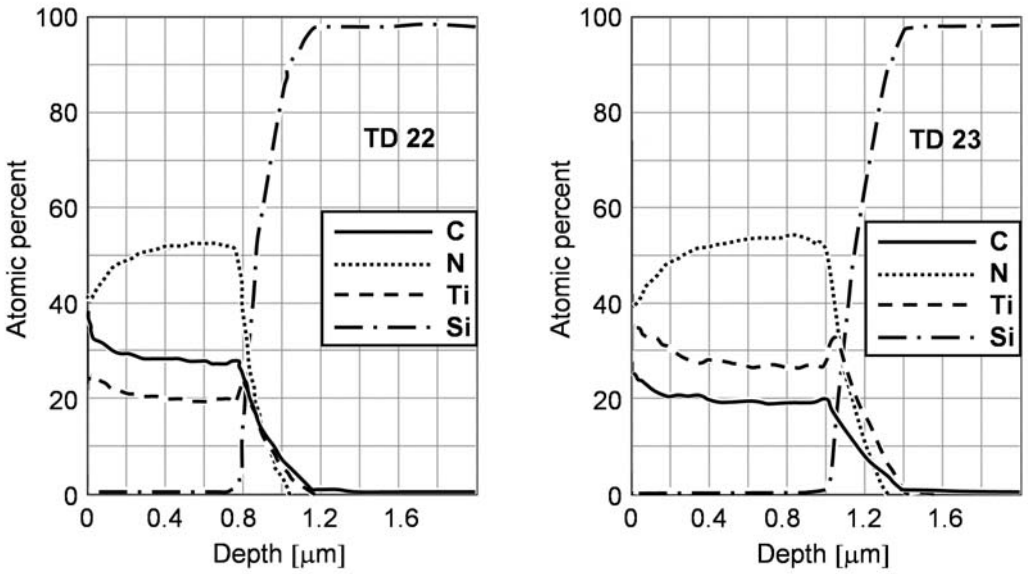

Fig. 3 *Example of atomic concentration of elements in TiCN films (GDOES).*

Conclusions

In this contribution there were summarized our experiences and reached results with newly constructed hybrid laser-magnetron deposition system. Several configurations was tested to cover homogeneously area of 3 cm x 3 cm. Layers of TiC and TiCN were synthesized. Smooth, nanocrystalline TiC were created at room substrate temperature. The films of TiCN deposited also at room temperature Ts were amorphous. The XPS measurement confirmed TiC or TiCN bonds. The PLDMS is much complicated compared to PLD, because of additional deposition variables as geometrical configuration of deposition arrangement. Two different energetic fluxes (up 1 keV for laser ablation and several eV for magnetron species) of material deposited on the same substrate and geometrical versatility offer much possibilities to create films of new properties. The method allows also easily and smoothly change composition profile along layer thickness (see Fig. 3) by changing of laser repetition rate and magnetron

power. The PLDMS system is a suitable tool for fabrication of specially tailored layer at new deposition conditions.

Acknowledgements

The research was supported by the Grant Agency of the Czech Republic, projects no. 106/08/1243 and no. 220/07/0591.

References

[1] D.B. Chrisey, G.K. Hubler: Pulsed Laser deposition of Thin Films (John Wiley& Sons, Inc., New York 1994).
[2] M. Jelinek, J. Lancok, J. Bulir, M. Novotny: Laser Physics 12 (2002), 306.
[3] A.A. Voevodin, J.S. Zabinski: Diamond and Related Materials 7 (1998), 463.
[4] A.A. Voevodin, J.J. Hu, T.A. Fitz, J.S. Zabinski: J. Vac. Sci. Technol. A 258 (2002) 1434.
[5] M. Jelinek, T. Kocourek, J. Kadlec, V. Vorlicek, M. Cernansky, V. Studnicka, A. Santoni, P. Bohac, F. Uherek: Thin Solid Films 506-507 (2006) 101.
[6] T. Kocourek, M. Jelinek, J. Kadlec, C. Popov, A. Santoni: Plasma Process. Polym. 4 S1 (2007) 651.

PRESENCE OF HYDROGEN PEROXIDE IN SnO_2 THIN FILMS PREPARATION

M. Macalík[1], M. Sedlaříková[1], J. Vondrák[2]

[1] Department of Electrotechnology, FEEC, BUT, Údolní 53, 602 00 Brno, CZ
[2] Institute of Inorganic Chemistry of the ASCR,v.v.i., 250 68 Řež near Prague, CZ

Corresponding author: M. Macalík
E-mail: michal.macalik@phd.feec.vutbr.cz

Introduction

Tin dioxide, SnO_2, is a semiconductor exhibiting good electric conductivity, optical transparency and reflectivity in infrared irradiation. Good transparency is connected to the 3 eV width of the band gap. These properties can be modified easily by a variety of additives such as compounds of antimony, fluorides, metal salts and others. This material can be used in many applications, such as transparent electrodes for displays [1], solar cells [2, 3], semiconductor technology [4], gas sensors [5], heating elements or electromagnetic shielding and antistatic surfaces [6].
Various technologies for thin layer deposition are under investigation nowadays. Magnetron sputtering [7], vacuum evaporation [8], spray pyrolysis deposition [2], methods based on CVD [9] or dip coating [1] are among them. The spray deposition is very cheap and does not require any sophisticated device.

Experimental

Tin dichloride dihydrate was used for preparation of starting solution. In the first set of samples, 1,5M $SnCl_2 \cdot 2H_2O$ was dissolved in 75ml of methanol. In the second set, 25,3g $SnCl_2 \cdot 2H_2O$ was dissolved by slowly added 10ml of H_2O_2 solution under permanent agitation and finally methanol was added to total volume of 75ml. 10ml, 25ml a 40ml of each solution were used for spray deposition by means of a air – driven atomizer on pre-heated soda-lime glass substrate. The temperature of substrates was controlled by thermocouple. Samples prepared with using H_2O_2 are labelled by symbol “A” and samples without H_2O_2 are labelled by symbol “B” in this article.
The surface morphology and thickness of the films were investigated by scanning electron microscope (Tescan VEGA 5135) and profilometter (Talysurf CLI 1000). Type of charge carrier, concentration and mobility were determined by room temperature Hall effect with standard Van der Pauw arrangement. Transmittance spectra of the films were measured between 325-900nm wavelength by spectrophotometer (Thermo Spectronic, Helios Delta). Differential thermal and thermogravimetric analysis were produced by DTA – TGA device (NETZSCH STA (QMS) 409 analyzer). Sheet resistance was measured by a linear four-probe type resistance meter (Jandel RM3). Temperature was controlled down to –50^{o}C in a cryogenic cell cooled by solid CO_2.

Result and discusion

At first, the presence of hydrogen peroxide in prepared tin hydroxides was investigated. The heating of precipitated hydroxides is indicated in Fig. 1 on DTA curves. The peroxide treated sample just losses weight while the untreated one increases its mass between 200 and 400°C; this is apparently accompanied by oxidation by atmospheric oxygen to Sn^{4+} species. Evidently, hydorogen peroxide contribute to tin oxidation and its valence change directly in starting solution.

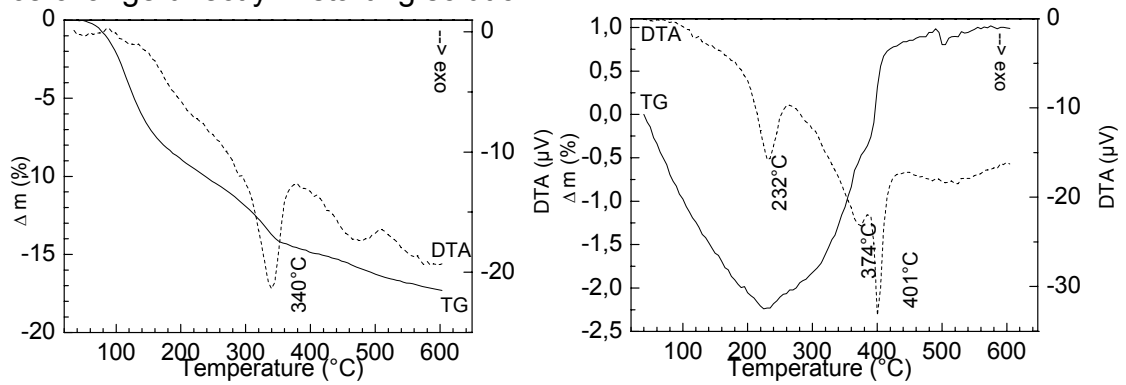

Fig. 1 *DTA cruves of hydrogen peroxide treated (left) and untreated sample (right)*

The microphotographs of both types of layers are shown in Fig. 2. Better homogenity of the layer is visible there. The surface of the layer consists of small particles formed probably by rapid evaporation of the solution droplets.

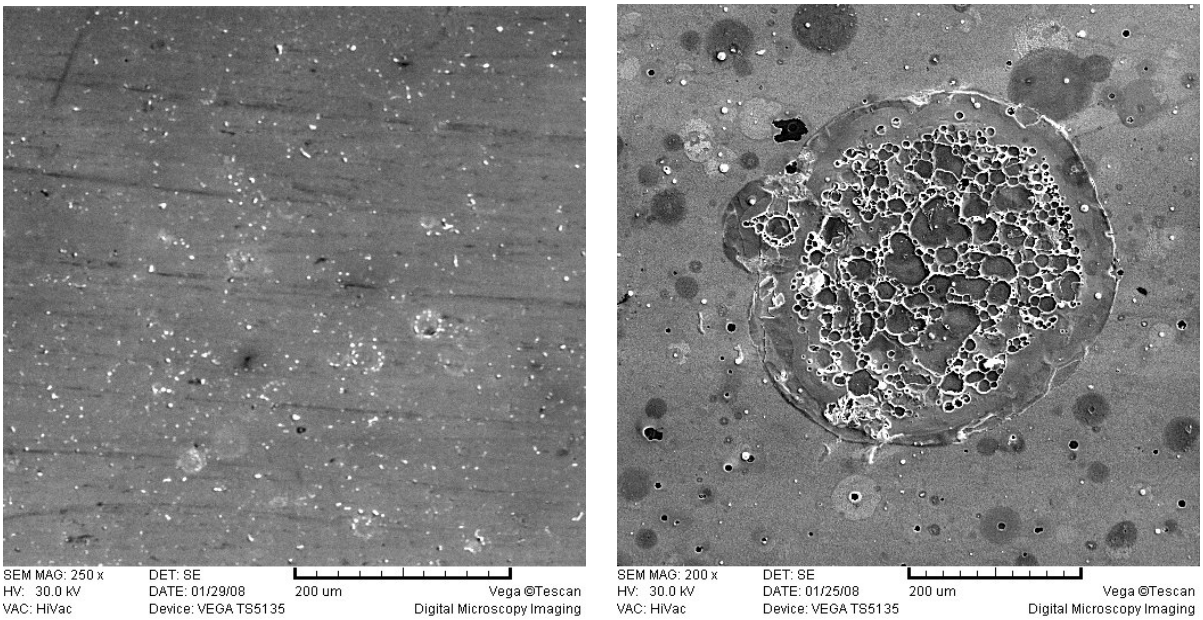

Fig. 2 *SEM images of hydrogen peroxide treated (left) and untreated (right) samples prepared from 25ml solution*

Thin films of SnO_2 prepared by spray pyrolysis method form $SnCl_2$ precursor without hydrogen peroxide using are darker and browny than almost clear and colourless films prepared from solution with adding H_2O_2. It is in good agreement with colouring of precipitated hydroxides from previous paragraph. Optical transmission curves from

prepared samples measured in the range of wavelength 325 – 900nm are depicted in figure 3. Peroxide treated samples are more transparent than untreated samples.

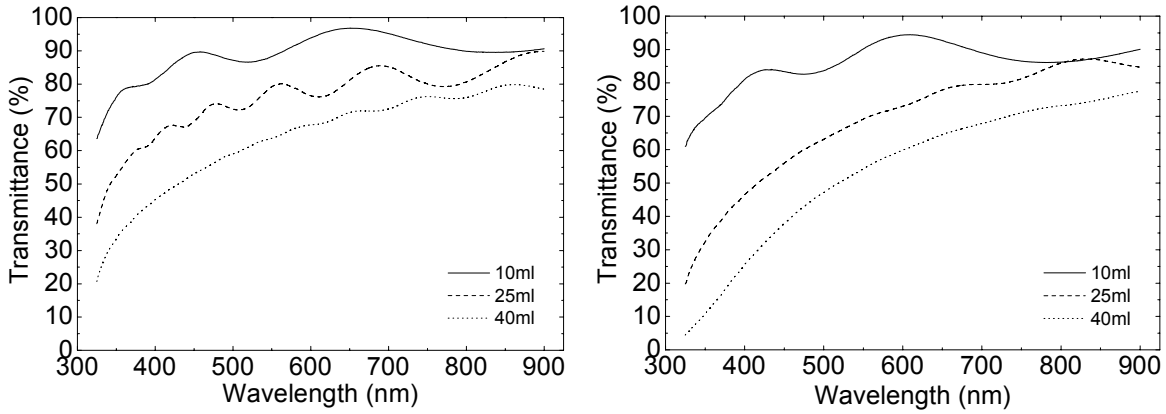

Fig. 3 *Transmission spectra of hydrogen peroxide treated (left) and untreated sample (right)*

The resistance dependence on temperature is shown in Fig. 4. In general, no behavior typical for a semiconductor was observed. At temperatures over zero, the resistivity increases with increasing temperature, while it is almost constant below that limit. We suppose that the material should be described as a highly doped or degenerated semiconductor in which the conductivity is controlled by numerous defects in the crystal lattice and by the mean free path of charge carriers. On the other hand, the improvement of charge carrier mobility by the peroxide addition is clearly visible. Also the decrease of resistivity with increasing of the layer thickness is apparent from Figs. 4.

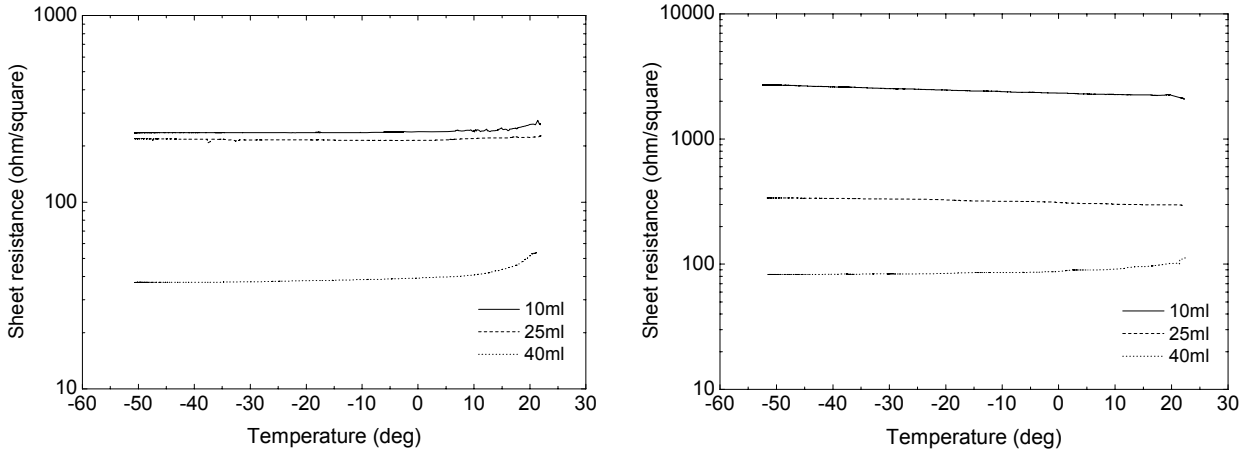

Fig. 4 *Temperature dependence of sheet resistance (peroxide treated left, untreated right)*

Hall effect measurement on SnO_2 thin films on glass substrates from the 40ml solution in room temperature show again the hydrogen peroxide contributes to lowering electrical resistivity due to increased concentration and mobility of charge carriers.

Table 1 *Sheet resistance and Hall effect measurement of 40ml solution samples*

Sample	Thickness (μm)	$R_{\square}$ (Ω/□)	ρ, 10^{-5} (Ωm)	n, 10^{25} (m^{-3})	μ_H, 10^{-3} ($m^2V^{-1}s^{-1}$)	Cond. type	% of ionization
without H_2O_2	1.23	64.79	7.97	4.82	1.62	N	$1.7x10^{-1}$
with H_2O_2	1.35	29.18	3.94	7.56	2.10	N	$2.7x10^{-1}$

A good criterion to define the quality of highly transparent and conductive thin film is through the introduction of a figure of merit calculated using Haacke's equation $\Phi=T^{10}/R_{\square}$ (Ω^{-1}).

Table 2

Sample		T (%) at λ = 550nm	$R_{\square}$ (Ω/□)	Figure of merit, Φ (Ω^{-1})
without H_2O_2	10ml	90.2	1982.0	$1.7931_{x}10^{-4}$
	25ml	69.2	421.4	$5.9406_{x}10^{-5}$
	40ml	54.3	64.8	$3.4161_{x}10^{-5}$
with H_2O_2	10ml	88.3	326.3	$8.8947_{x}10^{-4}$
	25ml	79.2	225.2	$4.3711_{x}10^{-4}$
	40ml	63.7	29.2	3,8156*10-4

Conclusion

The action of hydrogen peroxide in the precursor for SnO_2 deposition by spray method seems to be based on two factors. First it is the oxidation of divalent tin to tetravalent one before the spraying process. Second, we must not forget the formation of peroxoanions which are well soluble and which are undoubtedly present in the precursor. Both these effects yield in the formation of smooth, almost transparent and well conductive layer of tin dioxide. Essentially, the oxidation of the precursor by hydrogen peroxide yields in material with better transparency, lower coloration and higher conductivity. All these benefits are probably caused by better stoichiometry and lower concentration of structural defects in the peroxide treated material. This precursor is predominant over $SnCl_4$ precursor in technology because it does not irritate people and is non – corrosive.

Acknowledgements

This work was supported by the Ministry of Education, Youth and Sports (project MSM 0021630516).

References

1. GUZMAN, G. at al. *Thin Solid Films*. 2006, vol. 502, p. 281-285.
2. HICHOU, A. at al. *Thin Solid Films*. 2004, vol. 458, p. 263-268.
3. GOETZBERGER, A., HEBLING, CH. *Solar Energy Materials and Solar Cells.* 2000, vol. 62, p. 1-19.
4. MORGAN, D. V. at al. *Renewable Energy*. 1996, vol. 7, p. 205-208.
5. KOROTCENKOV, G. at al. *Senzore And Actuators B*. 2001, vol. 77, p. 244-252.
6. PUETZ, J. at al. *Thin Solid Films*. 2003, vol. 442, p. 40-43.
7. HOSHI, Y., KIYOMURA, T. *Thin Solid Films*. 2002, vol. 411, p. 36-41.
8. BANERJEE, R., DAS, D. *Thin Solid Films*. 1987, vol. 149, p. 291-301.
9. ISHIDA, T. at al. *Thin Solid Films*. 1996, vol. 281-282, p. 228-231.

SYNTHESIS AND SUPERCAPACITOR BEHAVIOUR OF NI-MN HYDROXOCARBONATES

O.A. Shlyakhtin[1,4], A.M. Skundin[2], Jung-Ho Ahn[3], Jeon-Kook Lee[1], Young-Jei Oh[1]

[1] Korea Institute of Science and Technology, Thin Film Materials Research Centre, Seoul 136-791, Korea
[2] Institute of Physical Chemistry and Electrochemistry RAS, 119991 Moscow, Russia
[3]Andong National Univ., Dept. of Materials Engineering, Gyungbuk 760-749, Korea
[4] Institute of Chemical Physics RAS, 119991 Moscow, Russia

Corresponding author: Prof. Young-Jei Oh
E-mail: youngjei@kist.re.kr
Phone: +82 2 958 5553, Fax: +82 2 958 5554

Introduction

A number of the recent papers on the alternative electrode materials for electrochemical supercapacitors deal with individual oxides and hydroxides of nickel and manganese. Both groups of materials were used previously as battery electrode materials though following studies demonstrated their reasonable electrochemical performance at high discharge rates. Rectangular shape of CV curves of the MnO_2-based materials is usually associated with true capacitive behavior of the system while complex-shaped CV curves of many NiO-based electrodes show at the considerable faradaic contribution. However, the electrochemical behavior of the corresponding Ni-Mn hydroxides and hydroxocarbonates is studied rather poor until now. Recent studies revealed that electrochemically deposited amorphous NiMn hydroxide films (Ni/Mn = ½) demonstrate considerable reversible electrochemical capacity similar to the MnO_2-based materials [1]. Synthesis and thermal evolution of the carbonate-containing Ni-Mn layered double hydroxides (LDH) is studied in details in [2]. Meanwhile, the Ni/Mn ratio recommended by authors [1] is reciprocal to the common Me^{2+}/Me^{3+} ratio in the LDH's [3]. Phase formation and thermal behavior of hydroxide phases with considerable Mn content is studied in much less details. Authors [4] reported the formation of poorly crystalline calcite-like hydroxocarbonate during coprecipitation of Ni and Mn by sodium bicarbonate. Further heat treatment causes decomposition of this product into the complex mixture of oxides at T = 400°C followed by the formation of single phase $NiMn_2O_4$ spinel at T = 750°C.
Taking into account these considerations and well-known ability of the freeze drying synthesis method [5] to promote retaining the native structure of coprecipitated species during following thermal processing[6], our study was aimed at the synthesis of the bulk Ni-Mn hydroxocarbonates and evaluation of their electrochemical performance at high discharge rates.

Experimental

Synthesis of the Ni-Mn hydroxocarbonates was performed by coprecipitation from the aqueous solution by 1M $NaOH/Na_2CO_3$ = 1/1 at various temperatures (20 – 80°C) followed by filtering, careful washing and freeze drying (P = 5 10^{-2} mbar; Christ Alpha 2-4). Dried products were isothermally processed in air at T = 100 - 400°C. for 2 hours. As-obtained powders (80 mass %) were mixed with carbon black (16 %) and PTFE binder (4%) in ethanol, dried in air and pressed onto Ni foam (8-10 mg of active material per cm^2). Analysis of the electrochemical behaviour of these electrodes was performed in 3% aqueous KOH with Hg/HgO reference electrode and Pt foil counter electrode using WBCS 3000 battery cycler (WonATech) for galvanostatic/chronopotentiometric (CP) studies and IM6ex electrochemical workstation (Zahner elektrik) for cyclic voltammetry (CV).

Results and Discussion

XRD analysis of the synthesis products obtained at various processing temperatures demonstrated that in all cases crystallographic structure of the products was identical and similar to calcite-like compounds observed in [4]. However, the crystallinity of the products demonstrated clear correlation with the synthesis temperature varying from the amorphous state to the rather perfect structure. Apart from thermally dried products described in [4], thermal processing of the freeze dried calcite-like hydroxocarbonates ("calcites") causes considerable amorphization of intermediates followed by the formation of the ilmenite-type Ni-Mn oxide earlier observed in [7] during decomposition of Ni-Mn oxalates (Fig.1). Poor crystallinity of as-obtained product does not allow detecting the extra Mn oxides that should be formed during thermal processing according to the ilmenite stoichiometry (Ni/Mn = 1/1).

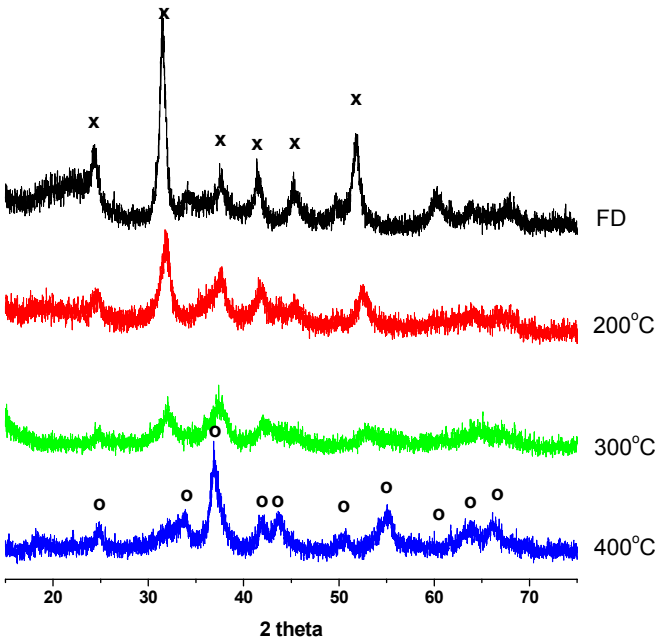

Fig. 1 *Thermal evolution of the freeze drying product during thermolysis. x – calcite-like phase; o – ilmenite.*

Morphological analysis of these powders by TEM and SEM demonstrated the essentially nanocrystalline character of as-obtained hydroxocarbonates. The plate- like primary crystallites are packed into round-shaped 100-200 nm agglomerates. Occasionally, crystallographic transformation of calcite to ilmenite during thermal processing has little or no influence on the size of primary particles. In spite of particle rearrangement and intergrowth, the product remains to be essentially nanocrystalline even after processing at 400°C.

XPS analysis of obtained products showed only minor changes of the valence state of Mn during thermal processing. A position of the main peak of Mn is very close to the corresponding value for Mn_2O_3 though small shift to higher values and poorly resolvable shoulder implies contribution of Mn^{4+}. The position of Ni peaks in the freeze dried product corresponds quite well to Ni^{2+} in Ni hydroxides while the Ni peak in the ilmenite-type product is shifted to lower values and fits well to Ni^{2+} spectrum in the Ni oxides. Evolution of the XPS spectra of oxygen also reflects the transformation of the system from the hydroxide to oxide. However, significant OH-shoulder contribution to the O-peak allows interpreting the ilmenite-like product as Ni-Mn oxyhydroxide,

Evaluation of the electrochemical performance of thus obtained products by cyclic voltammetry (CV) confirmed their expected substantial electrochemical activity (Fig.2). Essential and unusual feature of their properties is rather large operating potential window (-1.2 to +0.8V vs Hg/HgO). The boundaries of this range have been determined experimentally by the characteristic traces of oxygen and hydrogen evolution reactions (OER and HER, respectively) at the positive and negative sides of CV curves. In spite of complex-shaped CV curves and large operating window often associated with accelerated degradation of the electrodes, all samples demonstrated well-reproducible charge-discharge processes with energetic efficiency over 90%.

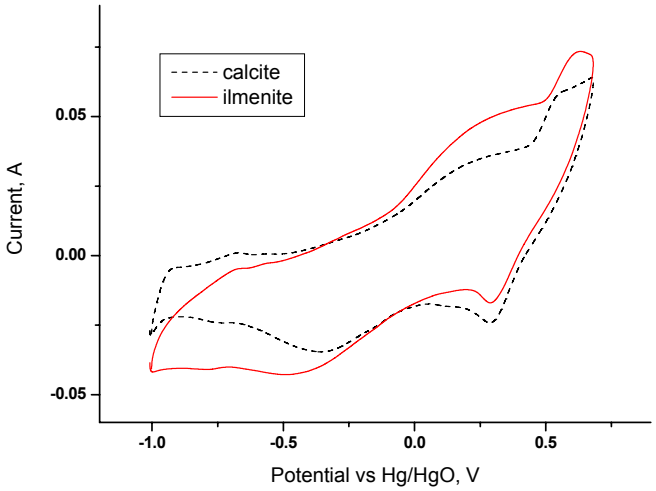

Fig. 2 *Cyclic voltammograms of the samples processed at 100°C (calcite) and at 400°C (ilmenite); scan rate 100mV* s^{-1}.

Clearly asymmetric CV curves can be divided into two parts, at positive and negative potentials. The right sides with more or less definite peaks show at the electrochemical processes occurred during cycling while left side can be rather associated with charge

redistribution in the double layer near the electrode surface. Despite significant Mn content in the composition, all observed CV curves exhibited distinct peaks at +0.4 and -0.3 V specific for the nickel oxides and hydroxides. Trial experiments with preliminarily platinized Ni foam as current lead demonstrated that these peaks couldn't be attributed to the foam-related nickel oxides.
Galvanostatic cycling of obtained electrodes also confirmed that obtained materials could be reversibly recharged at rather large voltage windows. Nonmonotonous character of the CP curves and substantial difference between ascending and descending branches of curves (Fig.3) correlate quite well with observed features of the CV curves and also show at the faradaic background of charge storage mechanisms. Further experiments confirmed that these electrodes retain eversible electrochemical capacity of 65-70 mAh g^{-1} at I = 30-70 mA cm^{-2} for several hundred cycles.

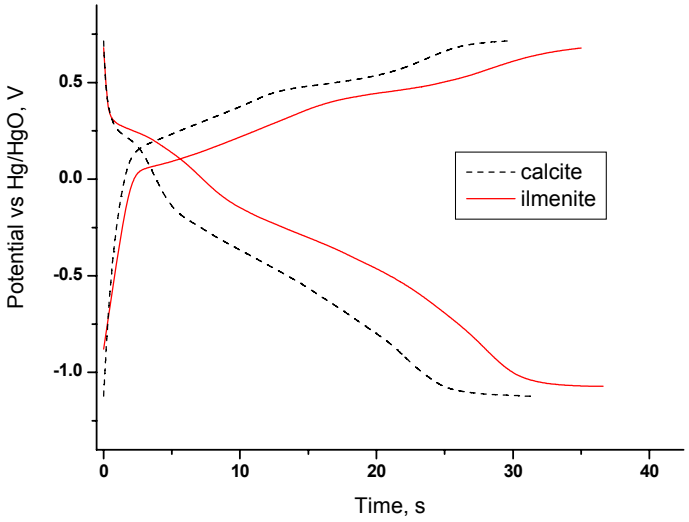

Fig. 3 *Galvanostatic charge and discharge curves of the samples processed at various temperatures (I = 70 mA cm^{-2}.).*

Conclusions

Freeze dried Ni-Mn hydroxocarbonate with calcite-like structure and products of its thermal processing demonstrated substantial reversible electrochemical activity in the alkaline solutions at high discharge rates that makes feasible their further study as electrode materials for electrochemical supercapacitors and high rate batteries.

Acknowledgements

Financial support of the Korea Research Foundation grant funded by the Korea Government (MOEHRD) and KIST Institutional Program is gratefully acknowledged.

References

1. K.R. Prasad, N. Miura: Electrochem. Comm. 6 (2004) 1004.
2. F. Kovanda, T. Grygar, V. Dorničak: Solid State Sciences 5 (2003) 1019.
3. G. Williams, D. O'Hare: J. Mater. Chem. 16 (2005) 3065.
4 D. Mehandjiev, E. Zhecheva, G. Ivanov, R. Ioncheva: Appl, Catal. A 167 (1998) 277.
5 O.A. Shlyakhtin, N. N. Oleinikov, Yu. D. Tretyakov, *Cryochemical synthesis of materials*, In: *Chemical Processing of Ceramics* (2nd. Edition), (B.I. Lee, E.J.A. Pope and S. Komarneni, eds.) (Materials Engineering, vol. 28) CRC Press LLC, NY, 2005, p. 77.
6. O.A. Shlyakhtin, Young-Jei Oh: Inorganic cryogels for energy saving and conversion, J. Electroceramics (2008) in press.
7. Xiao-Xia Tang, A. Manthiram, J.B. Goodenough: J. Less-Common Metals 156 (1989) 357.

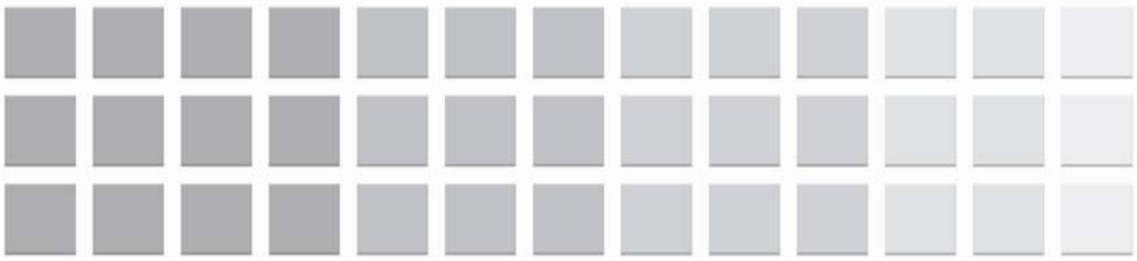

9th ABA

BRNO 2008

Advanced Batteries and Accumulators

Solid and polymeric conductors

CATHIONIC POLYMER ELECTROLYTES FOR LITHIUM-ION POWER SOURCES

O.Chervakov[1], M.Andriianova[1], R.Apostolova[1], E.Shembel[1,2], L.Neduzko[1], V.Ryabenko[1]

[1]SHEI "Ukrainian State Chemical Technology University", Dnipropetrovs'k, Ukraine
[2]Enerize Corporation, Florida, USA

Corresponding author: E. Shembel
E-mail: chervakov@email.dp.ua
Phone, Fax: +380 562 472 491

Introduction

Now search of alternative ways of energy production and also increasing performance of the existing power sources (lithium power sources, fuel cells, etc.) is the actual problem.

The operational characteristics of lithium sources in many respects are determined by a nature of active substance of a cathode material. Electrolytic sulfides and oxide of transition metals (Fe, Ni, Co) have been approved as electrode material [1]. It is known [2], that in lithium chemical power sources (CPS) the electrochemical interaction of lithium with sulfides of transition metals is accompanied by reactionary decomposition of liquid electrolyte components and, first of all, of the aprotic solvent. Used in lithium accumulators the liquid aprotic electrolytes based on ethylene carbonate (EC), dimethyl carbonate (DMC), propylene carbonate (PC) can degrade at repeated cycling of lithium power source [3]. Thus, the degradation ability appreciably is determined by nature of an active material and its catalytic activity.

Proceeding from the above the replacement of liquid phase electrolyte on solid phase polymeric electrolytes (PE) with electrochemical stability up to 2.80-0.02V relative to lithium and good serviceability within a wide temperature range is topical.

In the work the research results of polymeric electrolyte based on ammonium interpolymeric complexes (AIPC), for their use in the thin-film lithium-ion power sources are presented.

Experimental

Synthesis of the film materials based AIPC was carried out in two stages.
At the first stage has been received a solution of for-interpolymeric complex by joint condensation of homopolymer epichlorohydrin (PECH) with poly-4-vinylpyridine (P-4-VP) in a mixture of the organic solvents acetone:tetrahydrofurane (1:1, v/v) at constant mixing of solution and 40-50°C during 1.0-1.5 hours.

At the second stage cooled up to 20-25°C a solution of for-interpolymeric complex poured out on glass or Teflon substrate. Then the final condensation was carried out during 1.5-2.0 hours at temperature 100-120°C with simultaneous removal of the solvents up to obtaining of insoluble in water and organic solvents spatially cross-linked film material of the following structure:

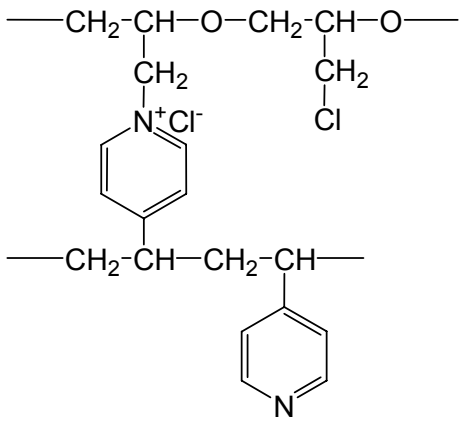

The received film materials based on AIPC have ion exchange capacity ~5.2 meq/g and conductivity $4.5 \cdot 10^{-6}$-$6.5 \cdot 10^{-6}$ $Om^{-1} \cdot cm^{-1}$ at room temperature.

At using of AIPC as binding for cathode material a solution of for-interpolymeric complex cast out on the stainless steel electrode with the earlier deposited cobalt sulfide. Then final condensation of AIPC on the electrode surface at 100-110°C during 1.5-2.0 hours was carried out. After drying the composite electrode material which comprised the mass ratio of cobalt sulfide:AIPC 1.0: (1.0-4.0) was obtained.

Testing of polymeric electrolytes was carried out in the lithium power sources prototype of two kinds: 1 - coin (size 2325), 2 – prismatic (size 3x3 cm), obtained with using of laminated aluminum foil.

As cathodes in prototypes have been used electrolytic cobalt sulfides obtained by cathodic reduction of solutions containing cobalt sulfate and sodium thiosulfate [1]. The deposits of sulfide materials obtained on a grid from stainless steel were connected to the body of CPS by means of the spot weld. The lithium plates were used as the anodes in prototypes of CPS.

Composition of liquid electrolyte in prototype of CPS: 1M solution of $LiClO_4$ in a solvent mixture of the EC:DMC=1:1 (v/v).

Result and Discussion

The film materials based on AIPC are capable to absorb and to keep in themselves significant amount of the liquid electrolytes, in particular,1M solution of $LiClO_4$ in a mixture of the solvents EC:DMC (AIPC:liquid electrolyte=1.00:4.29, wt). Ionic

conductivity of the activated membranes does not concede to conductivity of traditional liquid electrolytes used in lithium CPS, and equal to $3.9 \cdot 10^{-3}$ $Om^{-1} \cdot cm^{-1}$.

Utilization of AIPC as electrolyte in lithium CPS

With using of polymeric electrolytes based on AIPC and electrolytic cobalt sulfide (e-Co_9S_8) the coin prototypes of lithium-ion accumulators were produced. The discharge-charge curves of such e-Co_9S_8/AIPC:EC:DMC:$LiClO_4$/Li system are shown at figure.

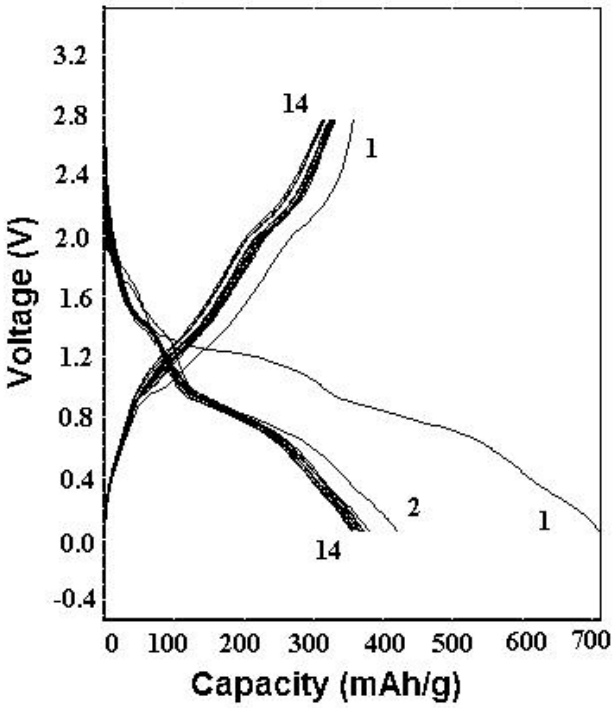

Fig. 1 *Discharge-charge characteristics of coin (size 2325) CPS prototypee-Co_9S_8/AIPC:EC:DMC:$LiClO_4$/Li. Number at curves is cycle number. I_{disch}=0.05 mA/cm^2, I_{charge}=0.03 mA/cm^2. Mass of Co_9S_8 = 1 mg/cm^2.*

Discharge capacity of prototype at the first cycle is about 700 mAh/g. After 3-rd cycle a capacity is stabilized at a level more than 350 mAh/g. The obtained testing data of lithium power sources prototypes (discharge-charge characteristics) with electrolyte of composition AIPC:EC:DMC:$LiClO_4$ in many cases are similar obtained for analogous prototype with the liquid electrolyte. The advantage of offered electrolyte is capability strongly to keep in the structure of ionogenic polymer matrix the liquid electrolyte of composition EC:DMC:$LiClO_4$. This is promoted by presence in structure of AIPC the electron-donor atoms of nitrogen and oxygen. It is known, that the polymeric materials containing in own structure the quaternary ammonium groups are capable to complexation with lithium salts, thus the significant increase of ionic conductivity is observed [4]. In this connection, the application of such electrolytes allows to solve a problem of safe operation of lithium power sources at the expense of prevention of the liquid electrolyte outlet from CPS at its seal failure.

Utilization of AIPC as binder for cathode materials of lithium CPS

With the purpose of the problem decision of adhesion increasing of active material to the current collector we carried out works on research of the use opportunity of AIPC as binder for cathode material. It is established, that the mass ratio of cobalt sulfide:AIPC influences on cycling duration of lithium CPS.

Investigations of lithium CPS prototypes based on the cathode with AIPC film have been shown that an increase of AIPC content in cathode leads to the adhesion improvement of electrolytic cobalt sulfide to the electrode surface.

The lithium CPS prototypes with composite cathode (e-Co_9S_8:AIPC) are stable cycling during more than 35 cycles.

Conclusions

As a result of the carried out work the use opportunity of ammonium interpolymeric complexes as a polymeric matrix for electrolytes and binding agent for cathodic materials of lithium power sources was established.

References

1. R.D. Apostolova, E.M. Shembel, I. Talyosef, J. Grinblat, I. Genish, B. Markovsky: 8th International conference ABA (Advanced Batteries and Accumulators). Brno, Czech Republic (2007) 23-26.
2. K. Kumagai, T. Ikeya, K. Ishihara, T. Iwahori: J. Power Sources 70 (1998) 235-239.
3. L. Gireaund, S. Grugeon, S. Laruelle, S. Pilard: J. Electrochem. Soc. 152 (2005) A850-A857.
4. Yuko Ikeda, Makoto Ikeda: 14th International Conference of Solid State Ionics. – Monterey, USA (2003) IXP08.

LI^+ AND H^+ SINGLE-ION CONDUCTING POLYMER ELECTROLYTES

Jakub Reiter[1], Jiří Michálek[2,3], Martin Přádný[2,3], Dana Chmelíková[2], Jakub Širc[2,3]

[1] Institute of Inorganic Chemistry of the ASCR, v. v. i., 250 68 Řež near Prague, CZ
[2] Institute of Macromolecular Chemistry of the ASCR, v. v. i., 162 06 Prague, CZ
[3] Centre for Cell Therapy and Tissue Repair, Charles University, 150 18 Prague

Corresponding author: Jakub Reiter (reiter@iic.cas.cz)
Phone: +420 266 172 198
Fax: +420 220 941 502

Introduction

Gel polymer electrolytes (GPEs) attract the attention since M. Armand's introduction of the electrolytes based on poly(ethylene oxide) [1, 2] for their suitable electrochemical and mechanical properties including high electrochemical and dimensional stability, good ionic conductivity, high design flexibility and long-term durability. The main application is in the technology of lithium and lithium-ion batteries. Generally, the lithium electrolytes, both liquid and polymer suffer from strong tendency of ion-ion association and low transference number of the lithium cation $t^+(Li^+)$. This process is linked to a decrease of the bulk electrolyte conductivity. Moreover, there is an important difference between the determination of $t^+(Li^+)$ by methods based on alternating current and real situation in the lithium-ion batteries and fuel cells, where one can found a direct current flow during charge and discharge processes. During these long-term processes a concentration gradients of ions in the electrolytes are formed and due to the rising IR drop (ohmic polarisation) the capacity of the device is decreasing.

Our recent task is to develop a new polymer electrolyte with a high transference number of Li^+, thus the current will be carried by the cations mainly. This will be caused by immobilising the anion to the polymeric network by a covalent bond such as in the case Nafion H^+-conducting electrolyte. Fig. 1A presents structures of a gel polymer electrolyte with long polymer chains randomly cross-linked and with homogenously distributed ions of $LiClO_4$ as a representative of a bi-ion conductor. The single-ion conducting electrolyte is shown on Fig 1B.

In the presented contribution we describe new copolymers of methacrylic acid (MA) or lithium methacrylate (LiMA) with 2-ethoxyethyl methacrylate (EOEMA) and poly(ethylene glycol) methyl ether methacrylate (EGMEMA) as pure cationically conducting Li^+ or H^+ electrolytes and covalently bonded carboxylic group.

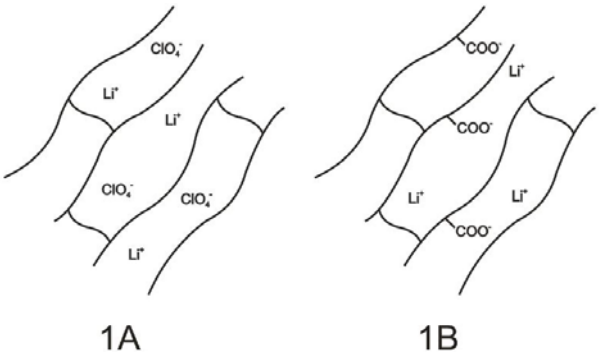

Fig. 1 *Structure of bi-ion (1A) and single-ion (B) electrolyte (solvent molecules are not shown).*

Experimental

Polymer electrolytes were prepared by direct, UV-initiated radical polymerization of the initial mixture of monomers, cross-linking agent and initiator (benzoine ethyl ether, Sigma-Aldrich). In the case of electrolytes with co-solvent, propylene carbonate (99.7%, anhydrous; Sigma-Aldrich) or N,N-dimethylformamide (anhydrous; Merck) were also added to the initial mixture.

The cross-linking agents hexamethylene dimethacrylate (Fluka) for EOEMA and ethyleneglycol dimethacrylate (Mr ≈ 330; Sigma-Aldrich) for EGMEMA were used in 0.3 mol. % concentration for improvement of the mechanical properties and following our previous results [3] also for the improvement of conductivity.

The polymerization proceeded for 1.5 - 2 hours at room temperature under UV light emitted by a pair of 15W UV lamps (Hagen, Czech Republic). The cell for the electrolyte preparation was described previously [3].

The potentiogalvanostat 30 (Eco Chemie, The Netherlands) was used for the electrochemical measurements including the FRA-2 module for impedance measurements. The electrochemical potentials in the text are related to the PMMA/Cd/Cd2+ reference system, E(PMMA-Cd-Cd2+) = -0.44 V vs. SCE in propylene carbonate [4].

The simultaneous TGA-DTA measurement was taken in air at the heating rate of 5 °C.min^{-1}. Experiments were performed with a Simultaneous Thermal Analysis Netzsch STA 409 (Germany).

Results and Discussion

The first task was to find suitable combination of a monomer with the carboxylic group and an aprotic monomer that is also present in the polymer network. This procedure has to consider both mechanical (reasonable elasticity, no phase-to-phase separation) as well as electrochemical properties (mainly ionic conductivity). The best results were found in the case of electrolytes with EOEMA or EGMEMA present as a copolymer.

Beside good mechanical properties, the interaction with H^+ and Li^+ cations with the oxygen atoms in the polymer network increases their mobility.

Table 1 summarises prepared representatives of various single ion electrolytes together with their conductivity at 20 °C. In the case of H^+ electrolytes with copolymerised methacrylic acid, the binary system poly(MA-EOEMA) exhibits very low conductivity that is strongly enhanced by more than three orders of magnitude by present aprotic solvent of a high dielectric constant – propylene carbonate.
The investigation of mechanical properties that the combination of MA and EOEMA ensures good mechanical properties, when the molar ratio MA : EOEMA is 1 : 1. Even a small difference from this ratio makes both the mechanical properties and conductivity worse (see table 1). Due to the low dissociation of the carboxylic group in methacrylic acid or its copolymer with EOEMA or EGMEMA, values in the range of 10-6 $S.cm^{-1}$ can be considered as acceptable.

Table 1 *The specific conductivities of H^+ and Li^+ single ion electrolytes with methacrylic acid or lithium methacrylate.*

Electrolyte	Composition [mol. %]	σ (20 °C) [$S.cm^{-1}$]
poly(MA-EOEMA)	5 : 95	$1.0 . 10^{-9}$
poly(MA-EOEMA)-PC	15 : 15 : 70	$2.2 . 10^{-6}$
poly(MA-EOEMA)-PC	20 : 30 : 50	$8.7 . 10^{-9}$
poly(MA-EGMEMA)-PC	20 : 5 : 75	$2.1 . 10^{-6}$
poly(LiMA-EOEMA)	non-compatible	-
poly(LiMA-EOEMA)-PC	non-compatible	-
poly(LiMA-EOEMA)-DMF	8 : 17 : 75	$5.4 . 10^{-5}$
poly(LiMA-EGMEMA)-PC	non-compatible	-
poly(LiMA-EGMEMA)-DMF	10 : 5 : 85	$1.9 . 10^{-4}$

The preliminary solubility tests of lithium methacrylate in various aprotic solvents showed that LiMA is not soluble in carbonates (propylene, ethylene, dimethyl or diethyl carbonate) or tetraethyleneglycol dimethylether. On contrary, LiMA is well soluble in N,N-dimethylformamide. Our experiments also showed that LiMA is not chemically compatible with EOEMA and EGMEMA, in the presence of propylene carbonate. DMF as another solvent with high dielectric constant showed remarkably high positive effect of LiMA dissociation in the polymer electrolytes. Values of 0.19 $mS.cm^{-1}$ were reached for poly(LiMA-EGMEMA)-DMF electrolyte at 20 °C (see table 1).

Considering the practical application, the influence of temperature on conductivity was studied in the range from -25 to 70 °C. Fig. 2 presents the Arrhenius plot for MA and LiMA single-ion electrolyte compared to the bi-ionically conducting PEOEMA electrolyte with H3PO4-PC. Here one can see remarkably different slope of the relationship conductivity vs. temperature. Using the Arrhenius equation for fitting the data we obtained the values of apparent activation energies for conduction. EA for poly((MA-EGMEMA)-PC and poly(LiMA-EGMEMA)-DMF electrolytes are 21.3 and 17.7 $kJ.mol^{-1}$

respectively. This a markedly lower value that 40.2 kJ.mol^{-1} determined for H3PO4-poly(EOEMA)-PC electrolyte [5], but similarly high values are generally found in other bi-ionic conductors. This difference indicates different conduction mechanism in the single-ion electrolytes.

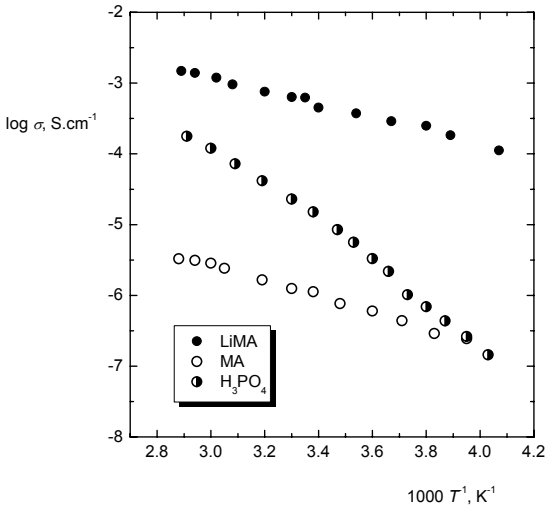

Fig. 2 *Arrhenius plot of the ionic conductivity for poly(MA-EGMEMA)-PC (20:5:75), poly(LiMA-EGMEMA)-DMF (10:5:85) compared to the bi-ionic electrolyte H3PO4-poly(EOEMA)-PC (42:34:24 mol. %).*

Concerning the applications, thermal stability is another principal parameter to be considered along with electrochemical and long-term stability and reasonable conductivity. Figure 3 shows TGA curve of selected MA and LiMA copolymers. The poly(MA-EOEMA) electrolyte exhibits highest thermal stability up to almost 200 °C, when methacrylates generally start do decompose [6]. In the presence of DMF or PC is the thermal limit is lowered down to 105 - 115 °C due to partial solvent evaporation.

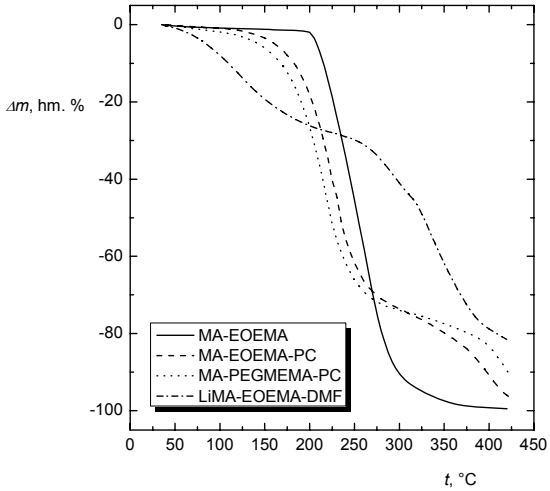

Fig. 3 *Simultaneous TGA and DTA curves of poly(MA-EOEMA), poly(MA-EOEMA)-PC, poly(MA-EGMEMA)-PC a poly(LiMA-EOEMA)-DMF (5 °C.min^{-1} heating rate, temperature range 30 - 380 °C; air atmosphere).*

Conclusions

New single-ion conducting electrolytes based on methacrylates were prepared using direct, radically initiated polymerisation: copolymers of methacrylic acid (MA) or lithium methacrylate (LiMA) with 2-ethoxyethyl methacrylate (EOEMA) and poly(ethylene glycol) methyl ether methacrylate (EGMEMA) as pure cationically conducting Li+ or H+ electrolytes and covalently bonded carboxylic group. For the conductivity improvement, a set of electrolytes with embedded aprotic solvent (propylene carbonate PC or N,N-dimethylformamide DMF) was prepared. After optimalisation of the electrolyte composition, highest conductivity values were found in the case of samples poly(MA-EOEMA)-PC (2.2 . 10-6 $S.cm^{-1}$) a poly(LiMA-EGMEMA)-DMF (1.9 . 10-4 $S.cm^{-1}$). The accessible potential window was estimated on gold electrode to be ca. 1.75 - 2 V for H+ electrolytes and over 3.5 V for the Li+ electrolytes.

Acknowledgements

This work was supported by the Academy of Sciences (Research Plan AV0Z40320502), by the Grant Agency of the Academy of Sciences (B400320701) and by the Ministry of Education (project MSMT LC523).

References

1. M. B. Armand, Solid State Ionics 9-10 (1983) 745.
2. M. B. Armand, Adv. Mater. 2 (1990) 278.
3. J. Reiter, J. Michálek, J. Vondrák, D. Chmelíková, M. Přádný, Z. Mička, J. of Power Sources 158 (2006) 509.
4. J. Reiter, J. Vondrák, Z. Mička, Solid State Ionics 177 (2007) 3501.
5. J. Reiter, J. Velická, M. Míka, Electrochim. Acta (under review).
6. H.S. Kim, J.H. Shin, S.I. Moon, M.S. Yun, J. Power Sources 482 (2003) 119.

POLYMER ELECTROLYTES FOR LITHIUM-ION BATTERIES OPERATING AT ELEVATED TEMPERATURES

Jakub Reiter[1], Robert Dominko[2], Ivo Jakubec[1], Jiří Michálek[3,4]

[1] Institute of Inorganic Chemistry of the ASCR, v. v. i., 250 68 Řež near Prague, CZ
[2] National Institute of Chemistry, Hajdrihova 19, SI - 1000 Ljubljana, Slovenia
[3] Institute of Macromolecular Chemistry of the ASCR, v.v.i., 162 06 Prague, CZ
[4] Centre for Cell Therapy and Tissue Repair, Charles University, 150 18 Prague

Corresponding author: Jakub Reiter (reiter@iic.cas.cz)
Phone: +420 266 172 198
Fax: +420 220 941 502

Introduction

Recently developed cathode materials ($LiFePO_4$, Li_2MSiO_4 (M=Fe and/or Mn) suffer from low intrinsic conductivity (10^{-9} - 10^{-12} $S.cm^{-1}$ at room temperature). This drawback can be minimized by reducing the conduction path length, e.g., by preparing nano-size [1,2] or nano-porous particles [3,4], and by decorating them with a thin electronically conducting layer (generally carbon). Electrochemical tests at elevated temperatures (60 - 90°C) give much better electrochemical behaviour of orthosilicate-based cathode materials due to improved conductivity by several orders of magnitude. This benefit of improvement of intrinsic conductivity has a negative effect on the commercial electrolyte stability in the potential range where mainly orthosilicates can deliver capacity. Namely it is known phenomena that commercial electrolytes (DMC-EC, DEC-EC, etc.) are stable to the potentials up to 4.2 V vs. Li/Li^+, above this potential range sporadic reactions like oxidation of electrolyte on carbon black and surface of cathode particles occur. These degradation reactions are even faster at elevated temperatures usually used for electrochemical testing of Li_2MSiO_4 based cathode materials (M=Fe, Mn).

An attempt to solve this is in employment of polymer gel electrolytes. Here, we can overcome drawbacks mentioned above due to their main advantages:

- improved thermal stability (up to 110 °C);
- lowered vapour tension (volatile solvents such as DEC or DMC are not used, PC is entrapped in the polymer structure);
- lower reactivity, thus larger potential window, especially at high potentials.

We have been studying various methacrylate-based systems with $LiClO_4$-PC electrolyte exhibiting reasonable ionic conductivity (10^{-3} $S.cm^{-1}$) together with electrochemical stability over 4.8 V (cit. [5, 6]). The presence of polymer is lowering the electrolyte reactivity and possibly participates on the SEI formation on both anode and cathode. Due to the reason that aluminium (serving as a current collector) is anodically oxidised in the presence of perchlorate anion leads us to investigate polymer electrolytes based on

2-ethoxyethyl methacrylate (EOEMA) with immobilised lithium bis(oxalato)borate (LiBOB) - PC solutions (see fig. 1).

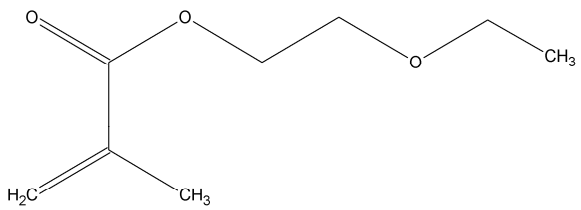

EOEMA

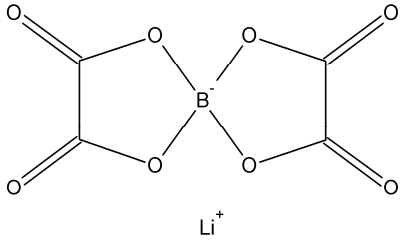

LiBOB

Fig. 1 *Molecular formulas of 2-ethoxyethyl methacrylate (EOEMA) and lithium bis(oxalate)borate (LiBOB) used for the electrolyte preparation.*

Experimental

The polymer electrolytes were prepared using direct, radical, thermally initiated polymerisation following our previous experiments [5, 6]. The initial mixture was prepared in a glove box (MBraun, USA) and contains monomer (EOEMA, Sigma-Aldrich), cross-linking agent (hexamethylene dimethacrylate; 0.3 mol. % of monomer; Sigma-Aldrich), polymerisation initiator 2,2'-azobis(isobutyronitrile) (AIBN), 1 mol. % of monomers; Sigma-Aldrich) and 0.7M solution of LiBOB (Chemetall) in PC (Sigma-Aldrich, 99.7%, anhydrous). The cell for the electrolyte preparation consists of PTFE and polypropylene plate (60 x 60 mm) with inserted spacer (silicone rubber, 1 mm). The polymerisation proceeded for 2 hours at 80 °C.

The basic electrochemical measurements were performed in a glove box using potentiostat PGSTAT 30 (EcoChemie, Holland) on gold electrode (∅ 1.6 mm). The electrochemical characteristics against metallic lithium were measured in vacuum-sealed triplex foil (coffee bag foil) cells. Electrochemical cells with polymer electrolyte were assembled from polymerized electrolyte on Al or Cu substrate against metallic lithium as a counter electrode, without using additional separator. For comparison we assembled also electrochemical cells with liquid electrolyte. The electrolyte used was a 0.8M solution of LiBOB in EC:DEC (1:1 vol.; Sigma-Aldrich). Solvents and the salt were used as received. The working (Cu or Al substrate) and the counter electrode consisting of metallic lithium were separated with a glass wool separator which was immersed into the electrolyte. The cyclovoltametric measurements were performed using a VMP3 potentiostat/galvanostat at a constant temperature of 80 °C with a scan rate of 2 $mV.s^{-1}$ in the potential range from 1 V - 5 V vs. Li/Li^+ when Al substrate was used and in the potential range 0 V – 3 V vs. Li/Li^+ when Cu substrate was used.

Results and Discussions

Prepared electrolytes form sticky, homogenous and transparent membranes of suitable elasticity. No phase-to-phase separation was observed after storage for several months. The electrolytes are thermally stable up to 130 °C.
While system PEOEMA-PC exhibits very low conductivity (below $1.2 \cdot 10^{-8}$ S.cm^{-1}), presence of LiBOB grants the ionic conductivity in the range around 10^{-4} S.cm^{-1} at 20 °C. At temperatures above 70 °C, the conductivity is ca. one-order higher (see table 1).

Table 1 *Ionic conductivity of PEOEMA-PC-LiBOB electrolytes at 20 and 70 °C.*

electrolyte composition (mol. %)	σ at 20 °C (S.cm^{-1})	σ at 70 °C (S.cm^{-1})
61:36:3	$2.1 \cdot 10^{-5}$	$2.2 \cdot 10^{-4}$
51:45:4	$4.6 \cdot 10^{-5}$	$3.7 \cdot 10^{-4}$
40:56:4	$1.4 \cdot 10^{-4}$	$1.0 \cdot 10^{-3}$

Cyclic voltammetry on gold electrode showed reversible lithium reduction and oxidation with preceding reduction waves corresponding to the SEI formation. The anodic limit is at 4.8 - 5 V with appearing wave of partial oxidation of propylene carbonate (see Fig. 1).

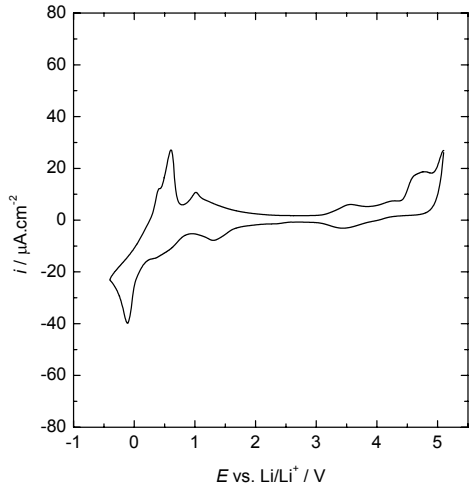

Fig. 2 *Cyclic voltammogram of PEOEMA-PC-LiBOB (40:56:4 mol. %) electrolyte on the gold electrode (5 mV/s scan rate, counter glassy carbon).*

Another set of electrochemical measurements using a “coffee bag” technology was done on aluminium and copper foil. Fig. 3 presents cyclic voltammograms of PEOEMA-PC-LiBOB electrolyte compared to the same measurements of DEC-EC-LiBOB electrolyte. One can see that the electrochemical reactivity is lower in the case of polymer electrolytes. This is important mainly for the high potentials, above 4.5 V.

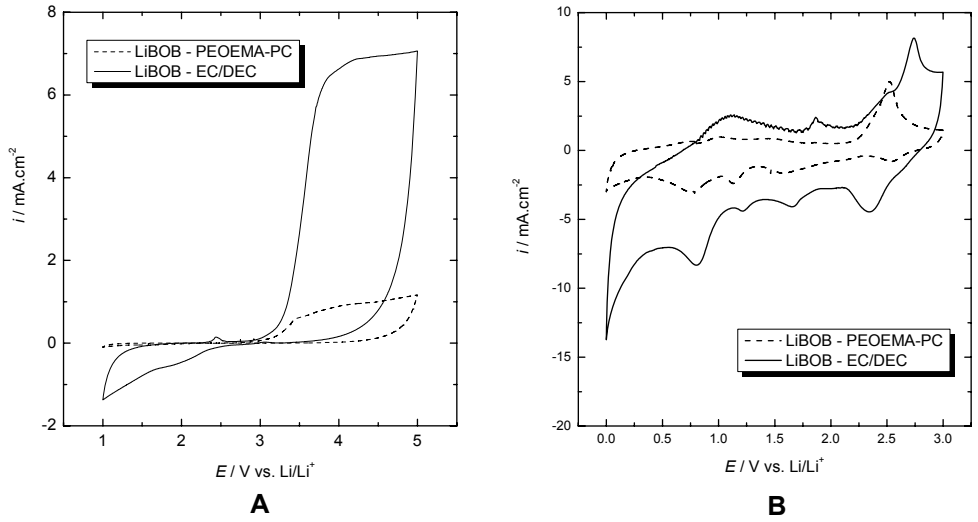

Fig. 3 *Cyclic voltammograms of LiBOB-EC/DEC and PEOEMA-PC-LiBOB electrolyte on aluminium (A) and copper (B) foil (2 mV/s scan rate, 80 °C temperature, counter lithium foil).*

Conclusions

The immobilisation of the LiBOB-PC solution in the polymer network of EOEMA lowers its electrochemical reactivity especially at high potentials close to 5 V vs. Li/Li^+. Considering the improved thermal stability and electrochemical stability towards oxidation, the polymer electrolytes are now being tested with $LiFePO_4$ cathodes at elevated temperatures (60 - 80 °C).

Acknowledgements

This work was supported by the Grant Agency of the Academy of Sciences of Czech Republic (grant No. B400320701), the Ministry of Education, Youth and Sports, Czech Republic (project MSMT LC523 and Czech-Slovenian project Contact MEB 090806) and by the Academy of Sciences (Research Plan AV0Z40320502).

References

1. N. Ravet, J.B. Goodenough, S. Besner, M. Simoneau, P. Hovington, M. Armand, 196th ECS Meeting, Honolulu, Hawaii, 1999, Proceedings, abstract 127.
2. H. Huang, S.C. Yin, L.F. Nazar, Electrochem. Solid-State Lett., **4** (2001) A170.
3. R. Dominko, M. Bele, M. Gaberscek, M. Remskar, D. Hanzel, S. Pejovnik, J. Jamnik: J. Electrochem. Soc. **152** (2005) A607.
4. R. Dominko, J.M. Goupil, M. Bele, M. Gaberscek, M. Remskar, D. Hanzel, J. Jamnik: J. Electrochem. Soc. **152** (2005) A858.
5. J. Reiter, J. Michalek, J. Vondrak, D. Chmelikova, M. Pradny, Z. Micka: J. Power Sources **158** (2006) 509.
6. J. Reiter, J. Vondrak, J. Michalek, Z. Micka: Electrochim. Acta **52** (2006) 1398

EFFECT OF HIGH FILLER CONTENT ON THE CHARACTERISTICS OF GEL POLYMER ELECTROLYTES BASED ON PVDF/HFP AND FUNCTIONALIZED SILICAS.

Monika Osińska, Mariusz Walkowiak, Marek Rusinek

Institute of Non-Ferrous Metals, branch in Poznan, Central Laboratory of Batteries and Cells, Forteczna 12, 61-362 Poznań, Poland

Corresponding author: Monika Osińska
E-mail: monika.osinska@claio.poznan.pl
Phone. +48618793153, Fax. +48618793012

Introduction

The aim of the presented work is to demonstrate a new kind of polymeric, lithium cation conducting membranes which could replace traditional liquid electrolytes suffer from unsatisfactory safety level in advanced Li-ion batteries. Dry polymer electrolytes contain only polymer and lithium salt. Gel polymer electrolytes comprise additionally some low-molecular weight solvent. Composite polymer electrolytes are obtained by dispersing fine ceramic powders in the polymer matrix. Polymer electrolytes membranes contained dispersed modified silica filler of lithium conducting systems are regarded as particularly promising and have been subject of numerous scientific reports [1-3].

Experimental

The membranes were prepared in the following way: PVdF/HFP copolymer (Kynarflex, Antofina) was added to acetone together with dibutyl phthalate (DBP; >99%, Merck-Schuchardt) and silica (SYLOID 244, Grace; SYLOID 244 modified with methacryloxy functional groups; SYLOID 244 modified by silicon tripodands which are a specific group of silanes in which three polyoxaethylene chains are pinned together by the central silicon atom. The weight ratios of silica in the composite matrices varied from 10% to 70%. The mixtures were stirred vigorously for two hours, followed by five minutes of ultrasonic shaking. Each solution was cast on a glass plate and left for a slow solvent evaporation. Dry membranes were immersed in diethyl ether (pure p.a., Chempur) and left under stirring for eight hours to extract DBP.

Scanning electron microscopy (SEM) micrographs of membranes have been taken with the application of Vega 5135MM microscope (Tescan).

Liquid phase uptake and evaporation kinetics were studied by immersing round pieces dry membranes in liquid electrolyte for Li-ion batteries:1M solution of LiPF6 (99.99%, Aldrich) in the 1:1 w/w mixture of diethyl carbonate (EC, anhydrous, 99%, Sigma-Aldrich) and dimethyl carbonate (DMC, anhydrous, 99%, Sigma-Aldrich). The membrane pieces

were removed from the solution, weighted and placed immediately again in liquid electrolyte in definite interval of time. After 72h the membrane pieces were removed from liquid electrolyte and allowed for free solvent evaporation. In predefined moments of time the pieces were weighted.

Conductivities were measured in two electrode Swagelok-type cells with stainless steel electrodes. The conductivities were determined at several temperatures (0ºC -70ºC) on the basis of impedance spectra by means of Solatron impedance analyzer in the frequency range 100 kHz-100 Hz. The cells were thermostated using Vötsch climatic chamber.

Results and discussion

Fig.1. shows the typical pores in composite membranes where the filler was SYLOID 244 modified with methacryloxy functional groups. With increasing the filler load, the pore spaces become more packed with silica grains.

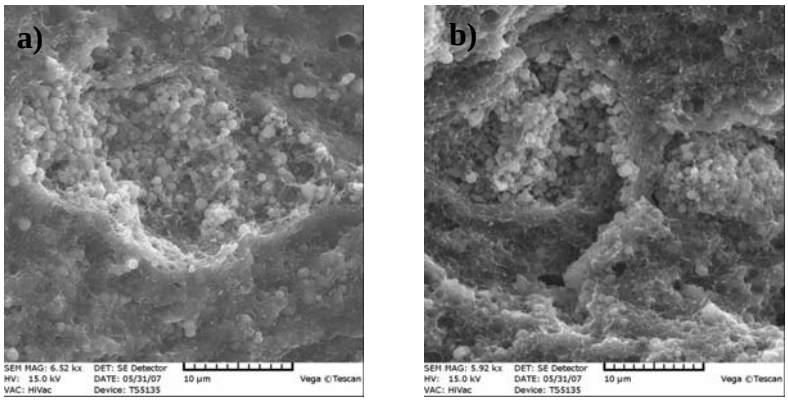

Fig. 1 *SEM pictures taken from the membrane fractures: a). 30% of filler, b). 50% of filler*

Fig.2. compares the liquid phase uptakes after 24h of swelling for all the membranes filled with SYLOID 244 modified with methacryloxy functional groups. The membranes are practically fully swelled after 24h and further weight increase is rather negligible. It can be observed during free solvent evaporation that increasing the filler content suppresses the solvent evaporation.

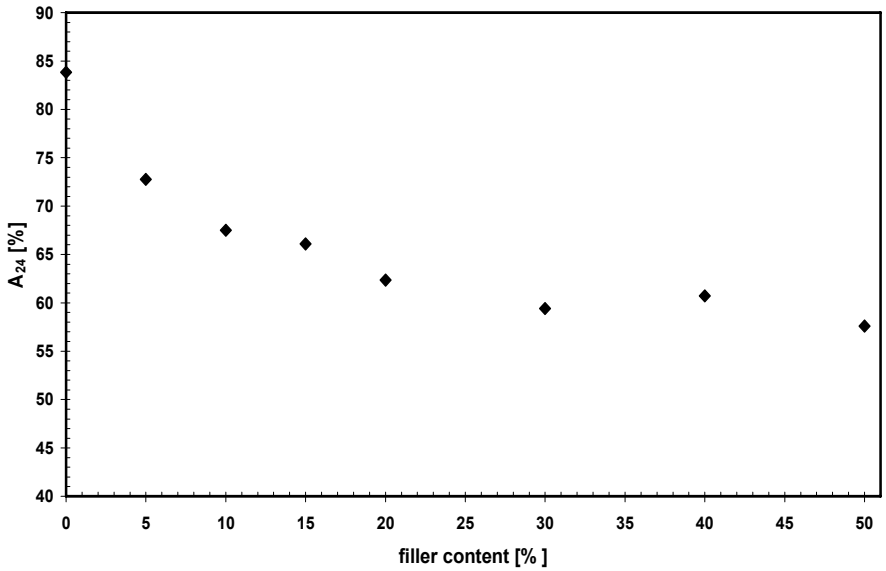

Fig. 2 *Liquid phase uptaken after 24h as a function of filler content of for membranes in 1M $LiPF_6$ solution in EC/DMC.*

The conductivity (Fig.3.) for the membranes with different filler contents of SYLOID 244 SYLOID 244 modified with methacryloxy functional groups has tend to increase with increasing the filler content and temperature even for very high filler concentration.

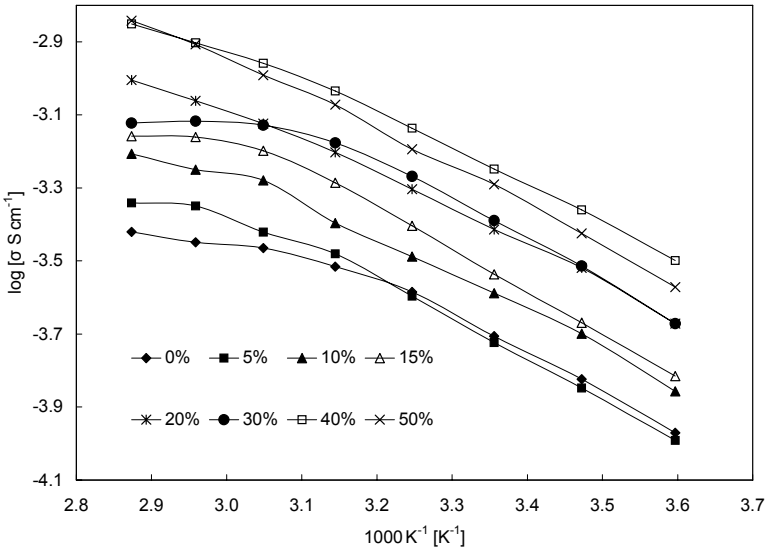

Fig. 3 *Arhenius plots determined for membranes with various silica contents swelled with liquid electrolyte.*

Conclusion

It can be found that conductivity increase of composite gels is not directly correlated with the liquid electrolyte uptake. Thin layers of electrolyte adsorbed on the filler grain

surfaces can ensure sufficiently favorable transport environment for ions. Overlapping space-charge layers coming from silica packed in the pores create fast conduction pathways, thus contributing to the conductivity increase.

References

1. B.Kumar, L.G.Scanlon, Polymer-ceramic composite electrolytes, J. Power Sources 52 (1994) 261-268
2. E.Quartarone, P.Mustarelli, A.Magistris, PEO-based composite polymer electrolytes, Solid State Ionics 110 (1998)1-14
3. M.Walkowiak, New concepts of composite polymer-ceramic electrolytes for Li-ion batteries, in S.S.Zhang (Ed.), Advanced materials and methods for lithium-ion batteries, Transworld Research Network, Trivandrum, India, 2007, Chapter 15

A STUDY OF PMMA BASED GEL ELECTROLYTES CONTAINING NA+ IONS BY NUCLEAR MAGNETIC RESONANCE

J. Vognar[1], M. Macalík[1], P. Špičák[1], J. Vondrák[1,2], V. Novák[1], O. Krejza[1], K. Bartušek[3]

[1] Department of Electrotechnology FEEC BUT, Údolní 53, 602 00 Brno, CZE
[2] Institute of Inorganic Chemistry of the ASCR, v.v.i.,250 68 Řež, CZE
[3] Institute of Scientific Instruments of the ASCR, v.v.i., Královopolská 147, 612 64 Brno, CZE

Corresponding author: J. Vognar
E-mail: jirikv@email.cz

Introduction

The investigation of polymer gel electrolytes is a most important not only for all solid-state rechargable lithium or lithium-ion batteries, but also for many branches of other electrochemical devices such as supercapacitors, electrochromic windows, and sensors [1]. The polymer gel electrolytes have lot of advantages opposite liquid electrolytes. At the beginning of nineties of 20th century, gels were called "third generation gel electrolytes". It consisted of an electrolyte such as lithium salt in propylene carbonate (or other suitable aprotic solvent) thickened to the consistency of a gel by suitable polymer (polymethylmetacrylate, polyvinyl chloride, polyacrylonitrile etc.). Plenty of papers appeared in last 10 years, which indicated clearly that this field was (and still is) extremely vivid. Nuclear magnetic resonance (NMR) can be used for non-destructive examinations of gel electrolytes. Spin-lattice relaxation time: (T1)-weighted inversion recovery spin-echo images of ^{23}Na nuclei in gels were acquired [2]. Inversion recovery spin-echo NMR microimaging may be useful for studying internal microstructure of the gels. A method for quantitative T2 imaging has been presented by Edzes [3]. This method covers the large range of T2 values in gels electrolytes (5 to 2000 ms) simultaneously. The transverse relaxation is characterized by phase-sensitive measurement of many echo images in a multi-echo magnetic resonance imaging sequence. The characterization of transverse relaxation by multi-echo image acquisition opens a new route for studies of sodium nuclei in gel electrolytes.

Experimental

The relaxation times T_1 and T_2 of ^{23}Na nuclei in the gel electrolytes and their changes during the gel ageing were experimentally measured. Relaxation time T_1 was measured by the Inversion Recovery (Tab 2, Fig 1). The relaxation time T_2 was measured by two methods: Hanh echo (Tab 3, Fig 2) and by determination half-width of spectral line from FID signal (Tab 4, Fig 3). T_2 determinated from half-width is according to

$$T_2 = \frac{1}{\pi \cdot \Delta \nu},$$

where $\Delta\upsilon$ is the half-width of the spectral line measured.
Two types of gel were prepared. Base of each one was 1M solution of $NaClO_4$ in PC (4ml of basic solution, sample 2). To this solution has been added:
1.type: 6ml of liquid monomer MMA (99%), 40ul of netting agent EDMA a 100mg of polymerization agent AIBN (samples 3-6).
2.type: 2,8g industrial polymerization agent SUPERACRYL® (Spofadental, Czech Republic) (sample 7 and 8).

Volume of each sample was about 10 ml. Sample 1 was measured in time 0 minutes only. The samples 2-7 were heated on 80°C (polymerization temperature), sample 8 was polymerized in room temperature and they were polymerized for 3 hours. Sample compositions and measuring ageing time step are displayed in Table 1.
The measurement was done on MR tomography with resonance frequency 200MHz and basic magnetic B_0 = 4,7T in Institute of Scientific Instruments of the ASCR, v.v.i.

Table 1 *Marking of samples, their composition, measuring time step nad thermic option*

Sample	Composition	Time (min)	Thermic option
1	H_2O + 10% wt. NaCl	0	not heated (23°C)
2	$NaClO_4$ + PC	0, 180	heated (80 °C)
3	$NaClO_4$ + PC + MMA	0, 180	heated (80 °C)
4	$NaClO_4$ + PC + MMA + EDMA	0, 180	heated (80 °C)
5	$NaClO_4$ + PC + MMA + AIBN	0, 180	heated (80 °C)
6	$NaClO_4$ + PC + MMA + EDMA + AIBN	0, 30, 60, 90, 120, 150, 180	heated (80 °C)
7	$NaClO_4$ + PC + SUPERACRYL®	0, 30, 60, 90, 120, 150, 180	heated (80 °C)
8	$NaClO_4$ + PC + SUPERACRYL®	0, 30, 60, 90, 120, 150, 180	not heated (23°C)

Table 2 *T_1 relaxation times (inversion recovery) measured at different polymerization time*

	t [min]						
Sample	0	30	60	90	120	150	180
1	42,6						-
2	1,7						1,8
3	5,5						6,1
4	5,3						6,1
5	5,1						*
6	5,1	0,4	0,1	0,2	0,1	0,4	0,0
7	4,3	1,7	1,8	1,6	1,7	1,8	1,8
8	3,9	2,5	2,2	2,1	1,9	1,9	1,8

T1 [ms]

* noised signal

Table 3 *T_2 relaxation times (hahn echo) measured at different polymerization time*

	t [min]						
Sample	0	30	60	90	120	150	180
1	94,9						-
2	2,7						3,0
3	6,5						7,4
4	6,5						7,2
5	6,2						2,1
6	6,6	0,9	1,1	1,0	0,5	0,7	1,0
7	4,5	1,4	1,5	1,3	0,8	1,0	1,0
8	4,0	3,0	2,4	2,1	1,7	1,6	1,4

T_2 [ms] (Hahn echno)

Table 4 *T_2 relaxation times (half-width) measured at different polymerization time*

	t [min]						
Sample	0	30	60	90	120	150	180
1	10,2						
2	1,5						1,4
3	3,4						3,9
4	3,4						3,1
5	3,5						0,3
6	3,3	0,4	0,4	0,3	0,3	0,4	0,4
7	2,2	0,8	0,8	0,6	0,6	0,5	0,4
8	2,2	1,6	1,3	1,1	0,9	0,8	0,7

T_2 [ms] (half-width)

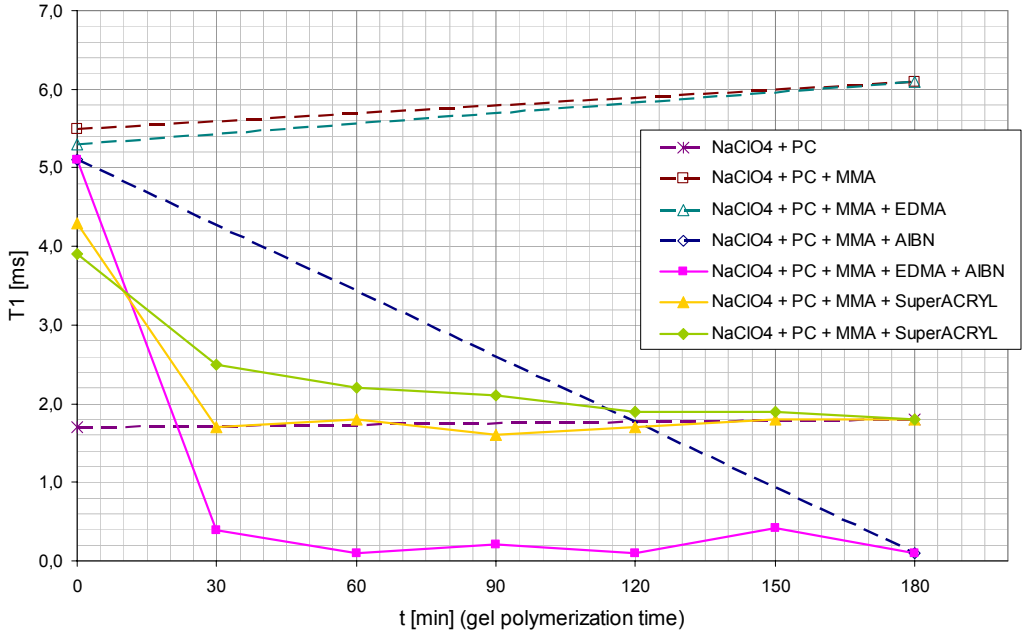

Fig. 1 *T_1 relaxation (inversion recovery) as a function of gel ageing*

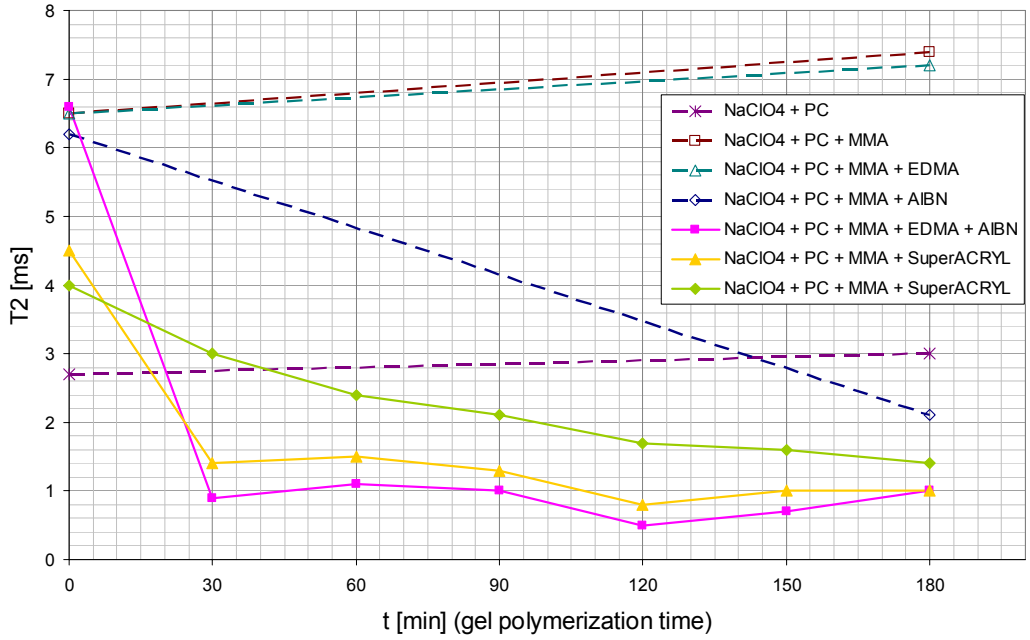

Fig. 2 *T_2 relaxation (hahn echo) as a function of gel ageing*

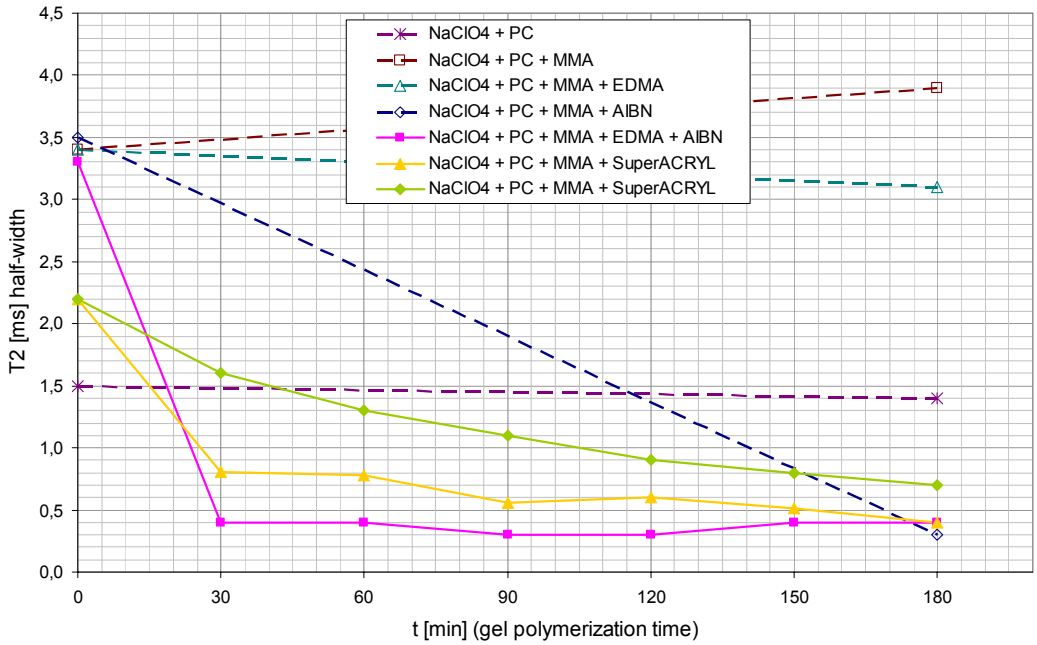

Fig. 3 *T_2 relaxation (half-width) as a function of gel ageing*

Result and discusion

Mixture of liquid MMA and PC displays significantly longer relaxation times T_1 and T_2 than clear solution of $NaClO_4$ in PC. Possibly reason is that the presence of MMA release solvatation of ions Na^+ by propylencarbonate. After beginning increase both relaxation times always decrease. This is the evidence of intensive binding of Na+ ionts to neighbouring environment. This decrease is very intesive in the case of gel polymerated by homogenous iniciator AIBN. On the other side, polymeration by heterogenous iniciator SUPERACRYL is not directed to whole repression of relaxation times. Na^+ ionts stays more mobile obviously in channels surrounding grains of polymerization activator (it is PMMA with organic peroxides on the surface). This heterogenous structure has been recently evidenced by optical observation of gel colored by methylviolet.
Due to considerable mobility of Na^+ ions is also different ion conductivity of gels prepared with AIBN and SUPERACRYL. Conductivity of AIBN gels is usually lower. It could be caused by more powerful ions binding to gel structure attended by decreasing of ion moveabily.

Acknowledgements

Academy of Sciences, Research Plan AV/0Z4030502, Ministry of Education of Czech Republic, Project MSM002130516, Grant Agency of the Academy of Sciences, Grant No. B208130604, Ministry of Environment of Czech Republic, Grant No. VaV SN/3/171/05, Czech Science Foundation, Grant No. 104/06/1471

References

1. F.M. Gray, Solid Polymer Electrolytes – Fundamentals and Technological Applications, VCH, New York, 1991.
2. T.J. Schaafsma, H. Vanas, W.D. Palstra, J.E.M. Snaar, P.A. Dejager, Magnetic Resonance Imaging 10 (5), p. 827-836, 1992.
3. H.T. Edzes, D. van Dusschoten, H. van As, MAGNETIC RESONANCE IMAGING 16 (2), p. 185-196, 1998.

APROTIC GEL POLYMER ELECTROLYTES

Jiří Vondrák[1], Marie Sedlaříková[2], Ondřej Krejza[2]

[1] Institute of Inorganic Chemistry, Academy of Sciences of the Czech Republic, Řež near Prague 25068, Czech Republic
[2] Department of Electrical and Electronic Technology, Brno University of Technology, Údolní 53, Brno 60200, Czech Republic

Corresponding author: Jiří Vondrák
E-mail: vondrakj@iic.cas.cz
Phone Number: +420 266 172 198
Fax Number: +420 220 941 502

Introduction

The systematic research of gel polymer electrolytes started in the days of 1st and 2nd Lithium Battery Meetings in Italy. The idea was rather unique – to „thicken" an aprotic solution of lithium salt with an inert polymer.
We have started this research 12 years ago approximately. Our first object was gel polymer based on MMA and Li salt in PC.
Two main methods to obtain them are the Method called casting and direct polymerization of a mixture of the monomer and aprotic salt solution. We have decided to perform the latter.
We have started with methyl methacrylate and solution of salts in PC. In essential, two methods of mentioned polymerization exist:

a) The use of industrial heterogeneous polymerization agent.
b) The use of a homogenous polymerization initiator such as ABIN and proper physical means (temperature or UV radiation).

The aim of this contribution is to describe widely the differences between two mentioned methods of polymerization.

Experimental

The industrial polymerization agent SPOFAKRYL® is a powder of PMMA (grain size 20 to 100 μm) on the surface of which is anchored the polymerization initiator on the basis of organic peroxides. The polymerization starts immediately after mixing the components and can be finished at 80 – 90°C.

Polymerization initiator ABIN (asobis isobutyro nitride) is added to the reaction mixture and the polymerization occurs on heating to the same temperature. The mixture is sufficiently fluid before the exposition to heat.

Conclusions

- Morphology: Spofakryl polymerized gels are heterogeneous and they contain small residuum of the particles, as it was shown on microphotographs.
- Electrical conductivity: The conductivity of ABIN polymerized gels is by one order of magnitude lower. In both cases. The conductivity of lithium containing electrolytes is higher than that of sodium.
- The influence of nanoparticles: Nanosized alumina quite appreciably increases the conductivity of SUPERAKRYL gels.
- Electrochemistry of redox systems: It was tested using ferrocene – ferricinium couple. This system is quasireversible. However, the diffusion coefficient is higher in SUPERAKRYL gels.
- Transference numbers: At this moment, they were investigated only on SUPERAKRYL gel. In general, smaller ions are less mobile than larger ones.
- NMR mobility: The process of polymerization can be monitored by the NMR line (^{7}LI or ^{23}Na, respectively). The polymerization by ABIN seems to be more extended. This is in accordance with lower conductivity of these gels. The comparison of Li and fluorine (in gels containing $LiBF_4$) did not reveal any essential interaction of just one ion with the gel matrix until now. This work should continue now.
- Other systems under investigation are based on monomers and solvents different from MMA and PC, and on special salts offering high transference number of Li ions. Dr. Reiter is the initiator of the latter orientation.

Acknowledgements

The investigations were supported by:
Academy of Sciences, Research Plan AV/0Z4030502,
Ministry of Education of Czech Republic, Project MSM002130516,
Grant Agency of the Academy of Sciences, Grant No. B208130604,
Czech Science Foundation, Grant No. 104/06/1471.

HETEROGENEITY OF PMMA-PC BASED GEL ELECTROLYTES

Ondřej Krejza[1], *Petr Špičák*[1], *Marie Sedlaříková*[1], *Jiří Vognar*[1], *Jiří Vondrák*[2]

[1]*Institute of Electrotechnology, Brno University of Technology, Czech Republic*
[2]*Institute of Inorganic Chemistry of the ASCR, v. v. i., Czech Republic*

Corresponding author: Ondřej Krejza
E-mail: ondrej.krejza@phd.feec.vutbr.cz
Phone: (+420-5) 41146170, Fax: (+420-5) 41146147

Introduction

Since 1997 our research team has been extensively dealing with an electrochemical research on acrylic based gel polymer electrolytes (GPEs) for several-mostly aprotic applications. Despite elevated PMMA content (58 wt%) the PMMA GPEs prepared from commercial resin SUPERACRYL® (SPOFA Dental Co., Czech Republic) (further abbreviated as MMA/SA) exhibit high ionic conductivity at RT (10^{-4} $S.cm^{-1}$) while retaining good mechanical and dimensional stability. The drawback of MMA/SA GPEs is undefined chemical composition of oligomeric precursor and its sensitivity to moisture uptake. Surprisingly, the conductivity drop upon substitution of SA by direct 2,2'-azobis(isobutyronitrile) (AIBN) polymerized MMA (further abbreviated as MMA/AIBN) was observed and will be discussed. The nature of SUPERACRYL® based samples seems to be in an agreement with a number of literature definitions of gels as submicroscopic colloidal systems [1]. The purpose of this study is to confirm previously reported [2] heterogeneous nature of MMA/SA based GPEs by optical means using methyl violet indicator.

Experimental

The two types of PMMA gels with trace elements of 2B methyl violet dye were prepared. As a charge carrier the $LiClO_4$ dissolved in propylene carbonate (PC) in 0.1 $mol.l^{-1}$ concentration was used. The two samples were thermally polymerized using either SUPERACRYL® (commercial resine based on PMMA particles covered by Dibenzoyl peroxides serving as an initiator of polymerization) or standard polymerization agent AIBN. The chemical composition in wt% of the systems was as follows: 0.33/36/42.5/21.2 ($LiClO_4$/PC/MMA/SA) for MMA/SA and 0.38/41.5/57.2/0.94 ($LiClO_4$/PC/MMA/AIBN). The membranes were cured in an oven for 90 minutes and then sliced and sandwiched in between two blocking stainless steel electrodes for conductivity check. The conductivity was derived from a Nyquist plot gathered by Potentiogalvanostat PGSTAT 12 (Eco Chemie, The Netherlands). For optical inspection the microscope OLYMPUS BX40 working in reflected light mode was used.

Results and Discussion

During preparation, the AIBN polymerized sample was virtually homogenous while the SUPERACRYL® prepared gel showed high inhomogeneity caused by PMMA particles originating from the precursor. In case of MMA/SA gels, dispersed particles of precursor are clearly visible by naked eye. After polymerization there are no precursor residues. Except the visible surface unevenity of MMA/SA sample there were no visible differences in between both membranes.

Figure 1 shows the temperature-conductivity dependence. The MMA/SA sample had overall higher conductivity values than MMA/AIBN based membrane. The apparent activation energy was estimated from linear section (0 to +70 °C) of the curves where both systems appeared to obey single reaction rate constant dependency. Visible change of slope in conductivity curve, due to polymer host solidification, occurred at -20 °C. Using simplified Arrhenius equation $Ea=-2.303.A.R$ [KJ.mol^{-1}], where A is a constant and R is a gas constant, we received $Ea_{(MMA/SA)}$ = 23.9 kJ.mol^{-1} and $Ea_{(PMMA/AIBN)}$ = 26.8 kJ.mol^{-1}. Despite the fact that MMA/AIBN gel has increased amount of solvent in a solvent/monomer (41.5/57.2) ratio in the system, which was earlier proved to be crucial for obtaining high conductivity values [3], the conductivity is lower than in case of MMA/SA.

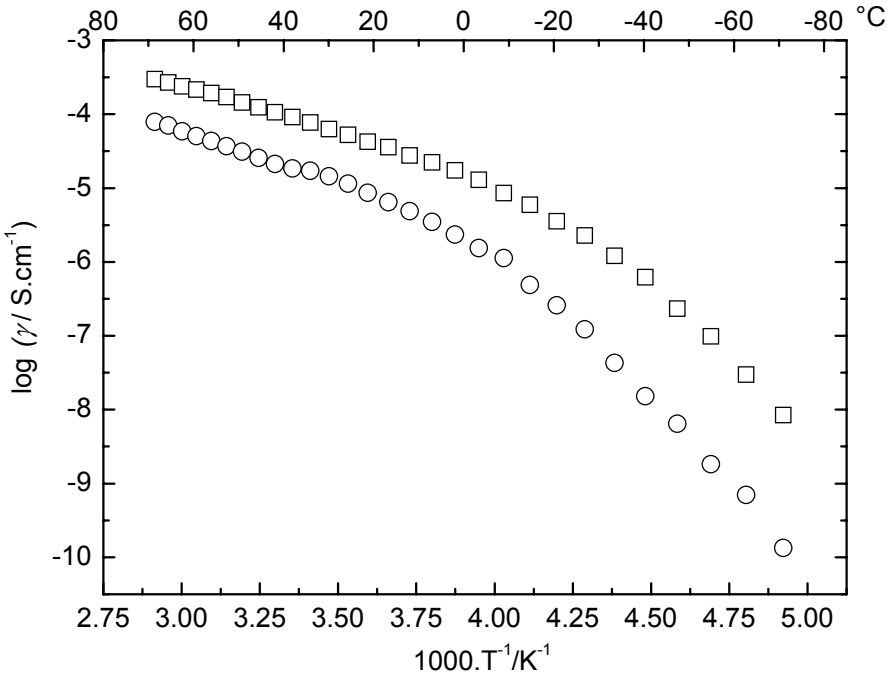

Fig. 1 *The comparison of MMA/SA (squares) and MMA/AIBN (circles) based GPEs, 0.1M $LiClO_4$ in PC (from -70 to +70 °C).*

In order to be distinguished in the bulk properties we have added 2B methyl violet (Sigma Aldrich) in very small amount into both samples. The methyl violet dye is first evenly dispersed in the blend and lately inhibited during polymerization. Prepared thin slices were checked in microscope which is indicated as an example on Fig. 2. From

Figure 2 (on the left) formation of channels with low PMMA resp. high solvent-salt concentration between solid PMMA particles (dispersed white spots) is clearly visible. On the other hand the MMA/AIBN sample showed excellent bulk homogeneity, in Fig. 2 on the right, with suppressed liquid phase on behalf of the ionic conductivity increase.

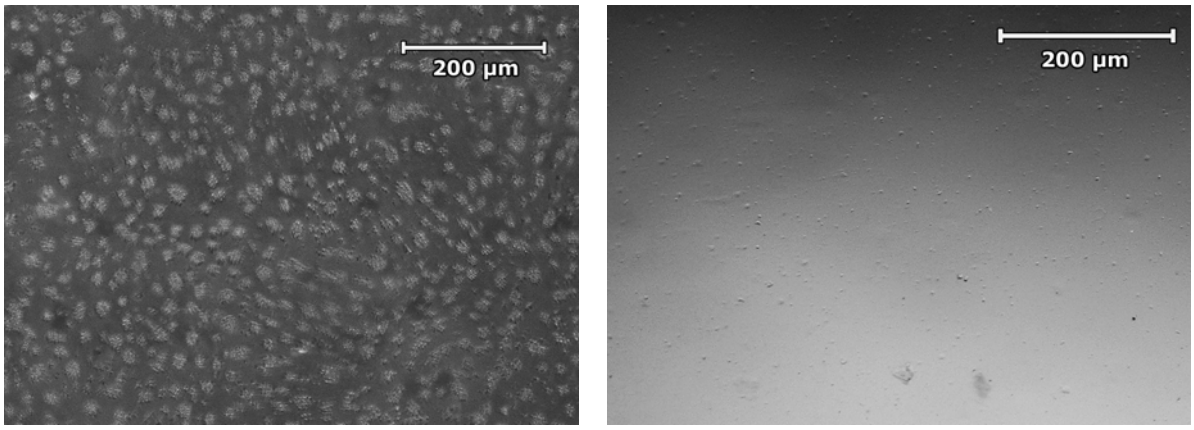

Fig. 2 *The scan of MMA/SA (left) and MMA/AIBN (right) based GPEs with a trace element of methyl violet.*

Conclusions

The gels differ in their properties in several points which indicate the benefit of gels prepared by the use of SUPERACRYL®; (a) the specific conductivity of gel is considerably higher, (b) the increase of specific conductivity by the presence of nano - Al_2O_3 in lithium gels is also higher [4] and (c) formation of channels with low PMMA concentration between solid PMMA particles must be expected in this case.
We can conclude that the positive impact on ionic conductivity of the MMA/SA based GPEs can be assigned to increased liquid phase in the system.

Acknowledgements

This work was supported by the Academy of Science of CR (No. AVOZ40320502), Ministry of Education of Czech Republic (No. MSM0021 630516), Grant Agency of Academy of Science of CR (No. B208 130 604) and by Czech Science Foundation (No. 104-06-1471).

References

1. C. J. Brinker, G. W. Scherer, Sol-Gel Science, The Physics and Chemistry of Sol-Gel Processing, Academic Press, New York, 1990 (p. 8.)
2. J.Reiter, J. Vondrák, Z. Mička, Electrochim. Acta 50 (2005) 4469-4476.
3. O. Bohnke, G. Frand, M. Rezrazi, C. Rousselot, and C. Truche, Solid State Ionics 60 (1993) 97-104.
4. O. Krejza, J. Velická, M. Sedlaříková, J. Vondrák, Journal of Power Sources 178 (2008) 774–778.

DETERMINATION OF DIFFERENCE OF T_2 RELAXATION TIME MEASUREMENT WITH PMMA BASED GEL ELECTROLYTES

J. Vognar[1], M. Macalík, P. Špičák, K. Bartušek[3], V. Novák[1], J. Vondrák[2]

[1] Department of Electrotechnology FEEC BUT, Údolní 53, 602 00 Brno, CZE
[2] Institute of Inorganic Chemistry of the ASCR, v.v.i.,250 68 Řež, CZE
[3] Institute of Scientific Instruments of the ASCR, v.v.i., Královopolská 147, 612 64 Brno, CZE

Corresponding author: J. Vognar
E-mail: jirikv@email.cz

Introduction

T2 relaxation is a complex phenomenon, but at its most fundamental level, it corresponds to a decoherence of the transverse nuclear spin magnetization. Random fluctuations of the local magnetic field lead to random variations in the instantaneous NMR precession frequency of different spins. As a result, the initial phase coherence of the nuclear spins is lost, until eventually the phases are disordered and there is no net xy magnetization. Because T2 relaxation involves only the phases of other nuclear spins it is often called "spin-spin" relaxation.T2 values are generally much less dependent on field strength, B, than T1 values.

In present paper T_2 relaxation times were measured using PMMA based aprotic gel electrolytes with $NaClO_4$ conducting agent. T_2 was measured by detecting direct FID signal after HF pulse and by hahn echo method. This work submitted measured differences of T_2 and discussed accuracy of T_2 determination.

Experimental

The relaxation time T_2 of ^{23}Na nuclei in the gel electrolytes and their changes during the gel ageing were experimentally measured. The relaxation time T_2 was measured by two methods: Hanh echo and by determination half-width of spectral line from FID signal.
T_2 values of Hanh echo reported in this work were calculated by fitting a series of single Hahn echoes to exponential decay function of the type

$$S(T_E)=A \exp(-T_E/T_2), \quad (1)$$

where $S(T_E)$ is the signal intensity at echo time T_E, T_E is echo time, A is the signal amplitude at a T_E of zero, T_2 is calculated T_2 (hahn echo) relaxation time (Fig. 3).
T_2 determinated from half-width is according to

$$T_2 = \frac{1}{\pi \cdot \Delta \nu}, \quad (2)$$

where $\Delta\upsilon$ is the half-width of the spectral line measured.

Two types of gel were prepared. Base of each one was 1M solution of $NaClO_4$ in PC (4ml of basic solution, sample 2). To this solution has been added:

1.type: 6ml of liquid monomer MMA (99%), 40ul of netting agent EDMA a 100mg of polymerization agent AIBN (samples 3-6).
2.type: 2,8g industrial polymerization agent SUPERACRYL® (Spofadental, Czech Republic) (sample 7 and 8).

Volume of each sample was about 10 ml. Sample 1 was measured in time 0 minutes only. The samples 2-7 were heated on 80°C (polymerization temperature), sample 8 was polymerized in room temperature and they were polymerized for 3 hours. Sample compositions and measuring ageing time step are displayed in Table 1.,

The measurement was done on MR tomography with resonance frequency 200MHz and basic magnetic B_0 = 4,7T in Institute of Scientific Instruments of the ASCR, v.v.i.

Table 1 *Marking of samples, their composition, measuring time step nad thermic option*

Sample	Composition	Time (min)	Thermic option
1	H_2O + 10% wt. NaCl	0	not heated (23°C)
2	$NaClO_4$ + PC	0, 180	heated (80 °C)
3	$NaClO_4$ + PC + MMA	0, 180	heated (80 °C)
4	$NaClO_4$ + PC + MMA + EDMA	0, 180	heated (80 °C)
5	$NaClO_4$ + PC + MMA + AIBN	0, 180	heated (80 °C)
6	$NaClO_4$ + PC + MMA + EDMA + AIBN	0, 30, 60, 90, 120, 150, 180	heated (80 °C)
7	$NaClO_4$ + PC + SUPERACRYL®	0, 30, 60, 90, 120, 150, 180	heated (80 °C)
8	$NaClO_4$ + PC + SUPERACRYL®	0, 30, 60, 90, 120, 150, 180	not heated (23°C)

Low noise measurement

As vivid example sample no. 3 was examinated. No iniciaor of polymerization (AIBN) has been added to this sample, so as expected, NMR response didn't change through polymerization time (no polymerization occured). Signal was strong, so no filtration of noise had to be used. T_2 relaxation times are described in Tab 2. T_2(0,5) and T_2(0,38) were obtained from time domain of FID signal at 0,5 and 0,38 value of the peak (Fig. 1). Then time domain has been converted to frequency domain and using equation (1) T_2 (half-width) was determinated (Fig. 2). T_2 (hanh echo) was obtained by measuring hanh echo of NMR signal (Fig. 3).

Table 2 *T_2 relaxation times measured by FID and hahn echo at different polymerization time*

Sample 3	t [min]	
Method [ms]	0	180
T2(0,5)	4,2	4,9
T2(0,38)	5,9	6,7
T2(half-width)	3,4	3,9
T2(hanh echo)	6,5	7,4
T1 (inversion recovery)	5,5	6,1

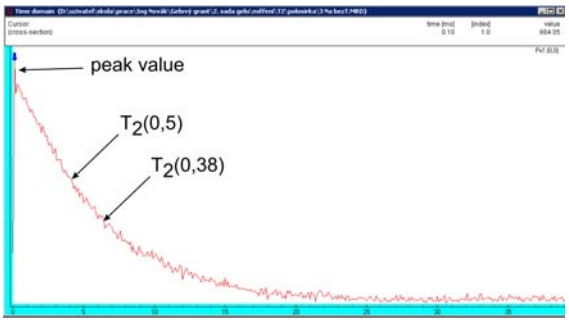

Fig. 1 *FID signal (time domain) for sample no.3 with determination of $T_2(0,5)$ and $T_2(0,38)$*

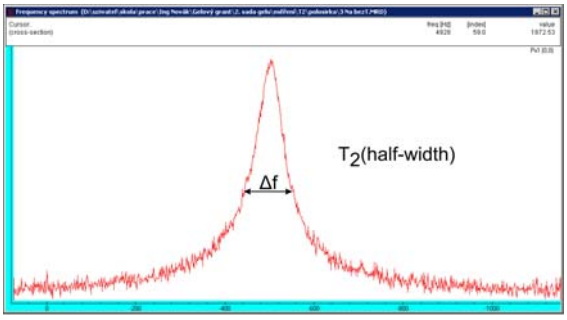

Fig. 2 *FID signal (frequency domain) with detemination T_2 (half-width)*

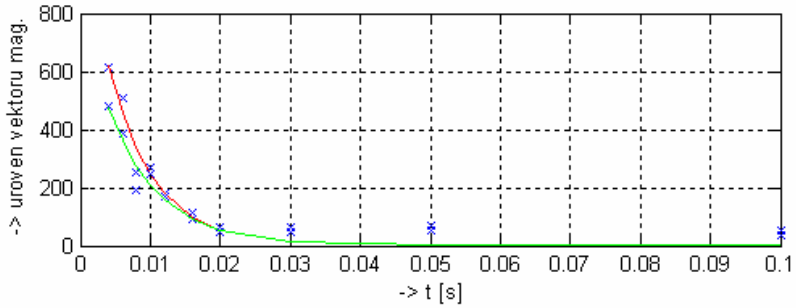

Fig. 3 *Matlab analysis of hanh echo data, T_2(hanh echo) detrminated from exp function (1). Red line - 0 minutes, green line - 180 minutes.*

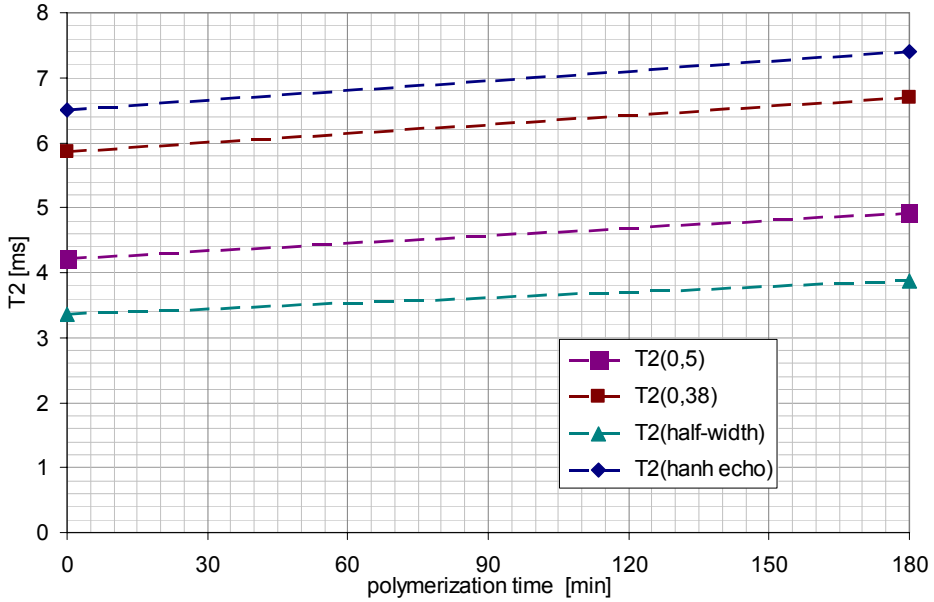

Fig. 4 *T_2 relaxation times obtained by different methods (T_2 (0,5), T_2(0,38), T_2(half-width) from FID signal; T_2(hahn echo) from hahn echo)*

Result and discusion

T_2 relaxation time has been measurent by different methods.
First method was direct FID signal after HF pulse is used for determination of T_2 from time domain of FID signal (0,5 or 0,38 value of peak maximum - Fig.1) and from frequency domain (half-width - Fig.2). Pulse sequence is ussually writen as $\pi/2$ - *AQ* (Fig. 5). This type of measurement is used for short T_2 response, because there is no

time delay between HF pulse and readout. Disadvantage of this method is influence of inhomogenity of magnetic field ΔB_0. From theory the value T_2 (0,38) obatined from time domain should be almost the same as value T_2 (half-width) obtained from frequency domain. Our measurements show that more acurate to T_2 (half-width) is value T_2 (0,5).

Otherwise, the second method, Hahn echo response is not so influenced by inhomogenity of magnetic field. But for shorter T_2 response do not acurately describes real T_2, because of τ delay (Fig 6,7).

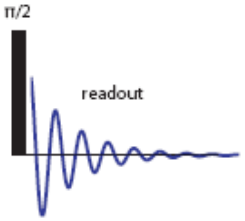

Fig. 5 *Signal sequence for direct FID signal after HF pulse*

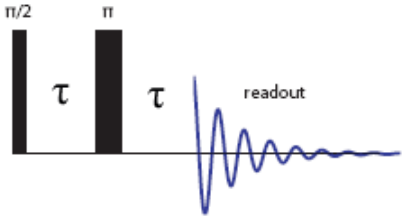

Fig. 6 *Signal sequence for Hahn echo signal*

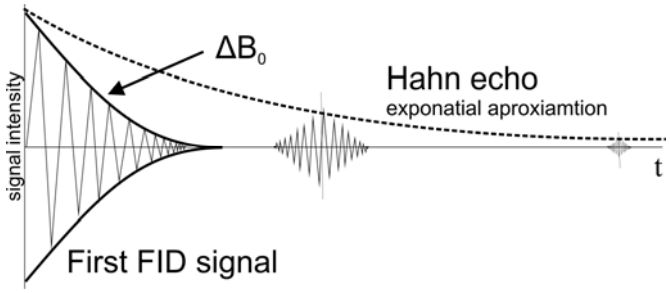

Fig. 7 *Difference between T_2 obtaining*

Values obtained by T_2(0,38) are closest to T_2(hahn echo). T_2 obtain by Hahn echo is greater T_1 by inversion recovery. From theory T_2 value should be considably lower than T_2 for solid materials and lower or equal for liquid solutions. Because of iregularities of both used methods, the value T_2(0,5) could be potencial result of T_2 measurement.

Acknowledgements

Academy of Sciences, Research Plan AV/0Z4030502, Ministry of Education of Czech Republic, Project MSM002130516, Grant Agency of the Academy of Sciences, Grant No. B208130604, Ministry of Environment of Czech Republic, Grant No. VaV SN/3/171/05, Czech Science Foundation, Grant No. 104/06/1471

References

1. F.M. Gray, Solid Polymer Electrolytes – Fundamentals and Technological Applications, VCH, New York, 1991.
2. T.J. Schaafsma, H. Vanas, W.D. Palstra, J.E.M. Snaar, P.A. Dejager, Magnetic Resonance Imaging 10 (5), p. 827-836, 1992.
3. H.T. Edzes, D. van Dusschoten, H. van As, MAGNETIC RESONANCE IMAGING 16 (2), p. 185-196, 1998.

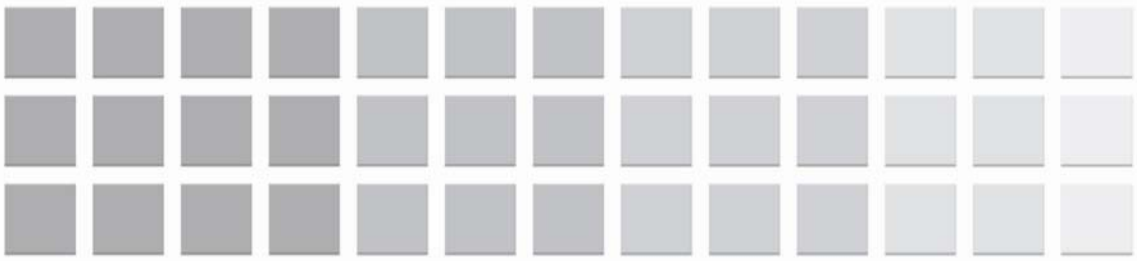

9th ABA

BRNO 2008

Advanced Batteries and Accumulators

Fuel Cells

MOLYBDENUM OXIDE–CARBON NANOTUBES NANOCOMPOSITES FOR FUEL CELL OXYGEN ELECTRODE

M.O. Danilov[1], N.D. Ivanova[1], A.V. Melezhyk[2], E.I. Boldyrev[1], O.A. Stadnik[1]

[1)]Institute of General and Inorganic Chemistry of the Ukrainian National Academy of Sciences, prospekt Palladina 32/34, Kyiv 142, Ukraine
[2)]TM Spetsmash Ltd., vul. Viskoznaya 5, build. 23, 02660, Kyiv, Ukraine. E-mail: nanocarbon@rambler.ru

Corresponding author: Danilov M.O.
E-mail: danilovmickle@rambler.ru

Introduction

Carbon nanomaterials, particularly carbon nanotubes (CNT), can be used as supports for catalysts. Electrode materials containing catalytically active particles supported on CNT often exhibit higher specific electrochemical characteristics compared to the same catalysts and CNT separately due to effect of synergism. This effect arises from interaction of catalyst particles with nanocarbon structures.

In this work we have prepared and studied nanocomposite electrode materials based on molybdenum oxide supported on CNT.

Multiwalled carbon nanotubes were prepared by CVD method with use of ethylene as source of carbon [1]. Outer diameter of nanotubes was nearly 10-30 nm, specific surface was 230 m^2 g^{-1}. Mineral impurities (rests of catalyst) were removed from nanotubes by treatment with a hydrofluoric acid solution.

CNTs have high electrical conductivity and surface area. Aggregates of CNT form conductive mesoporous structures with large specific pore volume. These factors are favorable for creating electrode materials containing supported catalysts. Due to tubular structure it is possible to expand the oxygen-electrode-electrolyte ternary contact zone where generation of current takes place. This allows increasing of working current density.

Results and discussion

In this work molybdenum oxides were studied as catalysts for electrochemical reduction of oxygen. MoO_x/CNT nanocomposites were prepared by electrochemical deposition of molybdenum oxides on CNT [2]. Mass content of molybdenum in composites was determined by spectral analysis and amounted 0.2%, 3.5%, and 4.5%. Valency of molybdenum was estimated with using XPS method. One definite peak at 231.8 eV was

observed which corresponds to oxide compound of molybdenum with Mo oxidation level +5.

Gas-diffusion electrodes made of these composites were investigated as oxygen electrodes in model fuel cell with alkaline electrolyte (6M KOH). All potentials were measured relatively to standard hydrogen electrode. Electrode potential vs current density plots are shown in Figure. As is seen, electrode materials can be arranged by decrease of activity in the order: (0.2 wt% Mo) > (3.5% Mo) > (4.5% Mo). Such behavior of electrochemical parameters probably is caused by increasing dispersion of MoO_x with decreasing mass content of it. This conclusion was proved by electron images of MoO_x/CNT nanocomposites.

Electrode containing 0.2 wt% Mo has the best parameters. This electrode gives current density nearly 400 mA/cm^2 at polarization of 200 mV. Such parameters are comparable with electrodes containing platinum catalyst.

Thus, nanocomposites containing molybdenum oxides supported on CNTs are promising catalysts for fuel cell oxygen electrodes. These materials can replace expensive platinum containing catalysts.

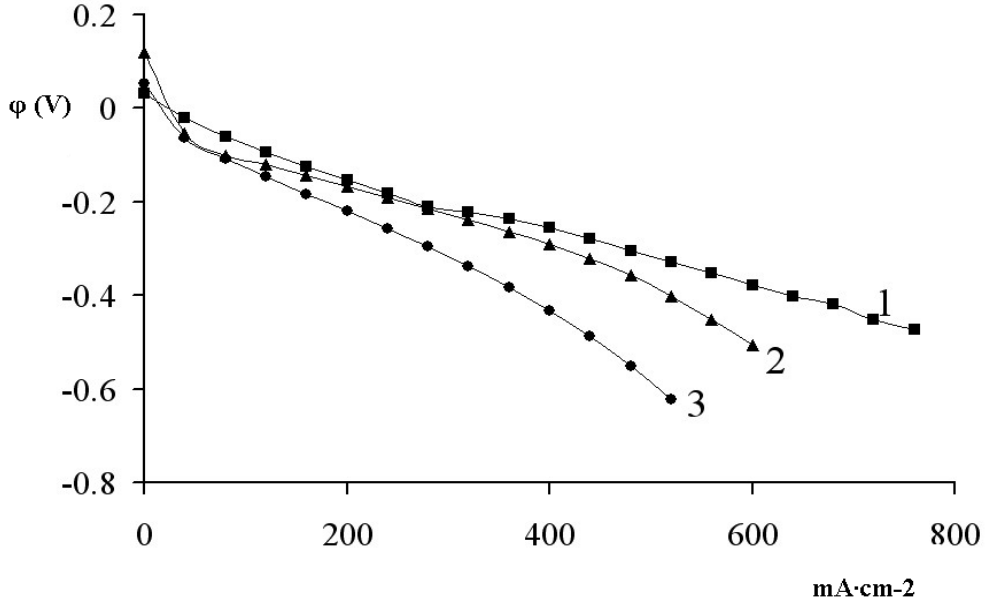

Fig. 1 *Electrode potential vs current density plots for electrodes containing different amounts of MoO_x (wt%) supported on CNT:1 – 0.2%, 2 – 3.5%, 3 – 4.5%.*

References

1. A.V. Melezhyk, Yu.I. Sementsov, V.V. Yanchenko, J. of Applied Chem. (Russian), 2005, v. 78, No 6, p. 938-944.
2. N.D. Ivanova, S.V. Ivanov, Russian Chemical Reviews, 1993, v. 62, No 10, p. 907-918.

COMPLEXES OF 3D METALS WITH HEXAMETHYLENEDIAMINETETRAACETATE AS PRECURSORS FOR OXYGEN REDUCTION ELECTROCATALYSTS

A.V. Berezovska, Yu.K. Pirsky, V.S. Kublanovsky

V.I. Vernadsky Institute of General and Inorganic Chemistry,
Ukrainian National Academy of Sciences
prosp. Palladina 32/34, Kiev 142, 03068, Ukraine

Corresponding author: Yu.K. Pirsky
E-mail: pirsky@ionc.kar.net
Phone: +380 (44) 424 33 11
Fax: +380 (44) 424 30 70

Introduction

In electrochemical power sources, fuel cells and sensors, platinum metals or pyropolymers of N_4 complexes applied to carbon supports are usually used as oxygen reduction electrocatalysts [1]. However, although they possess stable and good electrocatalytic characteristics, their cost is rather high for practical application. As was shown earlier [2-4], it is possible in principle to replace electrocatalysts based on noble metals and pyropolymers of N_4 complexes by cheaper and more readily available organometallic complexes or their pyrolysis products possessing good characteristics.

Of special interest is the development of novel highly efficient oxygen reduction electrocatalysts based on homo- or heteropolynuclear complexes. In such complexes there are several metal atoms, which form a bond to ligand through nitrogen and oxygen atoms, which facilitates in heat treatment the formation of spinels or oxides of nonstoichiometric composition in the form of catalytically active centres of oxygen reduction reaction [3-5]. Therefore, the aim of the present work was to investigate electrocatalysts based on homobinuclear and heteropolynuclear complexes of 3d metals with hexamethylenediaminetetraacetate (HDTA) and to determine the effect of the above ligand and metal ion on the activity of the catalysts synthesized.

Experimental

To synthesize complexes as precursors of electrocatalysts, hexamethylenediaminetetraacetic acid was used, which is an analog of ethylenediaminetetraacetic acid and is distinguished from the lather by longer

hydrocarbon chain, which consists of six methyl groups. In such complexes, the central atoms are far apart and are not bonded to one another.

Homobinuclear complexes were prepared by interaction between aqueous solutions of appropriate metal salts and HDTA at the ratio M:HDTA = 2:1, where M= Cr^{3+}, Mn^{2+}, Fe^{2+}, Co^{2+}, Ni^{2+}, Cu^{2+}, Zn^{2+}, and heteropolynuclear complexes at the ratios Co^{2+}:Ni^{2+}:HDTA as 2:1:2, 1:1:1 and 1:2:2. Electrocatalysts were prepared as follows: calculating on the ratio of metal to SIT-1 carbon 1:10, complexes were adsorbed onto the carbon surface from aqueous solutions of salts of appropriate metal ions with HDTA, at 50°C. After that, they were dried at room temperature in air for a day. Then a weighed amount of ~200 mg of carbon with adsorbed complex was placed in a tubular quartz reactor, through which argon was passed, heated gradually to the required temperature, held for an hour, and the temperature was lowered to the room temperature. Samples were heat-treated at 200–800°C with a step of 200°C.

Electrochemical characteristics were derived from stationary polarization curves of oxygen electroreduction, taken at a floating gas-diffusion electrode [6] in 1M KOH and air atmosphere at 20°C in a three-electrode electrolytic cell with separated cathode and anode chambers. The floating gas-diffusion electrode was prepared and catalyst was applied in the same way as in Ref [4]. The stationary polarization curves were taken under potentiostatic conditions by points on a PI-50-1.1 potentiostat with a step of 10 mV. Current variation was measured with an M 2020 milliammeter.

Results and Discussion

The dependence of oxygen electroreduction rate on pyrolysis temperature for homobinuclear complexes is shown in Fig 1.

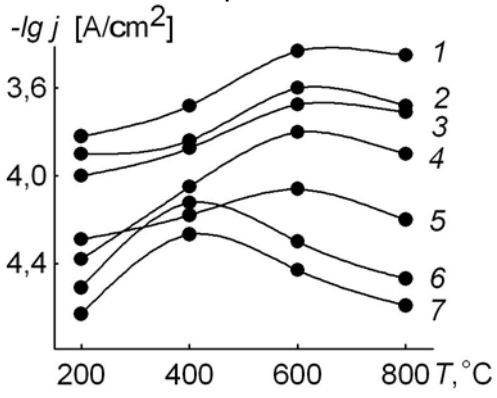

Table 3 *Dependence of the activity of oxygen reduction electrocatalysts on pyrolysis temperature, where 1 –Co^{2+}, 2 – Cu^{2+}, 3 – Fe^{2+}, 4 – Mn^{2+}, 5 – Zn^{2+}, 6 – Ni^{2+}, 7 – Cr^{3+}.*

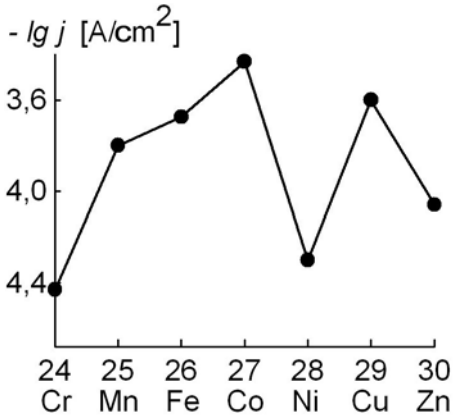

Fig. 2 *The activity of oxygen reduction electrocatalysts based on homobinuclear complexes with HDTA as a function of the atomic number of transition metal.*

As is seen from Fig. 1, when the temperature increases for the complexes containing Co^{2+}, Cu^{2+}, Fe^{2+}, Mn^{2+}, Zn^{2+}, the electroreduction rate increases, and the optimum pyrolysis temperature is 600°C. The same follows from the kinetic characteristics of oxygen reduction reaction, which were obtain on catalysts; the largest exchange current

magnitudes are observed at a pyrolysis temperature of 600°C, which may be due to the formation of the maximum number of active centres.

For complexes with HDTA containing Ni^{2+} and Cr^{3+}, the highest characteristics were obtained at 400°C. As the temperature rises the activity of the catalysts based on complexes with Ni^{2+} and Cr^{3+} decreases toward the time of reaching 800°C, which may be due to breakdown of active centres and formation of inactive structures. The kinetic slopes of stationary curves are in the ranges b_1=54-68 mV, b_2=100-128 mV, and the exchange currents for electrocatalysts are in the range $2{,}30 \cdot 10^{-7}$ to $7{,}01 \cdot 10^{-6}$ A/cm^2, which corresponds to the oxygen reduction process with slowed-down attachment of the first electron.

Fig. 2 shows the dependence of catalyst activity on the position of transition metal in the periodic table. From the figure follows a dependence according to which the activity of catalysts increases in going from even number of 3d metal to odd number, and the nanostructures containing the metals in which the 4s and 3d electron shells are filled with more than half of the possible number of electrons but are not filled full, are most active. There data are in good agreement with the Boreskov law for 3d transition metal oxides [7], which may indirectly corroborate the fact that in our case, too, oxide structures are probably formed on the carbon support surface.

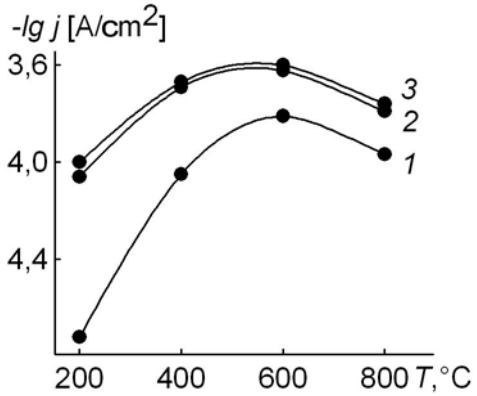

Fig. 3 *Dependence of the rate of oxygen electroreduction on catalysts with different ratio of Co^{2+}, Ni^{2+} and HDTA on pyrolysis temperature at the potential E =-0,15 V in 1M KOH at 20°C. Catalysts: 1- {Co^{2+}:Ni^{2+}:HDTA=2:1:2}, 2- {Co^{2+}:Ni^{2+}:HDTA=1:1:1}, 3- {Co^{2+}:Ni^{2+}:HDTA=1:2:2}.*

Figure 3 shows the dependence of oxygen electroreduction rate on the synthesis temperature of electrocatalysts based on heteropolynuclear complexes of cobalt (II) and nickel (II) with HDTA. It is seen from the figure that the ratio of cobalt (II) to nickel (II) and HDTA in heteropolynuclear complexes for the preparation of the most active oxygen electroreduction catalysts at a pyrolysis temperature of 600°C is 2:1:2. At this ratio, a high current output and largest exchange current magnitudes are observed. The kinetic slopes of stationary polarization curves for all catalysts are in the ranges: b_1 = 50 – 65 mV, b_2 = 100 – 120 mV.

Conclusions

Thus, the following conclusions can be drawn from the investigations carried out:

For homobinuclear complexes, the catalysts prepared on the basis of complexes of Co^{2+}, Cu^{2+}, Fe^{2+}, Mn^{2+} with HDTA at 600°C have the best characteristics;
The electrocatalytic activity of the catalysts obtained by the pyrolysis of homobinuclear complexes of 3d metal with HDTA depending on the central atom obeys the Boreskov law and is in the order:

$$Co > Cu > Fe > Mn > Zn > Ni > Cr;$$

Increasing the cobalt content of catalyst based on heteropolynuclear complexes with different Co^{2+}:Ni^{2+}:HDTA ratio improves their electrocatalytic properties, and the optimal ratio for the preparation of active catalysts in the oxygen reduction reaction is 2:1:2.

References

1. M.R. Tarasevich, K.A. Radyushkina, G.V. Zhutaeva: Russian Journal of Electrochemistry 11 (2004) 1174.
2. Yu.K. Pirskii, V.S. Kublanovskii, D.V. Shevchenko, V.N. Kokozei: Russian Journal of Applied Chemistry 12 (2006) 1964.
3. Yu.K. Pirsky, V.S. Kublanovsky, V.A. Potaskalov, A.A Andriiko: Dopovidi NAN Ukrayiny 11 (2006) 152.
4. Yu.K. Pirsky, A.V. Berezovska, Ye.A Shulzhenko, V.S. Kublanovsky: Voprosy Khimii i Khimicheskoi Tekhnologii 1 (2007) 141.
5. V.S. Kublanovskii, Yu.K. Pirskii: Russian Journal of Applied Chemistry 7 (2001) 1116.
6. G.V. Shteinberg, I.A. Kukushkina, V.S. Bagotskii, M.R. Tarasevich: Electrokhimiya 4 (1979) 527.
7. G.V. Boreskov: Catalysis.Problems of Theory and Practice (in Russian) Nauka, Moscow 1987, page 536.

MODIFICATION OF CARBON BY PYROLYSIS PRODUCTS OF HETEROBIMETALLIC MN^{II}/M^{II} AND ZN^{II}/M^{II} COMPLEXES (M=CU,NI) FOR THE ELECTROREDUCTION OF OXYGEN

Yu.K. Pirsky, V.S. Kublanovsky

V.I. Vernadsky Institute of General and Inorganic Chemistry, Ukrainian NAS, prosp. Palladina 32/34, Kiev 142, 03068, Ukraine

Corresponding author: Yu.K. Pirsky
E-mail: pirsky@ionc.kar.net Phone: +380 (44) 424 33 11, Fax: +380 (44) 424 30 70

Introduction

Carbon materials have been used many years in the chemical industry to manufacture electrodes for electrochemical power sources. The physicochemical properties, electronic structure and extended surface of activated carbons indicate them to have promise in electrocatalysis as matrices-support for various classes of compounds (metals, oxides and complex compounds, enzymes, etc) and in the development of efficient electrocatalysts [1]. The manufacture and use of electrocatalysts for fuel cells and electrochemical power sources are directly limited by their cost and electrochemical characteristics. Catalysts based on complexes of d metals with phtalocyanines and porphyrins [2, 3] (N_4 complexes) for the electroreduction of oxygen are well known, but their cost is high and comparable with that of platinum metals. Using heterobimetallic complexes containing ligands coordinated to the central atom through nitrogen atoms, it is possible to imitate pyropolymers produced by pyrolysis from N_4 complexes and to approach them in electroactivity. Such catalysts will require lower production costs in comparison with the known porphyrin and phthalocyanine complexes of d metals or platinum.

Experimental

In the works on using heterometallic compounds to obtain oxygen reduction electrocatalysts [4], the following complexes were taken as precursors: $Cu(L)MnCl_4$ (1), $Ni(L)MnCl_4$ (2), $Cu(L)ZnCl_4$ (3), $Ni(L)ZnCl_4$ (4), (L = 4,6,6-trimethyl-1,9-diamino-3,7-diazanone-3-ene), which were prepared by direct template synthesis [5].

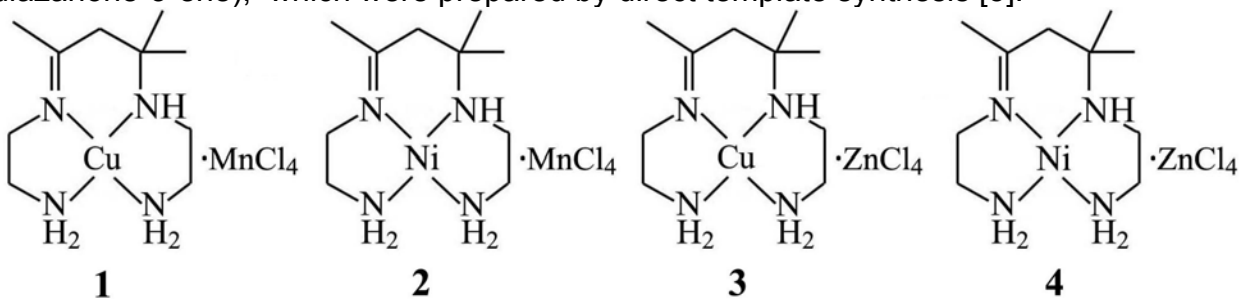

The electrocatalysts were prepared as follows: heterobimetallic complexes were dissolved in dimethyl formamide and adsorbed on a high-porosity carbon matrix (SIT-1) of under 50 μm fineness with a specific surface of 1050 m^2/g (according to BET). Then after drying, the carbon matrices obtained with complex compounds applied to them were heat-treated at different temperatures (200-800 °C) with a step of 200 °C in an argon atmosphere. To this end, a weighed 100 mg amount of SIT-1 carbon with a complex applied to it was permanently passed, and heated gradually to the required temperature, held for one hour, and then the temperature was lowered to room temperature. The electrocatalysts obtained in this way were tested for catalytic activity in oxygen electroreduction reaction by means of a floating gas-diffusion electrode [6] at 20 °C in a three-electrode electrolytic cell with separated cathode and anode chambers in 1M KOH solution. The reference electrode was a silver-chloride electrode. The polarization curves were taken under potentiostatic conditions on a PI – 50 – 1.1 potentiostat with a step of 10 mV; current was measured with an M2020 milliammeter. The floating gas-diffusion electrode was a structure in the form of a pellet of 0.95 g/cm^3 specific density, 10mm in diameter and 2 mm in thickness, made of 300 mg of acetylene black hydrophobized with 30% polytetrafluoroethylene; the pellet was pressed under a pressure of 50-70 kgf/cm^2, and a nickel-wire current tap was embedded in it. A layer of the electrocatalyst under investigation (~1 mg/cm^2) with a particle size of under 20 μm was applied to the electrode surface and pressed under a pressure of 50-60 kgf/cm^2. This amount of electrocatalyst ensured the kinetic conditions of the reaction [7]. The catalyst was held on the conducting porous substrate by adhesion forces. The amount of the catalytically active material under investigation was determined from the difference in the weight of the substrate before and after pressing powder.
The pyrolysis of the complexes was studied by thermal analysis in a range of 20–900°C in an argon atmosphere on a Paulik-Paulik-Erdey Q-1500 D MOM derivatograph (Budapest) (weighed amount ~ 140 мг, TG = 500, heating rate 10 $°C \cdot min^{-1}$, standart – as-calcined Al_2O_3), and by thermal desorption with mass spectroscopic analysis of desorbed species in a temperature range of 20–800 °C at a heating rate of 10 $°C \cdot min^{-1}$ (MX-1302M mass spectrometer, vacuum 10^{-6} Pa; weighed amount of complexes ~ 1 mg).

Results and Discussion

Thermogravimetric investigations reveal some regularities. Complexes 2 and 4 containing nickel are thermally more stable; their decomposition begins at 130°C. The final pyrolysis products of there complexes contain the following mixtures: metallic nickel – manganese chloride for complex 2, metallic nickel – zinc chloride for complex 4.

Complexes 1 and 3 containing copper are less stable. Their decomposition begins at 100 °C, but the final pyrolysis products contain, unlike complexes with nickel, compounds of copper with nitrogen and carbon, as well as manganese chloride for complex 1 and zinc chloride for complex 3. Pyrolysis products containing a metal, nitrogen and carbon were obtained in Refs [8, 9] as highly efficient electrocatalysts, and their high activity in the oxygen reduction reaction was shown.

For complex 1 containing copper and manganese, escape of HCl during pyrolysis is observed. Complex 2 containing nickel and manganese decomposes with escape of both molecular chlorine and HCl, and the decomposition of complexes 3 and 4 containing zinc involves escape only of chlorine and small amounts of chlorine – containing species.

The activity of the catalysts obtained was assessed by the value of the observed oxygen reduction current at the potential of -0.10 V and by slopes of $\partial E/\partial \lg j$ polarization curve (b_1; b_2). Plots of oxygen electroreduction rate against electrocatalyst synthesis temperature are shown in Fig. 1, from which it is seen that the catalysts obtained from complexes 2 and 4 have a lower activity in the oxygen electroreduction reaction.

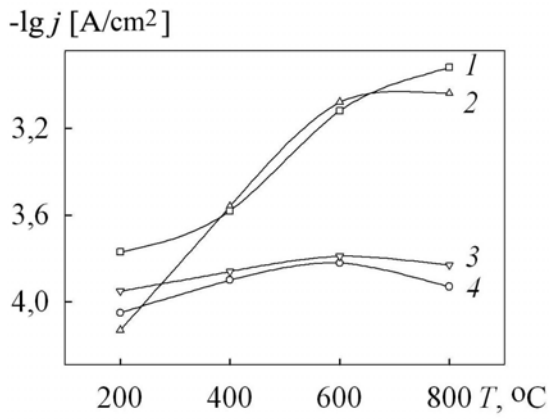

Fig. 1 *Plots of the rate of oxygen electroreduction in 1M KOH solution at 20 °C (E = -0,1 V) against pyrolysis temperature on catalysts obtained from complexes 1 – (1), 2 – (2), 3 – (3), 4 – (4).*

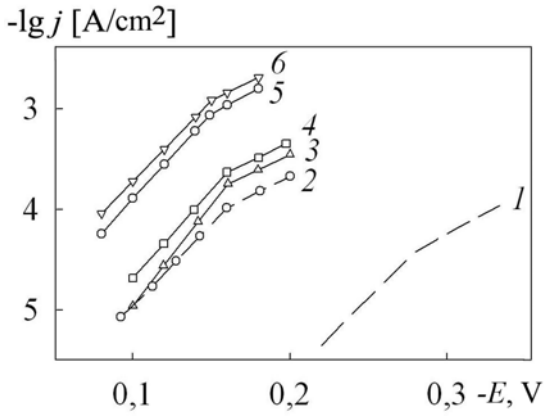

Fig. 2 *Potentiostatic polarization curves of oxygen electroreduction measured in 1M KOH solution at 20 °C on a hydrophobized carbon black substrate -(1), SIT-1 -(2) and for electrocatalysts prepared at 800 °C: {4 + (SIT-1)}– (3), {2 + (SIT -1)}– (4), {3 + (SIT -1)}– (5), {1 + (SIT -1)}– (6).*

This may be attributed to the formation of catalytically inactive nickel in pyrolysis products of there complexes. Unlike complexes 2 and 4, complexes 1 and 3 form during pyrolysis products containing organometallic fragments linked to the carbon surface, which ensures their high activity in the electroreduction of oxygen.

Electrocatalysts obtained at 700-800 °C for complexes with copper have the highest oxygen reduction current at -0.10V. The exchange current densities j_0 and slopes of stationary polarization curves (b_1, b_2) for them are: $j_0 = 5{,}9\cdot10^{-6}$ A·cm^{-2}, $b_1 = 0{,}063$ V, $b_2 = 0{,}118$ V (complex 1), $j_0 = 4{,}4\cdot10^{-6}$ A·cm^{-2}, $b_1 = 0{,}060$ V, $b_2 = 0{,}098$ V (complex 3), $j_0 = 5{,}5\cdot10^{-7}$ A·cm^{-2} , $b_1 = 0{,}063$ V, $b_2 = 0{,}120$ V (complex 2) и $3{,}2\cdot10^{-7}$ A·cm^{-2} , $b_1 = 0{,}047$ V, $b_2 = 0{,}118$ V (complex 4).

It is known that the electrocatalysts obtained from porphyrin and phtalocyanine N_4 complexes at 800°C form active centers chemically bonded to the carbon support in organometallic fragments of pyrolyzed complexes [2, 3, 10]. In our case, the temperature range 700-800°C is also optimal for the preparation of the most active catalysts from

complexes 1 and 3, which can form, on decomposition on the carbon support, pyrolysis products linked to its surface.

Stationary polarization curves of oxygen reduction for catalysts obtained at 800°C in an argon atmosphere are shown in Fig. 2, from which it is seen that the change in the stationary potential of electrocatalysts relative to the substrate is above 0.15 V. The shift of polarization curves towards positive potentials in comparison with SIT-1 carbon was 0.08 V (complex 1), 0.07 V (complex 3), 0,02 V (complex 2) and 0,01 V (complex 4), and the slopes of $\partial E/\partial \lg j$ curve are analogous to those for SIT-1 activated carbon, indicating a similar oxygen electroreduction mechanism. Basing on the values of slopes, it may be assumed that the electroreduction of oxygen proceeds by a one – electron mechanism with slowed-down attachment of the first electron via the hydrogen peroxide formation stage, which is typical of activated carbons [1].

Conclusions

Thus, the electrocatalysts obtained by the thermal destruction of heterobimetallic complexes in an argon atmosphere at 700-800 °C have the highest activity. Their activity is higher when complexes with copper are used, and in the case of the same metals, e.g. with copper or nickel, the catalysts obtained with manganese are more active than those with zinc.
The catalytic activity of the oxygen reduction catalysts synthesized depends on the nature of metals and decreases in the order of heterobimetallic complexes:

{Cu-Mn} > {Cu-Zn} > {Ni-Mn} > {Ni-Zn}

References

1. M.R. Tarasevich: *Electrochemistry of Casbon Materials (in Russian),* Nauka, Moscow 1984, 253 p.
2. M. R. Tarasevich; K. A. Radyushkina; G. V. Zhutaeva: Russian Journal of Electrochemistry 11 (2004) 1174.
3. M. R. Tarasevich; K. A. Radyushkina; V.A. Bogdanovskaya: *Electrochemistry of Porphyrins (in Russian)*, Nauka, Moscow 1991, 312 p.
4. Yu. K. Pirskii: Visnyk Kharkivskoho Universytetu, 648 (2005) 55.
5. Shevchenko D.V., Petrusenko S.R., Kokozay V.N., Skelton B.W: J. Coord. Chem., -. 57 (2004) 1287.
6. G.V. Shteinberg, I.A. Kukushkina, V.S. Bagotskii, M.R. Tarasevich: Electrokhimiya 4 (1979) 527.
7. Yu.A. Shizmandzhev, V.S. Markin, M. R. Tarasevich, Yu.G. Chirkov: *Makrokinetics of Processes in Porous Media (in Russian)*, Nauka, Moscow 1971, 364 p.
8. Jaouen F., Dodelet J-P.: Electrochimica Acta 52 (2007) 5975.
9. Liu G., Zhang H.M., Wang M.R., Zhong H.X., Chen J.: Journal of Power Sources: 172 (2007) 503.
10. M.R. Tarasevich. L.A. Beketaeva, B.N. Yefremov et al.: Russian Journal of Electrochemistry, 40 (2004) 542.

PREPARATION OF GAS DIFFUSION ELECTRODES BY ELECTROPHORETIC DEPOSITION

N. Furuya, R. Mohri

Department of Applied Chemistry, Faculty of Engineering, University of Yamanashi, Takeda-4, Kofu, 400-8511, Japan

Corresponding author: Nagakazu Furuya
E-mail: Furuya@ab11.yamanashi.ac.jp
Phone: +81-55-220-8559, Fax: +81-55-220-8560

Introduction

The manufacture of the gas diffusion electrode by the electrophoresis was reported in the previous paper (1). The gas diffusion electrode is composed of carbon black and PTFE dispersion with a catalyst. The production technique of this gas diffusion electrode is complicated (2, 3). The electrode materials are dispersed in aqueous solution with a surfactant. The dispersion becomes the electrode sheet by flocculation, filtration, drying and sheeting process. Afterwards, the sheet is dried, removed the surfactant, and it is finally hot-pressed. Reduction of the process is necessary in order to obtain the cheaper gas diffusion electrode. It was noticed that carbon black and PTFE dispersion were disperse system using the non-ion surfactant. The zeta-potential is almost -30mV on carbon black and PTFE particles in the dispersion. It puts the high voltage in this dispersion, because the conductivity is small. By inserting the Pt and Ni electrodes in the dispersion, it was electrolyzed. The Pt anode was covered with mixture of the carbon black and PTFE particles, that is, it was found that mixture of the carbon black and PTFE could be electrodeposited by the electrophoresis. However, there is a defect with the productive crack, when large gas diffusion electrode is produced. The crack was noticed in the water which was included for the sediment, because it occurred by the process of removing the water.
In this paper, the solid concentration of the dispersion for the electrophoresis was optimized.

Experimental

The dispersion was composed of a hydrophobic carbon black (acetylene black, AB-6, DENKA) in aqueous solution containing of surfactant. First a hydrophobic carbon black with ultra pure water (Milli-Q) including a non-ion surfactant (N-100) was dispersed 5 times for 5min each time using Jet mill (Genus) at 150 MPa/cm^2. The final electrophoresis dispersion was obtained by mixing the concentrated CB-dispersion and PTFE dispersion (AD-911, ASAHI GLASS CO., LTD) (CB : PTFE = 60 : 40). The particle size in the dispersion was measured with Fiber-Optics Particle Analyzer (FPAR 1000, Otsuka Electronics Co., Ltd) and AcoustoSizer II (Colloidal Dynamics). The zeta-

potential of the dispersion was analyzed with AcoustoSizer II (Colloidal Dynamics). Electrophoresis cell was 7 by 8 by 1 centimetres. Anode and cathode gap are 1cm. The applied cell voltage is 40V. Drying the deposition sheet at 393K for 15hr and sintering at 633K for 3 hr produced the gas diffusion sheet.
The composition of the gas diffusion sheet was analyzed by a fluorescence X ray analyzer (JSX-3201, JEOL). Tensile strength was measured by AGS-J Series Autograph (SHIMADZU). Electric conductivity was measured by using Resistivity Meter (LORESTA-GP MCP-T600, DIA INSTRUMENTS Co.Ltd, 4-pin probe, constant-current method). The gas penetrability was measured in soap-Film Flow Meter. The surface state was observed using SEM (Tiny-SEM 1710, Technex Lab Co., Ltd).

Results and Discussion

Figure 1 show electrodeposition time and electrodeposition efficiency in using the various concentration dispersions. The yield lowers by the increase in the solid concentration of the dispersion.

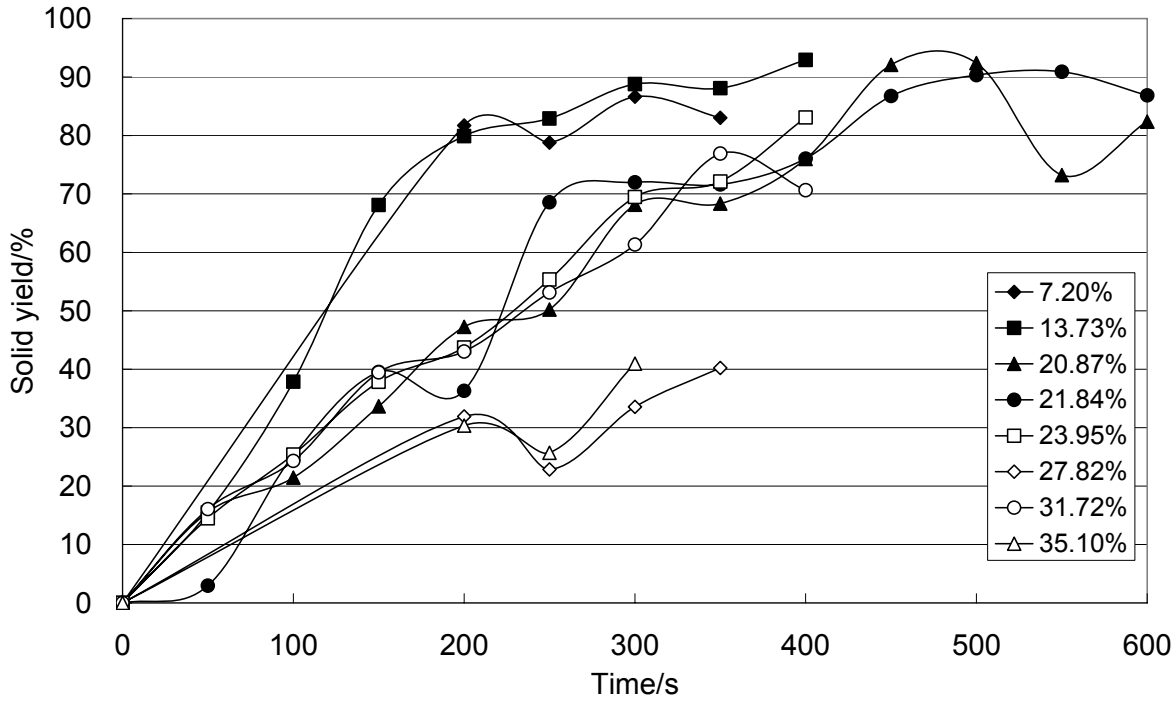

Fig. 1 *Relationship between electrodeposition time and electrodeposition efficiency in using the various electrodeposition dispersions.*

The good yield was shown to 27.82% from 7.20% at the solid concentration of the dispersion. When the electrodeposition time is adjusted to 400 seconds or more, yield exceeds 80%.
Electrodeposition time dependence of the solid concentration of the electrodeposition is shown in Fig. 2. It is proven that the water content of the electrodeposition in the dispersion to 20.87% from 23.95% was small. When solid of the deposit becomes 50% or less, the seat is not obtained.

The relationship between electricity yield and for the electrodeposition hour was shown in Fig. 3. The electricity yield is low with that the concentration of the dispersion is low. It is proven that over 20% is suitable on the concentration of the dispersion, when it is considered from the electricity yield.

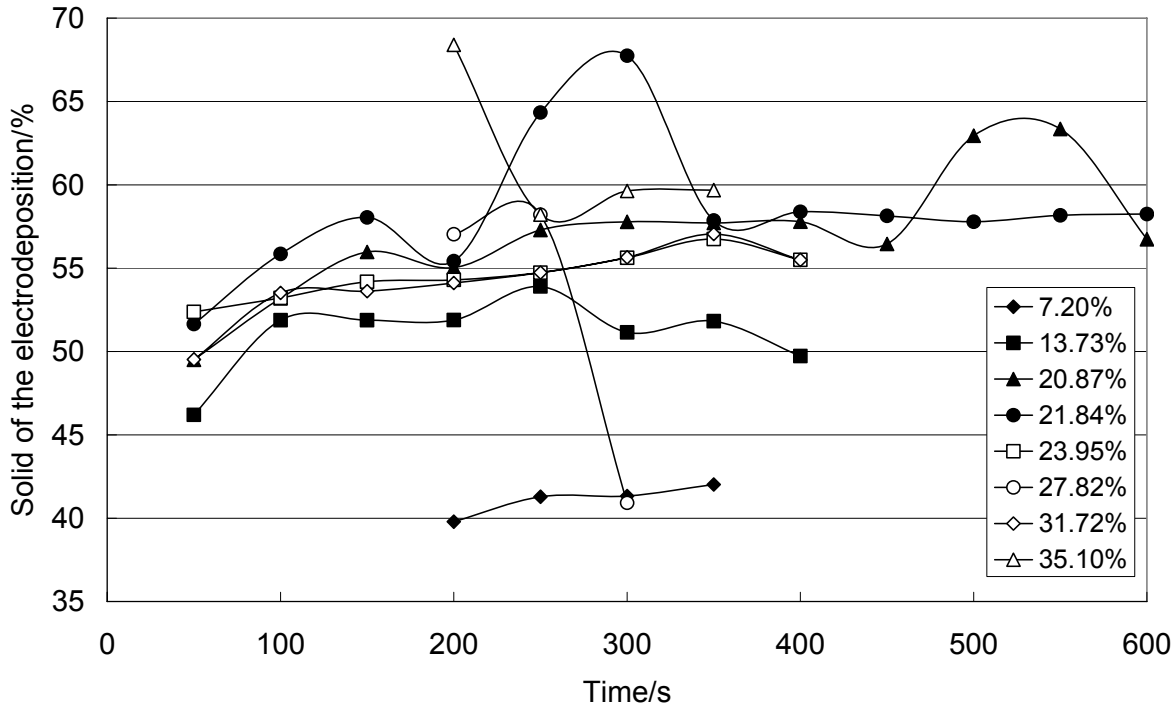

Fig. 2 *Electrodeposition time dependence of the solid concentration of the electrodeposition.*

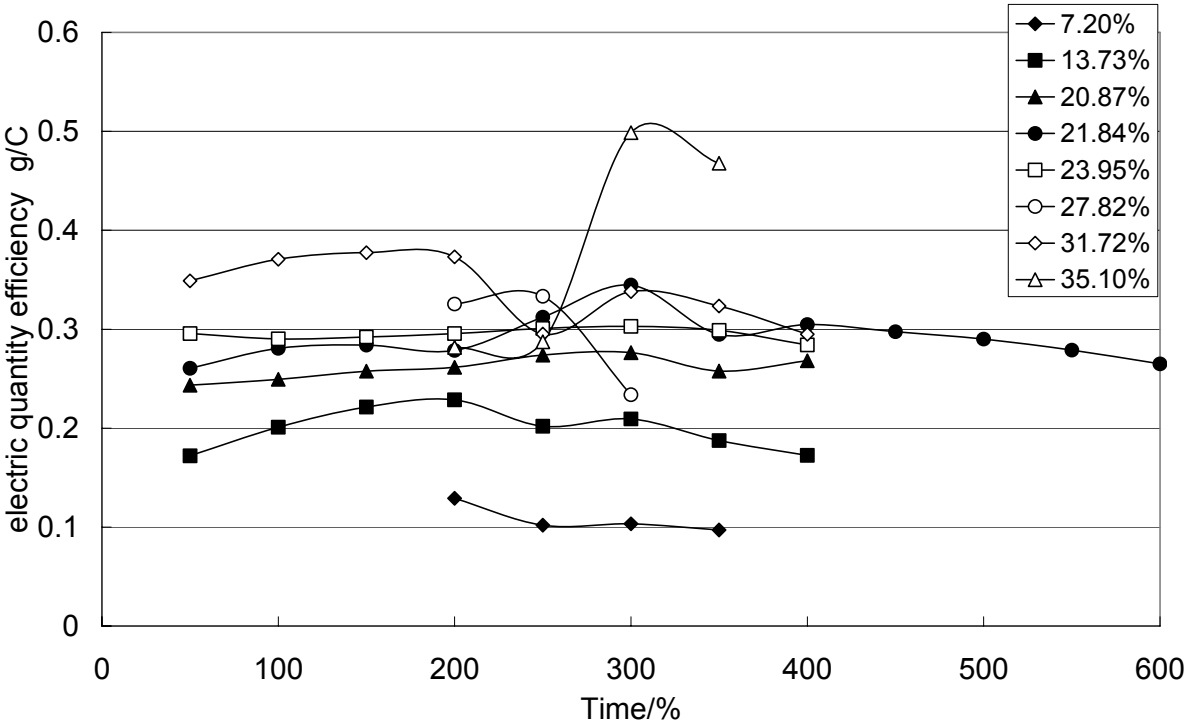

Fig. 3 *The relationship between electricity yield and for the electrodeposition time.*

Table 1 shows the shape of the electrodeposition sheet after heat treatment (360℃, 3hr). The sheet without the crack in 23.95% dispersion was obtained from 200s to 350s for deposition time.

Conclusions

Dispersion concentration used for the electrophoresis electrodeposition technique was examined. In the electrophoretic deposition, it has understood from 14 to 24% of solid of the dispersion to obtain an excellent depositon. The sheet without the crack in 23.95% electrodeposition dispersion was obtained.

Table 1 *The shape of the electrodeposition sheet after heat treatment (360□, 3hr).*

	200s	250s	300s	350s
7.20%	C	C	C	C
13.73%	A	B	A	B
20.87%	A	B	B	B
23.95%	A	A	A	A
27.82%	C	C	C	C
31.72%	B	B	C	C
35.10%	B	B	C	C

A; no crack, B; crack, C; piece

References

Fig. 1 N. Furuya, J. Solid State Electrochem., 8, 48(2003)
8. S. Motoo, M. watanabe and N. Furuya. J. Electroanal. Chem. 160, 351(1984).
9. 3. N. Furuya, N. Aoki and S. Motoo, Denki Kagaku, 56, 658(1988).

HYDROGEN STORAGE ALLOYS AS ANODE MATERIALS FOR THE ALKALINE FUEL CELL

M. Kopczyk[1], A. Kowal[1,2], A. Sierczyńska[1], K. Lota[1], G. Lota[1,3]

[1] Institute of Non-ferrous Metals Department in Poznan, Central Laboratory of Batteries and Cells, 61-362 Poznan, Forteczna 12, Poland
[2] Institute of Catalysis and Surface Chemistry, Polish Academy of Sciences, 30-239 Krakow, Niezapominajek 8, Poland
[3] Poznan University of Technology, Institute of Chemistry and Technical Electrochemistry, 60-965 Poznan, Piotrowo 3, Poland

Corresponding author: Maciej Kopczyk (kopczyk@claio.poznan.pl)
Phone: +48 61 879 33 91
Fax: +48 61 879 30 12; tel.

Introduction

Fuel cells are attractive energy conversion devices to their higher efficiency and low pollution. Hydrogen storage alloy used as a source of hydrogen are attracted because of high energy density and satisfactory value of working potential [1-5]. Multilayer alloys AB_5 are attractive for hydrogen storage due to their high ability to adsorb hydrogen and to store it safely at low pressure. The alloy: $MmNi_{3.55}Al_{0.3}Mn_{0.4}Co_{0.75}$ was studied in our laboratory as an anode in nickel - metal hydride batteries [6]. This alloy is characterized by high value of hydrogen to metal ratio (H/Me is about 1.0 wt.%).

Experimental

The AB_5 – type alloy $MmNi_{3.55}Al_{0.3}Mn_{0.4}Co_{0.75}$ (Mm: La-rich mischmetal) was used as hydrogen storage alloy. Polyvinyl alcohol (PVA) of 3 wt% solution was added to the powders as a binder. To prepare the testing electrode, the alloy powder sample was mixed with carbonyl nickel and polyvinyl alcohol. Then the mixture was spread onto a 4 x 5.5 cm foam nickel sheet to which a nickel wire was point-welded as current collector. After drying at room temperature, the testing electrode was pressed under a pressure of 10 MPa. The testing electrodes prepared on such way were subjected to chemical pre-activation.
A two-electrode measurement system was composed of the testing electrode and a platinum grid. Nafion®1135 (Aldrich) membrane was placed between the two electrodes to obtain the sandwich structure. Nafion membrane was chemical pre-activated before the assembly. In the Pt/N/MH cell 1 M KOH aqueous solution was used as an electrolyte. A schematic diagram of such a cell is shown in Fig. 1.
The electrochemical impedance spectroscopy (EIS) measurements and the cyclic voltammetry experiment were carried out using a PGSTAT 30 potentiostat – galvanostat - frequency response analizer system produced by Autolab Eco Chemie B.V. The scan

rate in cyclic voltammetry experiments was 25 mV/s and scanning range was: $E_0 \rightarrow 1,5$ V$\rightarrow$ 0 V$\rightarrow E_0$, (E_0 is equilibrium potential of two-electrode system).

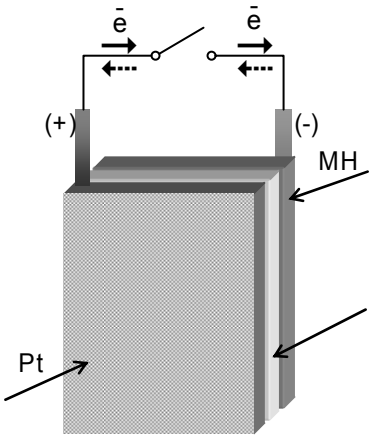

Fig. 1 *A schematic diagram of Pt/Nafion/MH cell*

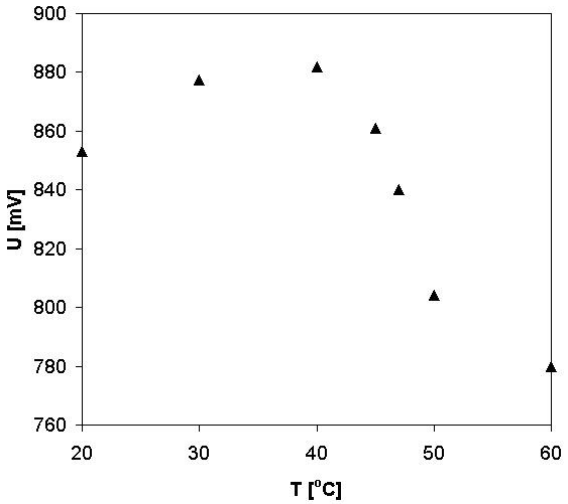

Fig. 2 *The potential difference for the Pt/N/MH system as a function of temperature*

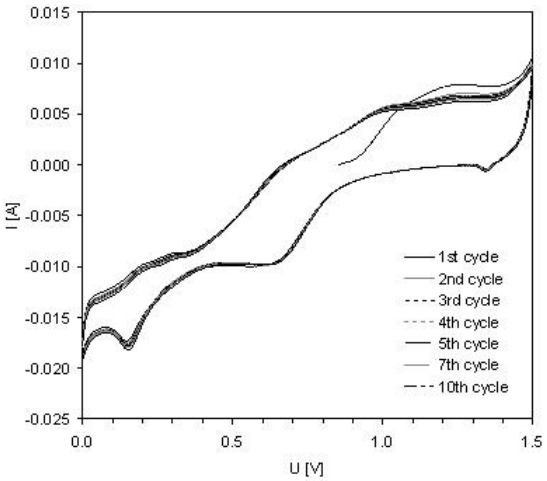

Fig. 3 *Cyclic voltammetry characteristics recorded for Pt/N/MH system as a function of cycle number, $E_0 \rightarrow$ 1.5 V$\rightarrow$ 0 V$\rightarrow E_0$; E_0 = 0.855 V, scan rate 25 mV/s.*

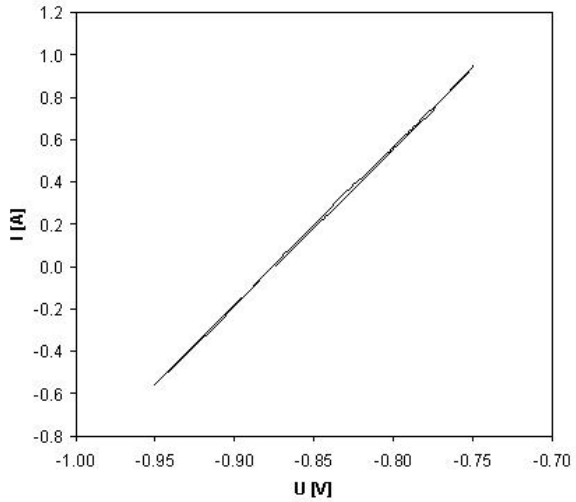

Fig. 4 *Cyclic voltammetry characteristics recorded for M/MH electrode vs. Hg/HgO, $E_0 \rightarrow$ - 0.95 V$\rightarrow$ -0.75 V$\rightarrow E_0$; E_0 = -0,880 V, vs. Hg/HgO, scan rate 25 mV/s.*

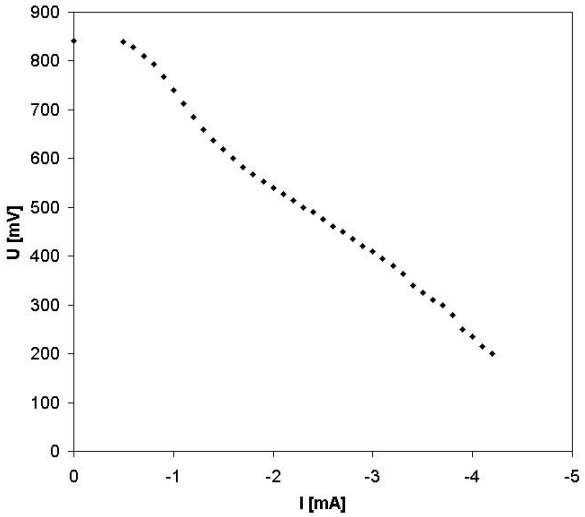

Fig. 5 *Polarization curve for Pt/N/MH system*

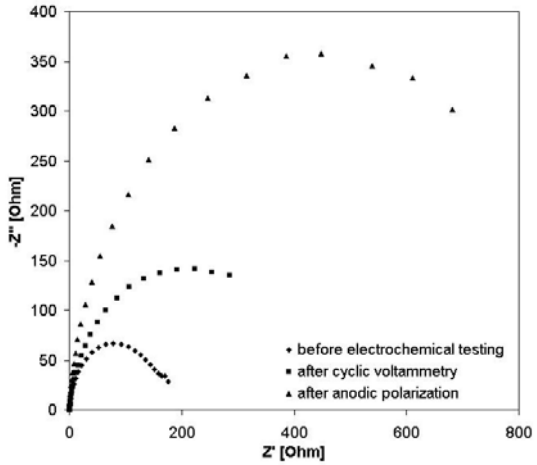

Fig. 6 *Impedance spectroscopy for Pt/N/MH system.*

Results and discussion

The effect of temperature on the equilibrium potential of Pt/N/MH system was investigated in sandwich configuration: Pt/Nafion membrane/tested MH (Fig. 1). As it is shown in Fig.2 the potential difference of Pt/N/MH system systematically increases in the temperature range from 20 to 40 ^{o}C. At temperatures higher than 40 ^{o}C, this difference, measured between the tested and Pt electrode, decreased. The decrease of Pt/N/MH potential difference was connected with the properties of the tested MH electrode.

After recording the potential vs temperature dependence (Fig. 2), the cell was stabilized at room temperature. When it reached the value 0.815 V, the electrochemical impedance test was carried out. The impedance investigation was done at room temperature, at frequency range from 1MHz to 10 MHz, with use of alternating current signal of $\pm$10 mV amplitude and at open circuit potential (OCP=0.815 V). In the next stage the potential window of Pt/N/MH system was studied, starting from the equilibrium potential (E_o), and broadening the potential range from E_o – 50 mV to E_o + 50 mV. Various scan rates of potential shift were applied: 1, 10, 25, and 50 mV/s.

Cyclic voltammetry characteristics recorded for the sandwich system at scan rate 25 mV/s are shown in Fig. 3. For comparison the some cyclic voltammetry characteristics were recorded for tested MH electrode versus Hg/HgO electrode (Fig. 4). Comparing cyclic voltammetry characteristics presented in Fig. 3 and Fig. 4., one can conclude that all peaks presented in Fig. 3 shows the processes occurring on Pt electrode.

The polarization curve of Pt/MH system was recorded starting from constant current of -0.5 mA (discharge) and then decreasing the current in 0.1 mA steps until the potential reached the value of 0.2 V. The results of this measurement as shown on Fig. 5 is not very satisfactory, but the system is composed of platinum grid which is only polarized.

The electrochemical impedance spectroscopy measurements were carried out before electrochemical testing, after investigation leading to the determination of potential

window of the system (OCP=0.865) and finally after the determination of polarization curve (OCP=0.834). As one can see in Fig. 6, after each step of investigation, the inner resistance of the system increased.

Conclusion

The nature of potential- temperature dependence is significant but has not been established so fare
The potential window which was determined for the Pt/N/MH system promises the possible application of multicomponent alloys in modern fuel cells.
The sandwich structure: Pt/Nafion/ $MmNi_{3.55}Al_{0.3}Mn_{0.4}Co_{0.75}$ (Mm: La-rich mischmetal) is an interesting system for further investigations.

References

1. B. Hong Liu, S. Suda, *J. Alloys Compd*. 454 (2008) 280-285.
2. X.H. Wang, Y.Y. Bei, X.C. Song, G.H. Fang, S.Q. Li, C.P. Chen, Q.D. Wang, *Int. J. Hydrogen. Energy* 32 (2007) 4011-4015.
3. L. Wang, Ch. Ma, X. Mao, J. Sheng, F. Bai, F. Tang, *Electrochem. Commun.* 7 (2005) 1477-1481.
4. Y. Chen, C.A.C. Sequeira, Ch. Chen, X. Wang, Q. Wang, Internat. *J. Hydr. Energy* 28 (2003) 329-333.
5. Y. Nakamura, H. Nakamura, S. Fujitani, I. Yonezu, T. Saito, N. Nishizawa, M. Tsutsumi, *J. Alloys Compd*. 231 (1995) 898-902.
6. M. Kopczyk, A. Sierczynska, W. Majchrzycki, E. Jankowska, 6th Advanced Batteries and Accumulators – ABA (2005) 150-154.

MESOPOROUS NICKEL-NICKEL OXIDE FOR THE FUEL CELL CATALYST

Peter Barath[1,2], Tereza Uhlířová[1], Jakub Reiter[1]

[1] Institute of Inorganic Chemistry of the ASCR, v. v. i., 250 68 Řež near Prague, Czech Republic
[2] Institute of Electrotechnology, Technical University of Brno, 602 00 Brno, Czech Republic

Corresponding author: Jakub Reiter (reiter@iic.cas.cz)
Phone: +420 266 172 198
Fax: +420 220 941 502

Introduction

A novel approach to preparation of mesoporous metals and oxides reported in recent years [1-5] has involved electrodeposition from lyotropic liquid crystals (LLCs). The ability of several non-ionic surfactants to form self-assembled liquid crystalline phases on addition of aqueous solutions or pure water [6, 7] results in a facile synthesis of a variety of dimensionally variable templates in which the electrodeposit morphology is the inverse of the template.
The liquid crystal structure is determined by the system composition, surfactant type and temperature. Fig. 1 shows one of basic structures (hexagonal), which can be found in the LLC containing Brij® 56 in water. For the application of LLC in the nanotechnology, the hexagonal phase is the most important one due to its characteristic dimension less than 100 nm.

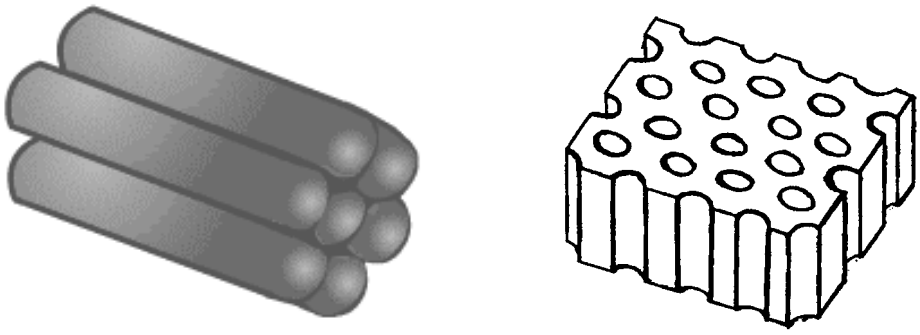

Fig. 1A and 1B Hexagonal structure of the lyotropic liquid crystal Brij® 56 – water (A - left) and a schematic structure of the mesoporous material prepared from the hexagonal phase of the LLC (B - right; from [8]).

The structure of the deposited material can be expressed similarly to Fig 1B, when regular structure provide very high surface area in comparison with the smooth sample surface prepared by conventional electrolytical method. The electrode surface with highly organised structure is much better accessible for the molecules of gaseous or

liquid compounds. This effect is strongly welcomed in the technology of fuel cells, where high catalytic activity of the material is expected.

Our recent work is aimed at the preparation of mesoporous nickel for its application in low-temperature H_2-O_2 fuel cells. In this area, the main task is to substitute expensive materials (platinum catalysts, Nafion-based ion-exchange membranes) with more affordable components such as nickel or manganese oxide [9].

Experimental

The lyotropic liquid crystal was prepared from Brij® 56 (poly(ethylene glycol)hexadecyl ether; Fluka) and aqueous nickel bath (0.2M $(CH_3COO)_2Ni$, 0.5M CH_3COONa, 0.2M H_3BO_3) in the 50 – 50 wt. % ratio. The procedure of preparation followed literature [8].
The electrochemical measurements were performed using potentiostat-galvanostat PGSTAT 30 (Eco Chemie, Holland). Nickel was deposited galvanostatically on a glassy carbon electrode (∅ 3 mm) at 30 °C. For comparison, nickel was also electrodeposited directly from the nickel bath under the same conditions. The electrochemical investigation of prepared materials was done on a rotating disc electrode RDE; Metroohm) and aimed mainly at measurements of the hydrogen oxidation reaction (HOR).

Results and Discussions

The voltammetrical measurements presented on Fig. 2 show formation and consequent reduction of several Ni(OOH) monolayers between the potentials 0.1 and 0.5 V vs. Hg/HgO and this process is independent on the method of sample preparation. Considering the same charge used for the nickel electrodeposition, the only factor influencing the reactivity of nickel is the presence of channels and pores in the structure of nickel deposited from the LLC.

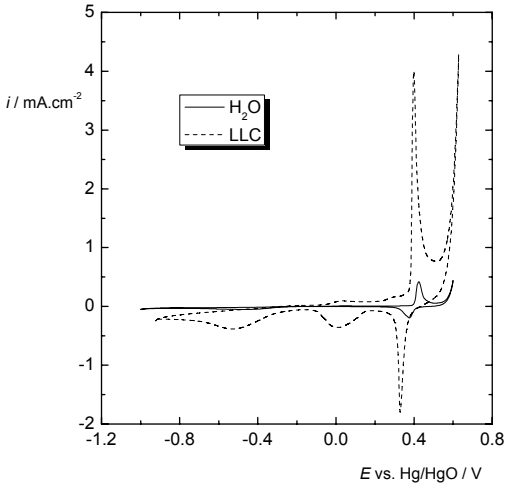

Fig. 2 Voltammograms of nickel deposited from the liquid aqueous and LLC phase (1M KOH electrolyte, both samples deposited galvanostatically at 2.25 $C.cm^{-2}$).

The areas of the oxidation peak of nickel are in ratio 8.9 : 1 in favour of the mesoporous sample. The oxidation also occurs at lower potential and both oxidation and reduction peaks are sharper, what can be explained by its higher reactivity. The voltammetrical measurements done at higher scan rates (up to 100 $mV.s^{-1}$) showed rapid charge transfer and fast transport to the mesoporous surface.

Our recent research is aimed at the hydrogen oxidation reaction (HOR) on prepared mesoporous nickel at moderately elevated temperatures. Here, higher reactivity of the catalyst and fast species (H_3O^+ and H_2) transport will be employed. Our first results of the measurement on a rotating disk electrode showed distinctive catalytic activity.

Conclusions

Prepared mesoporous nickel-nickel oxide material showed high catalytic activity towards hydrogen. Our recent investigation is aimed at its application in the H_2-O_2 fuel cells, where the Ni/NiO catalyst will be combined with similarly prepared MnO_2 materials doped with bivalent cations [9] serving as a catalysts for the oxygen reduction.

Acknowledgements

This work was supported by the Academy of Sciences (Research Plan AV0Z40320502), by The Grant Agency of the Academy of Sciences (grant KJB200320801) and the Ministry of Education, Youth and Sports, Czech Republic (project MSMT LC523).

References

1. G.S. Attard, J.C. Glyde, C.G. Göltner, Nature **378** (1995) 366.
2. G.S. Attard, M. Edgar, C.G. Göltner, Acta Mater. **46** (1998) 751.
3. A.H. Whitehead, J.M. Elliott, J.R. Owen, J. Power Sources **81-82** (1999) 33.
4. P.N. Bartlett, P.N. Birkin, M.A. Ghanem, P. de Groot, M. Sawicki, J. Electrochem. Soc. **148** (2001) C119.
5. J.M. Elliott, G.S. Attard, P.N. Bartlett, N.R.B. Coleman, D.A.S. Merckel, J.R. Owen, Chem. Mater. **11** (1999) 3602.
6. G.S. Attard, P.N. Bartlett, N.R.B. Coleman, J.M. Elliott, J.R. Owen, Langmuir **14** (1998) 7340.
7. J.M. Elliott, J.R. Owen, Phys. Chem. Chem. Phys. **2** (2000) 5653.
8. P.A. Nelson, J.M. Elliot, G.S. Attard, J.R. Owen, Chem. Mater. **14** (2002) 524.
9. J. Vondrák, B. Klápště, J. Velická, M. Sedlaříková, J. Reiter, I. Roche, E. Chainet, J.F. Fauvarque, M. Chatenet: J. New Mat. Electrochem. Syst. **8** (2005) 209-212.

ELECTROCHEMICAL CARBON STUDY PART I. ENVIROMENTAL SEM VIEW

J. Vognar[1], P.Dvořák[1], P. Černoch[1], V. Novák[1], J. Vondrák[2], M. Sedlaříková[1]

[1] Department of Electrotechnology FEEC BUT, Údolní 53, 602 00 Brno, CZ
[2] Institute of Inorganic Chemistry, Academy of Science CR, 250 68 Řež, CZ

Corresponding author (name underlined): J. Vognar
E-mail: jirikv@email.cz

Introduction

Graphite and amorfous carbon (carbon black) structure is widely used as electrode material for batteries, fuel cells and supercapacitors. In this paper SEM study assortment of carbon samples was accomplished. One can observe significant difference between graphite, nanotech and carbon black samples. These variations deteminate usage of carbons for specific occasions. Study is replenished with data sheets of used samples such as specific surface area and powder density.

Experimental

Carbon is occured in nature in three alloptropic substances - diamond (Fig.1a), graphite (Fig.1b) and amorphous carbon (Fig.1c). Other modifications such as fullerens (Fig.1d) and nanotubes (Fig.1e) were syntetized in laboratory.

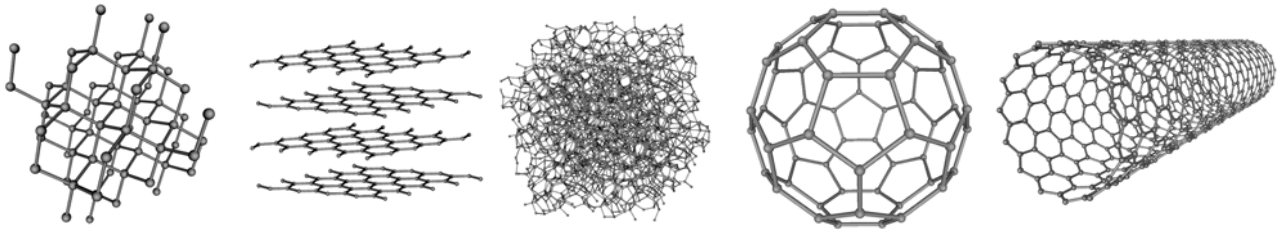

Fig. 1 *Carbon alloptropic structures*

Our twelve carbon samples contain amorphous carbon (sample no. 1,2,10,11,12), graphite (7,8,9,10), nanotubes (4,5) and graphite with fullerens (3). Table 1 describes basic carbon parameters.
Samples for SEM were made from carbon ink. 10mg of carbon has been added to 2:1 distilled water and ethanol solution. This solution was sonicated for 10 minutes in ultrasonic bath. After that 10 wt. % of PTFE has been added and sonicated again for 15 min. This mixture was pippeted to aluminium foil and sintered for 20 minutes in 80 °C. So prepared samples were ready for scanning.

Scanning electron microscope used segment ionizer detector (SID). This type of detector detects mainly backscattered electrons, where brighter place represent shapes or poor conducting areas.

Result and discusion

From SEM pictures are markedly visible differences between carbon black and graphite samples. Nanotech samples (3,4,5) have a stucture similar to graphite without micro porous structure observed on carbon black samples. This effect could affect catalytic activity in oxygen reduction reaction. Higher overpotential is needed to ORR when using non carbon black electrode material. Further investigation will carry out.

1. *Selected parameters of carbon samples*

Type of carbon	Specific [m2/g]	Powder [g/dm3]	Carbon [%]	Minerals [%]	Fullerens [%]	Ash [max %]	Electrical [Ωcm]
Chezacarb A	min. 800	112	99,5	0,5	-	0,9	150
Chezacarb B	min. 800	115	99,4	0,6	-	1,7	150
Nanosorb	1700	-	-	-	20	-	-
Nanotrubice 632B	340	29	80	20	-	-	
Nanotrubice 632C	340	-	99	<1	-	-	-
Exp. grafit	2500	-	-	-	-	-	-
Exp. grafit EG-B	2500	-	-	-	-	-	-
Cond 2 995	20	-	>96 %	-	-	4%	-
CR 5 995	10	180	>99,5 %	-	-	0,50%	-
Vulcan XC72	250	263	-	-	-	-	-
Vulcan XC72R	250	96	-	-	-	-	-
Black Pearls 2000	1400	-	-	-	-	-	-

* by N2 adsorption/desorption

Acknowledgements

This work was supported by the Ministry of Education (project MSM 0021630516), by the Ministry of Environment (grant VaV SN/3/171/05), by Czech Science Fundation no. 104/06/1471.

References

1. J. Vondrák, J., Sedlaříková, M., Novák, V. Electrocatalysts based on carbon-manganese oxide for alkaline fuel cells cathodes. Journal of New Materials for Electrochemical Systems, 1998, Vol. 1, No. 1, pp. 25-30.
2. Vondrák, J., Klápště, B., Velická, J., Sedlaříková, M., Reiter, J., Roche, I., Chainet, E., Fauvarque, J. F., Chatenet, M.Journal of New Materials for Electrochemical Systems, 2005, Vol. 8, pp. 209-212.
3. J. Vognar, J. Vondrák, J. Novák, M. Sedlaříková. Kinectic properties of MnO_x positive electrode with different dopants, Advaced Batteries and Accumulators Proceedings 2007, Vol.1, pp. 147-151, ISBN 978-80-214-3424-0

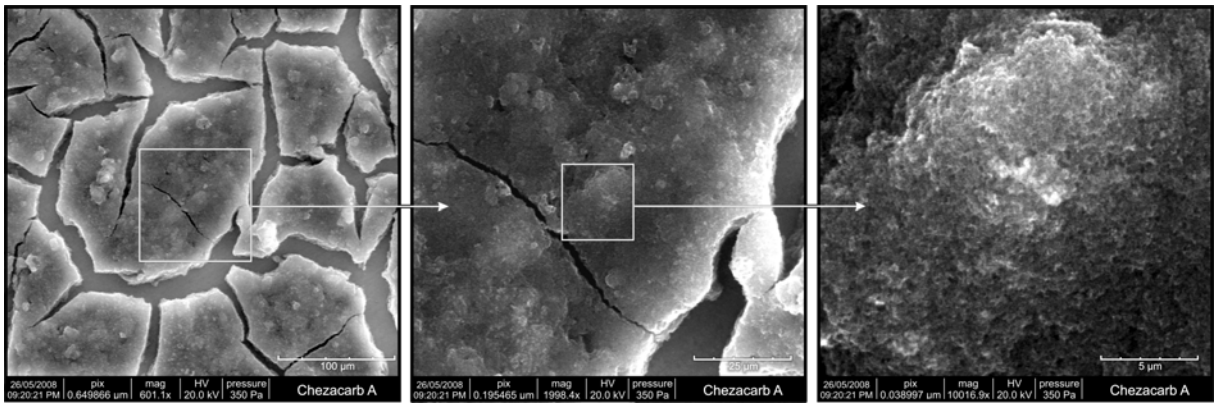

Fig. 2 *Chezacarb A*

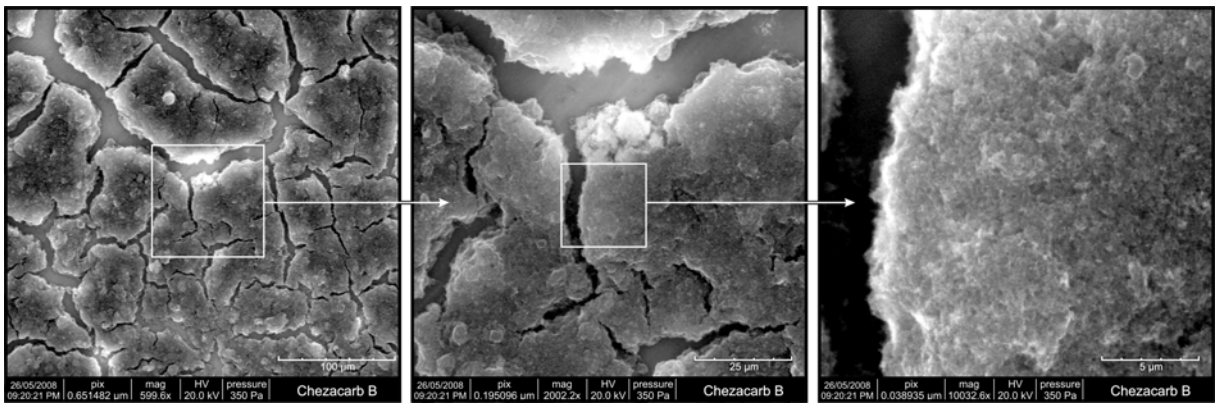

Fig. 3 *Chezacarb B*

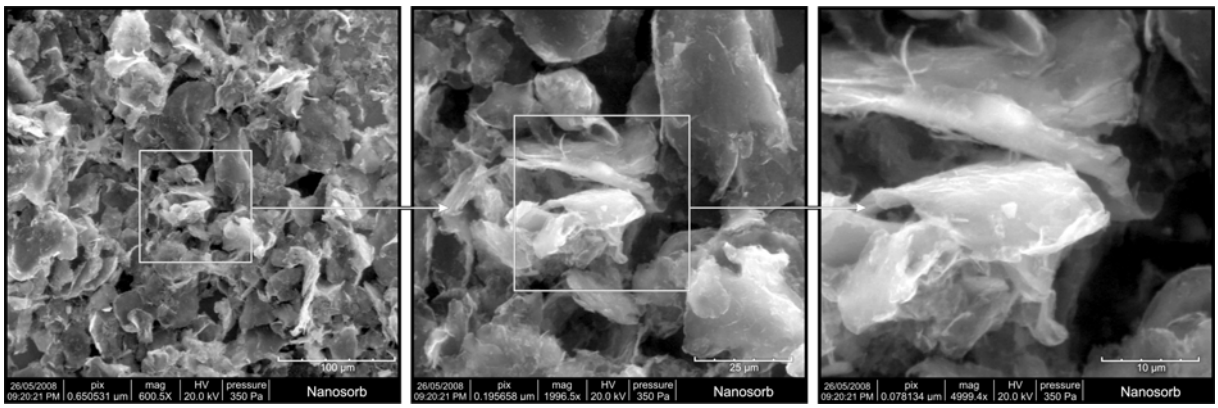

Fig. 4 *Nanosorb*

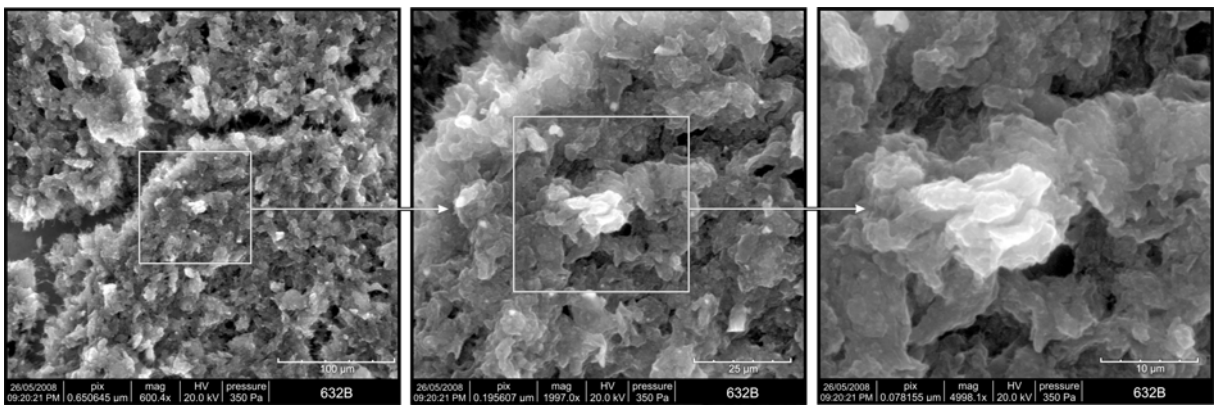

Fig. 5 *Nanotrubice 632B*

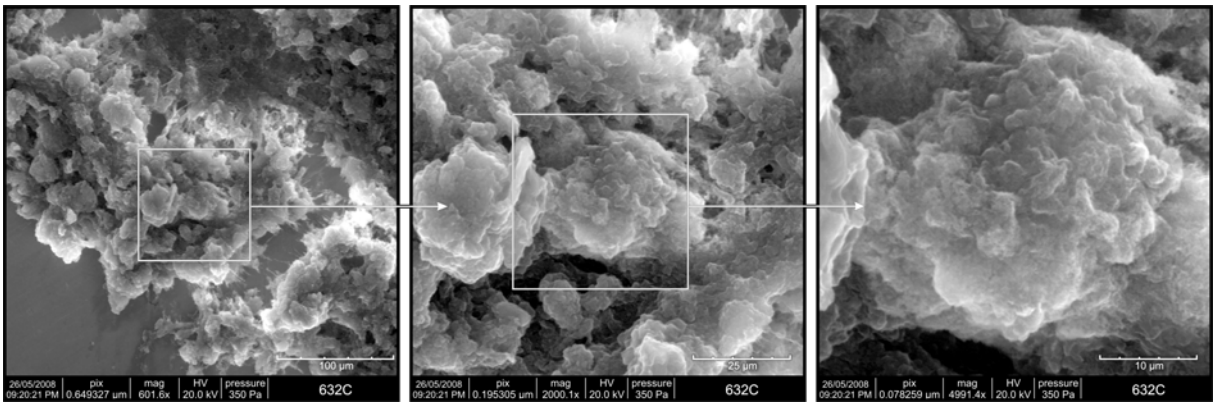

Fig. 6 *Nanotrubice 632C*

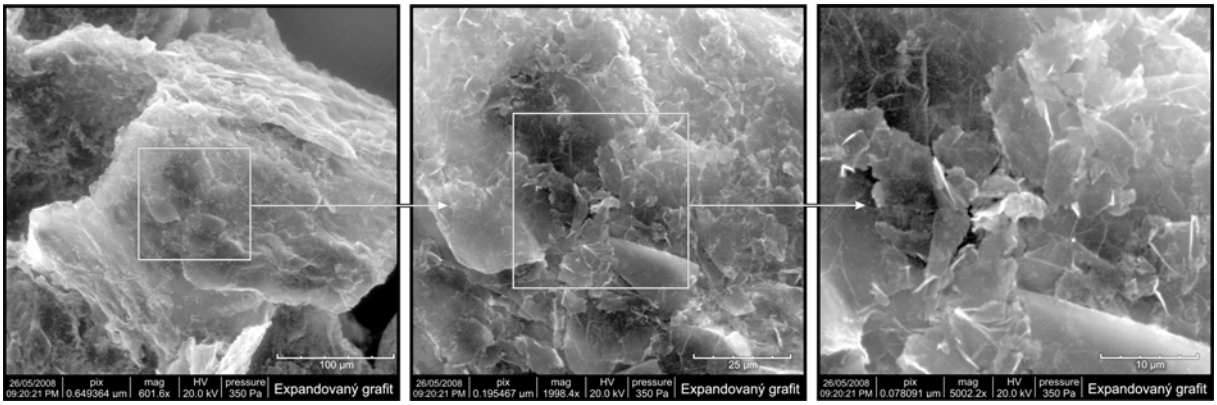

Fig. 7 *Expandovaný grafit*

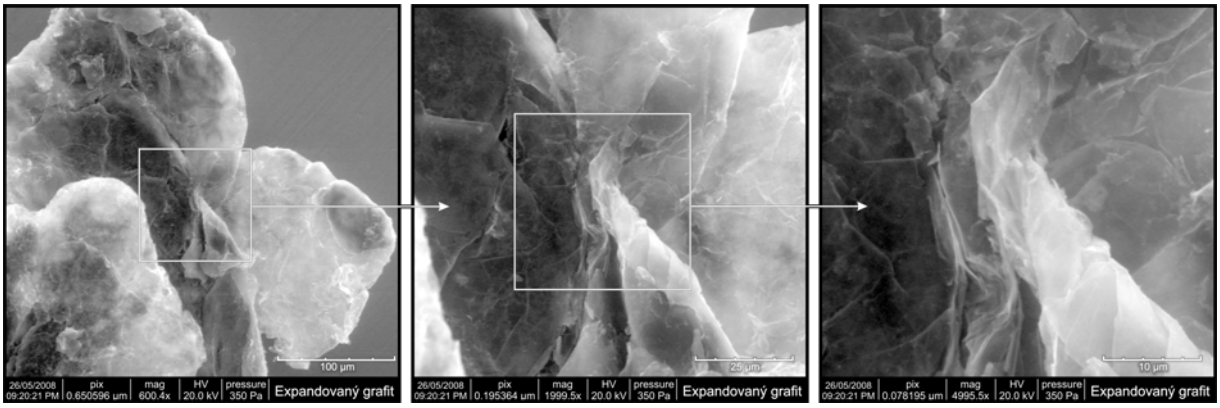

Fig. 8 *Expandovaný grafit EG-B*

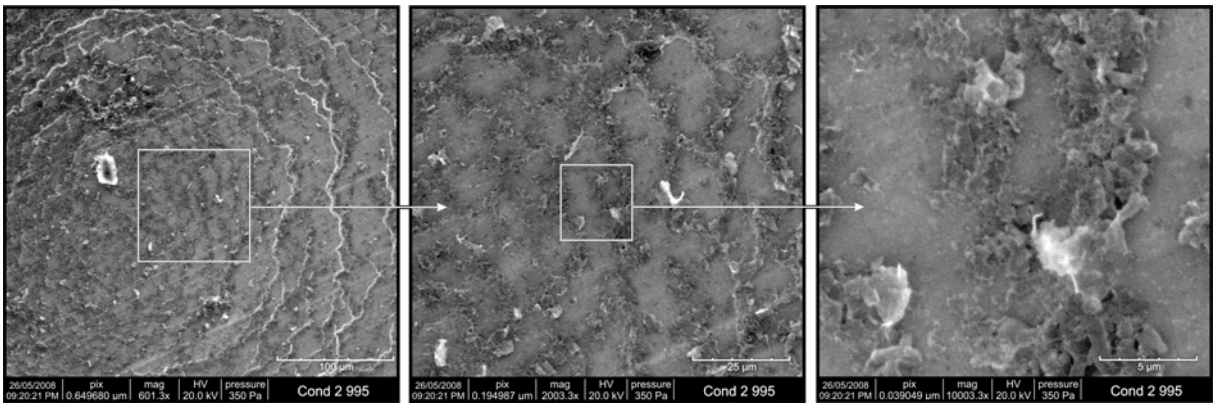

Fig. 9 *Cond 2 995*

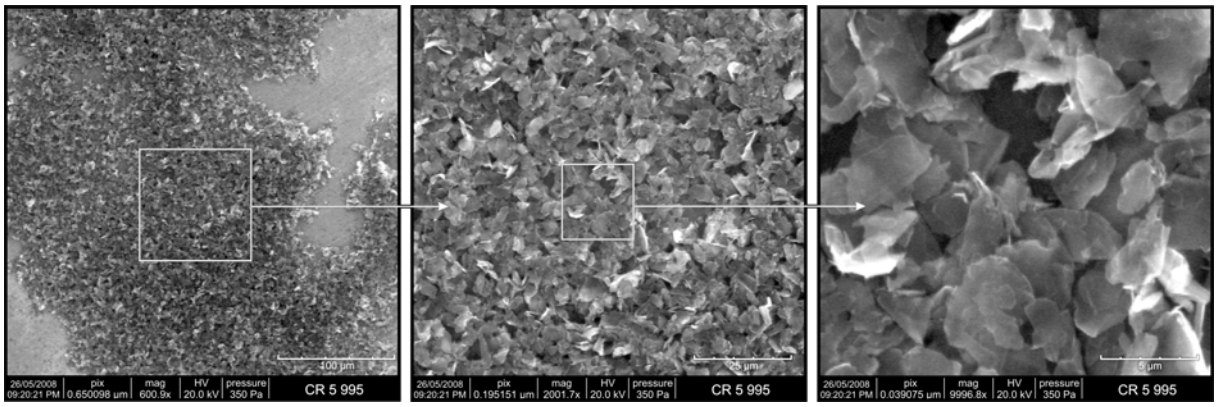

Fig. 10 *CR 5 995*

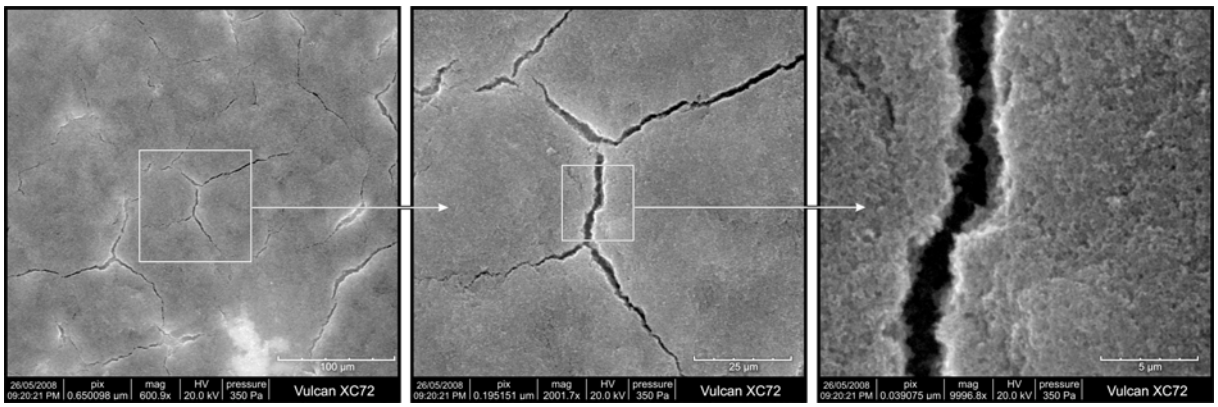

Fig. 11 *Vulcan XC72*

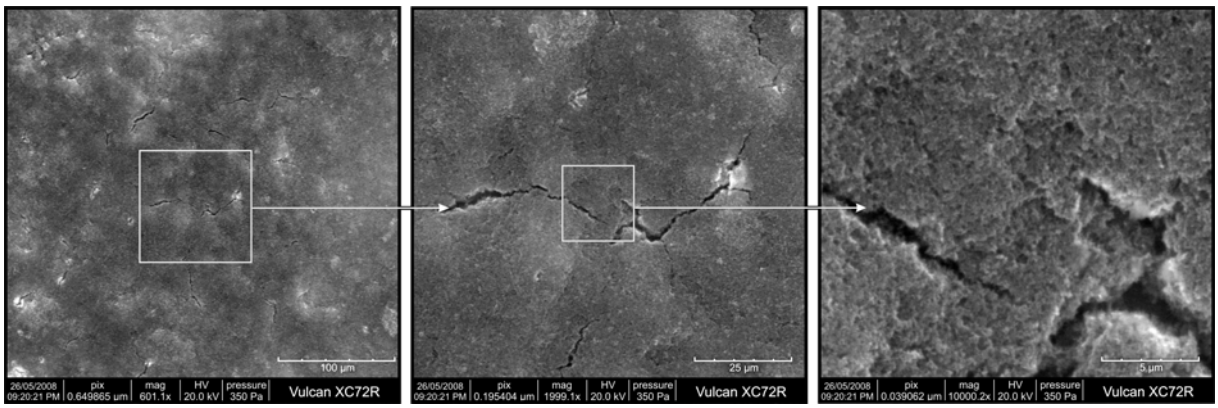

Fig. 12 *Vulcan XC72R*

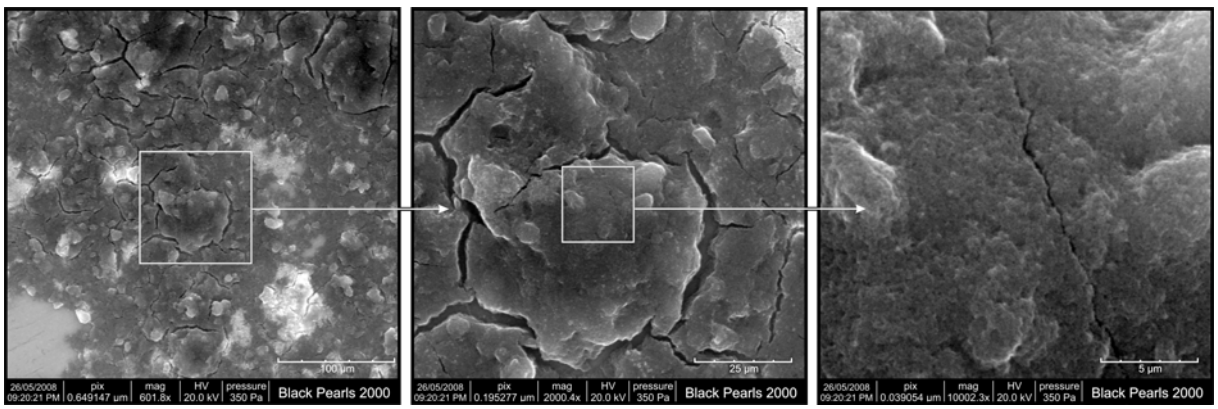

Fig. 13 *Black Pearls 2000*

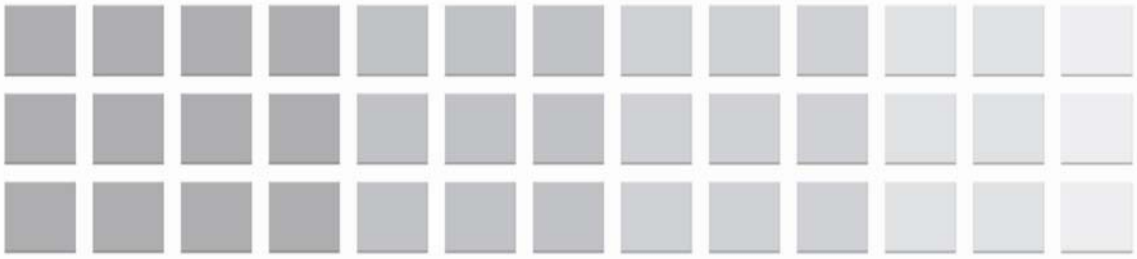

9th ABA

BRNO 2008

Advanced Batteries and Accumulators

Special electrochemical components

SUPERCAPACITORS BASED ON NICKEL OXIDE/CARBON MATERIALS COMPOSITES

Katarzyna Lota[1], Grzegorz Lota[1,2], Agnieszka Sierczyńska[1]

[1]Institute of Non-ferrous Metals Department in Poznan,Central Laboratory of Batteries and Cells, 61-362 Poznan, Forteczna 12, Poland
[2]Poznan University of Technology, Institute of Chemistry and Technical Electrochemistry, 60-965 Poznan, Piotrowo 3, Poland

Introduction

Electrochemical capacitors have generated great interest because of their possible use in high power applications such as lasers and for propulsion in electric vehicles. There are a number of electrode materials being developed for electrochemical capacitors. The main electrode materials are microporous activated carbons with high specific areas, which take advantage of capacitance arising from charge separation at an electrode/electrolyte interface and can be used with either aqueous or organic electrolytes [1-3]. However new trends for supercapacitors development are connected with application of materials with pseudocapacitance properties associated with fast and reversible surface redox-type reactions using e.g. transition metal oxides or conducting polymers [4,5]. To utilize both advantage of double layer capacitance and pseudocapacitance many composite materials consisting active carbon and metal oxide have been investigated as electrode materials for electrochemical capacitors [6,7]. In our work composites with different proportion of nickel oxide/carbon material were prepared. Nickel oxide was prepared by chemically precipitating nickel hydroxide on carbon active and heating the hydroxide in the air in 300°C. We studied electrochemical performances of composite electrode used in electrochemical capacitor and moreover properties of electrode consisting only active carbon and only nickel oxide.

Experimental

Nickel oxide was prepared by directly chemically precipitating nickel hydroxide on active carbon (AC) NORIT® SX2 (POCH-Poland) from the $Ni(NO_3)_2$ solution. NaOH solution was slowly dropped into above mixed solution; the molar ratio of $Ni(NO_3)_2$/NaOH was 1:2. The precipitated materials were washed with distillated water and then dried at a temperature 80°C. Then composites or nickel hydroxide were heating in the air at 300°C for 2 hours. Phase compositions of the products were characterized by X-ray diffraction (XRD) analysis using CuKα radiation. Specific surface area measurements (BET) were performed using ASAP 2010 M. The capacitor electrodes were formed as pellets consisting of 85% active material, 10% binder (PVDF, Kynar Flex 2801) and 5% acetylene black (to ensure good conductivity). The composites were tested in 6 M KOH aqueous electrolyte using two- and three-electrode Swagelok® system. The electrochemical measurements have been carried out using cyclic voltammetry, galvanostatic charge/discharge and impedance spectroscopy using AUTOLAB

ECOCHEMIE BV-PGSTAT 30/FRA2. The capacitance values were calculated per active mass of one electrode.

Results and discussion

Compositions of the composites were characterized by X-ray diffraction (XRD) analysis. Fig. 1 shows the XRD pattern of the deposited nickel hydroxide (β-$Ni(OH)_2$) and nickel oxide (NiO) on active carbon before and after calcination process. Calcination process has influence on increase of crystallinity. During calcination process from room temperature to 200°C hydrated water is lost. Next at 300°C nickel hydroxide is converted into nickel oxide and water [8]. The BET surface area of the composite after calcination is higher with visible increase of microporosity. Before calcination, specific surface area is 514 m^2/g and after annealing process is 574 m^2/g.

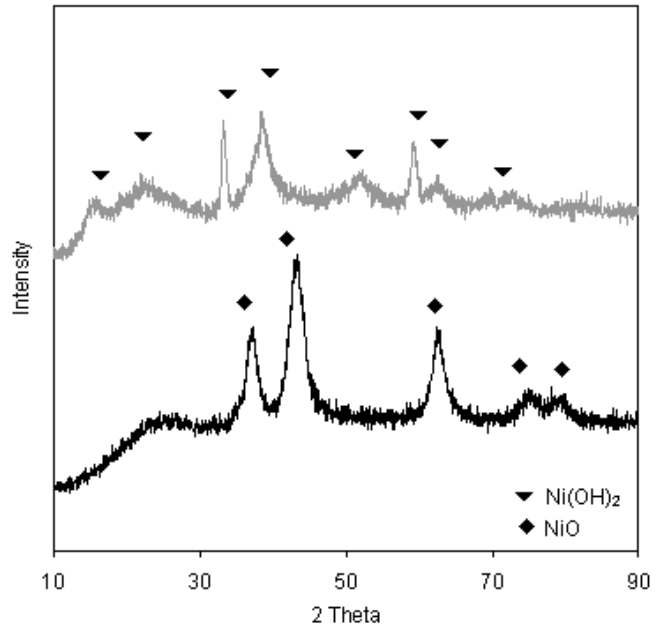

Fig. 1 *XRD pattern of the deposited nickel hydroxide on AC and nickel oxide on AC.*

The values of capacitance for nickel oxide, active carbon and 34% NiO/66% active carbon composite varied from 11 to 74 F/g depending on the ratio of these two components. The capacity of pristine nickel oxide is very low. In spite of the fact that capacity of active carbon is negligibly higher than that of the composite, there are some advantages of such composite, which are shown on Fig. 2. The bare NiO has only pseudocapacitive properties. The CV curves for AC and composite material have much more rectangular shape, which is a characteristic of a double-layer capacitive behavior. ESR (equivalent series resistance) estimated from impedance spectroscopy measurements at 1 k Hz for AC is 0.991 Ω, and for composite material 1.231 Ω, and confirm that active carbon has capacitance mainly from double-layer whereas nickel oxide/active carbon has both characteristic from double-layer and from surface redox-type reactions. To establish electrochemical nature of the composite investigations were made in three electrode system. The composite material seems to be an excellent

candidate as negative electrode. The application of an asymmetric configuration with materials of different nature is advisable, because of the possibility of increasing the operating voltage in aqueous solution which affects power and energy of supercapacitior. Direct chemical precipitation of nickel hydroxide on active carbon seems to be good method to obtain composite material. Process of annealing at 300°C allows to convert nickel hydroxide into nickel oxide. There is a need to prepare composite material with smaller amount of nickel oxide.

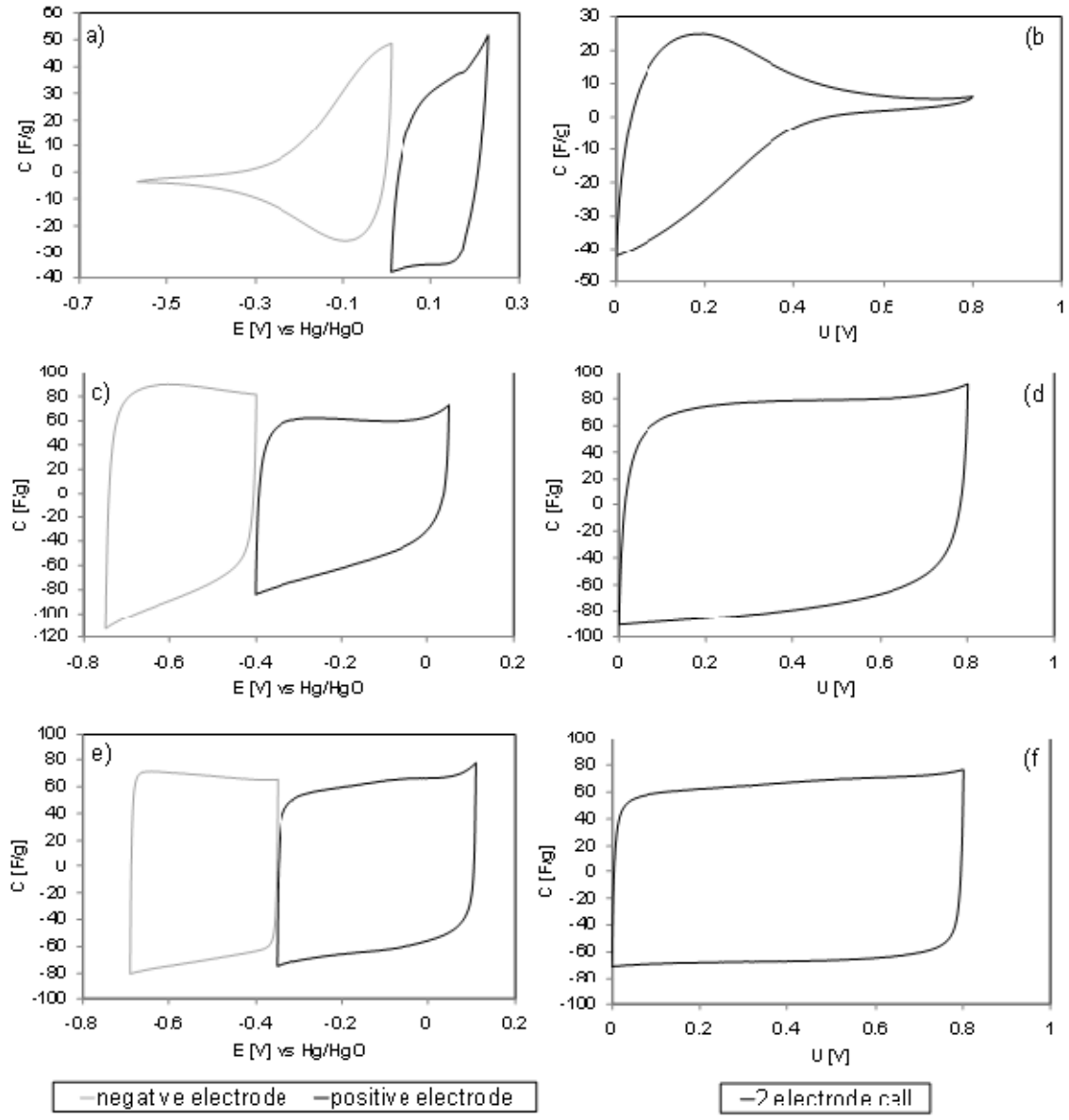

Fig. 2 *Voltammetry characteristics of: NiO (a,b); AC (c,d); composite NiO/AC (e,f). The CV b, d, f are made in two-electrode swagelok system at a scan rate 10 mV/s, while curves a, c, e are made in three-electrode swagelok system at a scan rate 5 mV/s.*

Conclusion

The chosen method for chemical precipitating nickel hydroxide and the temperature of calcination process allow to obtain composite material with quite good capacitance properties. The electrochemical investigations show that the composite nickel oxide/active carbon needs further investigations as a negative electrode in asymmetric configuration of electrode materials in electrochemical capacitor.

Acknowledgements

The authors acknowledge the financial support of grant DS 419/E-138/F/2008.

References

1. G. Lota, T.A. Centeno, E. Frackowiak, F. Stoeckli Electrochim. Acta 53 (2008) 2210.
2. Ch. Emmenegger, Ph. Mauron, P. Sudan, P. Wenger, V. Hermann, R. Gallay, A. Zuttel J. Power Sources 124 (2003) 321.
3. B. Fang, L. Binder J. Power Sources 163 (2006) 616.
4. D. Rochefort, A. Pont Electrochem. Commun. 8 (2006) 1539.
5. E. Frackowiak, V. Khomenko, K. Jurewicz, K. Lota, F. Beguin J. Power Sources 153 (2006) 413.
6. G. Yuan, Z. Jiang, A. Aramata, Y. Gao Carbon 43 (2005) 2913.
7. Q. Huang, X. Wang, J. Lui, C. Dai, S. Gamboa, P.J. Sebastian J. Power Sources 164 (2007) 425.
8. M. Wu, H. Hsieh Electrochim. Acta 53 (2008) 3427.

CARBON BASED ELECTRODE MATERIALS FOR SUPERCAPACITORS

Petr Dvořák[1], Jiří Vognar[1], Jiří Vondrák[2], Marie Sedlaříková[1]

[1]Brno University of Technology, Faculty of Electrical Engineering and Communication, Department of Electrical and Electronic Technology, Údolní 53, 602 00 Brno
[2]Academy of Sciences – Institute of Inorganic Chemistry, 250 68 Řež near Prague

Corresponding author: Petr Dvořák
E-mail: petr.dvorak@phd.feec.vutbr.cz
Phone Number: +420 54114 6142

Introduction

Research into supercapacitors is divided into two main spheres according their energy storage principles. Redox supercapacitors are the first group, they store electrochemical charge using highly reversible surface redox reactions. The second are electrochemical double layer capacitors which store electrical charge in an electrical double layer at the electrode-electrolyte interface.
EDLC stores energy by charge separation. It is a similar principle as is used in traditional electrolytic capacitors, but the supercapacitors can store much more energy because the highly extended electrode surface. Various carbon forms are extensively examined and widely utilised electrode materials. The carbon materials have been used in electrodes of energy storage devices as conductive, catalysts, porosity surface area and capacity agents for long time. For these properties, carbon materials are also well suited as the electrode materials for EDLCs.
This work is a study of different commercially available carbon materials produced by Cabot Corporation.[1,3,4]

Experimental

Materials
VULCAN® XC72R, VULCAN® M, VULCAN® P, VULCAN® 3, VULCAN® 6

Preparation
Each carbon material were boiled in water with isopropanol for one hour, then 4 wt % PTFE was added as a binder agent. After 24 hours the solution was filtered and dried at 120 ^{o}C for 2 hours.

Instrumentation and methods
Cyclic voltammetry and impedance spectroscopy experiments were carried out with a potentiostat AUTOLAB PGSTAT 30. Samples were measured in a three electrode cell

with lithium auxiliary and reference electrodes. A 0.5 M $LiClO_4$ solution and propylencarbonate was used as an electrolyte. The cell was placed into dry box with argon atmosphere.
Cyclic voltammetry (CV) was measured from 0 to 3 V, GPES as measuring software was used. Impedance spectrum of carbon electrodes were acquired after CV always at constant DC potential 2 V in frequency range from 10 kHz to 0.1 Hz.

Results and Discussion

Cyclic voltammetry
Fig. 1 shows two cyclic voltammograms of measured samples (solid line) and calculated capacity per gram (dotted line). Vulcan XC72R reached the highest specific capacity 48 F/g. Interesting is capacity behaviour between 0.5 and 1.5 V. The specific capacity raise to approximately 20 F/g and when the voltage is higher then 1.5V, the capacity fall down (Vulcan M, Vulcan P and Vulcan 6) or increase to 34 F/g (Vulcan 3) and 48 F/g (Vulcan XC72R).

Capacity was calculated by the formula:

$$C = \frac{1}{2} \cdot \frac{\Delta I}{\alpha} \qquad [F] \qquad (1)$$

a)

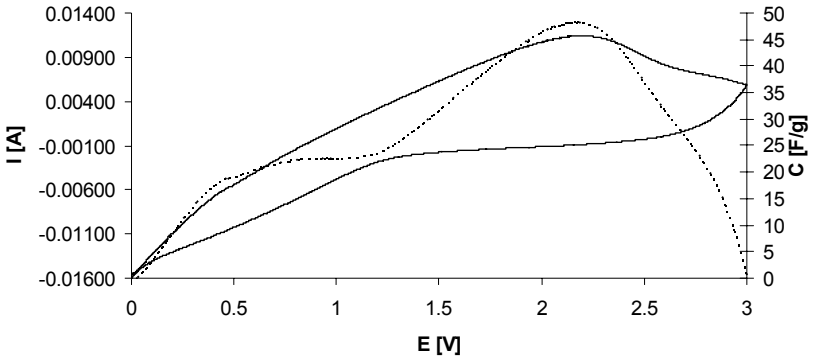

b)

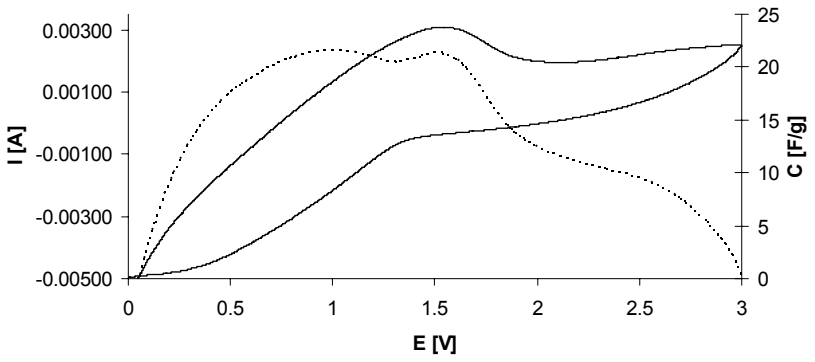

Fig. 1 *Two examples of voltammograms a) Vulcan XC72R and b) Vulcan 6*

Table 1 *The highest reached capacity of measured samples*

Type of material	Specific capacity [F/g]
Vulcan XC72R	48
Vulcan M	20
Vulcan P	20
Vulcan 3	34
Vulcan 6	21

Impedance spectroscopy

In Fig. 2, two Nynquist plots of the experimental electrochemical impedance spectra of Vulcan XC72R and Vulcan 6 are shown. At high frequencies a depressed capacitive semicircle is observed, due to the influence of the porosity on the electrode's AC response.

a) b)

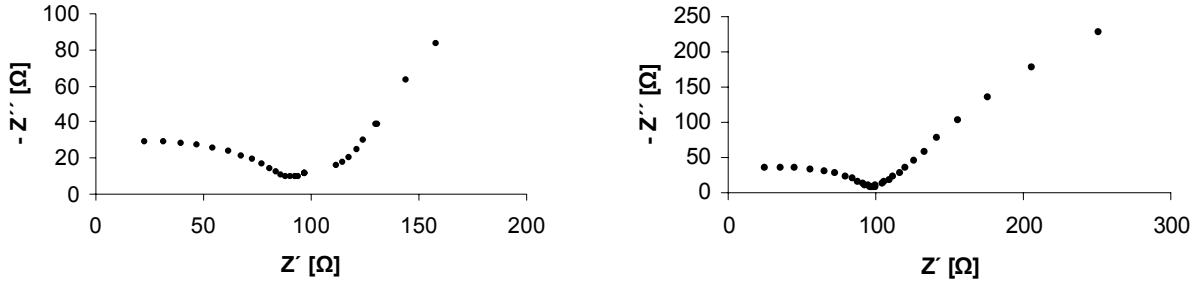

Fig. 2 *Nynquist plots a) Vulcan XC72R, b) Vulcan 6*

To achieving the relevant electrochemical data from the spectra a model describing the porous electrode is necessary. Very advanced model is in [3] (Fig. 3).

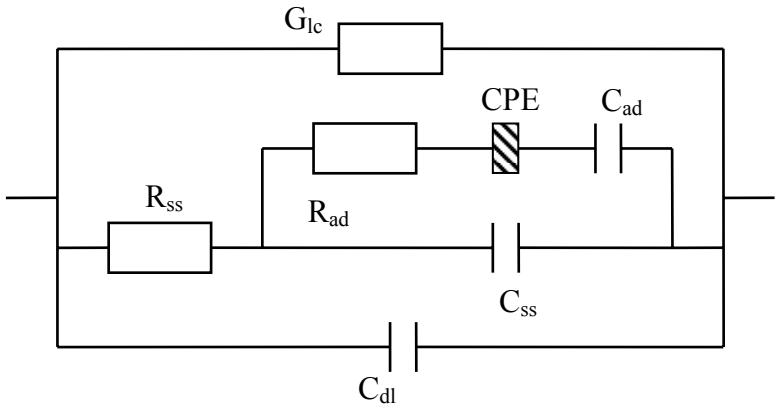

G_{lc} ... leack current conductance
C_{dl} ... double layer capacitance
R_{ss} ... surface state charging resistance
C_{ss} ... surface state charging capacitance
R_{ad} ... adsorption resistance
C_{ad} ... adsorption capacitance
CPE ... constant phase element

Fig. 3 *Electrical equivalent circuit*

To discuss the results summarized in table 2, we start with resistivity and information from datasheets. Vulcan XC72R belongs into group of high conductivity carbon blacks. It explains low values of R_{ss} and R_{ad}. Values of C_{ad} are proportional to number of absorbing "active" surface sites [2]. Vulcan XC72R has the higher value of C_{ad} but other capacities are lower. The good conductivity and higher C_{ad} of the Vulcan XC72R gave

the highest specific capacity calculated from CV. Samples Vulcan M and Vulcan P have higher values of C_{dl} and C_{ss} it could be very interesting to reduce their resistivity.

Table 2 *Parameters of the electrical equivalent circuit*

	Vulcan XC72R	**Vulcan M**	**Vulcan P**	**Vulcan 3**	**Vulcan 6**
G_{lc} [S/g]	0.045	0.057	0.035	0.144	0.044
C_{dl} [F/g]	$2.64 \cdot 10^{-5}$	$5.571 \cdot 10^{-5}$	$6.07 \cdot 10^{-5}$	$2.581 \cdot 10^{-5}$	$3.815 \cdot 10^{-5}$
R_{ss} [Ω/g]	4632	22807	19052	22719	8864
C_{ss} [F/g]	$3.445 \cdot 10^{-4}$	$2.26 \cdot 10^{-3}$	$3.904 \cdot 10^{-3}$	$3.004 \cdot 10^{-4}$	$6.037 \cdot 10^{-4}$
R_{ad} [Ω/g]	1575	6615	3336	13929	3220
C_{ad} [F/g]	2.057	1.305	1.19	1.56	1.765
CPE [S/g]	0.994	0.239	0.53	1.012	0.776
n	0.257	0.616	0.566	0.254	0.561

Conclusions

The cyclic voltammetry and impedance spectroscopy studies were made. It was observed parameters of the electrical equivalent circuit of the high conductive carbon material and other carbon blacks. According to obtained parameters from impedance spectroscopy we can improve carbon black parameters and get higher capacity of supercapacitors.

Acknowledgements

This work was supported by the Ministry of Education (project MSM0021630516).

References

[1] Conway, B.E., *Electrochemical Supercapacitors: Scientific Fundament and Technological Application*, Kluwer Academic, New York, 1999, 698 s, ISBN 0-306-45736-9
[2] F. L. Mantia, J. Vetter, P. Novák: Electrochimica Acta, 53 (2008) 4109
[3] A. G. Pandolfo, A. F. Hollenkamp: J. Power Sources, 157 (2006) 11
[4] P. Simon, A. Burke: Interface, 1 (2008) 38

GALVANIC DEPOSITION OF METALS WITH ELECTROCATALYTIC PROPERTIES

Tomáš Knotek[2], Miroslav Kunovjánek[2], Peter Barath[1,2], Jiří Vondrák [1,2]

[1] Institute of Inorganic Chemistry of the ASCR, v. v. i., 250 68 Řež near Prague, Czech Republic
[2] Institute of Electrotechnology, Technical University of Brno, 602 00 Brno, Czech Republic

Abstract

This work deals with problems of preparations galvanic deposition of metals formation alloys emphasis. Next activation these alloys, first of all alloy Ni-Zn and corrode out their component in hydrochloric acid. End of part deals with check activation galvanic deposition of metals Ni-Zn and found out their electro catalytic properties.

Introduction

This work was created for better understanding to galvanic deposition of metals and electrocatalytic properties of these depositions. This knowledge will by use to create best of electrode for electrolysis tank for hydrogen production.

Experimental

Galvanic deposition was doing in nickel plating bath and plating bath SLOTOLOY ZN 80. First of parts was create samples. Brass was plated with nickel and then with Ni-Zn alloy. Steel only was plated with Ni-Zn alloy and nickel only was plated with Ni-Zn too. We can see sample with theirs alloy in table 1.

Table 1 *Basic materials with their alloys*

Basic material	**Alloy**	**Current density**	**Time**
Brass	Ni + NiZn	Ni-1A/dm^2 + NiZn-2,5 A/dm^2	Ni-5min + NiZn-15min
Steel	NiZn	NiZn-2,5 A/dm^2	NiZn-20min
Nickel	NiZn	NiZn-2,5 A/dm^2	NiZn-15min

Second of part was immersing into hydrochloric acid for 15 second for corrode out zinc components. End of part was preparing for measuring on device AUTOLAB 12 (Eco Chemie) and samples were evaluating with program GPES. The supporting electrolyte was 1M KOH in distilled water. Measuring setup has three parts reference electrode – REF (SCE), counter electrode - CE (Pt) and working electrode - WE (measure sample). Connection diagram is in Fig. 1. Samples were tested in described way by means of cyclic voltammetry.

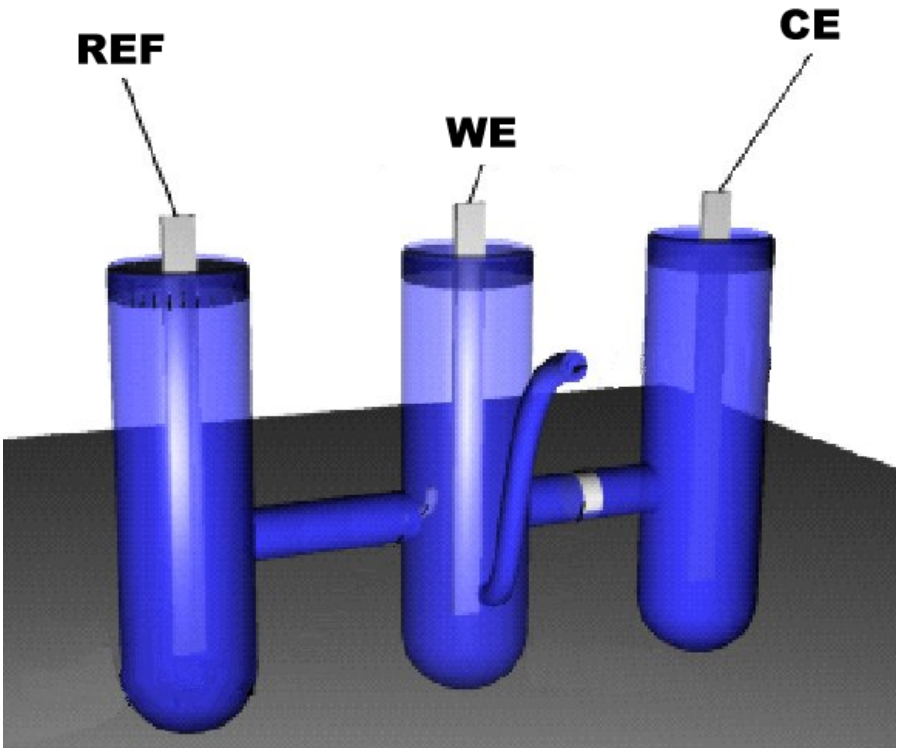

Fig. 1 *Connection diagram*

Results and Discussions

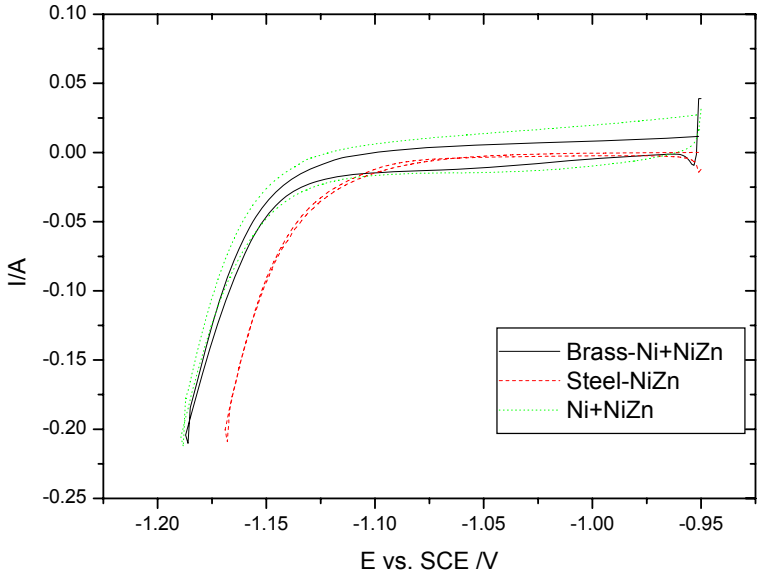

Fig. 2 *Voltage-current curves*

How we can see in graph of all samples, the sample Steel-NiZn is the most acceptable. In this case difference potential before dissolution of zinc component and after it only is 0,1 V. The samples Brass-Ni+NiZn and Nickel-NiZn have very similar curves and difference potential before dissolution of zinc component and after it is about 0,18 – 0,22 V.

Conclusions

Purpose of this work was to create galvanic deposition of metals with electrocatalytic properties. This galvanic deposition will be used to prepare the high efficient electrodes for electrolysis cell for hydrogen production. It is clear, that we can create suitable surface for electrodes. Hence, the reduction of energy by their use is possible.

Acknowledgements

This work was supported by the Ministry of Education, Youth and Sports, Czech Republic (project MSMT 0021630516).

References

[1] KNOTEK, T.: Diplomová práce, Ústav elektrotechnologie VUT, Brno 2007
[2] G. Vatankhah, J. Lessard, G. Jerkiewitz: Electrochimica Acta 48 (2003)1613-1622
[3] Barek J., Opekar F., Štulík K. Elektroanalytická chemie KAROLINUM
[4] Regner A. Elektrochemické pochody v anorganickém průmyslu SNTL

9th ABA

BRNO 2008

Advanced Batteries and Accumulators

Accumulators

ELECTROLYTIC IRON SULFIDES IN LITHIUM POWER SOURCE MODEL WITH PVDF ELECTROLYTES

R. Apostolova[1], L. Neduzhko[1] , S. Samoylov[1], E. Shembel[1, 2]

[1]Ukrainian State Chemical Technology University, Dnepropetrovsk,
[2] Enerize Corporation, Coral_Springs, Fl, USA

Corresponding author: E.Shembel
Tel., Fax:+380562 470391, E-mail: shembel@onil.dp.ua

Introduction

Until recently, iron sulfides (FeS, FeS_2) were used in the cathodes of lithium cells and were tested in mean - and high - temperature lithium secondary battery systems. Under room temperature, insignificant part of the theoretical specific power of natural pyrite (FeS_2) is released in actual lithium chemical power source at cycling together with a solar cell [1]. Besides, iron-sulfide products of electrolysis (e-Fe_xS_y) can be considered as the suitable electrode materials for low-temperature lithium secondary batteries [2, 3]. Their reversible capacity at electrochemical transformation in the electrolyte comprising PC (propylene carbonate), DME (dimethoxyethane), 1 M $LiClO_4$ is 200-320 mAh/g (for the 40-50th cycles). Since for the accident prevention and ecological purity of thin-layer lithium secondary batteries, gel electrolytes are preferable to liquid-phase ones, investigations of thin-layer (e-Fe_xS_y) are continued in the models of lithium chemical power sources with polymer electrolytes based on PVdF-matrix.

Experimental

Iron sulfide compounds with the mass 1-20 mg/cm^2 have been produced on Al foil (10x10, mm) by the cathode reduction of aqueous electrolytes comprising iron sulfate and thiosulfate ions [2]. Charge-discharge cycling of as-prepared Fe-sulfides electrodes was carried out at room temperature by galvanostatic mode using lithium as an anode. For preparation of polymer electrolytes for the models, the following materials were used: 1. Obtained from Solvay (polyvinylidene fluoride) – PVdF Solef 21508 and its co-polymers PVdF-CTFE, Solef 32008/1001, PVdF-HFP Solef 20508; 2. Lithium salts: $LiClO_4$ («Iodobrom», Saki, Ukraine, $LiPF_6$ (Merck), $LiN(CF_3SO_2)_2$ (Aldrich, USA); 3. Solvents: EC (ethylene carbonate, Merck), DMC (dimethyl carbonate, Merck), PC (propylene carbonate, Angara Chemical Reagent Plant, Russia), THF (tetrahydrofurane, Labskan, Ireland), acetone (Merck), n-MP (n-methylpyrrolidone, Labskan, Ireland). Polymer electrolytes (PE) were prepared by watering method. In the case (1), the films of 30-60 μm thickness or gelatinous mass were formed from polymer solution on e-Fe_xS_y-electrode. In the case of the procedure (2), at the beginning, the inert macroporous film (100-150 μm) was produced, then it was activated by electrolyte. Conductivity of PE was evaluated by EIS (electrochemical impedance spectroscopy)

method on the analytical radiometer VoltaLab PJZ301 in the cell with stainless steel electrodes. Galvanostatic cycling of the models was carried out within the voltage range of 2.8-1.1V on a test bench with computer provision at the discharge current density ranging from 25 up to 280 mA/g. Structure of the synthesized compounds was examined by X-ray diffraction analysis (DRON-2).

Results and Discussion

Iron sulfides FeS, FeS_2, Fe_3S_4, Fe_2S_3 are formed in electrolytic deposits. In this work, electrochemically active Fe-sulfide compositions in the reactions with lithium in the models of chemical power sources with liquid-phase electrolyte [2] were investigated in the models with polymer electrolytes. One of the compositions is shown in Fig.1. PE compositions for the models e-Fe_xS_y/Li and their characteristics are shown in Table 1, where L - thickness of PE film, σ – conductivity of PE. The test of PVdF, THF, dioxolane, 1 M $LiN(CF_3SO_2)_2$ electrolyte was also successful [4].

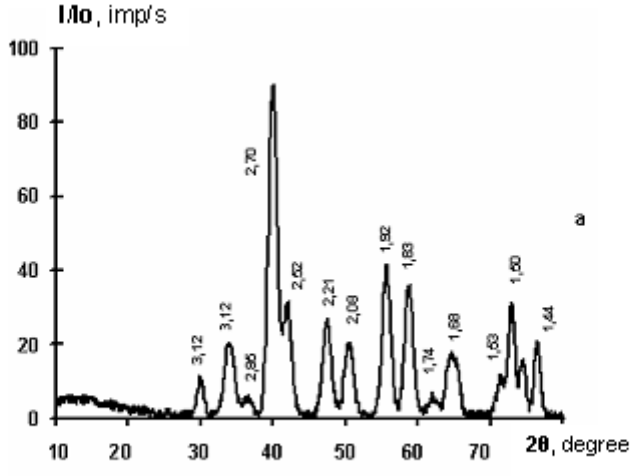

Fig. 1 *X-ray pattern of e-Fe_xS_y. Co-K_α radiation. (FeS_2-pyrite, FeS_2-marcasite, γ-Fe_2O_3.*

Table 1 *Compositions and characteristics of PE*

№ PE	Polymer Grade	Plasticizing solution		State of PE	L, μm	σ, mC/cm	Solvent
		Solvent	Salt				
PE 1(1)	PVdF-CTFE	EC, PC (1:1) volume	$LiClO_4$	Gelatinous mass		1.08	TGF, n-MP
PE 2(1)	PVdF-HFP	EC, DMC (1:1) Vol.	$LiPF_6$	Gelatinous mass		2.04	TGF
PE 3(2)	PVdF-CTFE	Activating solution EC, DMC (1:1 volume.), $LiPF_6$		Film	100-150	0.46	DMF
PE 4(1)	PVdF	EC, DMC (1:1) Vol.	$LiN(CF_3SO_2)_2$	Film	30-60		TGF, Acetone

Significant difference between discharge capacity (Q_p) in the first and subsequent cycles is the common regularity of discharge curves of the models with PE as well as with a liquid-phase electrolyte. In the first cycle, Q_{p1} exceeds 500 mAh /g, reaching 800 mAh/g. The Q_p value drops at cycling and becomes stable after 15-20 cycles. Fig.2 shows evolution of the discharge-charge curves of the model between the 40th and 86th cycles, where active cathode material is characterized by XRD (Fig. 1). At cycling, discharge capacity decreases and its 260 mAh/g value is at the 86th cycle. Discharge capacity loss is 0.2% for a cycle.

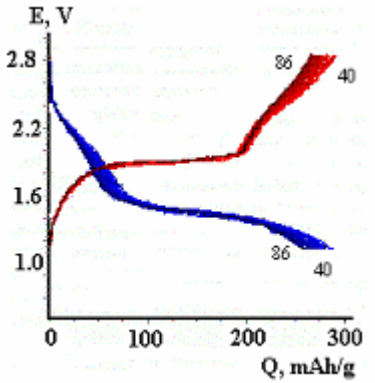

Fig. 2 *Discharge-charge curves of the model based on the composition of FeS_2 (pyrite), FeS_2 (marcasite), γ - Fe_2O_3 (mass m=3.7 mg/cm^2) with PE1(1).$I_{disch.}$=0.05 mA /cm^2, $I_{charge.}$=0.03 mA/cm^2.*

Temperature dependence of model discharge capacity with PE1(1) is determined. Effect of model cooling from 17 up to – 7°C on its discharge capacity is greater than heating from 17 up to 40°C. Discharge capacity decrease is nearly by 2 times greater at indicated temperature lowering. Discharge characteristics of the e-Fe_xS_y /PE 2(1)/Li models are the same as those of the models with PE1 (1). Discharge capacity of the model with PE2 (1) and the cathode material comprising FeS_2 (pyrite), FeS, S equal to 730 mAh/g in the 1st cycle is at the level of 280 mAh/g – in the 110th cycle at 0.05 mA.cm^{-2} current density. Dependence of discharge capacity on the discharge current density is determined, and it is established that 200 mAh/g can be obtained at the end of prolonged cycling at the high discharge rate (300 mA g^{-1}).

In the models based on electrolytic Fe-sulfide composition (FeS_2, FeS, γ -Fe_2O_3), with PE 3, produced by the method (2), discharge capacity decreases from the initial value of about 600 mA h·g^{-1} up to the order of 200 mA h·g^{-1} at the end of cycling.

At the concluding stage of investigation, the models within the dimension of flat real lithium secondary battery, with the cathode size of 30x50 mm were approved. On the surface of Fe-sulfide cathode, the PE4 (1) film with 30-40 μm thickness was formed, and then it was assembled with lithium counter-electrode in the package of laminated aluminum foil followed by package hermetic sealing by hot-pressing. During 125 cycles, the 200 mAh/g discharge capacity of the model was maintained.

The EIS results show that PE conductivity decreases at cycling with decreasing model discharge capacity. Thus, σ value for PE2(1) equal to 2.04 mC/cm before cycling, decreases by 10 and more times after discharge capacity drop up to <50 mA h/g. In this case micro-injection of liquid-phase electrolyte into the model increases σ and Q_p. This can be explained by presentation of PE consisting of two macroscopic phases: polymer and porous space, filled with the solution which properties are close to those of volume

solution. Polymer phase also comprises ions and molecules of solvent, but their individual properties are modified by interaction with polymer matrix. Consumption of liquid electrolyte in PE pores and accumulation of non-conducting interaction products of cathode material and PE can be considered as the factor determining degradation of e-Fe_xS_y /PE/Li system.

Conclusions

We have studied electrolytic iron sulfides as a promising electrode material for lithium secondary batteries with polymer PVdF-electrolytes. Iron – sulfide compositions produced by cathodic reduction of the solutions comprising $FeSO_4$, $Na_2S_2O_3$, in the models of lithium chemical power sources with PVdF electrolytes can be electrochemically transformed within the 2.8-1.1 V range and with the efficiency of 200-280 mAh/g during the 80-180 cycles.

Acknowledgements

The authors acknowledge with thanks the financial support provided by the Ministry of Education and Science of Ukraine *(Contract 42070390).*

References

1. R. Apostolova, E. Shembel. J. Appl. Chem. **68** (1995) 1483-1486. (In Russian).
2. E. Shembel, R. Apostolova, V. Nagirny, A. Baskevich., P. Litvin. Elektrokhimiya **40**. (2004) 843-851. (In Russian).
3. Pat. 67134, UA. Shembel E.M., Nagirny V.M., Apostolova R.D., Novak P.
4. Pat. 60953, UA, 7 H01M 10/24. Shembel E.M., Nagirny V.M., Apostolova R.D., Novak P

MODELING THE PROCESSES OF LI^+ INTERCALATION WITH THE PHASE TRANSITIONS IN THE MATERIALS OF LITHIUM POWER SOURCES

V.Tysyachny[1], R. Apostolova[2], E. Shembel[2,3]

[1]National Metallurgical Academy, Dnepropetrovsk, Ukraine
[2]Ukrainian State Chemical Technology University, Dnepropetrovsk,
[3]Enerize Corporation, Coral Springs, Fl, USA

Corresponding author: E.Shembel
Tel., Fax:+380562 470391, E-mail: shembel@onil.dp.ua

Introduction

To a great extent, the most important technical characteristics of lithium power sources are determined by kinetic and structural processes in the solid phase of electrode materials [1]. The rate of often observed at intercalation slow, poorly reversible phase transformations and connected with them hysteresis of charge/discharge processes influence on the rate, specific capacity and energetic parameters as well as on electrode cycleability. Co-existence of two-phase regions is typical for such widely used electrode materials as $Li_x NiO_2$ [2] $Li_xMn_2O_4$ [3], Li_xC_6 [4], Li_xCoO_2 [5].
Availability of horizontal plateau on OCV-Q curves (open circuit voltage – specific charge) [6,7], sharp peaks on cyclic voltammetry curves at slow potential scanning [5], current increase on the initial sections of curves in the method of potentiostatic impulse titration (PITT) instead of usual current decay in the absence of phase transitions [3,4], value of the parameter of lithium ion interaction in a solid phase equal to less (-4) are the characteristics of the first-order phase transitions in solid phase[6,8].
In two-phase region lithium intercalation is accompanied by moving phase boundary formation, which displacement is often a rate-determining stage of the process.
Mathematical modeling of intercalation processes within one phase is the basis of PITT and GITT (galvanostatic impulse titration) methods for determination of chemical diffusion coefficient [9] and does not present special problem [10]. Description of non-conventional diffusion processes with moving boundary in the systems with phase transformations represents some difficulties. Formal analytical solution can be obtained only for the limited number of similar tasks, for example, in infinite or semi-infinite media [11]. In other cases, e.g, in a finite media or in the media in the form of cylinder or sphere, only approximate solution or those obtained by numerical methods are possible.

In the work, two mathematical models of lithium ion intercalation in the materials of lithium accumulators taking into consideration and without consideration of phase transformations are compared. In the both models intercalation material is considered as a thin flat layer (unlimited plate) deposited on a conducting substrate. It is assumed that within each phase, lithium diffusion coefficients are constant. We neglect molar volume

change at phase transfer, unconventional Li^+ transfer and only diffusion in solid phase is considered as a rate determining process.
The problem of lithium ion intercalation in a two-phase system can be formulated in the following way (Fig.1):

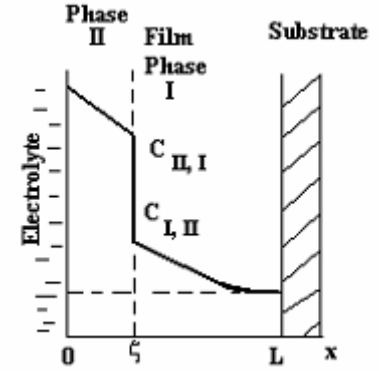

Fig. 1 *Concentration profiles of Li ions in electrode material at potentiostatic intercalation taking into account phase transition.*

$$\frac{\partial C_{II(x,t)}}{\partial t} = D_{II}\frac{\partial^2 C_{II(x,t)}}{\partial x^2} \qquad t\rangle 0, \quad 0\langle x\langle \xi \qquad (1)$$

$$\frac{\partial C_{I(x,t)}}{\partial t} = D_{I}\frac{\partial^2 C_{I(x,t)}}{\partial x^2} \qquad t\rangle 0, \quad c_\infty \rangle x\rangle \xi \qquad (2)$$

Initial condition: $C_{I(x,0)} = C_0$, t=0, $x \geq 0$ (3)

Boundary conditions: $C_{II(0,t)} = C_s$, $t\rangle 0$, $x = 0$ (4)

$$\frac{\partial C_I(L,t)}{\partial x} = 0, \quad t\rangle 0, \quad \text{x= } L \qquad (5)$$

Condition (5) means unavailability of Li^+ diffusion flow at the boundary film - current conducting substrate.

For the moving boundary $x = \xi$ we use the integral condition following from the material balance in accordance with the total quantity of Li^+ ions intercalated for the time "t" in the film:

$$q = (C_{II,I} - C_{I,II})\xi + \int_0^{\xi} C_{II(x,t)}dx + \int_{\xi}^{L} C_{I(x,t)}dx \qquad (6)$$

Quantity of Li^+ introduced during the time unit through a surface at $x = 0$ is:

$$\frac{dq}{dt} = -D_{II}\frac{\partial c_{II(0.t)}}{\partial x} \qquad (7)$$

Equation (6) will be substituted into (7):

$$(C_{II,I} - C_{C_{I,II}})\frac{d\xi}{dt} + \frac{d}{dt}\int_0^{\xi} C_{II(x,t)}dx + \frac{d}{dt}\int_{\xi}^{L} C_{I(x,t)}dx = -D_{II}\frac{\partial C_{II(0,t)}}{\partial x} \qquad (8)$$

Functions of $C_{II.}$ and C_I will be selected so that they satisfy the initial and boundary conditions. For phase II we shall apply linear distribution of concentration:

$$C_{II(x,t)} = C_s - \frac{(C_s - C_{II,I})}{\xi}\cdot x \qquad (9)$$

Equation (9) satisfies the boundary condition (4): at $x = 0$ $C_{II(0,t)} = C_s$.

For phase II we apply parabolic distribution of concentrations:

$$C_{I(x,t)} = C_{I,II} - \frac{\xi}{L}(C_{I,II} - C_0)(1 - \frac{x^2}{\xi^2}), \qquad (10)$$

that satisfies the conditions (3,5). Indeed, near a substrate at $x = L$ in the time moment "t"

$$C_{I(L,t)} = C_{I,II} - \frac{L - \xi}{L}(C_{I,II} - C_0) \qquad (11).$$

At initial moment, at t=0 $\xi = 0$, $C_{I(L,0)} = C_0$, when the boundary will reach a substrate, $\xi = L$ .and $C_{I(L,t)} = C_{I,II}$, as it should be.

Boundary condition (5) is also adhered.

Taking integrals in equation (6) in consideration of (9, 10), we shall obtain the differential equation:

$$(A - B\xi)\frac{d\xi}{dt} = \frac{D_{II}(C_s - C_{II,I})}{\xi}, \qquad (12)$$

where

$$A = \frac{3}{2}C_{II,I} - 2C_{I,II} + \frac{1}{2}C_s + \frac{4}{3}(C_{I,II} - C_0) \qquad (13)$$

$$B = \frac{4(C_{I,II} - C_0)}{3L} \qquad (14)$$

We integrate equation (12):

$$\frac{A}{2}\xi^2 - \frac{B}{3}\xi^3 = D_{II}(C_s - C_{II,I}) \cdot t + const \qquad (15)$$

Integration constant is found from the condition that at t=0. $\xi = 0$, from what ensues constant= 0.

In equation (15) we leave only the ξ^2 members taking into consideration that quadratic shift is proportional to a time:

$$\xi = \sqrt{\frac{2D_{II}(C_s - C_{II,I})}{A}} \cdot t \qquad (16)$$

Diffusion flux through the unit of surface at $x = 0$:

$$j_{x=0} = \sqrt{\frac{AD_{II}(C_s - C_{II,I})}{2t}} \qquad (17)$$

Electric current corresponding to this flux:

$$i = nFj_{x=0} = nF\sqrt{\frac{AD_{II}(C_s - C_{II,I})}{2t}} \qquad (18)$$

From (18) equation it is evident that it $^{1/2}$ is independent on time and it is a constant value, which can be calculated from the experimental values $C_s, C_{II,I}, C_{I,II}, C_0, D_{II}$.

Li^+ intercalation in one-phase limited system for little times $(t \langle\langle \frac{L^2}{D})$ is described by equation [9]:

$$i = nF(C_s - C_0) \cdot \sqrt{\frac{D}{\pi t}}, \qquad (19)$$

in accordance to which it $^{1/2}$ is also a constant value, known as a Cottrell slope.
For the great time intervals (t>> L2) in this case current changes in accordance with:

$$i = \frac{2nF(C_s - C_0)D}{L} \exp(-\frac{\pi^2 Dt}{4L^2}) \qquad (20).$$

From the equations (18, 19) it follows that

$$it^{1/2} = nF\sqrt{\frac{AD_{II}(C_s - C_{II,I})}{2}} \qquad (21)$$

$$it^{1/2} = nF(C_s - C_0)\sqrt{\frac{D}{\pi}}, \qquad (22)$$

In two-phase (equation 21) and one-phase (22) systems in the coordinates it- lg t, the horizontal plateau should be observed, by which value diffusion coefficients can be calculated.

We have calculated the $it^{1/2}$ value using the equations 21 and 22 for the obviously known two-phase system (graphite electrode) by the experimental data of work [4]. From the OCV - specific charge (Q) curve, Q_s=40 mAh/g, Q_0=15 mAh/g, $Q_{II,I}$=36 mAh/g, and according to EIS data $D_{II}=1.10^{-7}$ cm^2/c. Graphite density is recognized as equal to 2,26 g/cm^3 [12]. Calculation by (18) results in $it^{1/2}$ = 0.22 A $cm^{-2}c^{-1/2}$, and by equation (19) for graphite $it^{1/2}$ = 0.037 A $cm^{-2}c^{-1/2}$ i.e. the model of one-phase system gives the value $it^{1/2}$ by 1.7 times greater than two-phase one. Thus, calculation of the diffusion coefficient in the two-phase system by the experimental values of $it^{1/2}$ with the help of equation for the one-phase system (19) will overstate the values.

References

1. J. Desilvestro, O. Haas. J. Electrochem. Soc. **137** (1990) P.5C-22C.
2. M.D. Levi, K. Gamolsky, D. Aurbach, V. Heider, R. Oesten. Electroanal. Chem. **477** (1999) P.32-40.
3. M. D. Levi, K. Gamolsky, D. Aurbach, V. Heider, R. Oesten. J.Electrochem. Soc. **147** (2000) P.25-33.
4. A. Funabiki, M. Inaba, T. Abe, and Z. Ogumi. J. Electrochem. Soc. **146** (1999) P.2443-2448.
5. M. D. Levi, G. Salitra, B. Markovsky, H. Teller, D. Aurbach, V. Heider, and L. Heider. J. Electrochem. Soc. **146** (1999) P.1279-1289.
6. M.A. Vorotyntsev and J.P. Badiali. Electrochim. Acta **39** (1994) P.289-306.
7. W.R. McKinnon. Solid state electrochemistry ed. P.G.Bruce, Chapter 7, Cambridge University Press. 1995. P.163-197.
8. M.D. Levi, D. Aurbach. Electrochim. Acta **45** (1999) P.167-185.
9. W .Weppner, R.A. Huggins. Ann. Rev. Mater. Sci. **8** (1978) P.269-311.
10. V. Tysyachny, E. Shembel, R. Apostolova. Elektrokhimiya **38** (2002) C.883-885. (In Russian).
11. J. Crank. The Mathematics of Diffusion. Oxford Press, London. 1975.421 P.
12. A.C. Fialkov. Carbon, Interlaminar compounds and composites on its basis. M: Aspect Press, 1997, 718 P.

POSSIBILITY OF USING IONIC LIQUIDS WITH GRAPHITE ANODE: CORRELATION BETWEEN ELECTROCHEMICAL AND THERMAL PROPERTIES

Nam-Soon Choi, I.A. Profatilova, Saeweon Roh, Eui-hwan Song

Energy laboratory, Corporate R&D Center, Samsung SDI Co. LTD., 575, Shin-dong, Yeongtong-gu, Suwon-si, Gyeonggi-do 443-731, Republic of Korea

Corresponding author: Irina Profatilova
E-mail: irina.profatilov@samsung.com
Tel: 82-31-210-7571, Fax: 82-31-210-7555

Introduction

Nowadays, rechargeable lithium ion batteries (LIBs) have gained high momentum for its research activities in the field of high power systems. In this respect, reliabilities of LIBs, especially regarding a safety function to inhibit combustion must be improved to realize commercial application.

Over the last decades, graphitized carbon has been used as a major active material for an anode. Along with high specific capacity and superior cycling behavior of carbon anode, low thermal stabilities of lithiated graphite (LiC_6) should be noticed [1, 2]. Lithiated graphite in combination with carbonate-based electrolyte solution can serve as a source of thermal runaway of LIBs.

Ionic liquids are highly attractive for improving the safety of LIBs owing to their unique properties: essentially no vapor pressure, non-flammability, high thermal stability and high ionic conductivity [3]. The formation of unstable solid electrolyte interphase (SEI) layer by the reductive decomposition of ionic liquid on the anode surface restricts their application. Therefore, the appropriate selection of SEI-forming additives is a key factor to guarantee the electrochemical performances of ionic liquid containing electrolytes in LIBs.

We attempted to improve thermal stabilities of lithiated graphite anode by introducing room temperature ionic liquids to electrolyte solution. In addition, electrochemical properties of ionic liquid containing electrolytes with and without additive were investigated.

Experimental

An anode was prepared by casting slurry containing 97 wt % of graphite active material and 3 wt % of polyvinylidene fluoride (PVdF) binder on a copper foil. The resulting

electrode was dried in vacuum for 2 h. N-methyl,N-propylpiperidinium and ethylmethyl imidazolium trifluoromethane sulfonyl imides (MPPp-TFSI and EMI-TFSI respectively) were provided by Toyo-Gosei (Japan). N-Methoxylmethyl-N,N-dimethylethyl (MMDMEA) TFSI was provided by Otsuka-Stella (Japan).

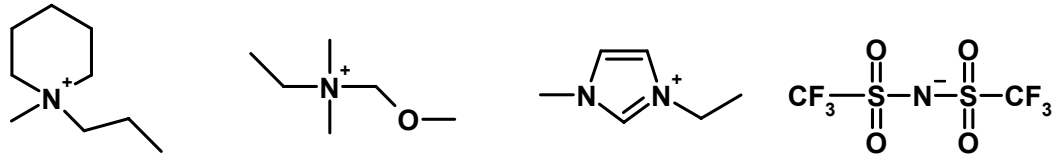

MPPp **MMDMEA** **EMI** **TFSI**

Electrolyte solution compositions are presented in Table 1. Lithium hexaflurophosphate ($LiPF_6$) was used as a salt in all the electrolytes.

Table 1 *Compositions of electrolytes used for cycling tests of coin half cells, initial coulombic efficiency (ICE) at first cycle and exothermic heat evolution in DSC experiments.*

Electrolyte abbreviation	EC (vol %)	EMC (vol %)	Ionic liquid (30 vol %)	FEC (wt %)	ICE (%)	Heat evolution (J/g)
Ref	30	70	-	-	94	435
MPPp_30	21	49	MPPp-TFSI	-	81	372
MPPp_FEC	21	49	MPPp-TFSI	5	92	370
MMDMEA_30	21	49	MMDMEA-TFSI	-	88	331
MMDMEA_FEC	21	49	MMDMEA-TFSI	5	93	321
EMI_30	21	49	EMI-TFSI	-	2	103
EMI_FEC	21	49	EMI-TFSI	5	93	182

Differential scanning calorimetry (DSC) experiments were performed using the DuPont TA model 2000 calorimeter and high-pressure DSC pans (Perkin Elmer). These pans are hermetic steel pans crimped with a gold plated copper seal. DSC scan was performed at a rate of 10 ^{0}C/min to a maximum of 380 ^{0}C to minimize the possibility of over pressurization. The ratio of entrapped electrolyte to graphite active material was 1 : 3.2 by weight.

Results and Discussion

Fig.1 shows differential capacity (dQ/dV) curves for coin half cells with various electrolytes at the first charge in a range from 0.1 to 1.2 V. This potential window mainly corresponds to the SEI layer. The dQ/dV curve for reference electrolyte (Ref) is shown in all the graphs, demonstrating the effect of ionic liquid on electrochemical properties of graphite. In the absence of ionic liquid, the reduction peak of SEI layer appears around 0.45 V apparently due to the electrochemical reduction of ethylene carbonate (EC) (Fig. 1, gray curve). Introduction of MPPp-TFSI to an electrolyte solution results in the intensive peak appearance at 0.48 V, which can be attributed to its reductive decomposition (Fig. 1(a)). The reduction of fluoroethylene carbonate (FEC) additive

occurs at 0.55 V. This indicates that stable SEI layer was formed preventing the reductive decomposition of MPPp-TFSI ionic liquid (Fig. 1(a)).

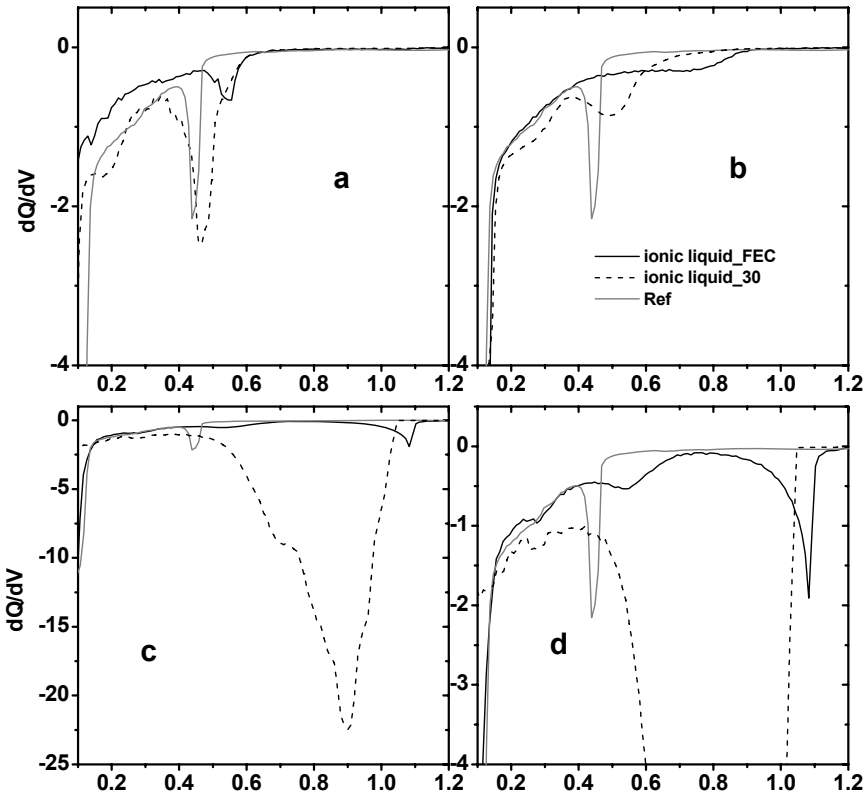

Fig. 1 *Differential capacity versus voltage at 1st cycle of coin half cells with electrolyte solutions containing (a) MPPp-TFSI; (b) MMDMEA-TFSI; (c) EMI-TFSI; (d) enlargement of graph (c).*

Similar effect was observed for MMDMEA_30 and MMDMEA_FEC electrolytes, as shown in Fig. 1(b). In the case of EMI_30 electrolyte, extremely intensive reductive decomposition was shown, as a result of poor electrochemical stability of EMI-TFSI. The reduction peak corresponding to EMI-TFSI decomposition was eliminated by using FEC additive in Fig. 1 (c) and (d).

The ICEs (Table 1) of coin half cells containing ionic liquid were improved by the introduction of FEC additive. It is likely that FEC additive increases the reversible capacity of graphite at the first cycle due to the formation of an electrochemically stable SEI layer.

Thermal interactions between fully lithiated graphite anodes and electrolyte solutions listed in Table 1 were measured by differential scanning calorimetry (DSC). A comparison of DSC profiles for all the electrolyte compositions is shown in Fig. 2. There is a common tendency for electrolyte solutions MPPp_30 and EMI_30: onset temperatures of the first exothermic peak are shifted to lower value compared to Ref electrolyte. This implies that the SEI layer, derived from decomposition of ionic liquid is thermally unstable.

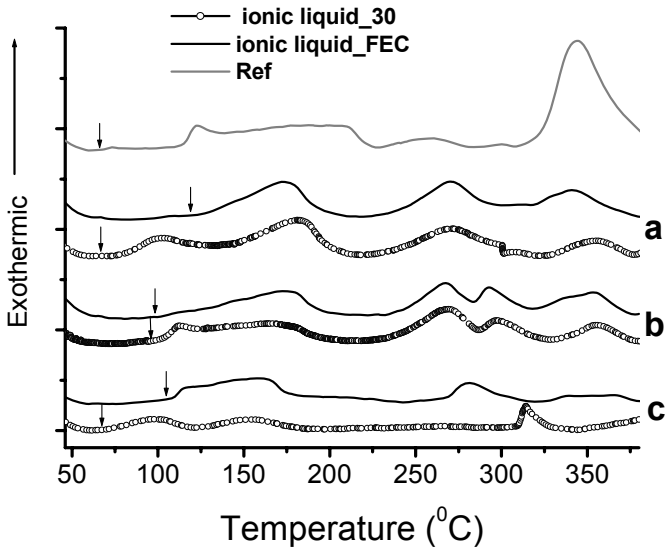

Fig. 2 *Differential scanning calorimetry (DSC) curves of the hermetic cells containing 100% lithiated graphite and ionic liquid based electrolyte solutions (a) MPPp-TFSI; (b) MMDMEA-TFSI; (c) EMI-TFSI. The onset temperatures of the first exothermic peaks are marked by arrows.*

In the presence of FEC additive, the onset temperature of the first exothermic peaks delayed and total heat evolutions were reduced (Fig. 2, Table 1).

Conclusions

Electrochemical and thermal properties of electrolyte solutions containing 30 vol % of ionic liquids were investigated. The reductive decomposition of ionic liquid resulted in the formation of electrochemically and thermally unstable SEI layer. Introduction of 5 wt % FEC to electrolyte solutions drastically improved both ICE values and thermal reactivities between lithiated graphite active material and electrolyte.

References

1. M. Richard, J. Dahn: J. Electrochem. Soc. 146 (1999) 2068.
2. J. Jiang, J. Dahn: Electrochim. Acta 49 (2004) 4599.
3. M. Gali´nski, A. Lewandowski, I. Stepniak: Electrochim. Acta 51 (2006) 5567.

CHEMICAL AND ELECTROCHEMICAL STABILITY OF SOLID STATE GLASSY INORGANIC ELECTROLYTE BASED ON THE SYSTEM LI_2O-LIF-P_2O_5

Elena Shembel[1,2], Alexander Nosenko[1], Artur Tron[1]

[1] Research laboratory of chemical power sources (NILhit), Ukrainian State Chemical-Technology Universality, 49005, 8, Gagarin Ave., Dnipropetrovs'k, Ukraine
[2] Enerize Corporation, Coral Springs, Fl, USA

Corresponding author: Elena Shembel
E-mail: shembel@onil.dp.ua
Phone, fax: +38 (0562) 47-03-91

Introduction

Inorganic glassy solid state electrolytes (GSE) suitable for application in lithium chemical power sources (CPS), as a minimum should satisfy for the following requirements:

- High ionic and low electronic conductivity;
- Chemical stability in the contact with electrode and constructional materials of lithium CPS;
- Electrochemical stability;
- Productivity

In this case, the chemical and electrochemical stability of GSE is one of the basic properties [1-4], therefore, their evaluation is necessary for solving the technological problems of these material application in lithium CPS.
According to [11,12], the satisfactory thermal chemical stability of the system of «GSE – metal lithium», on the whole, raises doubts due to the exceptional high reactivity of metal lithium.
In the works [5-7] there is shown the promising application of the glassy solid state electrolytes based on Li_2O-LiF-P_2O_5 system in lithium CPS. The electrical properties of such materials have been partially studied in [8-10]. However, the experimental data regarding their electrochemical and chemical stability are either not numerous or completely absent in the available literature.
This work is aimed at the evaluation of chemical and electrochemical stability of glassy solid state electrolyte in the Li_2O-LiF-P_2O_5 system relative to metal lithium.

Experimental

Glassy solid state electrolyte in the system Li_2O-LiF-P_2O_5 [5-7] was synthesized at the temperature up to 1000°C and was made in the shape of thin plates with the thickness up to 200 μm by the rolling method through the massive metal rollers.

Material samples were investigated by the method of X-ray phase analysis (DRON-3,0 in Co-K_α radiation , 35 kW, 10 mA).
The experimental samples from the synthesized glass for determination of its chemical stability relative to lithium were fabricated in the form of Ø25 mm discs with 3 mm thickness. The production technology included the following operations: glass plate grinding in agate mortar, wetting the produced coarse powder, pressing the samples in a metal mold (P=500 κG/cm^2), drying in the medium of dewatered argon at the temperature below by 10^{o}C than the temperature of glass softening (softening point) beginning.
After drying the sample was placed into the box filled with a dried argon, and was strongly gripped in clamp between the plates of non-metal lithium. Time of contact was 48 hours.
X-ray phase analysis of the sample surface before and past the contact with metal lithium was investigated with the help of X=ray plant DRON-3.0 in Co-K_α radiation (35kW, 10mA). The degree of surface degradation was evaluated with the help of optical microscope.
Electrochemical stability of GSE was determined by the method of cycling voltammetry. Cycling interval was 0,0÷4,5 V relatively to Li°/Li$^+$ at the potential scanning rate 0,5 mV·s^{-1}. For comparison and analysis, the background potentiodynamic characteristics of the electrode without solid electrolyte were determined.

Results and discussion

As a result of carried out thermodynamic calculations, stability of lithium phosphates relatively metal lithium rises at Li_2O/P_2O_5 ratio increase. At the ratio $Li_2O/P_2O_5 \geq 2$, the isobar isothermal potential of lithium phosphate reduction reactions takes positive values.

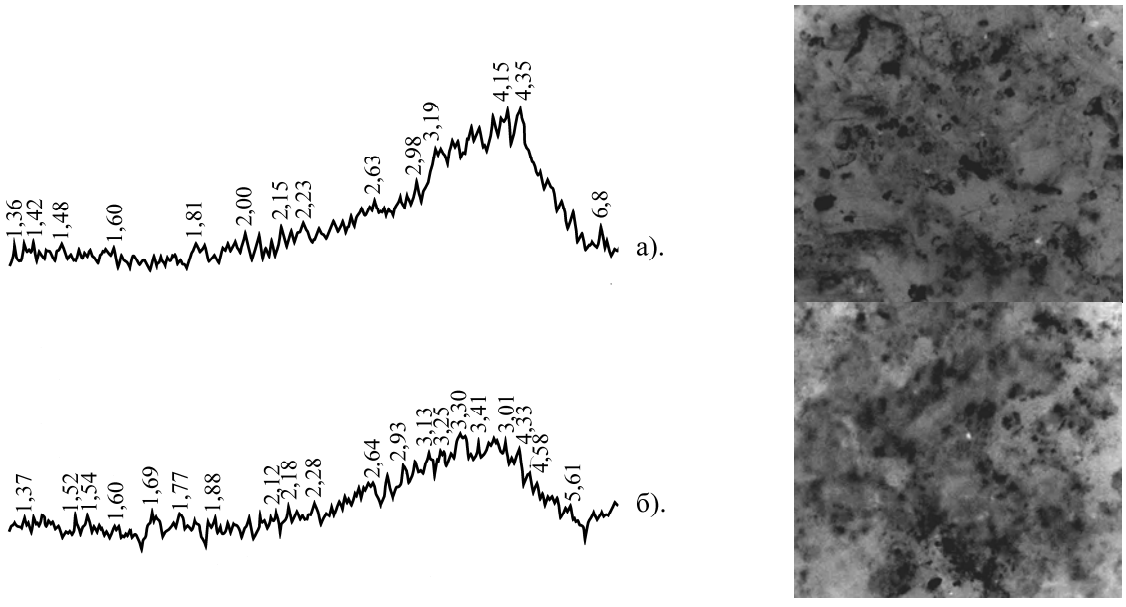

Fig. 1 *X-ray and micro- photographs of the surface of GSE sample in the system of Li_2O-LiF-P_2O_5 before (a) and after (b) the contact with metal lithium (48 hours)*

For the experimental control of thermal dynamic calculations, the surface of samples from glassy GSE in the system of Li_2O-LiF-P_2O_5 (Li_2O/P_2O_5 > 1) before and past the contact with metal lithium was investigated by the method of X-ray phase analysis (XRPA).
On the X-ray photograph of the sample surfaces from the produced material (Fig. 1-a), the very slight (as compared with a background) diffraction maximum of crystal lithium phosphate were identified [13].

Comparative analysis of X-ray and micro photographs of the sample surface before and after the contact (Fig.1-b) with metal lithium has shown their absolute identity. The fact that surface of metal lithium after a contact was shining is the indirect confirmation of the interaction absence between glass and metal lithium.
Electrochemical stability or the "electrochemical window" of solid electrolytes within the working potential range of lithium CPS [1-4] retains its stability, which is the important property at their use.
Absence of the additional peaks on the voltammetry characteristic for the electrode coated with GSE layer (Fig. 2-a) as compared with the electrode without it (Fig.2-b), is the indication of GSE electrochemical stability.

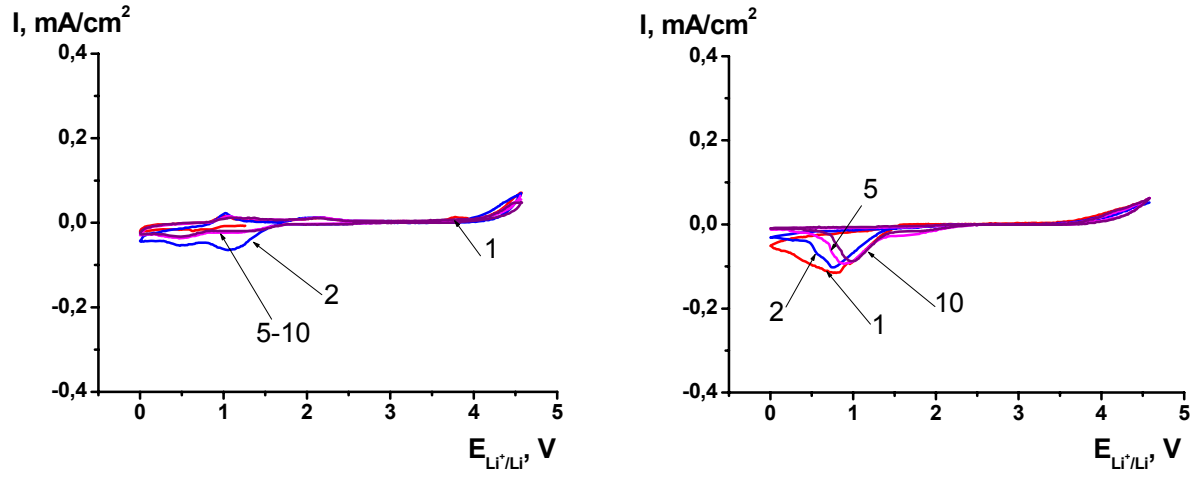

a). b).

Fig. 2 *Potentiodynamic characteristics of stainless-steel electrode coated with the thin layer of GSE (Fig. 2-a) and without it (Fig.2-b). Potential scanning rate is 0,5 mV·s^{-1}. Numerals on curves correspond to a cycle number. SS – stainless steel (12X18H10T).*

Analysis of electrode potentiodynamic characteristics (Fig.2) of the stainless steel electrode coated with the 20μm thickness layer of TEL (Fig.2-a) and without it (Fig.2-b) has shown that during cycling decreasing the current flowing through a cell takes place.
On the potentiodynamic characteristics the cells with GSE, appearance of the new peaks corresponding to the electrochemical reactions at the stainless steel / solid electrolyte interface is not noted. The value of current peaks in the cells with GSE is by 2-3 times lower as compared with the stainless steel electrode in a liquid electrolyte.

The experimental data of galvanostatic cycling of the electrode coated with solid electrolyte layer show the practical absence of solid state electrolyte electrochemical activity.

Conclusions

Chemical stability of GSE in the system of Li_2O-LiF-P_2O_5 ($Li_2O/P_2O_5 > 1$) regarding metal lithium has been established by the calculation and experimental methods.
The results of cycling voltammetry and galvanostatic cycling have shown the electrochemical stability of solid state electrolyte within the potential range of 0,0 - 4,5 V against lithium reference electrode
The obtained multi-lithium glassy ТЭЛ in the system Li_2O-LiF-P_2O_5 can be used in solid state lithium and lithium ion CPS.

References

1. Hayashi A., Tatsumisago M., Minami T.: J. Electrochem. Soc. 1999. 146 (9). P. 3472-3475.
2. Takada K., Aotani N., Iwamoto K., Kondo S.: Solid State Ionics. 1996. 86-88. P. 877-882.
3. Minami T., Hayashi A., Tatsumisago M.: Solid State Ionics. 2000. 136-137. P. 1015-1023.
4. Nosenko A.V., Kvasha A.M., Shembel E.M.: Problems of chemistry and chemical technology, 2003. №5. P. 149-154.
5. Julien C., Nazri G.A.: Kluwer Academic publishers, 1994. 625 c.
6. A.V. Tron', E.M. Shembel, A.V. Nosenko: Abstracts, The 2-nd All-Ukrainian scientific-practical conference of students, post-graduated students and young scientists. Kiev, 2007, P.59.
7. A.V. Tron', E.M. Shembel, A.V. Nosenko: Problems of chemistry and chemical technology, (in press)
8. Sokolov I.A., Ustinov N.Yu., Pronkin A.A.: Journal of Applied Chemistry, 2006. Vol. 79, Issue. 1. P. 346.
9. I.A. Sokolov, Il'in A.A., Valova N.A. et al: Physics and chemistry of glass, 2003. Vol. 29, № 3. P. 421-427.
10. Kedrinsky I.A., Dmitrenko V.E., Povarov Yu.M., Grudyanov I.I.: Krasnoyarsk: Publsh. By Rrasnoyarsk Univ., 1983. 243 P.
11. Andreyev O.L.: Abstr. Of Cand. Dis.: 02.00.04. Yekaterinoburgh/, 2002. 22 P.
12. Published by the American Society for testing materials (ASTM). Philadelphia.

IMPROVING LITHIUM BATTERIES BY CONDUCTING POLYPYRROLE

Andrea Fedorková[1], Hans-Dieter Wiemhöfer[2], Renáta Oriňáková[3], Andrej Oriňák[3], Alan Majerník[4], Dušan Kaniansky[1]

[1]Department of Analytical Chemistry, Faculty of Science, Comenius University, Mlynská Dolina,SK-842 15 Bratislava 4, Slovak Republic
[2]Department of Inorganic and Analytical Chemistry, Westfälische Wilhelms University, Corrensstrase 30, 481 49 Münster, Germany
[3]Institute of Chemistry, Faculty of Science, P.J. Šafárik University, Moyzesova 11, SK-04154 Košice, Slovak Republic
[4]Institute of Animal Biochemistry and Genetic SAS, Moyzesova 61, SK-90028 Ivanka pri Dunaji, Slovak Republic

Corresponding author, Phone: +421-55-2342327, Fax: +421-55-6222124,
E-mail address: fedorkova@fns.uniba.sk

Introduction

Electroactive conducting polymers (ECPs) are conjugated polymers that exhibit electronic conduction when partially oxidized or reduced and are capable of undergoing oxidation/reduction reactions [1]. Examples of ECPs include polypyrrole (PPy), polyaniline, polytiophene and polyphenylenevinylene. Polypyrrole is a polymer which also acts as a host material for Li^+-ion insertion/extraction in the voltage range of 2.0 – 4.5 V versus Li/Li^+, with a theoretical capacity of 72 mAh/g [2]. Therefore, PPy additives can be used as both conductive agents and cathode materials. The principal problems with a practical utilization of conducting polymers like polypyrrole include its poor mechanical properties like brittleness and low processibility. Blending insulating polymers is an attractive route to improve their mechanical properties without loosing their conductivity [3].
Recently, $FePO_4$ has been introduced as a promising material for low cost lithium batteries. The material is environmentally benign, inexpensive, nontoxic and is characterized by a high theoretical specific capacity 178 Ah/kg [4]. Due to its properties this material shows to be an excellent candidate for the cathode of a low-power, rechargeable lithium battery [5]. Usually, thin films of PPy were obtained by electrochemical synthesis and powders (named as pyrrole black) by chemical oxidative polymerizations.
Electrochemical polymerization is most often carried out at noble metal electrodes such as gold or platinum or sometimes at carbon electrodes. The direct electrochemical polymerization of pyrrole at active metal electrodes such as steel or aluminum is complicated by the oxidation (corrosion) of the metal at the positive potentials required for polymerization [1].
In this paper, we describe the direct electrodeposition of polypyrrole from non-aqueous media (PC, DMC) focusing on its electrochemical behaviour as well the polypyrrole

synthesized by simple oxidative polymerization on the $FePO_4$ powder. The electrochemical properties of PPy films were investigated by cyclic voltammetry and EIS. The next step in our research is preparation of polypyrrole coated $FePO_4$ and $LiFePO_4$ composite materials and its systematic characterization.

Experimental

Aluminum foil (0.25 mm thick, 99.99%) was purchased from Alfa-Aesar. Propylene carbonate (PC), dimethyl carbobante (DMC) and pyrrole (Py) were purchased from Alfa-Aesar. The electrodeposition solution contained 0.1 M or 0.2 M pyrrole, PC and DMC (1:1). Electrochemical polymerization was performed in three-electrode cell having an aluminum working electrode, a platinum plate counter electrode and an Ag/AgCl reference electrode. The polypyrrole films were electrodeposited using potentiostat Ecastat, (Istran, Bratislava). All the experiments were carried out in glove box (Forma Scientific, Anaerobic system 1024) with nitrogene atmosphere containing 4 % of hydrogen at room temperature.
80 % active material ($FePO_4$+PPy) and 20 % polyvinylidene fluoride (PVdF) binder in *N*-methylpyrrolidone (NMP) were homogeneously mixed. Resulting slurry was coated onto Al foil. After solvent evaporation, the electrodes were punched in the form of disk. Electrochemical properties of the active material were evaluated via coin cell containing 1M lithium bis(oxalato)borate / PC+DMC (1:1 in volume) electrolyte. The coin cell was assembled in glove box. Lithium foil was used as anode and polypropylene film was used as a separator. Cyclic voltammograms were recorded between 2 and 4 V. The electrochemical tests were carried out at room temperature.

Results and discussion

Polypyrrole was synthesized by electrochemical polymerization from non-aqueous solution.

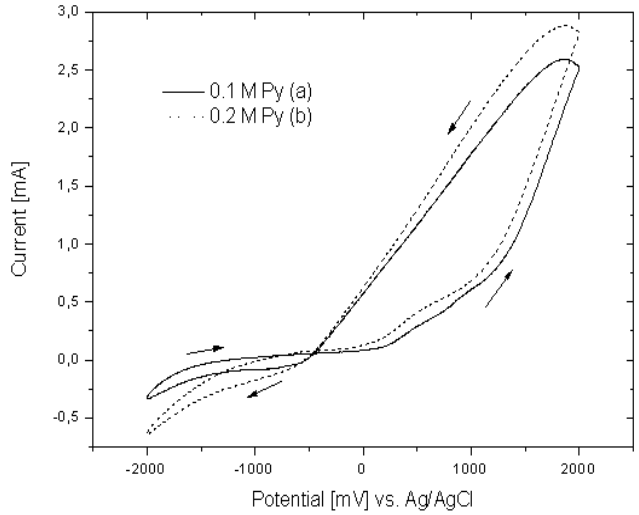

Fig. 1 *Cyclic voltammograms for PPy film electrodeposition from (a) 0.1 M Py, (b) 0.2 M Py solution at scan rate of 50 mV/s. All voltammograms were recorded after 10 CV scans in the same potential range -2 V → +2 V→ -2 V.*

Fig.1 shows the comparison between two voltammetry plots obtained during the anodic growth of the PPy film for different concentrations of monomer. The higher current intensity was observed for solution with higher Py concentration. The PPy films synthesized in nonaqueous media are more conductive than those synthesized in aqueous solutions [6].
From the plots in Fig. 2, which shows cyclic voltammograms for different scan rates, it can be seen that the area under the oxidation part of all plots grows due to an increase in the overall amount of charge passed during the process. The oxidation potential changes in negative direction with the increase in polarisation rate.

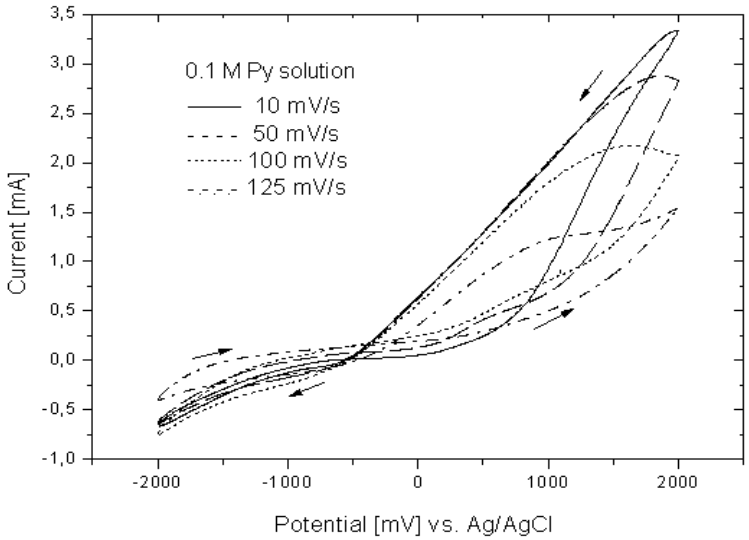

Fig. 2 *Cyclic voltammogramms for PPy film electrodeposition from 0.1 M Py solution at different scan rates. All voltammogramms were recorded after 10 CV scans in the same potential range -2 V → +2 V→ -2 V.*

The oxidative polymerization of pyrrole by hydrogen peroxide in aqueous HBF_4 medium as the regenerator was applied for the direct preparation of polypyrrole-$FePO_4$ composite powder [7, 8]. The impedance measurements were carried out in order to obtain more electrochemical parameters on studied PPy-$FePO_4$ samples.

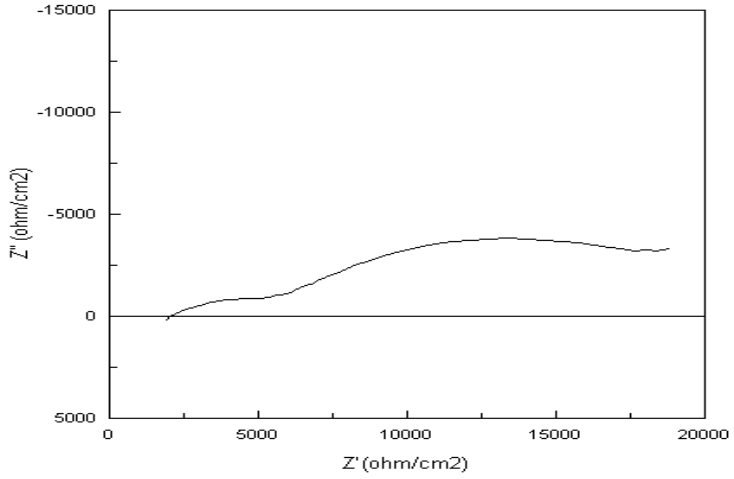

Fig. 3 *AC impedance spectra of $FePO_4$ + PPy electrode.*

The typical impedance diagram is shown in Fig. 3 for PPy-$FePO_4$ cathode prepared from powder synthesized by oxidative polymerization of pyrrole monomer on the surface of $FePO_4$ particles. The electrochemical response at higher frequencies consists in a semicircle, which could be associated to intergrain resistance. The response at the middle frequency region could be related to the electronic conductivity of the electrode.

Electrochemical behaviour of $FePO_4$-PPy samples was examined by cyclic voltammetry. A comparison of cyclic voltammograms for $FePO_4$-PPy and for untreated $FePO_4$ also proved that PPy presence in $FePO_4$ increases the conductivity and electrochemical activity of composite material.

Conclusions

Polypyrrole films were electrodeposited from nonaqueous solution containing pyrrole and its electrochemical behaviour was studied. An improved and at the same time simplified oxidative polymerization of PPy directly on $FePO_4$ powder, exploring its catalytic effect, shown to yield PPy-$FePO_4$ composite material with a highly conducting PPy network without any other doppants. It was found from voltammetry plots and impedance measurements that the PPy coating efficiently improves the electronic conductivity as well the electrochemical activity of studied materials.

Aknowledgements

We acknowledge the financial support from DAAD (grant No. 03042007/SMS) and Slovak Grant Agency VEGA (grant No. 1/0043/08).

References

1. D.E. Tallman, C. Vang, G.G. Wallace, G.P. Bierwagen: J. Electrochem. Soc. **149** (3) (2002) C173.
2. T. Osaka, T. Momma, K. Nishimura, S. Kakuda, T. Ishii: J. Electrochem. Soc. **141** (1994) 1994.
3. A. Kassim, H.N.M. Ekarmul Mahmud, L.M. Yee, N. Hanipah: Pacific J. Sci. Technol. **7** (2) (2006) 103.
4. F. Croce, A. D'Epifanio, P. Reale, L. Settimi, B. Scrosati: J. Electrochem. Soc. **150** (5) (2003) A576.
5. A. K. Padhi, K. S. Nanjundaswahi, J. B. Goodenough: J. Electrochem. Soc. **144** (4) (1997) 1188.
6. J. Arjomandi, R. Holze: J. Solid State Electrochem. **11** (8) (2007) 1093.
7. H.V. Rasika Dias, M. Fianchini, R.M. Gamini Rajapakse: Polymer **47** (2006) 7349.
8. A. Fedorková, H.D. Wiemhöfer, R. Oriňáková, A. Oriňák: 8th International Conference Advanced batteries and accumulators [A.B.A.-8], June 2007,Brno, Czech Republic.

NOVEL FUNCTIONAL CO-SOLVENT/ADDITIVE FOR LI-ION BATTERIES BASED ON SILANE COMPOUNDS

Mariusz Walkowiak [1], Daniel Waszak [1], Błażej Gierczyk [2], Grzegorz Schroeder [2]

[1] Institute of Non-Ferrous Metals Branch in Poznań Central Laboratory of Batteries and Cells, Forteczna 12, 61-362 Poznań, Poland
[2] Faculty of Chemistry, A. Mickiewicz University, Grunwaldzka 6, 60-780 Poznań, Poland

Corresponding author: M. Walkowiak
E-mail: walkowiak@claio.poznan.pl
Tel: +48 61 8793153

Introduction

Electrolytes for Li-ion batteries based on ethylene carbonate (EC) as film-forming component are today a technological standard. This particular solvent, however, in known to have certain inherent limitations, such as poor low-temperature behavior. On the other hand, propylene carbonate (PC), a potential alternative for EC, is incompatible with graphite anodes in terms of effective solid electrolyte interphase (SEI) formation. This is due to the phenomenons of solvent co-intercalation and graphite flakes exfoliation that occur upon first charging of graphite in PC. Strategies to overcome this problem include the application of suitable electrolyte additives or graphite surface modifications [1-6]. The presented work reports the application of new film-forming additive for PC (labelled as Additive A), based on podand-type silane compounds.

Experimental

Additive A has been prepared using the hydrosilylation reaction (see scheme below). The starting hydrosilane compound – 1,1,3,3-tetramethyldisiloxane (1 mmol) was dissolved in dry benzene (150 cm^3) and the stoichiometric amount of polyethylene glycol allyl methyl ether (average mol mass about 300 u; n = 3-7) was added. To the vigorously stirred mixture obtained, the catalyst (1,3-divinyl-1,1,3,3-tetramethyldisiloxane-platinium(0) complex - Karstedt catalyst) was added (0.2 mol% per 1 mol of SiH bond). The solution was heated under inert atmosphere at 50ºC until no allyl and SiH hydrogen atoms were detected (1H NMR), which happened after 60-100 h. Then the reaction mixture was filtered thought Celite and the solvent was evaporated in vacuum. The product was obtained as a slightly yellow liquid and was used for further experiments without purification (purity ~ 92-95%, NMR; yield 95%).

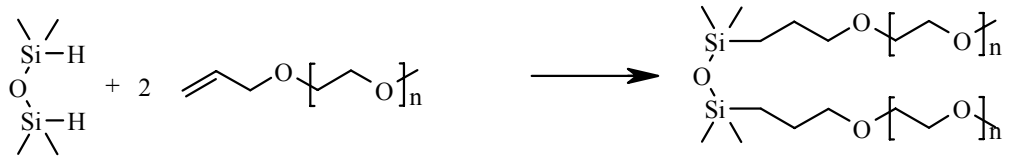

Electrolytes have been prepared by dissolving $LiPF_6$ (Aldrich, 99.99 %) in a mixture of propylene carbonate (Merck, 99.7 %, anhydrous) and the additive (10 % by weight). The electrolyte preparation was carried out in a glove box filled with dry argon (water content less than 20 ppm). For examination of the electrolyte behaviour during cathodic reduction highly crystalline SL-20 graphite (Superior Graphite Co.) was used as anode active material. The electrodes were prepared by applying a slurry consisting of the graphite and PVdF binder (5% w/w, Fluka) onto a copper foil current collector, followed by drying overnight in vacuum at 120 ºC. The graphite electrode and lithium foil counter electrode were sandwiched with a polypropylene separator (Celgard) and the whole stack was placed in a two-electrode Swagelok-type cell, followed by filling the cell by an excess of the investigated electrolyte composition. The cells were cycled galvanostatically at 10 mA per gram of active electrode mass in the voltage range 0 – 2 V vs Li/Li^+.

Results and Discussion

Fig. 1 shows galvanostatic curves recorded for graphite in electrolytes comprising PC as the main solvent and Additive A in three weight ratios. It is evident that in all cases intercalation of lithium into graphite occurs, however there is a clear evolution of elctrochemical behaviours with the best result observed for 15% of additive. The most pronounced differences can be observedin parts of galvanostatic characteristics responsible for SEI formation. For 5% of additive, there is still an important exfoliation-like behaviour, which is reflected in enormous irreversible charge between ca. 0.8 and 0.2 V. Traces of this pattern are still visible for 10% of additive, whereas in case of 15% of Additive A an effective SEI formation can be seen and the galvanostatic characteristics are close to these usually recorded for conventional Li-ion battery electrolytes.

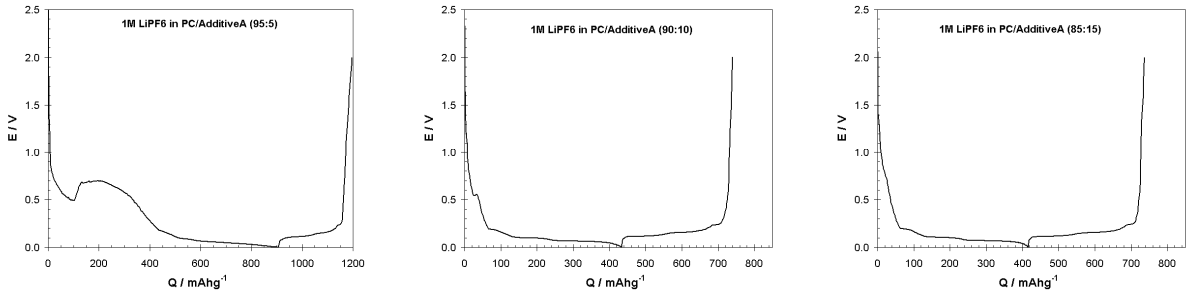

Fig. 1 *Galvanostatic charge/discharge curves in the first cycles recorded for graphite electrode in PC-based electrolytes with Additive A*

Numerical data collected in Table 1 confirm that the most beneficial effect of additive is observed for the highest content. In this case the reversible capacity of graphite reaches standard value of ca. 320 mAh/g, and efficiency of charging in the first cycle reaches maximum.

Table 1 *Basic electrochemical parameters of graphite anode charged/discharged in PC-based electrolytes with AdditiveA*

	First charge [mAh/g]	*First discharge [mAh/g]*	*Efficiency in the first cycle [%]*
1M LiPF6 in PC		*Not working*	
1M LiPF6 in PC/AdditiveA (5%)	*908*	*289*	*32*
1M LiPF6 in PC/ AdditiveA (10%)	*434*	*306*	*71*
1M LiPF6 in PC/ AdditiveA (15%)	*417*	*321*	*77*

Electrochemical data are supported by SEM analysis of graphite after cycling. In case of 5% of Additive A multiple splitting of graphite flakes can by seen, unlike in the case of 10% and 15%.

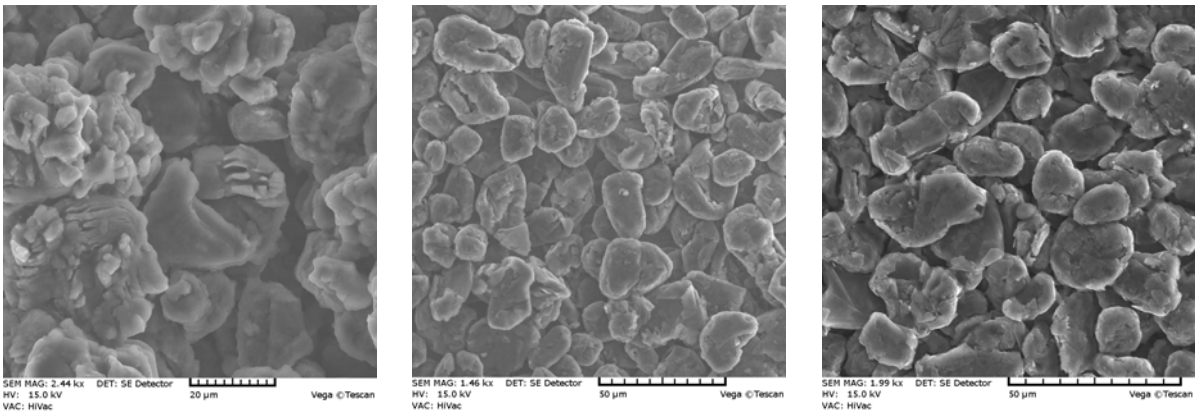

Fig. 2 *SEM micrographs taken from graphite anodes cycled in PC-based electrolytes with Additive A: left - 5%, middle - 10%, right - 15%.*

Conclusions

New silane additive for PC-based Li-ion battery electrolytes has been reported. The additive suppresses detrimental PC co-intercalation, enabling efficient SEI formation and reversible lithium intercalation into graphite. The beneficial action of Additive A depends on its content, with the best results observed for 15% content.

Acknowledgements

The authors gratefully acknowledge the financial support from the Ministry of Science and Higher Education of Poland, Grant No ERA-NET MNT/93/22006. The authors would

also like to thank all the MNT-ERA-Net project NANOLION partners, in particular Dr Petr Krtil and Dr Iratxe de Meatza, for fruitful discussions.

References

1. R. Oesten, U. Heider, M. Schmidt, Solid State Ionics 148 (2002) 391.
2. D. Aurbach, K. Gamolsky, B. Markovsky,Y. Gofer,M. Schmidt, U. Heider, Electrochim. Acta 47 (2002) 1423.
3. G. Schroeder, B. Gierczyk, D.Waszak, M.Walkowiak, Electrochem. Commun. 8 (2006) 1583.
4. G. Schroeder, B. Gierczyk, D.Waszak, M. Kopczyk, M.Walkowiak, Electrochem. Commun. 8 (2006) 523.
5. J. Gao, L.J. Fu, , H.P. Zhang, L.C. Yang, Y.P. Wu, Electrochim. Acta 53 (2008) 2376.
6. J. Gao, H.P. Zhang, T. Zhang, Y.P. Wu, R. Holze, Solid State Ionics 178 (2007) 1225.

STUDIES OF DOPED NEGATIVE VRLA BATTERY ELECTRODES

K. Micka[*], *M. Calábek, R. Bilko, P. Bača, P. Křivík, R. Lábus*

Department of Electrotechnology, Technical University, 602 00 Brno, Czech Republic
**J. Heyrovský Institute of Physical Chemistry, 182 23 Prague 8, Czech Republic*

Abstract

In our previous paper [1], we have discussed in detail the phenomenon of suppressed sulfation of negative lead-acid battery electrodes in the presence of powdered graphite and titanium dioxide and we came to the conclusion that steric hindrance of the crystal growth rather than the electrical conductivity of graphite plays a role in this case. Since suppression of sulfation is very important for VRLA batteries intended for hybrid electric vehicles and operating in the partial state of charge, we considered worthwhile to carry out systematic experiments using additions of inert powdered materials.

Keywords: Negative lead battery electrode; Cycle life; Graphite additive; Titanium dioxide additive

Experimental

1. Electrodes and Cells

We employed pasted negative electrodes of dimensions 55 × 20 × 2 mm placed between two pasted positives of dimensions 75 × 70 × 1 mm (cut out from commercial starting batteries) with 1.8 mm thick AGM separators. The lead grids contained Ca 0.2 and Sn 0.5 %. The initial capacity of the negative electrodes was about 2.5 Ah. The electrode packs were placed in vented cells filled with sulfuric acid of 1.28 g/cm^3 density, allowed to stand for an hour, and then subjected to formation. Afterwards, several conditioning cycles were performed: discharging at 0.5 A, charging at 0.5 A for 8 h with voltage limitation to 2.45 V, *i.e*. 2 cycles a day. The test cells (the vented state) were then subjected to accelerated cycling to determine their cycle life.

It was of interest, in view of the commercial VRLA cells, to arrange other experimental runs by using hermetically closed cells. These were prepared as indicated above except that the excess electrolyte was, after four conditioning cycles in the flooded state, removed, the cells were hermetically closed, discharged to determine their capacity (with a current C_4) and charged with constant current with voltage limitation to 2.45 V for 20 h. Thus, they obtained 105 – 110% of the original charge.

2. Accelerated Cycling Tests

Accelerated cycling in the PSoC regime was done as follows: Prior to every experiment, the cells were discharged to 50% capacity from the preceding conditioning cycle. Both discharging and charging currents were equal to 2.5 A, applied for 25 s. The standing time between switching over was 3 s. In the first run, the cells were cycled in this way

until their voltage dropped below 1.6 V. Afterwards, the cells were again subjected to several conditioning cycles and a new run was carried out.

Results obtained in the flooded regime

We employed six negative electrodes doped with different amounts of titanium dioxide and graphite and without additive.

Six PSoC cycling runs were performed, each ending at 1.6 V cell voltage. Both the charge and discharge currents were set to 1 A for 20 s, standing time was 2 s. As soon as one run ended, the cells were subjected to four conditioning charge-dicharge cycles and another run started. After the fourth run, the electrodes with 0.5% TiO_2, 2.5% TiO_2 and 0.5% C disintegrated and they had to be removed. The cumulative cycle life of the electrodes under test is illustrated in Fig. 1. It can be seen that the negative electrode containing 1% TiO_2 showed the best performance exceeding 200,000 cycles. The performance of the electrodes with graphite and without any addition was also quite good (more than 150,000 cycles).

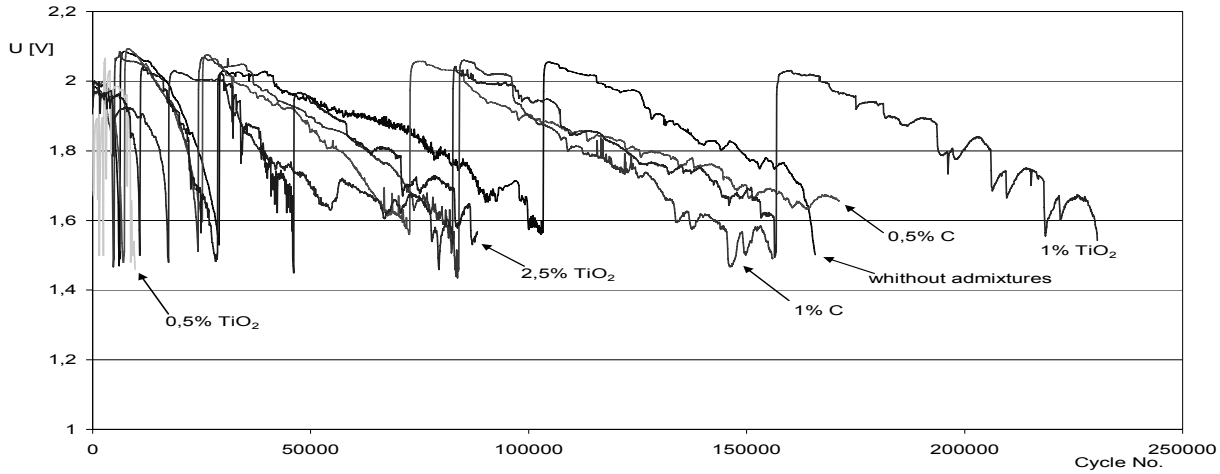

Fig. 1 *Cumulative cycle life of electrodes in the flooded system.*

Results obtained in the hermetic regime

We employed four negative electrodes doped with graphite, corund, titanium dioxide, and without additive. The cycling current was increased to 2.5 A, the time of charging and discharging was 25 s, and standing 3 s. Thus, the depth of discharge was approximately 0.7% which is somewhat higher than the value used by earlier authors (0.52%) [2, 3].

The cumulative results obtained from three subsequent runs are shown graphically in Fig.2. The cycle life was again highest for the electrode with 1% TiO_2 although somewhat shorter than in the preceding case. We assume that this difference is due to the higher depth of discharge used in the PSoC cycling. A similar effect has been observed in experiments with glass fibers. The experiments with aluminum oxide should be considered as preliminary. Measurements of the gas pressure in the cells showed that, in the first run, the pressure increased during 5000 cycles up to 130 kPa, the measuring range of the sensor used, except for the electrode without admixtures, as illustrated in Fig. 3. At the start of the second run, the overpressure was equilibrated with the atmosphere. The internal gas pressure then attained an equilibrium not exceeding 20

kPa. Apparently, the degree of drowning of the separators reached an optimum value enabling the oxygen cycle to proceed normally.

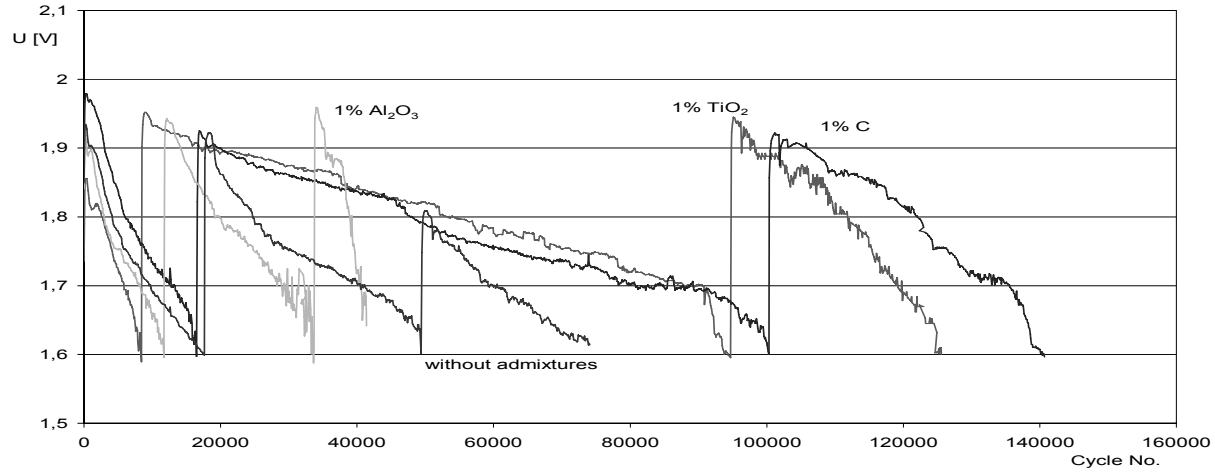

Fig. 2 *Cumulative cycle life of electrodes in the hermetic system.*

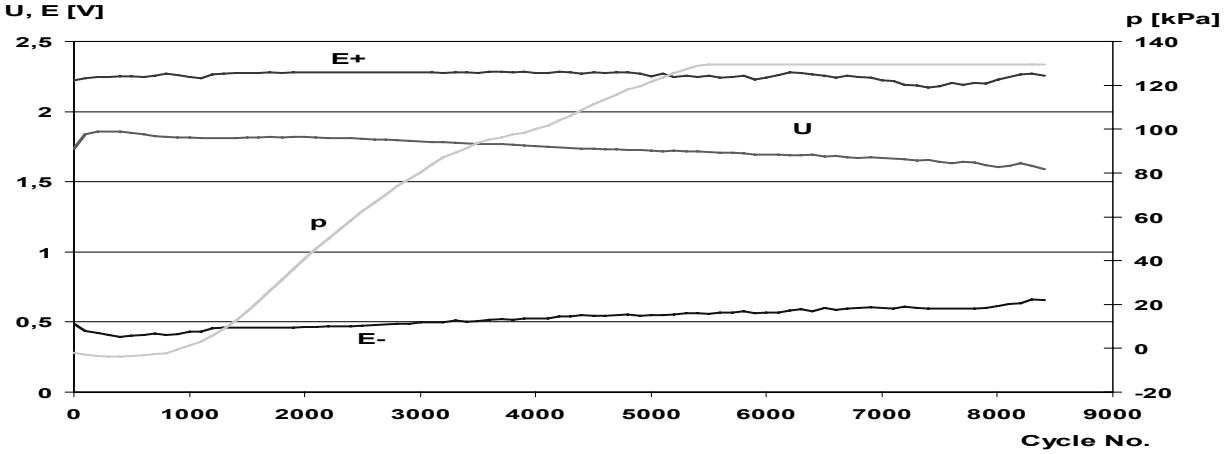

Fig. 3 *Voltage, potentials against Cd electrode, and internal pressure during the first PSoC run. Electrode containing 1% of graphite CR2996.*

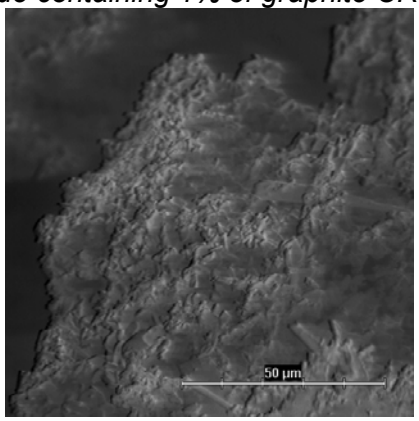

Fig. 4 Electrode without admixtures after 10,000 cycles.

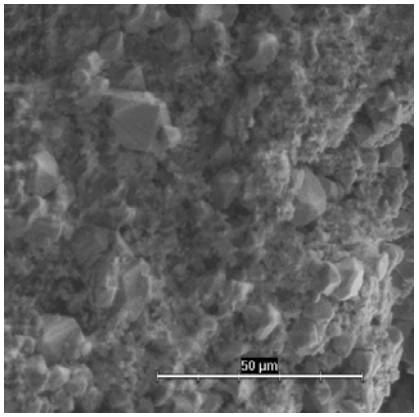

Fig. 5 Electrode without admixtures after 25,000 cycles.

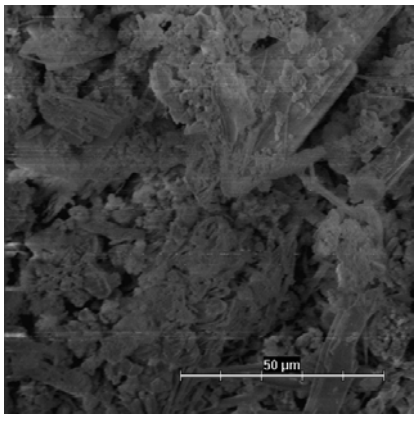

Fig. 6 Electrode containing 1% of TiO_2 after 10,000 cycles.

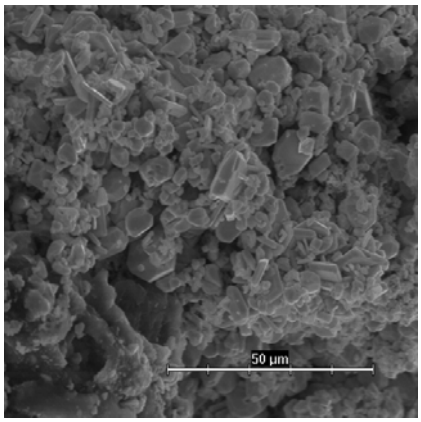

Fig. 7 Electrode containing 1% of TiO_2 after 42,000 cycles.

To find out whether the electrode structure is influenced by the presence of the additives, samples of the electrodes taken in different states of discharge in hermetic cells were investigated by the ESEM method. The electrodes were examined in the *charged* state. In Fig. 4 is shown a cross section of an electrode without admixtures after 10,000 of accelerated cycles, where crystals of lead sulfate are hardly discernible, and in Fig. 5 can be seen the same electrode after 25,000 cycles showing many crystals of lead sulfate. Many of these crystals are relatively large (10 µm or more) so that they could not be converted to lead during charging. A somewhat analogous situation can be observed with an electrode doped with titanium dioxide. After 10,000 accelerated cycles (Fig. 6), the crystals of lead sulfate are difficult to recognize, but after 42,000 cycles (Fig. 7) they are apparent, although smaller than in the preceding case (Fig. 5). And a very similar situation was observed with an electrode doped with 1% of graphite. These findings are in support of our concept published earlier [1] that finely powdered additives in negative lead electrodes may hinder the growth of lead sulfate crystals and thus enhance the cycle life during PSoC charging.

Conclusions

The hydrogen overpotential values measured on negative accumulator electrodes doped with different sorts of carbon, aluminum oxide, and titanium dioxide were found to be close to the electrodes witthout admixtures. Accelerated cycling in the partial state of charge showed that the electrodes with titanium dioxide performed better than those containing carbon. ESEM microphotographs revealed that lead sulphate crystals in the presence of admixtures are, on the average, smaller than in their absence, and thus easier to be reduced to lead.

Acknowledgement

This work was supported by the Advanced Lead-Acid Battery Consortium (Project No. C2.2) and by Research Project CR No. MSM 0021630516. The carbon samples APH 2939 and N 134 were provided by Ian Dyson, CMP Batteries, Ltd. The glass fibers were provided by Tony Ferreira, Hollingsworth&Vose Co., West Groton, Ma, USA.

References

1. M. Calábek, K. Micka, P. Křivák, P. Bača, J. Power Sources 158 (2006) 864.
2. M. Shiomi, T. Funato, K. Nakamura, K. Takahashi, M. Tsubota, JPS 64(1997) 147.

MODIFIED CONDUCTOMETRIC METHOD

P. Bača

Department of Electrotechnology, Technical University, 602 00 Brno, Czech Republic

Corresponding author. Petr Bača baca@feec.vutbr.cz

Introduction

Conductometry is analytic method that can be used to analyze character of electrolyte using measurement of the whole electrolyte conductivity. Each material participates in electric conductivity of electrolyte and we cannot recognize contribution to conductivity of each material. Thus conductometry is non selective analytic method that gives us information about total contents of materials in analyzed electrolyte.
The advantage of this method is that no electrochemical reaction (oxidation or reduction) occurs during measurement in the cell. During measurement of conductivity alternate current (A.C.) is used. Low frequency conductometry is used with frequency from 10^1 to 10^4 Hz and polarization events are not evident.
The advantage of high frequency conductometry (10^6 až 10^8 Hz) is in separation of contact between conduction electrodes and analyzed electrolyte.
When high frequencies are present, electromagnetic energy goes through walls of vessel, so conducting electrodes can be placed outside of the vessel, so they are not in direct contact with analyzed electrolyte. When high frequency alternate current is used in high frequency conductometry both components participate on total impedance equally, high frequency conductivity of electrolyte has complex character and it depends greatly on frequency of alternate current.
Analyzed electrolyte is during conductometric measurement in conducting (conductometric) vessel. To avoid polarization of electrodes, alternate current is leaded through electrodes. Conducting vessel shown at fig. 1 can be represented by electric circuit at fig. 2.

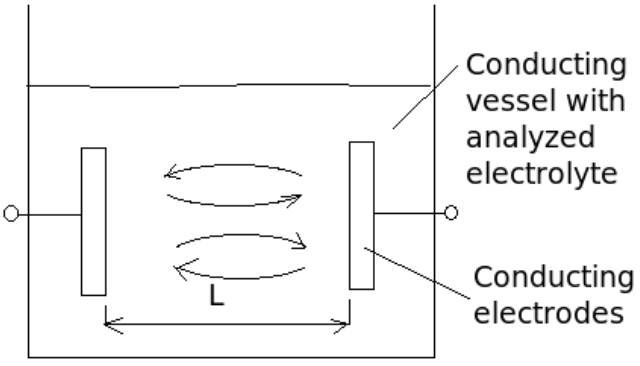

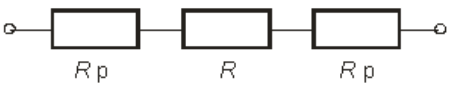

Fig. 1 *Conducting vessel with electrodes,*
Fig. 2 *R is resistance of vessel and Rp is resistance of wires.*

Conducting vessel has impedance character with capacitance component. Substitution diagram of real conducting vessel is more complex and it covers additional parts as it is shown in fig. 3.
When the electrode is inserted into the electrolyte chemical reactions occur that cause imbalance of charges. This imbalance is compensated by movement of charged ions to the electrode until imbalance is fully compensated. Near electrode there rises the double layer formed by charged ions and opposite charged electrode. This double layer acts as charged capacitor on certain potential [1,2]. Passing of charges through double layer is slowed by velocity of electron change between ions and electrode. This event has resistance character and it is called charge transfer resistance [1,2,3]. In the scheme there is represented by resistor R_{ct}. Z_w is Warburg's impedance and it is caused by limited diffusion velocity of ions from electrolyte to electrode [1,4]. Z_w and R_{ct} together makes Faraday's impedance that represent parasite behavior of cell together with parallel capacity C_{dl}.

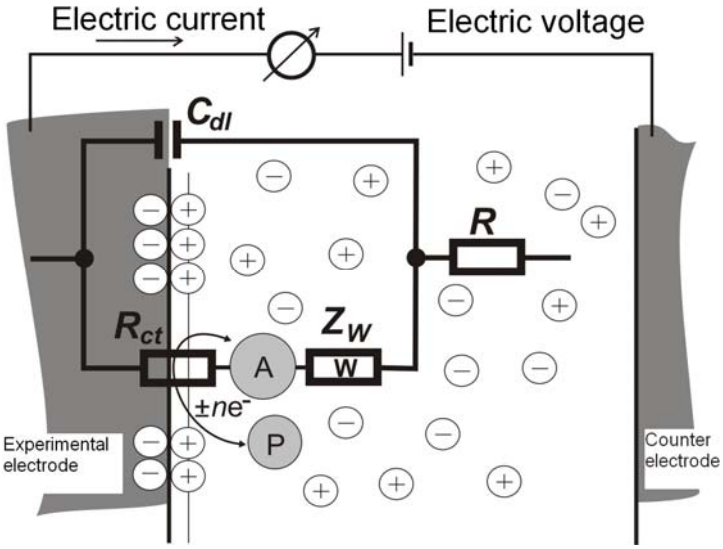

Fig. 3 *Randles circuit of electrochemical cell (R - resistance of electrolyte, C_{dl} - capacity of double layer, R_{ct} - charge-transfer resistance, Z_w -Warburgs resistance [5].*

In two-electrode configuration various layers can develop on electrodes, that contribute to the total resistance of vessel and also not completely compensated polarization of electrodes can occur. Size of current depends on total resistance in vessel i.e. not only on resistance of electrolyte, but also on health of electrodes and resistances of electrode/electrolyte. In the four-electrode configuration the current flows through one pair of electrodes and other pair is inserted between them. With the second pair of electrodes electric voltage with absence of current is measured. Measured voltage is not influenced by events on electrodes with current so it depends only on resistance of electrolyte.
You can see that four-electrode conductometric measurement can be used also for resistance measurement of interface of electrode/electrolyte. This resistance corresponds with health of electrode and because resistance of corrosion layer is greater then resistance of electrode itself we can assume the corrosion rate from resistance of corrosion layer.
Although primary use purpose of conductometric method is to measure conductivity of certain electrolyte and it needs inert electrodes (usually platinum electrodes), we can see

from previous article, that conductometric method can be used as a comparative method for determination of corrosion rate of certain electrode system. This method can be used to find optimal composition of lead alloy for grid of positive electrode of lead acid accumulator, which is first destroyed by corrosion during exploitation in sulfuric acid. Also for development of bipolar lead-acid accumulator these results can be useful, because corrosion of bipolar substrate is one of failure mode of bipolar lead-acid accumulators. On this account bipolar lead-acid accumulators cannot be industry produced.

Experimental

First of all we tried to verify functionality of conductometric method for resistance measurement of corrosion layer at the interface collector/electrolyte. We tried to determine how real and imaginary part of impedance depends on frequency and how it changes during time of measurement.
Experimental electrode was made from low-antimony lead alloy Pb Sb1.68 Sn0.05 (wt%). Individual ribs of electrode had dimensions 20x1 mm. Distance between ribs was 5.5 mm. Before we start with experiment we made experimental cell, that contained excess of electrolyte and negative active material from industry produced negative electrode of starting battery from AKUMA a.s. Mladá Boleslav. Negative electrodes were placed on both sides 2.5 mm far from experimental positive electrode. No separator was used. For creation of corrosion layer we charged the electrode with 0.2 A for 120 hours.
To find out optimal frequency, when the imaginary part of impedance would be minimal we analyze voltage U_1, U_2, U_3 and its phase difference in whole frequency range of power source of sine signal. To analyze values we used two channel digital oscilloscope ALIGENT CN45004070. From measured voltages and its phase difference we calculated Z_{abs}, Z_{real} and Z_{imag}.
Fig. 5 shows imaginary part on the real part of impedance for electrolyte (i.e. Nynquist chart) and its substitution diagram. By measurement on whole system effect is similar, but you can see also Warburg impedance Z_w. From fig results: For measurement is better to use lower frequencies. Our power source hat too much noise at 1 kHz frequency so we decide to measure at 5 kHz.
Sine generator was set to 5 kHz. And we tried to analyze time changes of absolute value of electrolyte impedance like in previous experiment. Impedance rises slowly during the time for system that consists of experiment electrode and also negative counter electrodes. Error of measurement is not higher than 1.5 %. In system with experimental electrode only there is error of measurement to 0.7%. Measurement with negative electrodes is influenced by error so we decided to do next measurement without them.
Influence of negative electrodes is more significant by measurements of whole system in two-wires wiring. With negative electrodes the absolute impedance decreases stably. Without negative electrodes the absolute impedance is stable – 0.5 % deviation.
Measured value of absolute impedance is always lower in system with negative electrodes. It is caused by high conductivity of active mass of negative electrodes. So some current flows through negative electrodes and lower the absolute impedance.

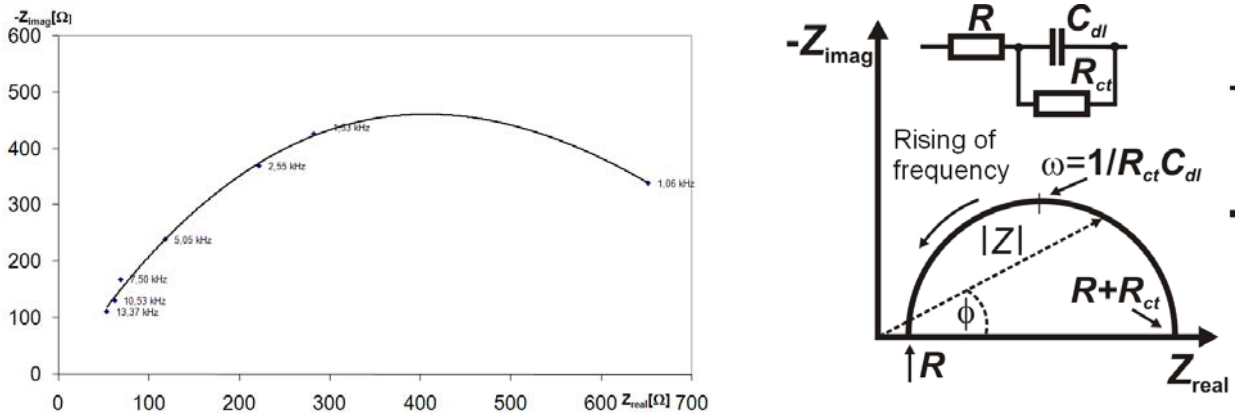

Fig. 4 *Dependency of imaginary part of electrolyte impedance on real part for various frequencies*

Results and discussion

Our preliminary experiments shows that conductometric method is acceptable for resistance of corrosion layer measurement at interface electrode/electrolyte and it can be used as comparative method for measuring of various collector alloys to find out corrosion rate of that alloy.

References

[1] Rieger, P.H.: Electrochemistry. Prentice-Hall, Inc., A Division of Simon & Schuster, Englewood Cliffs, New Jersey,1987.
[2] MacDonald, D.D.: Application of Electrochemical Impedance Spectroscopy in Electrochemistry and Corrosion Science. Techniques for Characterization of Electrodes and Electrochemical Processes, edited by Varma, R. and Selman, J.R., pp.515-580, John Wiley & Sons, Toronto, 1991.
[3] Jossinet, J., McAdams, E.T., Lackermeier, A., McLaughlin, J.A. & Macken, D.: The linear and non-linear electrical properties of the electrode-electrolyte interface. Biosensors & Bioelectronics, 10, pp.67-74, 1995.
[4] Moussavi, M., Schwan, E.T., Sun, H.H., Harmonic distortion caused by electrode polarisation. Med. & Biol. Eng. & Comput., 32, pp. 121-25, March 1994.
[5] Prof. RNDr. František Opekar, CSc. : Učební texty na Př.f. UK

CELL VOLTAGE AND ELECTRODE POTENTIAL COURSES OF LEAD ACID BATTERY IN PSOC REGIME

Petr Křivík

Department of Electrotechnology, Faculty of Electrical Engineering and Communication Technologies, Technical University of Brno, Czech republic

Introduction

World's research workers and battery manufacturers now face to a serious challenge, since their biggest market, namely market with automobile batteries SLI (Starting, Lighting and Ignition) must be prepared for situation, when conventional 12 V batteries will be mostly replaced by batteries designed for vehicles with increased requirements on electric power. Matter is that, that conventional 12 V SLI batteries aren't able to deliver such power that is required by new automobile systems with high power, with acceptable cycle life. Batteries for these systems with high power will work in PSoC regime (Partial State of Charge – about 50% of charge) and will be discharged and especially then again charged with high currents, even if only in short time intervals.
Nowadays there is also considerable attention to electromobiles and especially transient type between car with classical combustion drive and electromobile - hybrid electric vehicle (HEV). This vehicle is powered by electric motor, supplied (unlike classical electromobile) by relatively small battery, permanently charged with help of the combustion motor with not very big power, working in regime of optimum speed with minimum emissions. As one of possible sources for HEV shows to be economically advantageous lead-acid battery. Batteries for HEV must be able to receive electric charge at relatively high rates of charging (mainly at recuperative braking) and that is why they must work in regime PSoC. In such kind of regime it is shown that mechanism, limiting service life, includes gradual accumulation of lead sulphate inside negative electrode and it makes gradual lost of charging capacity (premature capacity loss - PCL or PCL3).
Efforts to improve parameters (especially service life) of batteries are oriented largely on new types of additives in active masses of negative electrodes, on optimalization of current collector (placement of bars) and pressure placed on active mass of electrodes.

Experiment

Experiment monitoring influence of additives in negative active mass of lead acid battery on cycle life of 8 experimental cells was done on experimental electrodes especially made for this purpose. In active masses negative electrodes there was added different additives – 1% of C in 1st and 2nd cell, 1% of TiO_2 in 3rd and 4th cell, 1% of corundum (Al_2O_3) in 5th and 6th cell and 7th and 8th cell without additives.
Pasted electrodes were set to the sealed vessel. Measured (negative) electrode was placed between positive counterelectrodes. Separator from glass fibres with high

porozity over 95% served to separation of both electrodes, minimalisation of inner resistance and to facilitation of oxygen cycle during charging. In separators there was absorbed electrolyte (solution of H_2SO_4 with concentration 1.24 g/cm^3).
After formation and of several cycles experimental cells were subjected to fast cycling in regime PSoC including charging, standing, discharging and other standing. Interval of charging and discharging was 25 s and interval of standing was 3 s. Charge and discharge current was 2.5 A. In given cycles there was done measuring of voltage and electrode potential courses of single electrodes during charging, discharging and standing.
Automated measuring station used for measurement of voltage and potential courses (see fig. 1) is composed from control unit (PC with measuring software programmed in VEE Pro 8.0), that is connected by GPIB cable with central measuring datalogger Agilent 34097A with multiplexer (MUX) card. Exits from MUX cards are connected to a positive, negative and referent (Cd) electrode. After start of measurement there proceeds fast measuring (in time interval 0.01 s) of cell voltage and potentials of electrodes. Resulting measured data are writen to MS Excel tables, where we can watch time courses graphically. Resulting graphic dependencies of voltage and potential courses of cell no. 1 with 1% of C at the beginning and at the end of life are presented on fig. 2 and 3.

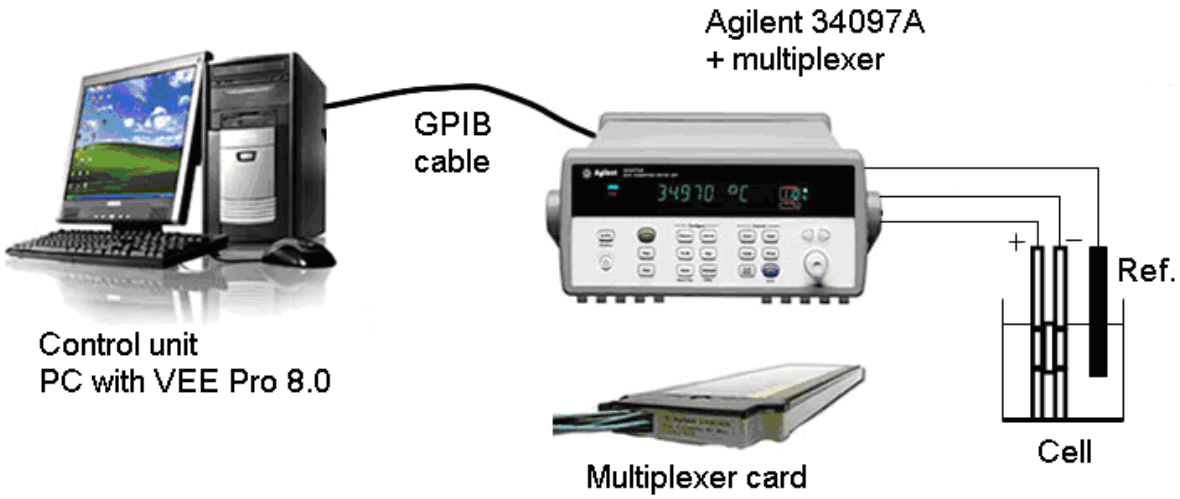

Fig. 1 *Scheme of automated measuring station*

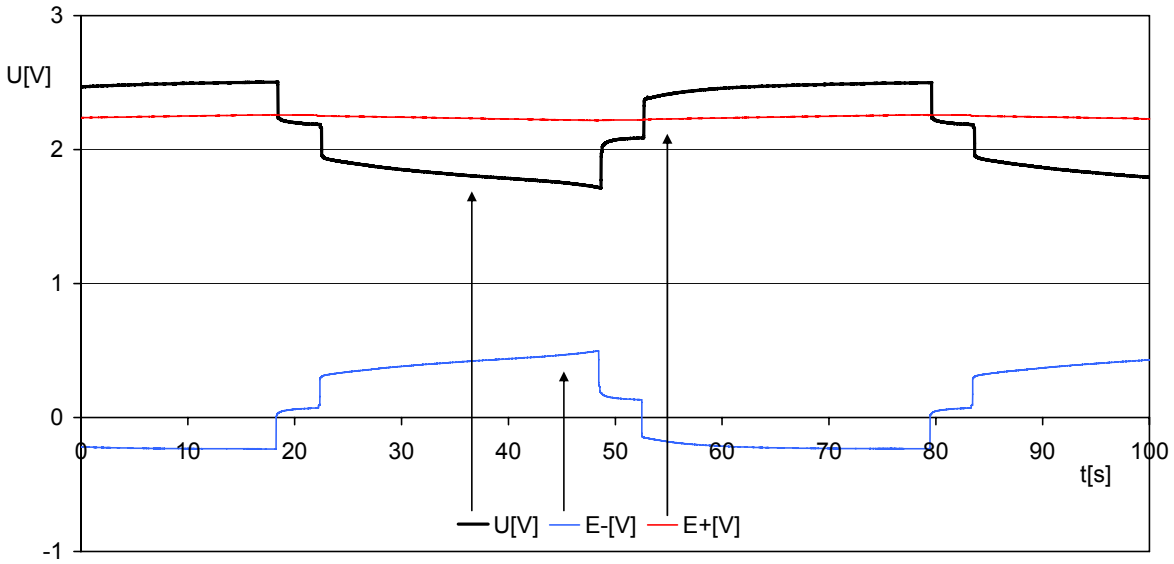

Fig. 2 *Time courses of cell voltage and electrode potentials during fast cycling in regime PSoC for 1st cell with 1% of C (beginning of life – 20th cycle).*

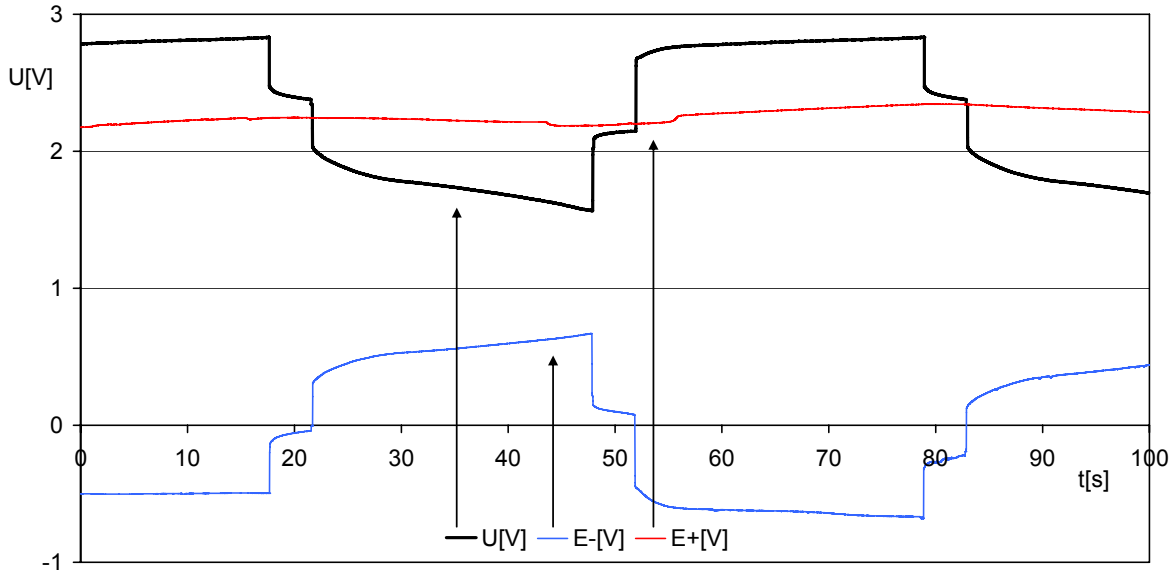

Fig. 3 *Time courses of cell voltage and electrode potentials during fast cycling in regime PSoC for 1st cell with 1% of C (end of life – 8220th cycle).*

From fig. 2 and 3 it is seen an evident difference in cell voltage and potential courses of electrodes. While on fig. 2 (beginning of life) it is variation between maximal value of voltage during charge and minimal value of voltage during discharge 0.79 V (max. U = 2.50 V, min. U = 1.71 V), on fig. 3 (end of life) it is variation between maximal value of voltage during charge and minimal value of voltage during discharge 1.27 V (max. U = 2.83 V, min. U = 1.56 V). It is related with growth of inner resistance owing to sulphation of negative active mass. Because of surplus of positive active mass potential course of positive electrode does not change too much during cycling and that is why for changes of cell voltage is major negative electrode all the time of cycle life.

From potential courses of single electrodes it is evident, that gas, which is released during charging is especially hydrogen (limiting electrode is negative – here releases hydrogen during charge, while oxygen on the positive one), which can be virtually dangerous (forms explosive mixture with oxygen). Therefore it is at most useful and needed to use separators from glass fibres, that, under the conditions of creation of air channels while there is small distance between electrodes, enable starting of so-called oxygen cycle. Oxygen, that releases during charging on positive electrode, travels through channels in separator to negative electrode, where's reduced to water according to equation:

$2Pb + O_2 + 2H_2SO_4 \rightarrow 2PbSO_4 + 2H_2O + Heat.$

Oxygen cycle shifts potential of negative electrode to less negative values and thereby essentially falls rate of hydrogen release on negative electrode.

Conclusions

Changes in voltage courses during cycling in PSoC regime reflect state of experimental lead acid battery cells and at the same time state of sulphation of negative electrodes. There plays an important role separator, that allows start of oxygen cycle and thereby it restricts growth of pressure in hermetical cell. Experiment exploring influence of ingredients in active mass of negative electrodes continues with the aim of finding of optimal quantity and type of additives with the aim of increasing of cycle life and other important parameters of lead acid batteries.

This work was sponsored by grant No. MSM0021630516.

Literature

1. P.T. Moseley, R.F. Nelson, A.F. Hollenkamp: The role of carbon in valve-regulated lead–acid battery technology, *Journal of Power Sources 157*, 2006, s. 3-10.
2. M. Calábek, K. Micka, P. Křivák, P. Bača: Significance of carbon additive in negative lead-acid battery electrodes, *Journal of Power Sources, 158, 2006*, s. 864-867.

MEASUREMENT OF THE CORROSIVE LAYER RESISTANCE OF LEAD ALLOYS USING MODIFIED CONDUCTOMETRIC METHOD

P. Abraham

Department of Electrotechnology, Technical University, 602 00 Brno, Czech Republic

Supervised by: P. Bača
Corresponding author. Pavel Abraham xabrah02@stud.feec.vutbr.cz

Introduction

Lead-acid accumulator is galvanic cell with lead based electrodes in sulphuric acid. Lead-acid accumulators are mostly used secondary electrochemical power sources. Main advantages are well managed produce technology, relatively low price and high electric power [1]. Bipolar lead-acid accumulators are great opportunity to use in hybrid vehicles due to their high power. But there are some problems for commercial production as heat removal during fast cycling and also lead grid corrosion in sulphuric acid. So we have focused to find out corrosion rate of lead alloys. We have used modified conductometric method to do so.
Conductometry is analytic method that can be used to analyze character of electrolyte using measurement of the whole electrolyte conductivity. Each material participates in electric conductivity of electrolyte and we cannot recognize contribution to conductivity of each material. Thus conductometry is non selective analytic method that gives us information about total contents of materials in analyzed electrolyte [2].
The advantage of this method is that no electrochemical reaction (oxidation or reduction) occurs during measurement in the cell. During measurement of conductivity alternate current (A.C.) is used to avoid polarization of electrodes [3,4].
Although primary use purpose of conductometric method is to measure conductivity of certain electrolyte and it needs inert electrodes (usually platinum electrodes), we can see from previous article, that conductometric method can be used as a comparative method for determination of corrosion rate of certain electrode system. This method can be used to find optimal composition of lead alloy for grid of positive electrode of lead acid accumulator, which is destroyed by corrosion during exploitation in sulfuric acid. Also for development of bipolar lead-acid accumulator these results can be useful, because corrosion of bipolar substrate is one of failure mode of bipolar lead-acid accumulators and it prevents from industry production of bipolar lead-acid accumulators.

Experimental

Experimental electrode was made from low-antimony lead alloy Pb Sb1.68 Sn0.05 (wt%). Individual ribs of electrode had dimensions 20x1 mm. Distance between ribs was 5.5 mm as it is shown at fig.1. Before we start with experiment we made experimental

cell, that contained excess of electrolyte and negative active material from industry produced negative electrode of starting battery from AKUMA a.s. Mladá Boleslav.
Negative electrodes were placed on both sides 2.5 mm far from experimental positive electrode. No separator was used. For creation of corrosion layer we charged the electrode with 0.2 A for 120 hours.

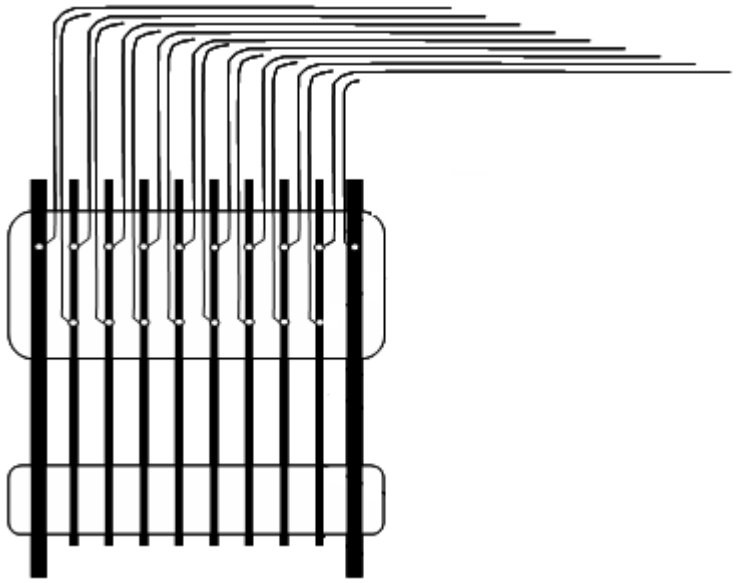

Fig. 1 *Experimental electrode*

To find out system voltage response to leaded current experiments were realized, when alternating sine current was gradually increased. This current was leaded through aforementioned electrode with system of disconnected parallel ribs in two wires scheme. Corrosion resistance should be nonlinear when higher voltages (and hence higher currents) occurs.
We found, that dependency is linear for currents higher then 15 mA, so total resistance of electrode system is invariable. But when the values of amplified sine signal are low (when values of leaded current flowing through system are low) the values of absolute impedance are nonlinear. This can be caused by non stability of used amplifier or by necessity to overcome barrier at interphase collector/electrolyte.
When you leave lead in sulfuric acid, lead sulphate originates at the surface, respective lead oxide (during charging), that has semiconductor character. So it is possible that interphase metal – semiconductor is made, that can lead to non linear voltages.
To verify dependency of voltage on current for higher currents, experiment was repeated with new non pasted electrode without high resistance corrosion layer. Results are shown at fig. 3 and 4. At figure 3 it is evident that from current 70 mA the inner impedance of whole system starts to be nonlinear. From current value 400 mA gas starts to develop at the electrode surface and electrolyte starts to blur.
When the experiment finished ribs were thinner. This corresponds with fig 3, where it is evident increase of resistance of electrode first, that can be explained by developing of resistance layer of $PbSO_4$ at the surface of the electrode. Then it decreases, this can be explained by shedding of surface elements of electrode to electrolyte thus conductivity of electrolyte increases.

Higher resistance of whole measuring system at the beginning and lower at the end of experiment can be explained by increasing of electrolyte conductivity by elements of lead from electrodes.
Removal of surface electrode layer corresponds with fig. 4. where dependency of imaginary part of impedance (capacitance) on connected current is shown.
Corrosion layer on the electrode ribs surface is removed when higher currents are used, hence capacity of whole electrode system decreases.

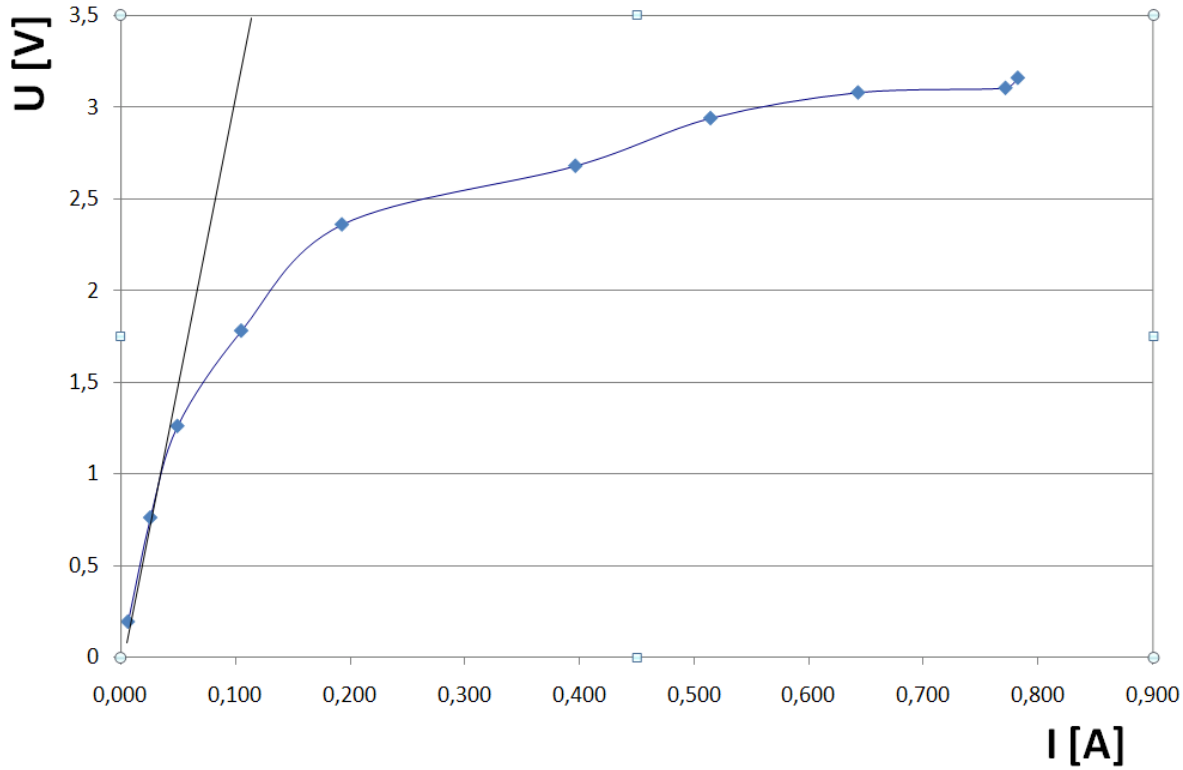

Fig. 2 *Dependency of maximal voltage on connected alternate current of electrode in two wires scheme*

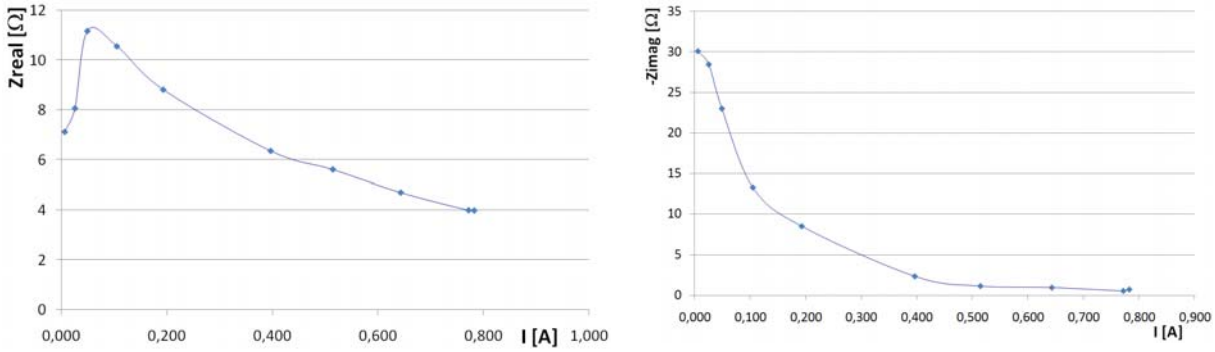

Fig. 3 and 4 *Dependency of real and imaginary part of impedance on connected alternate current of electrode in two wires scheme*

Results and discussion

Our experiments show that dependency of impedance on current is not linear in some cases. It is important to use low currents for measurements to avoid removing of corrosion layer from the ribs of electrode.

References

[1] www.wikipedia.cz
[2] Prof. RNDr. František Opekar, CSc. : Učební texty na Př.f. UK
[3] MacDonald, D.D.: Application of Electrochemical Impedance Spectroscopy in Electrochemistry and Corrosion Science. Techniques for Characterization of Electrodes and Electrochemical Processes, edited by Varma, R. and Selman, J.R., pp.515-580, John Wiley & Sons, Toronto, 1991.
[4] Jossinet, J., McAdams, E.T., Lackermeier, A., McLaughlin, J.A. & Macken, D.: The linear and non-linear electrical properties of the electrode-electrolyte interface. Biosensors & Bioelectronics, 10, pp.67-74, 1995.

THE DISTRIBUTION INTERNAL RESISTANCE AND TOTAL CHARGE PASSED ON THE SURFACE OF LEAD-ACID ACCUMULATOR ELECTRODES DURING DISCHARGE

Lábus Radek

Department of Electro technology, Technical University, 602 00 Brno, Czech

E-mail: xlabus00@stud.feec.vutbr.cz

Introduction

As a continuation of our past research work on the modelling of current distribution on the surface of standard lead-acid battery [1] plate electrodes and a cylindrical type VRLA cell [2] in the course of discharge for various configurations of the current tabs, we used a similar model also for 3-D modelling of internal resistance distribution and charge passed on the surface of standard lead-acid battery. Cell electrodes with position of current tabs are shown on top in Fig. 1. We have shown that our method can successfully be applied in the case of current distribution over the electrode surface in a lead-acid cell [1].

Experimental

Method of calculation
The mathematical model was based on an electrical equivalent circuit similar to that used by previous authors [1, 2]. It is assumed that the positive and negative grids have equal numbers of meshes of equal forms, thus corresponding, in the geometrical sense, to each other.
The internal resistances, R_{vk}, between the cell elements depend on the discharge current, I, and on the charge passed, Q. The course of this functional dependence was determined on a laboratory cell for various discharge currents. The values of R_{vk} involving the electrolyte resistance, contact resistance between the lead grid and the active mass and the active mass resistance were fitted by the following exponential function by using the least squares method (1):

$$R_{vk} = 0.32 + 4.2Q + 2.6 \times 10^{-5} \exp (730Q + 100I - 14) \qquad (1)$$

After application of the first and second Kirchhoff laws to nodes and loops of the whole equivalent circuit, we obtain a system of linear equations whose solution gives the sought distribution of local potentials and currents. To take into account the system changes with the time, the calculations were carried out in many steps as described in [1].
The results of the calculations of the internal resistance and charge passed distribution over the electrode surface are shown in the form of 3-D diagrams in figs. 1 – 2.

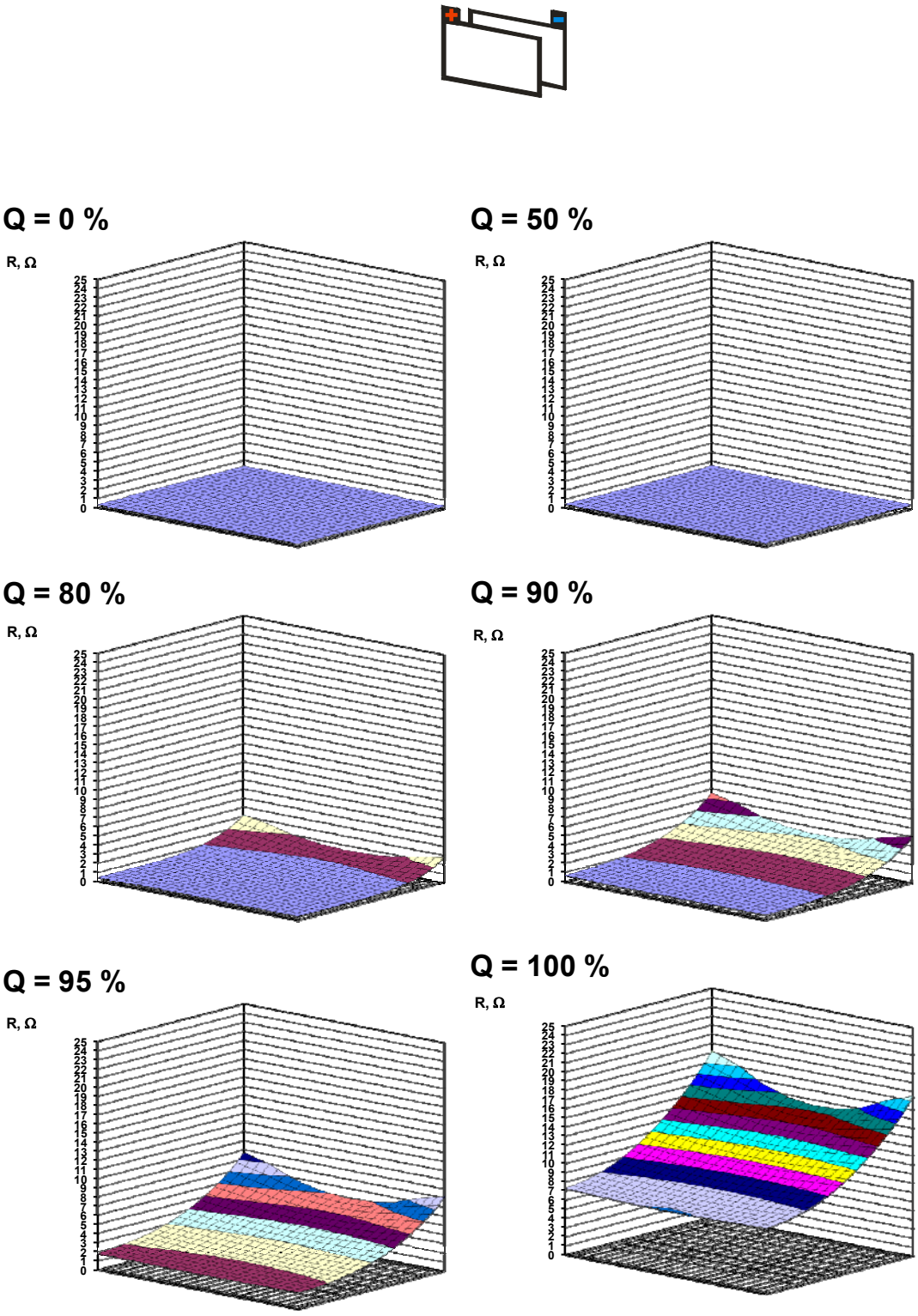

Fig. 1 *Internal resistance distribution over the plate electrode surface at increasing state of discharge, Q, from 0 to 100%.*

Analysis

Results from fig.1 - during discharge internal resistance dramatically increases as far as from 80 % of discharge.

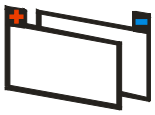

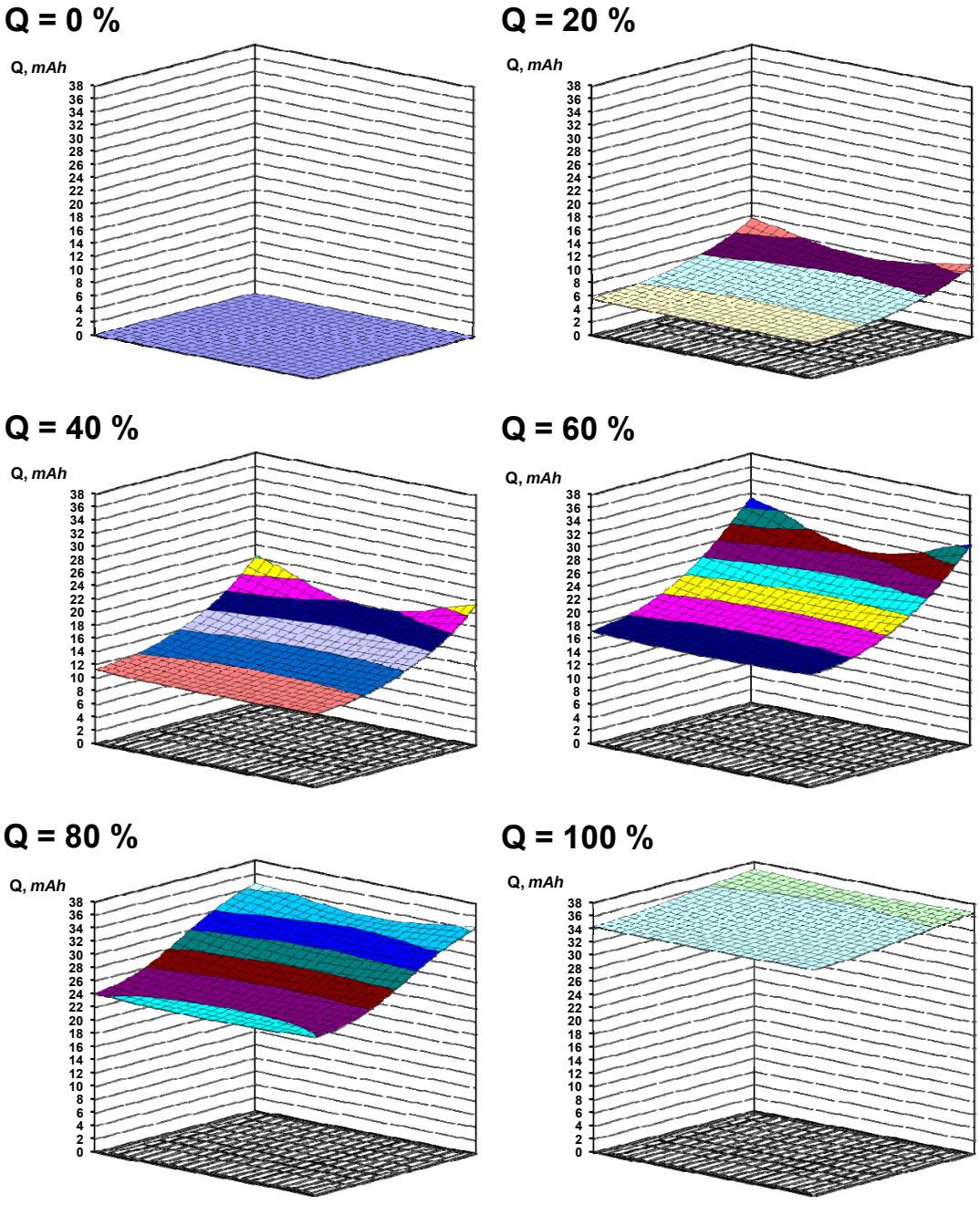

Fig. 2 *Charge passed distribution over the plate electrode surface at increasing state of discharge, Q, from 0 to 100%.*

The active mass is mostly exploited at current tabs especially on positive electrode (positive electrode has bigger resistance than negative electrode). At the end of discharge rate of R_{max}/R_{min} = 2.57.
Results from fig.2 - charge passed is increased equally during discharge. In half of discharge exploitation of charge passed increased on electrodes surface unevenly, especially active mass near current tabs (similarly as internal resistance on positive electrode) is exploited. At the end of discharge non-uniformity of exploitation of charge passed on electrodes surface is decreasing, even if at the end of discharge the active mass nearly current tabs is more exploited than in other regions of active mass (Q_{max}/Q_{min} = 1.09).

Conclusions

Mathematical model was created for recognition of internal resistance and charge passed distribution. Target of this work was limitation of degradation mechanism of lead-acid cells that is presented by distribution of internal resistance and charge passed. Unequally distribution of internal resistance and charge passed affected lay-out of current tabs located at opposite ends of the plate electrodes.

Acknowledgement

This work was supported by: The Research Project CZ No. MSM0021630516, ALABC (Project No. C2.2)

References

1. Petr Král, Petr Křivák, Petr Bača, Milan Calábek, Karel Micka: Current distribution over the electrode surface in a lead-acid cell during discharge, Journal of Power Sources, 105, 2002, s. 35-44.
2. Petr Křivák, Petr Bača, Milan Calábek, Karel Micka, Petr Král. Current distribution over the electrode surface in a cylindrical VRLA cell during discharge. Journal of Power Sources, 2006, 154, 2006, s. 518-522. ISSN: 0378-7753.

THE ELECTRODEPOSITION OF TIN IN ROOM TEMPERATURE MOLTEN SALTS

Lux S. F.[1], Schmuck M.[1], Balducci A.[2], Passerini S.[2] and Winter M.[2]

[1] Institute for Chemistry and Technology of Materials, Graz University of Technology, Stremayrgasse 16, 8010 Graz, Austria
[2] Institute of Physical Chemistry, Westfälische Wilhelms University of Münster Corrensstraße 28/30, 48149 Münster, Germany

Simon Franz Lux
simon@lux.at
phone: +43 (0) 316 873 8294
fax: +43 (0) 316 873 8272

Introduction

Electrodeposited tin is very common among the food and beverage industry and it is also seen as possible negative electrode material in Lithium Ion Batteries. However the electroplating of tin is carried out in aqueous bath types [1].
Room temperature molten salts also known as Ionic liquids (IL) possess physical properties such as a high thermal stability, a broad electrochemical window, a atoxicity and a low water content which make them attractive candidates for different electrochemical applications [2]. One of these applications is e.g. the electro-deposition of silicon in ionic liquids at room temperature [3].
In this study we deposited tin in an IL on a copper foil at room temperature to obtain a special kind of morphology of the tin alloy for a possible application as negative electrode in Lithium Ion Batteries.

Experimental

A commercial available three-electrode glass cell was used in all the experiments. Copper foil was established as working electrode and a high-purity tin foil was used as counter and reference electrode. The electrolyte was a solution of *N*-butyl-*N*-methylpyrrolidinium- bis(trifluoromethanesulfonyl)imide ($PYR_{14}TFSI$) with a content of 1 mol L^{-1} tin (IV) chloride. The so obtained film was cleaned using several organic solvents and/or ultrasound.

Results and Discussion

Prior to electrochemical analysis of the cycleability of these tin films, the foils were weight out, the electricity yield was calculated and the composition of the surface was analyzed with X-ray photon spectroscopy (XPS). These measurements indicate a

decomposition of the IL during the electroplating of the tin. The following cleaning experiments had an astonishing influence on the weight of the plated copper foil and also subsequent XPS analysis indicates a possible structure change of the deposited film after cleaning.
The cyclic voltammetry at 50 µV s^{-1} display the typical tin peaks and the scanning electron microscopy pictures also indicate the presence of tin which is backed up with the results of the XPS.
However, the XPS data and the behaviour of the films during cleaning also clearly indicates that the electrodeposition of tin in ILs is not following the same path as in aqueous electrolytes.

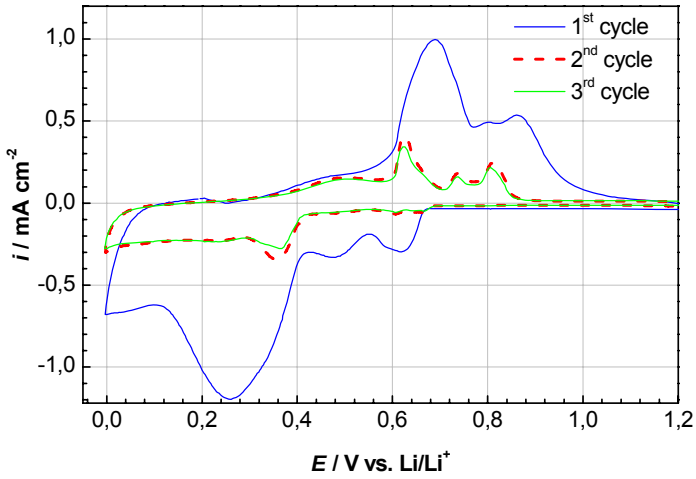

Fig. 1 *Cyclic voltammogram of deposited tin – 1M LiTFSI in propylene carbonate (50 µV/s scan rate).*

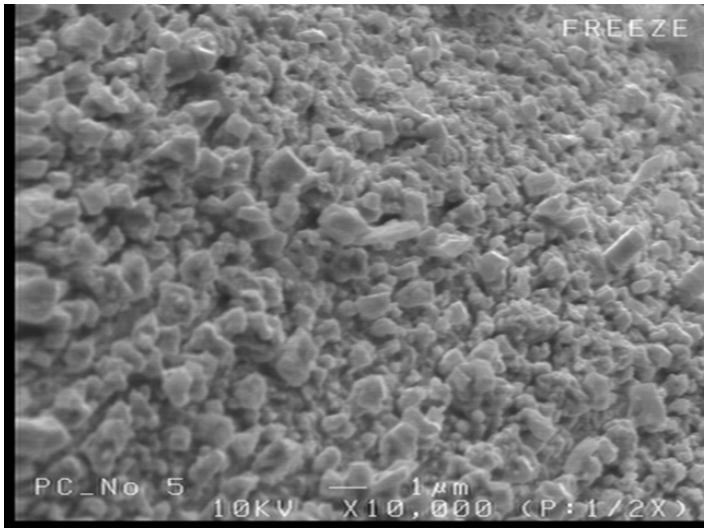

Fig. 2 *SEM – Image of deposited Sn*

Conclusions

The electrodeposition of tin in room temperature molten salts is possible, but there appear side reactions concerning the electrolyte which prevent the deposition of a homogeneous tin film. Also the conditions including the solvent during the cleaning process show an influence on the composition of the film and the possible application in Lithium Ion Batteries.

Acknowledgements

The authors acknowledge the European Commission for the financial support under contract NMP3-CT-2006-033181 (ILLIBATT, Ionic-Liquid-based Lithium Batteries).

References

[1] M. Schlesinger, M. Paunovic (Eds.); Modern Electroplating, fourth edition, The Electrochemical Society Inc, Pennington, NJ, Wiley, New York, 2000
[2] A. T. Tsuda, C. L. Hussey: The Electrochemical Society Interface 2007 42-49
[3] B. Zein El Abedin, et al., Electrochemistry Communications **6**(5) 2004 510-514.

NANOCOMPOSITE ELECTRODE MATERIALS WITH SPINEL STRUCTURE FOR LITHIUM-ION BATTERIES

Tibor Jirák[1], Jiří Vondrák[2], Marie Sedlaříková[1]

[1] Department of Electrical and Electronic Technology, Brno University of Technology, Údolní 53, Brno 60200, Czech Republic
[2] Institute of Inorganic Chemistry, Academy of Sciences of the Czech Republic, Řež near Prague 25068, Czech Republic

Corresponding author: Tibor Jirák
E-mail: tibor.jirak@phd.feec.vutbr.cz
Phone Number: +420 541 146 112
Fax Number: +420 541 146 147

Introduction

The article treats of electrode materials for lithium secondary batteries, concretely nanostructured $Li_4Ti_5O_{12}$. Material was chosen for research by virtue of very good intercalation / insertion characteristics, possibility utilization high charge and discharge rate and for his environmental safety. Low conductivity and voltage incident at $Li_4Ti_5O_{12}$ can be improved by many admixtures, e.g. multiwall carbon nanotubes and special modified exfoliated graphite.
Electrochemical properties and good stability in the electrochemical processes determine investigated material as an alternative to graphite in negative electrode or as headstone for positive electrodes lithium-ion batteries.

Experimental

The purpose of this work was obtained electrochemical characteristics prepared samples based on electrode materials $Li_4Ti_5O_{12}$. This spinel-type electrode material was delivered by company ELMARCO s. r. o. (Liberec, Czech Republic).
The electrode used for research was assembled in dry box from active mass ($Li_4Ti_5O_{12}$) and nickel mesh, which was used as carrier. The electrode was inserted into 3-electrode setup in experimental glass cell with 1 molar electrolyte based on lithium salt $LiPF_6$ in mixture of aprotic solvents - ethylene carbonate and dimethyl carbonate (ratio 1:1). Pure lithium subserved role counter and reference electrode in measuring system.
All measurements were executed in glove box Mbraun Labmaster with argon atmosphere. Purity values were checked and were hold at rates 0.1 ppm for H_2O and 0.1 ppm for O_2. Autolab PGSTAT 12 (ECOCHEMIE, The Netherland) was assessed for setting up standard electrochemical techniques (cyclic voltammetry) and recording achieving results. Structure analysis prepared samples were realized by high resolution electron microscopy (HRTEM) and by X-Ray diffraction.

Results and Discussion

Electrochemical behaviour of material in cycling process was researched via cyclic voltammetry. The examined material was transferred after executed experiments to HRTEM laboratory (laboratory high resolution electron microscopy) and laboratory X-Ray diffraction, where images and analysis of its structure were acquired. Results are presented via figures and tables.

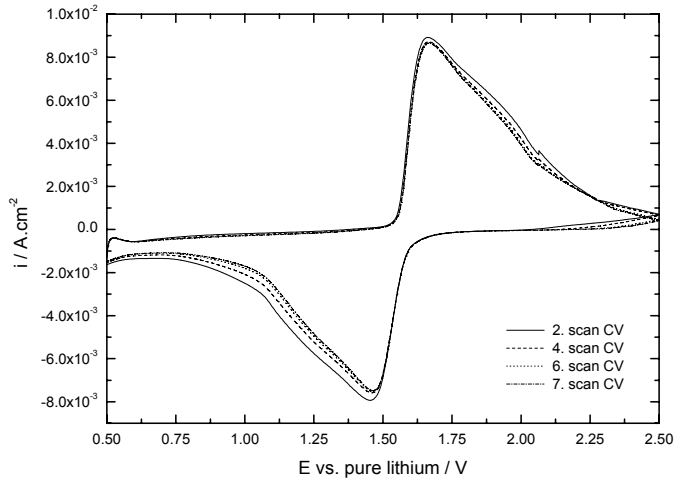

Fig. 1 *Cyclic voltammogram of $Li_4Ti_5O_{12}$ – electrolyte 1M $LiPF_6$ in EC-DMC (50:50 wt. %), parameters CV (0.4 mV.s^{-1} scan rate, 0.5 ÷ 2.5 V potential window), weight of electrode 18.5 mg.*

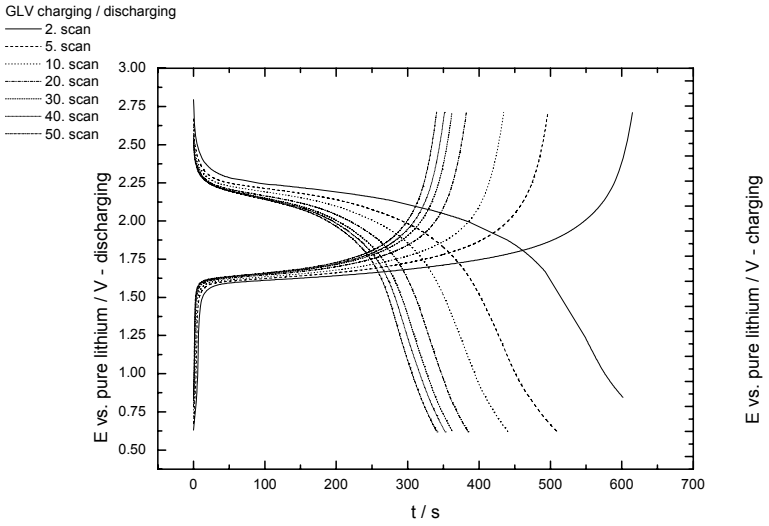

Fig. 2 *Galvanostatic measurements of $Li_4Ti_5O_{12}$ – electrolyte 1M $LiPF_6$ in EC-DMC (50:50 wt. %), parameters (2C charge/discharge rate, 0.5 ÷ 2.75 V potential range), weight of electrode 18.8 mg.*

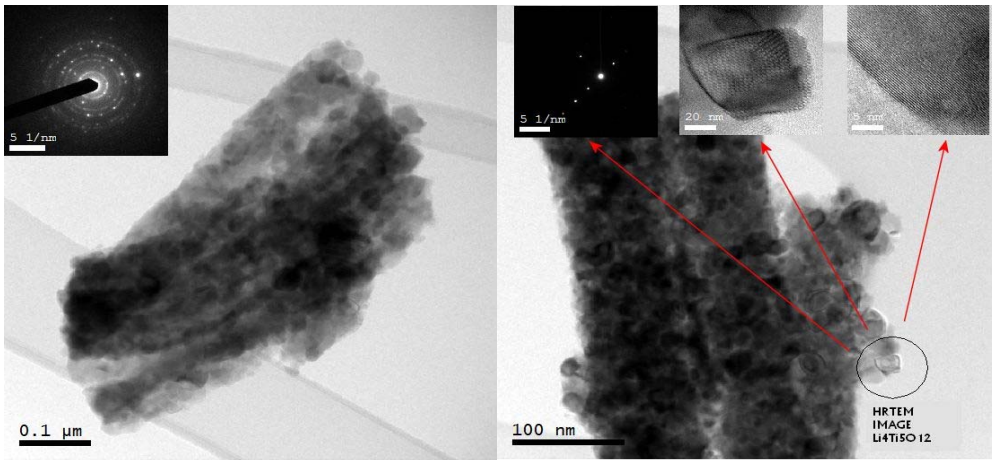

Fig. 3 *HRTEM photographs of $Li_4Ti_5O_{12}$ - nanoparticles $Li_4Ti_5O_{12}$ are deposited on binders (dark pipes).*

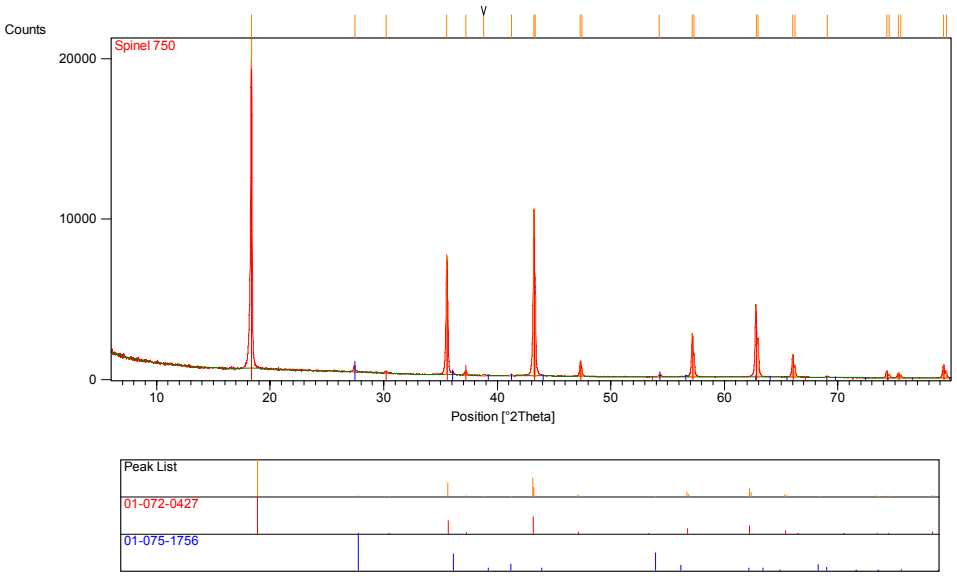

Fig. 4 *X-Ray diffraction of $Li_4Ti_5O_{12}$ - after electrochemical cycling.*

Table 1 *X-Ray diffraction results of $Li_4Ti_5O_{12}$.*

Code	Chemical formula	Mineral name	Quantity [%]
01-072-0427	$Li_4Ti_5O_{12}$	Lithium-titanate	96
01-075-1756	TiO_2	Rutile	4

Conclusions

Performed cyclic voltammetry and galvanostatic measurements of pure $Li_4Ti_5O_{12}$ without binder and conductive admixtures point to electrode material with good results in the field of reversibility reaction and electrochemical efficiency reaching values c. 95%. The scan rate was chosen fairly low by reason of achieving based behaviour of material $Li_4Ti_5O_{12}$. However, capacities of samples are lower than expected theoretical value 175 $mAh.g^{-1}$.

High resolution electron microscopy and X-Ray diffraction analysis confirm stability of electrode material $Li_4Ti_5O_{12}$ during electrochemical processes.
The ability of fast subduction / insertion of lithium ions and possibility of withdrawal bigger number of lithium ions from material structure without degradation allow using electrode material in high charge / discharge systems.

Acknowledgements

The investigations were supported by:
Academy of Sciences, Research Plan AV/0Z4030502,
Ministry of Education of Czech Republic, Project MSM002130516,
Grant Agency of the Academy of Sciences, Grant No. B208130604,
Czech Science Foundation, Grant No. 104/06/1471.

References

1. K. Kataoka, Y. Takahashi, N. Kijima, J. Akimoto, K.-I. Ohshima: Single crystal growth and structure refinement of Li4Ti5O12, in: Journal of physics and chemistry of solids. October 2007.
2. L. Kavan, J. Procházka, T. M. Spitler, M. Kalbáč, M. Zukalová, T. Drezen, M. Gratzel: Li insertion into $Li_4Ti_5O_{12}$ (Spinel). Charge capability vs. particle size in thin-film electrodes, in: Journal of The Electrochemical society, 150, p. 1000-1007. June 2003.
3. H. Ge, N. Li, D. Li, C. Dai, D. Wang: Electrochemical characteristics of spinel $Li_4Ti_5O_{12}$ discharged to 0.01 V, in: Electrochemistry communications, 10, p. 719-722. February 2008.
4. D. Djian, F. Alloin, S. Martinet, H. Lignier, J. Y. Sanchez: Lithium-ion batteries with high charge rate capacity: Influence of the porous separator, in: Journal of power sources, 172, p. 416-421. July 2007.
5. H. F. Xiang, Q. Y. Jin, R. Wang, C. H. Chen, X. W. Ge: Nonflammable electrolyte for 3-V lithium-ion battery with spinel materials $LiNi_{0.5}Mn_{1.5}O_4$ and $Li_4Ti_5O_{12}$.

COBALT ADITIVES IN NICKEL HYDROXIDE PREPARED BY ELECTRODEPOSITION

J.Vrbický[1], P.Špičák[1],V. Svoboda[1], J. Vondrák[2], M. Sedlaříková[1], J. Kazelle[1]

[1] Institute of Electrotechnology, Technical University of Brno, 602 00 Brno
[2] Institute of Inorganic Chemistry AS CR, 250 68 Řež, Prague

Corresponding author (name underlined): Jiří Vrbický
E-mail: xvrbic00@stud.feec.vutbr.cz
Phone Number, Fax Number: +420541146112, +420541146147

Introduction

Nickel hydroxide is the basic material for positive electrode of alkaline accumulators as Ni-Cd, Ni-MH and Ni-Fe. The three modification of nickel hydroxide is known, alpha, beta and gama.
The α-form has large interlayer space of 0,76 nm, whereas β-form offers layers which are just apart by 0,46 nm. Upon oxidation the α-nickel hydroxide converts to γ-nickel oxyhydroxide and β-nickel hydroxide to β-nickel oxyhydroxide. The theoretical specific capacity of α-γ couple is 456 $mAhg^{-1}$ as compared to 289 $mAhg^{-1}$ for β-β. It is based on 1.67 and 1.0 electron reversibly exchange during the redox reactions.
Alpha nickel hydroxide is stable in normal conditions, but in alkaline electrolytes is unstable and turns into β-$Ni(OH)_2$. When β-$Ni(OH)_2$ is overcharged to γ- NiOOH, the volume expansion is increasing so it occurs many construction and durability problems, it also solves the electrode made of α-$Ni(OH)_2$.
Possibility to prepare α- $Ni(OH)_2$ more stable in strong alkaline media is to add some other metals such as Al, Fe, Mn, Co and others. The aluminium doped α-$Ni(OH)_2$ was tested in various KOH electrolyte concentrations.
Samples were measured by cyclic voltammetry and EQCM microweights. Cyclic voltammetry is used for diagnostic of stability and charged to reversible capacity ratio. QCM tested changes of electrode weight and volume during cycles
An EQCM consists of a thin quartz single crystal, usually AT or BT cut, with two metal electrodes deposited on both sides of the crystal. A transverse shear wave across the thickness of the crystal
is generated that propagates into the film immobilized onto the metal layer on the crystal surface
In the electrochemical application (EQCM), one electrode of the crystal serves as the working electrode in the electrochemical cell. For thin rigid deposits, the change in the resonant frequency of the oscillating crystal (Δf) is proportional to the change in mass (Δm) per unit area (A) of the deposit on the working electrode as described by the Sauerbrey equation:

$$\Delta f = -\frac{2 * \Delta m * f_0^2}{A * (\mu\rho)^{1/2}} \quad (1)$$

where, f_0 is the fundamental frequency of the crystal and μ is the shear modulus ($2.947*10^{11}$ $g.cm^{-1}.s^{-2}$) and ρ is the density of quartz (2.648 $g.cm^{-3}$).

Experimental

The samples for cyclic voltammetry were deposited on nickel substrate from 0,05M solution of $Ni(NO_3)_2$ with various amount of $Co(NO_3)_2$. The deposition proceeded for 300s with current of 1mA Electrodes were measured by cyclic voltammetry, 3 electrode method, in 6 M KOH, counter electrode was platinum plate and reference electrode was SCE or Hg/HgO. Scan rate was 5 and 10 mV/s, potential window 0-0,45V (vs. SCE).

Results and discussion

The five samples with various amount of cobalt were measured. Nickel without cobalt on QCM, and samples with cobalt in various amounts as 19:1, 9:1, 7:3 and 6:4 parts nickel to cobalt. The best results gives the concentration of cobalt between 19:1 and 9:1. The concentration of 19:1 (Fig.1) has very stable behaviour in 6 mol/l KOH, but capacity is not so high like the 9:1molar ratio. The sample 9:1 (Fig.2) has higher capacity than the 19:1, but the structure degrades during the cycling.

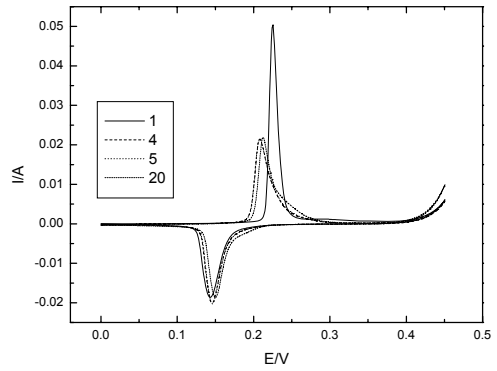

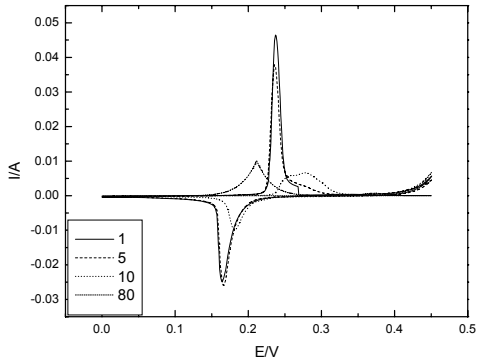

Fig. 1 Voltammogram NiCo 19:1

Fig. 2 Voltammogram NiCo 9:1

Higher concentrations of cobalt in nickel hydroxide structure has no favourable effect on this material. The cobalt create his own structures and the measurement of sample has two high peaks (Fig.3). The peaks has lower potential than the nickel hydroxide. The effective capacity of this material is lower than materials with one peak in higher potential.

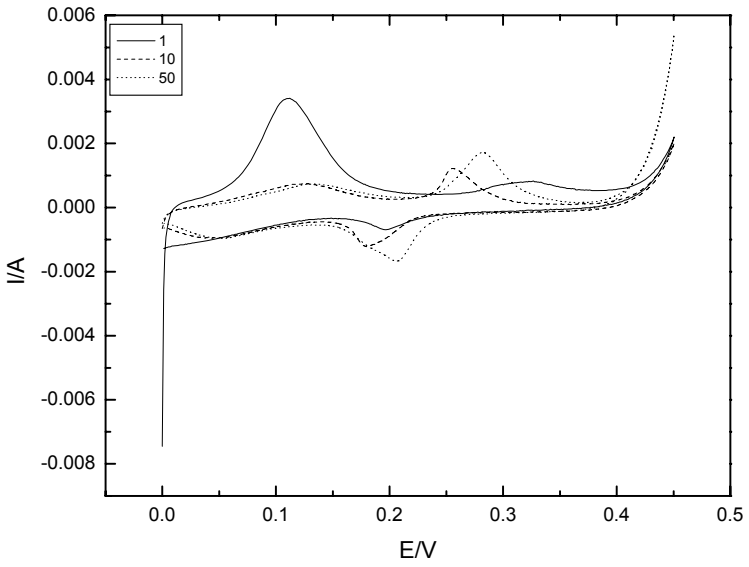

Fig. 3 *Voltammogram NiCo 6:4*

There is a different behaviour between 1 and 6 molar potassium hydroxide. During oxidation (charging) mass increased in the case of 1M KOH, in strong alkaline there is a decrease probably caused by expulsion of anions from interslab space on fig. 4 and 5. This can be the reason of partial degradation of α-$Ni(OH)_2$ into β- $Ni(OH)_2$. The remaining part of massogram is similar to 1M. Mass increasing/decreasing is due to cation uptake/expulsion from electrolyte ang proton intercalation/deintercalation.

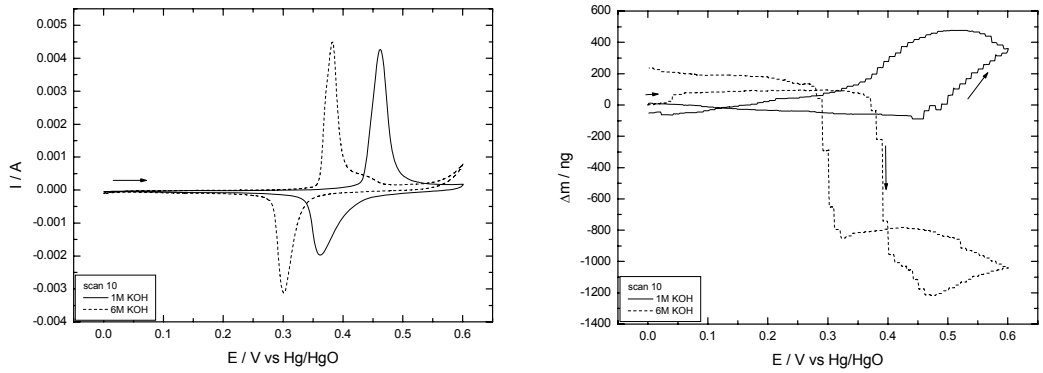

Fig. 4 *Comparison of electrodeposited Ni(OH)2 in 1 a 6M KOH, CV and EQCM*

Conclusion

The capacity and stability of cobalt substituted α- $Ni(OH)_2$ were investigated.
This stuff is unstable in highly alkaline media, this is caused by high pH and anion expulsion from interslab space. This result into closering of spaces to each other and drop of electrochemical specific capacity.
The cobalt additive has good influence on stability of nickel hydroxide in low concentration, maximally 1:9 to nickel. The higher concentration creates another structures and the electrode material has lower potential. The concentration of nickel-cobalt hydroxide between 19:1 and 9:1 will be investigated for optimalisation of capacity and stability.

Acknowledgment

Ministry of Education of Czech Republic, Project MSM0021630516, Ministry of Environment of Czech Republic, Grant No. VaV SN/3/171/05,

References

[1] M.A. Fetcenko , S.R. Ovshinsky, B. Reichman, K. Young,
C. Fierro, J. Koch, A. Zallen, W. Mays, T. Ouch: *Recent advances in NiMH battery technology,* Journal of Power Sources *165 (2007) 544–551*
[2] Rand, D.A.J., Woods, R, Dell, R.M.: *Batteries for electric vehicles* – Tauton, Somerset, England, Research studies press, 1998
[3] Falk, S.U., Salkind, A.J.: *Alkaline storage Batteries* - New York, The electrochemical society INC., 1969
[4] Zhao, Y.L., Wang, J.M., Chen, H., Pan,T., Zhang, J. Q., Cao, C.N.: *Al-substituted α-nickel hydroxide prepared by homogenous precipitation method with urea*, International Journal of Hydrogen Energy, 2004
[5] Wang, C.Y., Zhong, S., Konstantinov, K., Walter, G., Liu, H.K.: *Strucural Study of Al-substituted nickel hydroxide*
[6] GANESH-KUMAR, V., BAET,S. W., LEE, J. S., NAM, K. W., KIM, K. B., Contraction of Alpha-nickel hydroxide Layers by Excess Coulombic Attraction of Anions
[7] OHLIGSCHLASGER, T., SCHWITZGEBEL, G., EQCM contributions to the reactions of the nickel
oxide electrode. Phys. Chem. Chem. Phys., 2001, 3, 5290-5296
[8] WEHRENS-DIJKSMA M., MOTTEM P.H.L., Electrochemical Quartz Microbalance characterization of Ni(OH)2-based thin film electrodes. Electrochimica Acta 51 (2006) 3609–3621

INFLUENCE OF PRESSURE ON THE CYCLING STABILITY OF SILICON-ELECTRODES

Fuchsbichler B.[(1)], Kren H.[(2)], Schmuck M.[(1)], Sternad M.[(2)], Bayer C.[(1)], God C.[(1)], Lux S.[(1)], Stangl C.[(1)], Koller S.[(1)]*

[1] Graz University of Technology – Institute for Chemistry and Technology of Materials Stremayrgasse 16, A-8010 Graz
[2] Graz University of Technology – Institute of Electrical Measurement and Measurement Signal Processing, Kopernikusgasse 24, A-8010 Graz

E-mail: b.fuchsbichler@tugraz.at
Phone Number: +43 316 873 8264
Fax Number: +43 316 873 8272

Introduction

Presently graphite or other carbonaceous materials are the most common assembled active masses for negative electrodes in lithium ion batteries. The theoretical capacity (372 $mAh \cdot g^{-1}$) of the LiC_6-graphite-compound is compared to binary lithium alloys, for example $Li_{22}Si_5$ with a theoretical capacity of 4200 $mAh \cdot g^{-1}$, poor [1]. Unfortunately the high capacity of these lithium alloys is combined with a high volume change during lithium insertion and deinsertion [2], which causes disintegration of the silicon particles and leads to high capacity loss. A couple of efforts have been made to improve Li/Si alloy electrodes.

We studied the influence of extrinsic pressure during cycling on the Li/Si alloy electrodes to stabilize the structure. So the disintegration of the silicon particles is limited which causes a better cycling stability of the electrodes.

Experimental

Our silicon electrodes are composed of silicon nanoparticles, *Super P* and *CMC* as binder. The electrode slurry was prepared via an optimized dispersing technique.

The galvanostatical charge – discharge cycling tests were performed in a three electrode configuration swagelok-T-cell, using a lithium metal foil as counter and reference electrode and the silicon electrode as working electrode. To apply a defined pressure on the electrodes, the spring on the working electrode side was adjusted.

Results and Discussion

Our research results clearly indicate a significant positive influence of pressurized electrodes concerning cycling stability as well as capacity fading (figure 1). Additionally to the better cycling stability we achieved higher charge/discharge capacities when the pressure on the electrode was increased, these results are shown in table 1.

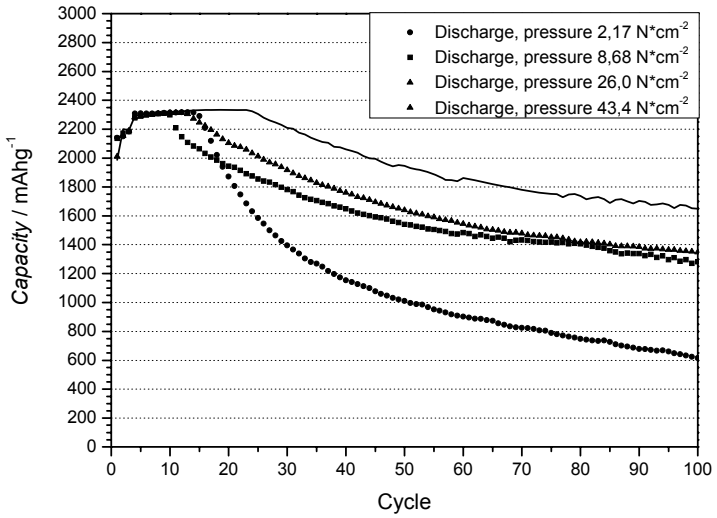

Fig. 1 *comparison of the cycling results of different pressurized silicon-electrodes*

Table 1 *comparison of the discharge-capacities at different pressures*

cycle	***discharge-capacity [mAh·g^{-1}]***			
	pressure			
	2,17 [N·cm^{-2}]	***8,68 [N·cm^{-2}]***	***26,0 [N·cm^{-2}]***	***43,4 [N·cm^{-2}]***
50	*1111*	*1539*	*1639*	*1978*
100	*615,4*	*1282*	*1347*	*1946*

References

1. B.A. Boukamp, G.C. Lesh, R.A. Huggins, J. Electrochem. Soc., **128** No4, 1981, pages 725-729
2. Winter M., J.O. Besenhard, M.E. Spahr and P. Novak, Adv. Mater., **10**, 1998, 725

ALLOYING OF ELECTRODEPOSITED SILICON WITH LITHIUM FOR THE USE AS ANODE MATERIAL IN LITHIUM ION BATTERIES

Martin Schmuck[1], Andrea Balducci[2], Barbara Rupp[1], Simon Lux[1], Stefano Passerini[2], Martin Winter[2]

[1] Institute for Chemical Technology of Materials, Graz University of Technology, Stremayrgasse 16, A-8010 Graz, Austria
[2] Institute for Physical Chemistry, University of Münster, Corrensstraße 28, D-48149 Muenster, Germany

martin.schmuck@tugraz.at
phone: +43 316 873 6264
fax: +43 316 873 8272

Introduction

Lithium-Ion Batteries (LIB) are today one of the most promising high energy power sources and extensive research still continues to achieve further improvements in terms of higher rate capability, time and cycle life, safety and to enlarge the temperature operation field.
Most state of the art Lithium-Ion Batteries use graphite or other carbonaceous materials for active mass in negative electrodes. A theoretical capacity of 372 mAh g^{-1} can be achieved from the LiC_6 compound but this is compared to 4200 mAh g^{-1} from $Li_{22}Si_5$ poor.
To obtain suitable thin film Silicon electrodes the method of electroplating can be a convenient one. Due to the redox potential of Silicon it is necessary to perform the electroplating in organic [1,2] or ionic liquid electrolyte [3,4]. In our investigations we used Propylene Carbonate (PC) and *N*-Butyl-*N*-methylpyrrolidinium bis (trifluormethanesulfonyl)imide ($Pyr_{14}TFSI$) as electrolyte solvent.

Experimental

The electroplating experiments were performed in a three-electrode homemade Swagelok ® cell. A copper foil was implemented as the working, lithium piston as the reference one, and lithium foil as the counter electrode. On the one hand the electrolyte solution used in this study was composed of 1M $SiCl_4$ as the silicon source, PC as solvent and 1M LiTFSI as conducting salt, on the other hand for the electroplating with ionic liquid we used 1M $SiCl_4$ and 1M LiTFSI in $Pyr_{14}TFSI$ room temperature Ionic Liquid. All samples were deposited at room temperature at 1.0 V vs. Li/Li^+ and characterized with SEM and CV.

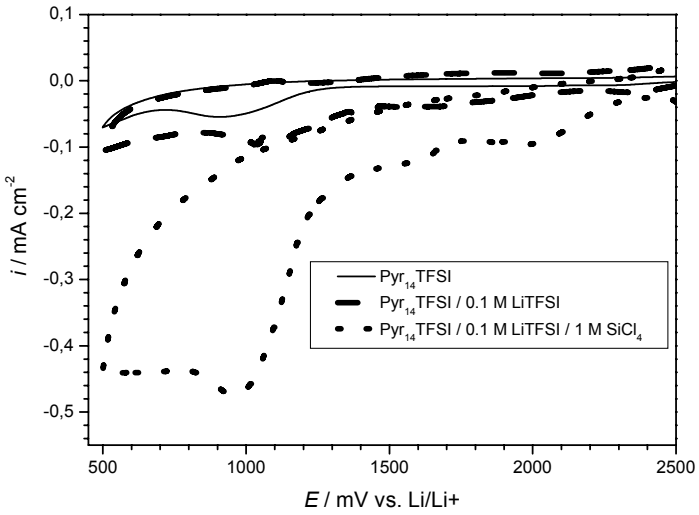

Fig. 1 *Cyclic voltammograms for a Cu electrode in $Pyr_{14}TFSI$ containing 1 M $SiCl_4$ and 0.1 M LiTFSI. Scan rate: 5 mV/s.*

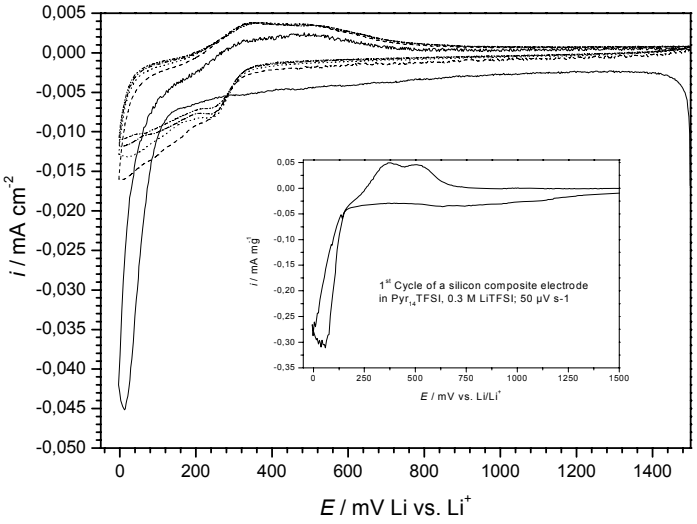

Fig. 2 *Cyclic voltammogram of a, in Ionic Liquid deposited, silicon electrode; in $Pyr_{14}TFSI$ containing 1M LiTFSI. Scanrate: 50 µV/s.*

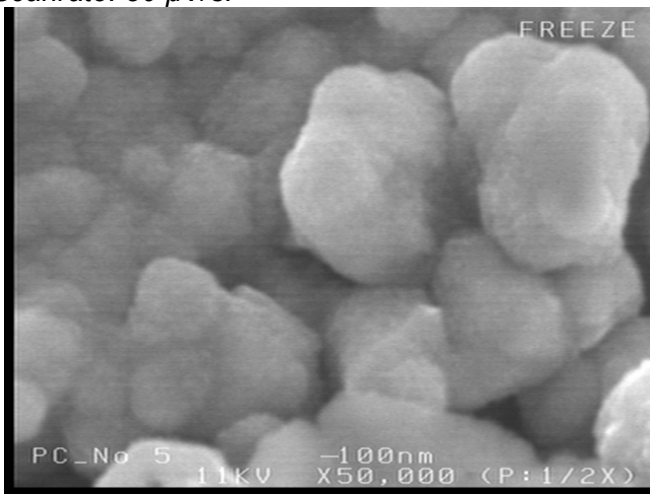

Fig. 3 *SEM imagine of silicon electrodeposited in $Pyr_{14}TFSI$.*

Acknowledgements

The authors acknowledge the European Commission for the financial support under contract NMP3-CT-2006-033181 (ILLIBATT, Ionic-Liquid-based Lithium Batteries).

References

1. A. E. Austin, U.S. Oat. 3990953 (1976)
2. Y. Takeda, R. Kanno, O. Yamamoto, T. R. Rama Mohan, C.H. Lee, F. A. Kröger, J. Electrochem. Soc., 128, 1221 (1981)
3. S. Zein El Abedin, N. Borissenko and F. Endres, Electrochemistry Communications 6, 5, 510-514, 2004
4. Yusaku Nishimura, Yasuhiro Fukunaka, Electrochimica Acta, 53, 1, 111-116, 2007

COMPREHENSION AND TAILORING OF CELLULOSE BASED BINDERS AS FUNDAMENT FOR APPLICABLE SILICON/GRAPHITE COMPOSITE ANODES

Koller S.[(1)], Fuchsbichler B.[(1)], Schmuck M.[(1)], , Bayer C.[(1)], God C.[(1)], Lux S.[(1)], Stangl C.[(1)], Kren H.[(2)], Sternad M.[(2)], Winter M[(3)]

[1] Graz University of Technology – Institute for Chemistry and Technology of Materials Stremayrgasse 16, A-8010 Graz
[2] Graz University of Technology – Institute of Electrical Measurement and Measurement Signal Processing, Kopernikusgasse 24, A-8010 Graz
[(3)] Institute for Physical Chemistry,
University of Münster, Corrensstraße 28, D-48149 Münster, Germany

E-mail: stefan.koller@tugraz.at
Phone Number: +43 316 873 8763
Fax Number: +43 316 873 8272

Introduction

Most state of the art Lithium Ion Batteries use graphite or other carbonaceous materials for active mass in negative electrodes. A theoretical capacity of 372 $mAh \cdot g^{-1}$, which can be achieved from the LiC_6 compound is compared to 4200 $mAh \cdot g^{-1}$ from $Li_{22}Si_5$ poor. Unfortunately the high capacity of the Si/Li-alloys is strongly addicted to high volume changes during Lithium insertion and deinsertion [1], which causes disintegration of the silicon particles and leads to unacceptable high capacity loss. Numerous efforts have been made to improve Li/Si alloy electrodes.

Experimental

Aqueous binders containing dispersed SBR-rubber and carboxy methyl cellulose (CMC) as viscosity regulating agent, got the subject of matter of many reports. We found, that SBR-rubber, dissolved in toluene without CMC, works similar bad like PVdF based binders. Furthermore CMC only works better than the combination of CMC and SBR-rubber[1]. This result is not expected, because the flexible SBR-rubber should bear the high volume changes much better than CMC, which is, like it had been shown by Dahn et. al., very brittle[2]. An explanation can be found, if we take a closer look on the structure of CMC. The carboxyl-groups are able to react with hydroxyl groups on the surface of the silicon particle in the way of esterification (*Figure 1, 2*). To provide evidence of this mechanism, we did ATR-IR studies. A shift of the carboxyl group from 1592 cm^{-1} to 1629 cm^{-1} was detected, which is a strong indication, that the carboxyl group is bounded to the silicon surface.

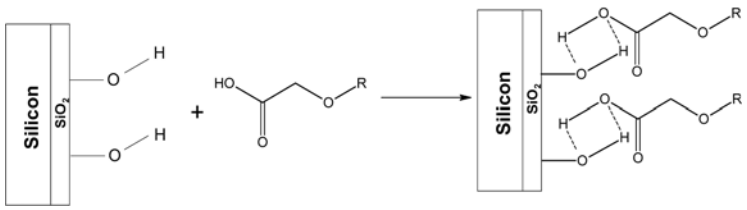

Fig. 1 *CMC coordinated with silicon particle*

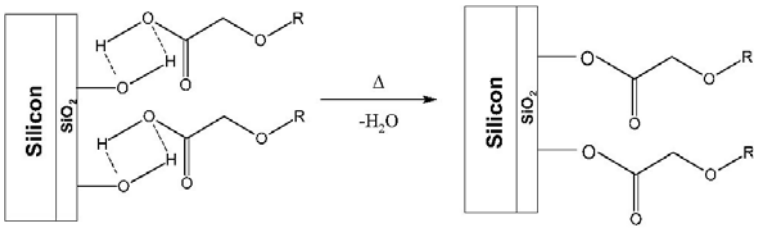

Fig. 2 *Silicon particle linked with CMC*

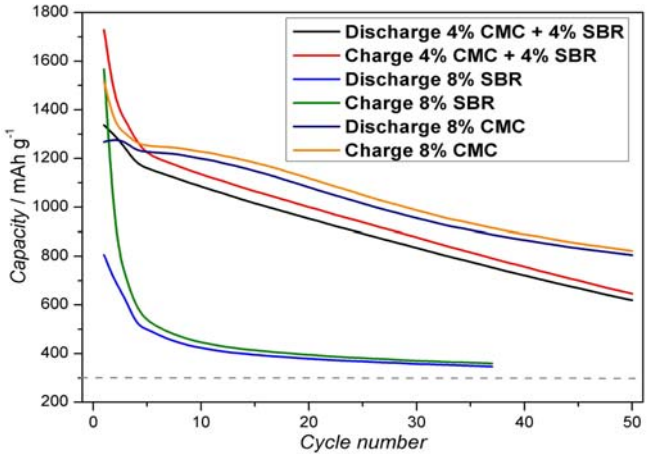

Fig. 3 *Comparison of differnt binder Systems*

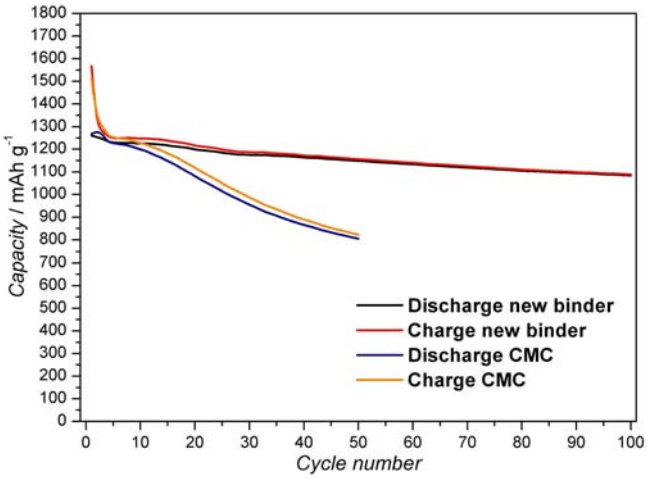

Fig. 4 *Comparison of commercial CMC and new cellulose binder*

Results and Discussion

This knowledge was used, to develop a new cellulose based binder, which improves cycling stability up to 12 % of capacity loss over 100 cycles [2].

References

1. B.A. Boukamp, G.C. Lesh, R.A. Huggins, J. *Electrochem. Soc*. Vol.128 No. 4, 1981, pages 725-729
2. Jing Li, R. B. Lewis, J. R. Dahn, *Electrochemical and Solid-State Letters,* 2007,10 (2) A17-A20

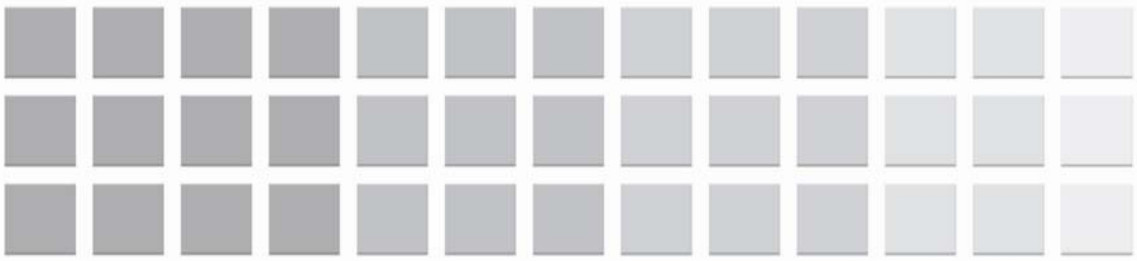

9th ABA

BRNO 2008

Advanced Batteries and Accumulators

Methods

LIGHT BEAM INDUCED VOLTAGE IN DYNAMIC MODE

Vaněk J., Jandová K., Sládek F.

Department of Electrotechnology,
Faculty of Electrical Engineering and Communication,
University of Technology Brno, Czech Republic

Introduction

This work deals with issues of technological process characterization and optimization by application of empirical models. The general aim is to create methodology for technological process optimization. The methodology consists of appropriate experimental plan that yields the most information from predetermined model with the least number of experiment runs. This statistical approach determines cause and effect relationships between technological variables and response with respect to the quality and reliability.

Experimental

LBIV measurement for solar cell local characterization has been developed and tested on mono-crystalline Si solar cells. Solar cells were locally illuminated by a focused light source in pulse mode (Fig. 2). The response (voltage) of the solar cell was filtered and converted to DC signal and measured at stationary conditions during scanning process. A large number of independent data with high spatial resolution are obtained. Applying an advanced fitting procedure on these data yields a set of local parameters for each point on the solar cell which give information on the distribution of the photo voltage, the series and shunt resistance, the lateral diffusion of minority carriers.

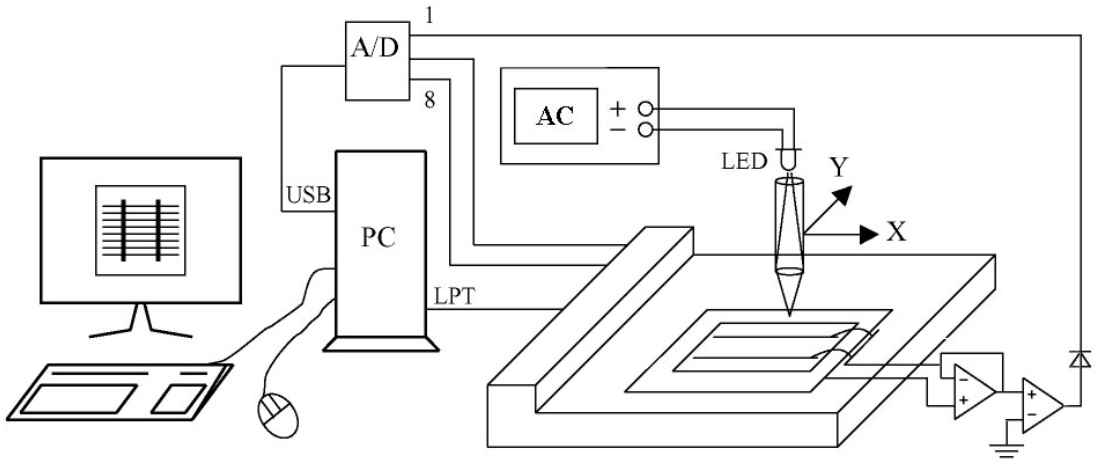

Fig. 1 *Workplace with the LBIV method.*

Light Beam Induced Voltage (LBIV) works on principle of exposure very small area of a solar cell, usually by laser beam of LED focused directly on the solar cell surface. This point light source moves over measured solar cell in direction of both X and Y axis. Thanks to local current response the XY current distribution in investigated solar cell can be measured. Acquainted data are then arranged in form of a voltage map and the behaviour of all solar cell single parts is thus visible. In such current map is therefore possible to determine majority of local defects.

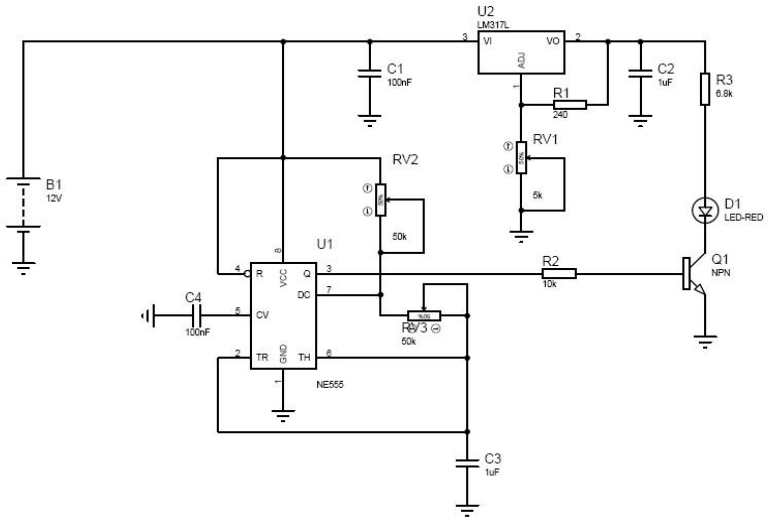

Fig. 2 *Power pulse source for LED diode used to illuminate solar cell in LBIV method.*

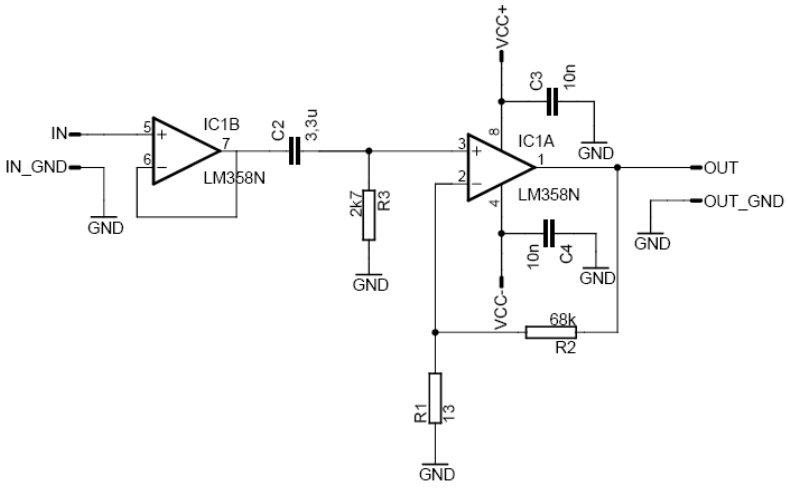

Fig. 3 *High impedance band-pass filter and amplifier used to LBIV method.*

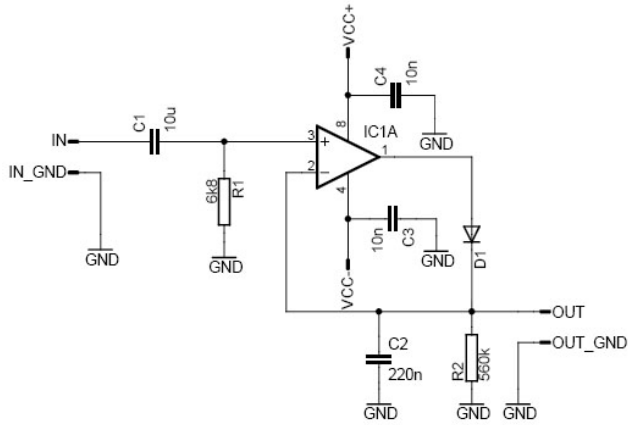

Fig. 4 *Voltage rectifier used to LBIV method.*

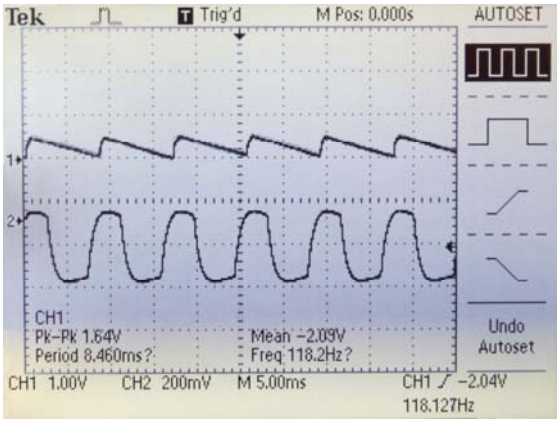

Fig. 5 *Signals measured on input and output of bandpass filter and rectirer.*

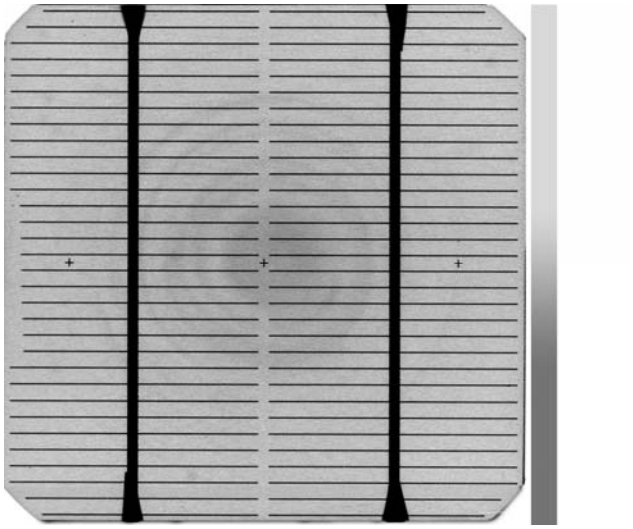

Fig. 6 *Result image of LBIV method in dynamic mode (Sample no.8)*

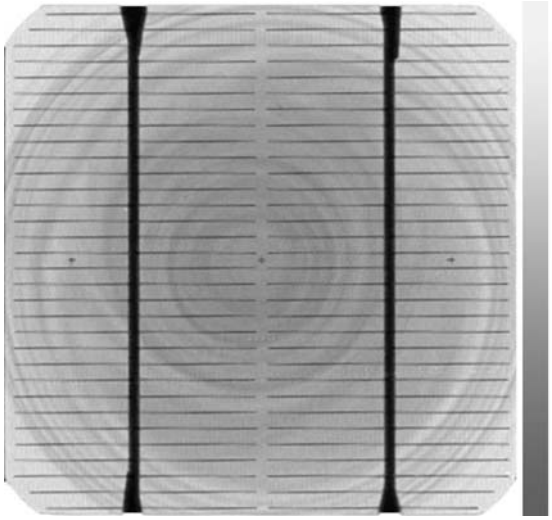

Fig. 7 *Result image of LBIV method in dynamic mode (Sample no.14)*

Results and Discussion

Pictures obtain by LBIV method contain different information about structure and defects of photovoltaic solar cells. Typical result of LBIV method is surface scan of material defects and shape of contacts bar. On the Fig. 6 there can be seen some defects and in homogeneity in diffusion layer and in middle of solar cell dark circles caused by oxide impurities in substrate – swirl defect. On the Fig. 7 there can be seen much more clearly the swirl defect in solar cell substrate.

Acknowledgements

This research has been supported by project MSM0021630516.

References

[1] Vanek, J., Brzokoupil, V., Vasicek, T., Kazelle, J., Chobola, Z., Barinka, R. *The Comparison between Noise Spectroscopy and LBIC* In The 11th Electronic Devices and Systems Conference. The 11th Electronic Devices and Systems Conference. Brno: MSD, 2004, s. 454 - 457, ISBN 80-214-2701-9
[2] Vasicek, T. *Diplomova prace*, 2004
[3] Pek, I. *Diplomova prace*, 2005
[4] Sladek. F. *Diplomova prace*, 2008
[5] Benda, V. - Macháček, Z. - Salinger, J. Diagnostic of the N+ Large Homogeneity in Large Area Silicon Solar Cells Using Local IrradiationIn: 21st European Photovoltaic Solar Energy Conference [CD-ROM]. Munich: WIP - Renewable Energies, 2006, s. 1512-1514. ISBN 3-936338-20-5.

EVALUATION OF SURFACE TEXTURE WITH CONFOCAL LASER SCANNING MICROSCOPE OLS 3000

Karel Maňas, Emil Svoboda, Jiří SUKÁČ and David KUSMIČ

Department of Mechanical Engineering, University of Defence in Brno
Kounicova 65, CZ-612 00, Brno, Czech Republic

Introduction

Surface texture (roughness) has a decisive impact on the performance features and behaviour of components and together with the surface layer properties is crucial for the useful life and functional reliability. At present, assessment of surface roughness and waviness can be performed using a number of methods. The contribution compares measurement of principal parameters of surface roughness with confocal microscope LEXT and with a classic 3D profilometer.

Experimental

1. Principles of measuring surface roughness with individual instruments

1.1. Microscope Olympus LEXT OLS 3000

Confocal laser microscope LEXT OLS 3000 allows for observation of surfaces both in 2D image and in 3D image enhances quality of acquired images and enables to measure lengths, shapes and surface roughness. It allows for 3D observation as well as high precision 3D measurement in real time. Thanks to its outstanding resolution of 0.12 μm and magnification range from 120x to 14 400x, confocal microscope LEXT can operate within the limits of common optical microscopes and scanning electron microscopes. The laser confocal microscope LEXT – scanning microscope – is the objective using to focus the laser beam on the very small point and in the x-y direction to moving. By the confocal optical system is in the place of focalization the diaphragm with a hole placed which separate the light beams from the unfocused places. The CCD detector entrap the reflected light beams from the sample surface and the software built up the 3D picture of the sample only from the focused vertical levels, every vertical level has his own height coordinate z. The 3D picture is built up from the x-y-z coordinates. Surface roughness measurement complements the operation program. Measurement can be performed only for 3D scanned surface using confocal optics, which is a case non-contact surface roughness measurement of components.

Talysurf CLI 1000

3D surface profiling system Talysurf CLI 1000 is effective for carrying out a fast spatial surface assessment, analyzing surface along three axes, including analyses assessing surface texture both from the section profile (2D) and from the surface (3D). At the inductive gauge is the diamond point on the gauge arm is moved through the surface. For this system is the small measuring power characteristic. Basic technical parameters in case of using the inductive gauge: contact measurement, ranging from 0,1 mm to 2.5

mm, excellent resolution – from 2 nm to 40 nm, measurement of internal surfaces and a high precision.

2. Conditions for correct measurement of surface roughness

Surface texture – is defined in the ISO 8785. The basic rules for the surface roughness evaluation are noted in the ISO 4288; the parameters of the surface structure (roughness) are defined in the ISO 4287.
Roughness – is the smallest peaks and valleys on the surface. The roughness can't be interchanged to the peaks and valleys with the greater values of wavelength, so-called waviness. The waviness characterizes the qualities of machines and tools.
The cut-off option is used for roughness measurement and obtaining "correct" measurement results will depend on setting of a number of parameters that can be selected both with the measuring instrument and in the process of assessment. To set the measuring instrument correctly, the cut-off must be properly chosen.
Cut-off – the limit wavelength represents the length. While the basic length is a physical quantity (length of the inspected surface), the limit wavelength (cut-off) is a software function. There are many guidelines for selecting the limit cut-off wavelength, e.g. in ISO 4288 (see Table. 1). It is recommended to set the profile filter at the value approximately corresponding with the spacing of peaks and valleys multiplied by five.

Table 1 *Recommended cut-off values (ISO 4288)*

Periodic profiles	Nonperiodic profiles		Cut-off	Principal /Assessed length
RSm [mm]	Rz [µm]	Ra [µm]	Λc [mm]	Λc / L [mm]
>0,04-0,13	>0,1-0,5	>0,02-0,1	0,25	0,25/1,25
>0,13-0,4	>0,5-10	>0,1-2	0,8	0,8/4
>0,4-1,3	>10-50	>2-10	2,5	2,5/12,5

The real field of view of LEXT is indicated in Table 2. In comparison with Table 1 it becomes evident that the measured length for surface roughness assessment is applicable only for the surfaces with roughness less than Ra < 0,1 µm and magnification 5x (zoom 1x and 2x) and magnification 10x (zoom 1x). In all other cases the length necessary for proper measurement of surface roughness is less.
If the surface has a value of Ra > 0,1 µm (the standard requires the basic length of 4 mm), then the required length will not be displayed in the field of view of the microscope.

Table 2 *Field of view of microscope Lext OLS 3000*

Objective magnification	Zoom			
	1x [mm]	2x [mm]	4x [mm]	6x [mm]
5x	2,56 x 2,56	1,28 x 1,28	0,64 x 0,64	0,427 x 0,427
10x	1,28 x 1,28	0,64 x 0,64	0,32 x 0,32	0,213 x 0,213
20x	0,64 x 0,64	0,32 x 0,32	0,16 x 0,16	0,107 x 0,107
100x	0,128 x 0,128	0,064 x 0,064	0,032 x 0,032	0,021 x 0,021

The comparison of Tables 1 and 2 results in the fact that the confocal microscope displays the length (surfaces) which is less than necessary for assessing the surface roughness with values higher than Ra = 0,1 µm.

3. Roughness measurement Methodology

3.1. Confocal laser microscope LEXT OLS 3000

In surface roughness measurement with confocal microscope LEXT OLS 3000 it is desirable to prepare the measured profile so that the profile is levelled with respect to the horizontal plane; for preparation of the measured surface prior to 2D surface texture assessment, two procedures have been chosen, which are linked with various types of surface treatment and profile treatment by means of filters:

Procedure A – a simplified procedure involving a gradual application of three filters (Fig. 1):

1. Filter - Tilt Correction 2. Filter - Height Noise Removal 3. Filter - Tilt Correction

Procedure B – a procedure involving a gradual application of six filters, which are suitable for a given profile (Fig. 1):

1. Filter - Tilt Correction 2. Filter - Height Noise Removal 3. Filter - Spike Removal
4. Filter - Profile Shape Correction 5. Filter - Smoothing 6. Filter - Tilt Correction

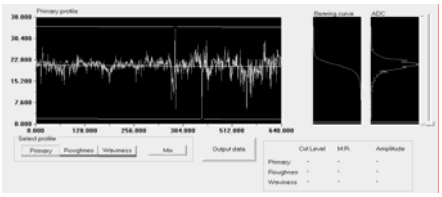

Procedure A

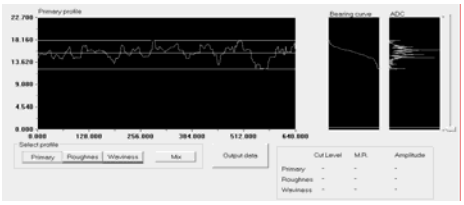

Procedure B

Fig. 1 *2D profiles after application of filters*

After this procedure, the software of microscope Lext OLS 3000 used the filter for identifying roughness and waviness deviations. The software offers the following options of filtering: without filter 1/3; 1/5; 1/10; 1/20 and 1/50.

Measurements were carried out on two etalons with a big difference in nominal values of surface roughness: lapped surface Ra = 0,05 μm and ground surface Ra = 0,8 μm. Three different cuts were chosen in the 3 D acquired images: one in the central part and two were symmetrically located on both sides. Then individual filters were applied to the profiles in compliance with the procedure A or B and surface roughness parameters were determined.

3.2. Talysurf CLI 1000

Surface roughness measurement of etalons was made in cut (2D profile) at the length of 4 mm with the step of 0,5 μm by the inductive gauge with the range of 523 μm in Z axis and resolution of 8 nm. Three profiles were measured in the same way as with confocal microscope Lext OLS 3000. Assessment of the obtained data was performed using program Talymap Platinum with cut off = 0,25 mm on the etalon profile with the nominal value of Ra = 0,05 μm and cut off = 0,8 mm on the etalon profile with the nominal value of Ra = 0,8 μm.

Results and discussion

Surface roughness was assessed by means of selected height and length parameters of roughness profile (Rx) and waviness profile (Wx):

1. Average arithmetic deviation of the profile Ra, Wa

2. Average quadratic deviation of the profile Rq, Wq
3. Average width of elements of the profile RSm, WSm

Assessment of results in measuring surface roughness with confocal microscope LEXT OLS 3000, their comparison with parameters obtain with 3D profilometer Talysurf CLI 1000 are shown in Tables 3 – 4.

Etalon roughness Ra 0,05 μm - Values of height parameters of surface roughness Ra captured with the confocal microscope using procedure A are comparable with the etalon nominal value and measurements performed with the profilometer only in magnification 100x without filtering (values in bold print in the table). When filtered, the parameters have lower values (cca 35 – 60 % of the original value).

The same tendency can be observed in parameters Rq and Wa. If lower levels of magnification are used, the values are higher (see Table 3).

Table 3 *Surface roughness Ra – etalon – lapped surface*

Procedure A							
Filter for roughness assessment	Average arithmetic deviation of roughness profile Ra [μm]						
	Magnification					Inductive gauge	Etalon
	5x	10x	20x	50x	100x		
unfiltered	10,656	1,557	0,496	0,204	0,056	0,057	0,05
1/3 ÷ 1/50	8,38÷7,38	1,44÷1,35	0,47÷0,43	0,2÷0,165	0,03÷0,02		
Procedure B							
bez	5,046	0,685	0,222	0,113	0,045		
1/3 ÷ 1/10	4,2÷3,9	0,54÷0,51	0,21÷0,21	0,09÷0,07	0,03÷0,02		
1/20	3,796	0,463	0,196	0,059	0,016		
1/50	2,608	0,337	0,143	0,049	0,009		

Length parameters RSm (Tab. 4) have a comparable value only with magnification 10x and filters 1/5 to 1/20; if the magnification is 5x, the values are up to ten times higher; if the magnification is 20x to 50x, the captured values are considerably lower and amount to 15 to 60 % of the value measured with the inductive profilometer. Comparable results were not obtained for parameter WSm with any magnification or filter – all values are substantially lower.

Table 4 *Parameter RSm; procedure A – etalon – lapped surface*

Filter in roughness assessment	Average width of profile elements RSm [mm]					
	Magnification					Inductive gauge
	5x	10x	20x	50x	100x	
without	0,112	0,018	0,009	0,004	0,006	0,015
1/5	0,050	0,016	0,009	0,004	0,004	
1/20	0,096	0,015	0,009	0,003	0,002	
1/50	0,069	0,014	0,008	0,003	0,002	

When applying procedure B the height parameters Ra, Rq, Wa reached on the whole lower values and for the length parameters RSm and WSm the measured values were higher. Comparable values of the surface roughness parameter Ra (Table. 3) could be measured only with magnification 50x and filters 1/20 and 1/50. All other height parameters Rq and Wa have a tendency similar to procedure A.

Length parameters RSm have a comparable value only with magnification 20x without filtering; in all other cases the measured parameters have the same tendency as in case

of procedure A, but the measured values are lower. No comparable results were obtained for parameter WSm in any measurement – all values obtained from the confocal microscope are considerable lower.
Etalon roughness Ra 0,8 μm - Values of height parameters of surface roughness Ra captured with the confocal microscope using procedure A are comparable with the etalon nominal value and measurements performed with the profilometer only in magnification 50x and filter 1/3. The same tendency can be observed in parameter Rq; parameter Wa has identical value only with magnification 100x and filter 1/3, all other parameters are substantially higher. Length parameters RSm have a similar value only if magnification 5x is used and any filer, but they are lower by about 10%. All other results are lower, regardless of magnification or filter. In case of parameter WSm, no comparable results were reached with any magnification or filter.
When applying procedure B the height parameters Ra, Rq, Wa reached lower values than in case of procedure A, while the length parameters RSm and WSm exhibited higher measured values. Comparable values of the surface roughness parameter Ra could be measured only with the magnification 20x and filters 1/3 and 1/5. All other values were higher. Parameter Rq has a similar tendency as parameter Ra. Parameter Wa reaches a comparable value only with magnification 100x and filter 1/3. Other values are higher. Length parameters RSm have a comparable value only with magnification 20x without filtering; in all other cases the measured values are lower. In case of parameter WSm, no comparable results were reached in any measurement (all measured values are considerably lower).
Generally speaking, the values of length parameters of surface roughness become lower with a higher magnification (5x to 100x), since roughness is assessed for a shorter length, which involves less uneven surface); filters have the same effect (without filter, 1/3 to 1/50), when the peak values are obtained without filtering and the lowest values using filter 1/50; it is in compliance with the principles of surface roughness assessment, as the small filter divides the profile for calculating the parameters into shorter lengths.

Conclusions

Following conclusions and recommendations can be drawn from the values of surface roughness measured with confocal microscope LEXT OLS 3000:
surface roughness assessment using height parameters is applicable to the surfaces having roughness Ra < 0,1μm in magnification 100x without filtering,
surface roughness assessment using length parameters is not suitable owing to a low correspondence,
lower values of surface roughness are obtained in procedure B than in procedure A – due to smoothing of the profile.
When measuring surface roughness with the confocal microscope it is recommended to compare the measured parameters with the parameters measured on an appropriate etalon of surface roughness, which was manufactured using the same technological process, since a more objective measurement can be obtained. Roughness measurement with the confocal microscope should be considered as complementary to analyses carried out with observation or measuring microscope.

Acknowledgements

The contribution has been prepared using the results of the research intent UO FVT 0000404 “Research and Development of modern materials and technologies for military equipment applications“as well as SV K216 “Application of materials and technologies in special equipment“and is a component in solving these research issues...

References

[1] ISO 4288:1998 - Geometrical product specifications (GPS) - Surface texture: Profile method - Rules and procedures for the assessment of surface texture
[2] ISO 8785:2000 - Geometrical product specification (GPS) - Surface imperfections - Terms, definitions and parameters
[3] ISO 4287:1999 - Geometrical product specifications (GPS) - Surface texture: Profile method - Terms, definitions and surface texture parameters
[4] Manual LEXT OLS 3000
[5] Manual Talysurf CLI 1000

IMPEDANCE OF LITHIUM-ION BATTERIES

V.A. Tarnopolsky [1], *T.L. Kulova* [2], *A.M. Skundin* [2]

[1]*Holding "Russian Accumulators", Moscow, Russia*
[2]*Frumkin Institute of Physical Chemistry and Electrochemistry RAS, Moscow, Russia*

Cylindrical and flat lithium-ion batteries (LIB) as well as symmetrical cells were studied using impedance spectroscopy. Equivalent circuit was proposed, its parameters and activation energies were evaluated for each of ion transfer stages.

Introduction

Lithium-ion cell is a complicated object for an impedance spectroscopy study. There are many works on the impedance of LIB [1-5], however only few of these works provide detailed analysis of the impedance data.

Experimental

Cylindrical 18650 and flat pouch test cells were assembled by "Sony" and "Samsung". Single-layer pouch test cells were manufactured using 41 x 22 mm electrodes. The active materials content was identical to that of commercial cells: anode consisted of graphite (90% by weight), cathode was made of lithium-nickel oxide, doped with cobalt and aluminum (83% by weight). The separator was 30 μm thick porous polypropylene membrane. 1.15M solution of $LiPF_6$ in a EC/DMC/EMC mixture was used as an electrolyte.
To obtain more reliable data on each of the electrodes cycled pouch test cells were disassembled in glovebox (dry Ar atmosphere) and symmetrical anode/anode and cathode/cathode cells were assembled and filled with fresh electrolyte. The same approach was used in [6,7]
The impedance spectra in 0.025 Hz – 100 kHz region were observed using frequency response analyzer "Solartron 1255 B" with "Solartron 1286" electrochemical interface. The voltage amplitude was 10 mV. The state of charge of the electrodes during the impedance measurements was 60% (which corresponds to 3.76V open circuit voltage in the full cell).
The parameters for the elements of the equivalent circuit were evaluated by minimization of square deviation of experimental impedance modulus from the theoretical value [8].
The impedance curves were measured at +25, 0 and −30 ^{o}C

Results and discussion

Figure 1 shows the typical impedance plot for the commercial 18650 lithium-ion cell. There are at least three elements in the curve: two semicircles and the straight region. Similar plots have been observed in [6,10-12].

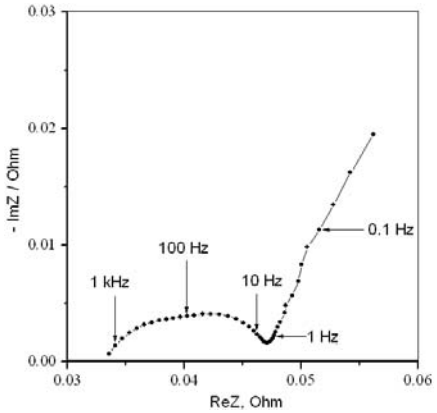

Fig. 1 Impedance plot for the commercial 18650 lithium-ion cell at 25 °C.

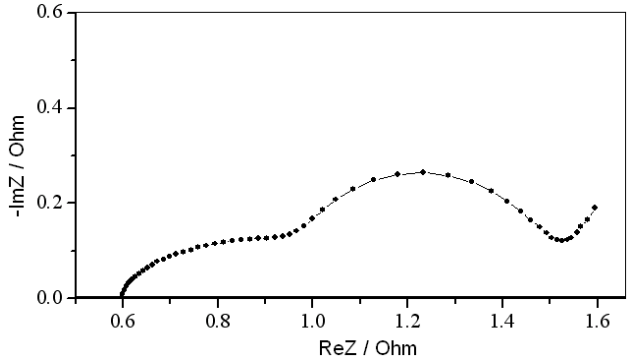

Fig. 2 Impedance plot for the flat single-layer pouch cell at 25 °C.

Fig. 2 shows the impedance plot for the flat single-layer pouch cell. The main features of this curve are similar to previously described, the differences in total resistance for each part arise from the different electrode surface area. The high-frequency curve intersection with the real axis corresponds to the ohmic cell resistance. The difference in these values at figures 1 and 2 exactly corresponds to the difference in separator thickness and electrode surface, so the electrolyte mainly contributes into the cell ohmic resistance.

The impedance plots of symmetrical cells, measured at different temperatures are shown on fig.3, 4 and 5. From the comparison of these data with impedance curves for the full cells it could be concluded that different electrodes contribute into the different stages of ion transport.

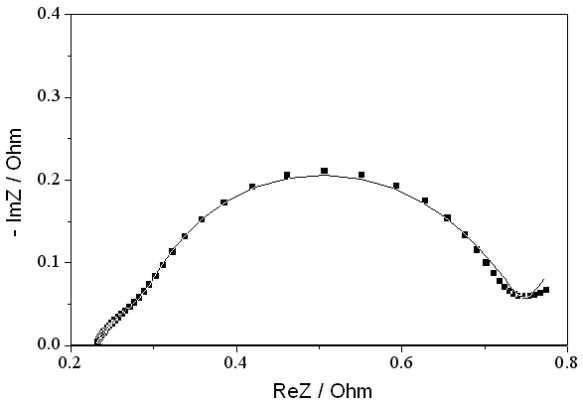

Fig. 3 **a** Impedance plot for the positive-electrode symmetrical cell, measured at 25 °C

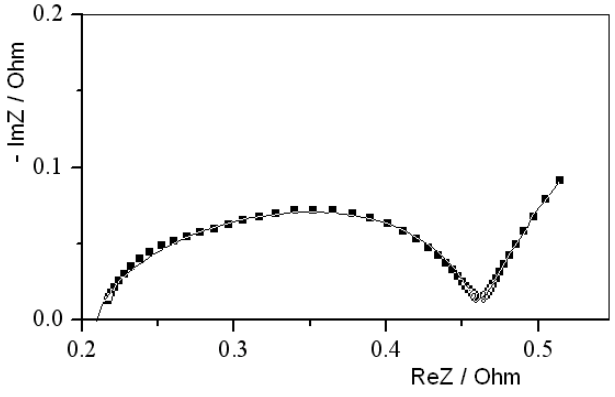

Fig. 3 b Impedance plot for the negative-electrode symmetrical cell, measured at 25 °C.

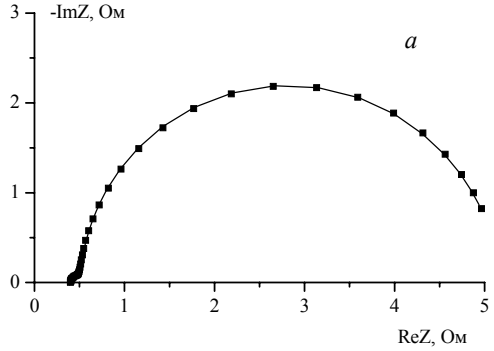

Fig. 4 **a** Impedance plot for the positive-electrode symmetrical cell, measured at 0 °C

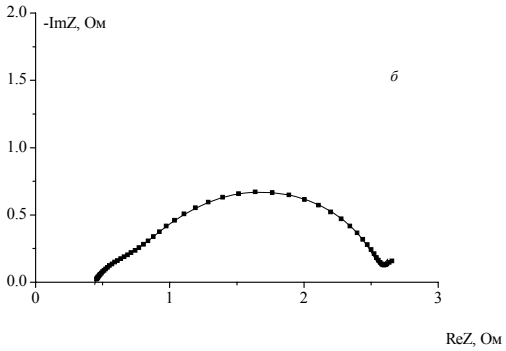

Fig. 4 b Impedance plot for the negative-electrode symmetrical cell, measured at 0 °C

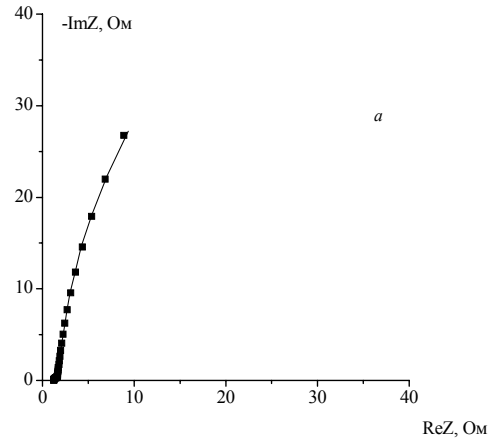

Fig. 5 **a** Impedance plot for the positive-electrode symmetrical cell, measured at -30 °C.

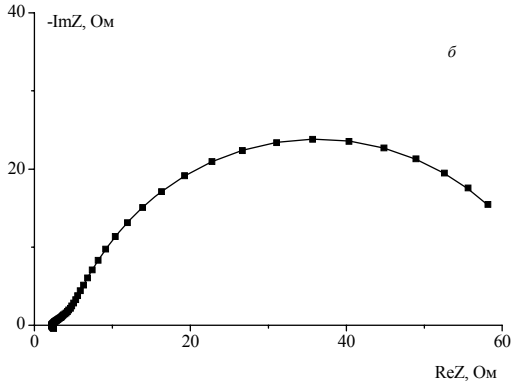

Fig. 5 b Impedance plot for the negative-electrode symmetrical cell, measured at -30 °C.

As the temperature decreases the resistance of all stages of charge transport grows with different rate.
The equivalent scheme shown on fig. 6 can be used to fit all the observed curves.

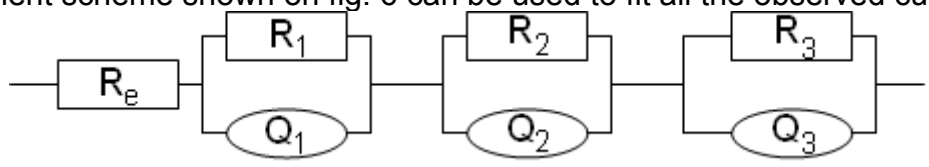

Fig. 6 *The universal equivalent scheme.*

The first element of this scheme (R_e) is the ohmic resistance. It follows the Arrhenius law with E_a = 22 kJ/mol. All the other elements of the equivalent circuit are parallel connections of active resistances R_i and constant phase elements (CPE) Q_i. Their nature is revealed from absolute values and low-temperature behaviour. Similar scheme was applied in works [1,2,6,10,13,14]

The results of impedance data fitting are shown on figures 3-5.
R_1Q_1 is assigned to the ion diffusion through SEI-layer. R_1 for the negative electrode is much more sensitive to the temperature change (Ea = 40 kJ/mol) than that of the positive side (Ea = 24 kJ/mol). We assume that the SEI-layer composition on cathode and anode sides is different.
R_2Q_2 element corresponds to the charge-transfer reaction on the active material/SEI-layer interface. Q_2 shows almost no dependence on the temperature, so we assigned the double-layer capacitance to it (≈ 11μF/cm^2). R_2 is the charge-transfer resistance.
R_3Q_3 is usually assigned to Li^+ solid -state diffusion [13]. At lower temperatures we were unable to track this element due to the shift of charge-transfer arc into the low-frequency region.
Thus in this work the electrochemical impedance study was applied to study positive and negative electrodes in the lithium-ion full cell or in symmetrical cells in -30°C-25°C temperature region.

References

1. Aurbach D., Levi M.D., Levi E., Teller H., Markovsky B., Salitra G., Heider U., Heider L. // J.Electrochem. Soc., 1998, V. 145, P. 3024
2. Levi M.D., Salitra G., Markovsky B., Teller H., Aurbach D., Heider U., Heider U. // J. Electrochem. Soc. 1999. V. 146. P. 1279
3. Levi M.D., Aurbach D. // Electrochimica acta. 1999. V. 45. P. 167
4. Aurbach D., Gamolsky K., Markovsky B., Salitra G., Gofer Y., Heider U., Oesten R., Schmidt M. // J. Electrochem. Soc. 2000. V. 147. P. 1322
5. Zhang S.S., Xu K., Jow T.R. // Electrochimica acta. 2006. V. 51. P. 1636
6. Chen C.H., Liu J., Amine K. // J. Power Sources. 2001. V. 96. P. 321
7. Shizuka K., Takano Sh., Okahara K. // J. Power Sources. 2007. V. 174. P. 1074
8. Boukamp B.A. // Solid State Ionics. 1986. V. 20. P. 31.
9. Chen C.H., Liu J., Amine K. // J. Power Sources. 2001. V. 96. P. 321
10. Itagaki M., Yotsuda S., Kobari N., Watanabe K., Kinoshita Sh., Ue M. // Electrochimica acta. 2006. V. 51. P. 1629
11. Tröltzsch U., Kanoun O, Tränkler H.-R. // Electrochimica acta. 2006. V. 51. P. 1664
12. Zhang S.S., Xu K., Jow T.R. // Electrochimica acta. 2004. V. 49. P. 1057
13. Kang Y.-J., Kim J.-H., Lee S.-W., Sun Y.-K. // Electrochimica acta. 2005. V. 50. P. 4784
14. Oh S.H., Lee S.M., Cho W.I., Cho B.W. // Electrochimica acta. 2006. V. 51. P. 3637

THE ELECTROCHEMICAL REDOX PROCESSES IN METHACRYLATE-BASED POLYMER ELECTROLYTES – STUDY ON MICROELECTRODES

Martina Nádherná[1,2], *Jakub Reiter*[1]

[1] *Institute of Inorganic Chemistry of the ASCR, v. v. i., 250 68 Řež near Prague, Czech Republic*
[2] *Department of Analytical Chemistry, Faculty of Science, Charles University in Prague, Albertov 2030, 128 40 Prague 2, Czech Republic*

Corresponding author: Jakub Reiter (reiter@iic.cas.cz)
Phone: +420 266 172 198
Fax: +420 220 941 502

Introduction

It is generally accepted that the motion in the structure of polymer gel electrolytes is partially restricted by the present polymer network. The motion of ions and molecules is located mainly in the embedded liquid microphase [1, 2]. We found out that the qualitative behaviour of various transition metal complexes are not influenced by the polymer in the case of poly(methyl methacrylate)-propylene carbonate (PMMA-PC) polymer electrolytes prepared from the commercial product Superacryl [3].

In our recent study we use different electrochemical methods for the description of qualitative and quantitative behaviour of ferrocene (Fc) in the liquid electrolyte (propylene carbonate) and corresponding polymer electrolytes with poly(methyl methacrylate), poly(ethyl methacrylate) and poly(2-ethoxyethyl methacrylate). Ferrocene-ferricinium couple is highly reversible redox system, when undergoes one-electron electrochemical reaction [4]:

$$Fc \leftrightarrow Fc^{+} + e^{-} \quad (1)$$

Several parameters were changed and their influence on the species mobility and electrochemistry are being studied:

- polymer polarity;
- cross-linking agent concentration;
- ratio polymer-aprotic solvent;
- ferrocene concentration.

Till now, several methods of determination of the apparent diffusion coefficients (D_0) have been published. In our project, results obtained on a rotating disk electrode (RDE), a large-scale electrode and a microelectrode were compared using various methods of D_0 evaluation.

Experimental

Polymer electrolytes were prepared by direct, thermally initiated radical polymerization (150 min at 80 °C) of the initial liquid mixture containing the monomer, solution of $5 \cdot 10^{-3}$ M ferrocene and 1 M lithium perchlorate in propylene carbonate, and a polymerization initiator (2,2'-azobis(isobutyronitrile); 1 mol. % of the monomer). The polymerization was carried out in a cell formed of polypropylene plate, packing distance frame (silicone rubber) and a glass plate. The study of redox processes of ferrocene was also studied in propylene carbonate. Here, 10^{-3} M solution of ferrocene was prepared in PC with 1M $LiClO_4$ as a supporting electrolyte.

The electrochemical characterization of prepared electrolytes was performed on a potentiogalvanostat PGSTAT 30 (Eco Chemie, The Netherlands). The voltammetrical and chronoamperometry measurements were done on platinum large-scale electrode (1.6 mm diameter; BASi), microelectrode (20 μm diameter, Eco Chemie) and in the case of liquid electrolytes also on a platinum rotating disk electrode (3 mm diameter, Eco Chemie). The measurements with the microelectrode were performed in a Faraday cage. All potentials are related to the PMMA-Cd-Cd^{2+} solid-state reference electrode developed in our laboratory (E(PMMA-Cd-Cd^{2+}) = 2.66 V vs. Li/Li^+ (cit [5]).

Results and Discussions

Ferrocene undergoes highly reversible electrochemical reaction in all studied aprotic systems. The peak potentials determined in liquid (PC) and polymer (PEMA-PC) electrolytes are almost identical as one can see from fig. 1. Here we can confirm our previous conclusion that aprotic polymers do not influence the electrochemical behaviour of the present metal complex.

Different methods were used for the determination of apparent diffusion coefficients of Fc and Fc^+:

- cyclic voltammetry on a platinum large scale electrode (non-stationary conditions approximated as a linear diffusion to the planar electrode);
- cyclic voltammetry on a platinum microelectrode (spherical diffusion - pseudo-stationary conditions);
- fast cyclic voltammetry (1 $V.s^{-1}$ scan rate) on a platinum microelectrode (non-stationary conditions);
- cyclic voltammetry on a platinum rotating disk electrode (stationary conditions);
- chronomamperometry (potential-step experiment) on a platinum microelectrode.

From obvious reasons, the measurements on the RDE could not be performed with the polymer gel electrolytes.

The electrochemical measurements showed highly reversible reaction both in liquid and polymer electrolyte (see fig. 1 and 2). During the polymerisation process is the mobility restricted only partially (15 – 50 times depending on the method of D_0 determination) as one can see from table 1. The previous study of PMMA-PC electrolytes based on Superacryl® [3] showed much lower mobility both of Fc/Fc^+ and $[Co(bpy)_3]^{2+/3+}$ redox

pairs ($D_0 \approx 10^{-9}$ cm^2.s^{-1}). Recently we optimised the polymer electrolyte composition leading to a higher ion and molecule mobility in the structure.

In the case of non-stationary conditions (measurements on a large-scale electrode) the diffusion coefficients of ferrocene were calculated using the Randles-Ševčík equation [6, 7]:

$$I_P = (2.68 \cdot 10^5)\, n^{3/2}\, A\, D_0^{1/2}\, v^{1/2}\, c\,, \qquad (2)$$

where I_P is the peak current (A), n number of transferred electrons, A area of the working electrode (cm^2), D_0 apparent diffusion coefficient (cm^2.s^{-1}), v scan rate (V.s^{-1}) and c concentration of the species (mol.cm^{-3}). The constant $2.68 \cdot 10^5$ was calculated at the measurement temperature of 22 °C.

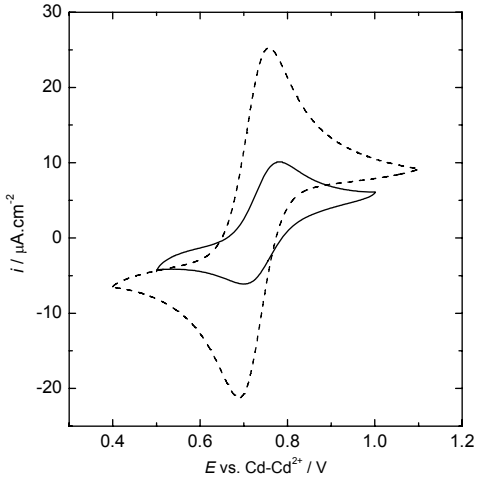

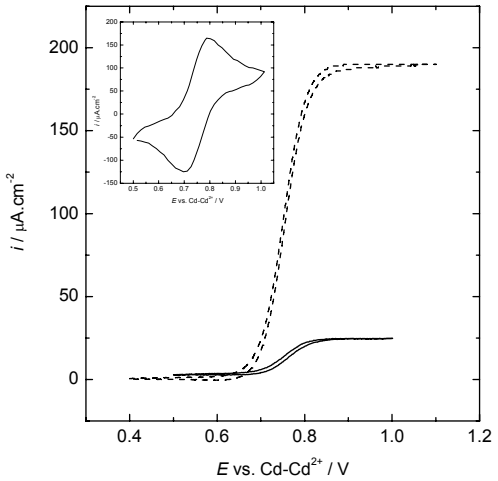

Fig. 1 *(left) Cyclic voltammograms of 10^{-3} M Fc in PC (dash line) and of $2.7 \cdot 10^{-3}$ M Fc in PEMA-PC-$LiClO_4$ (38:57:5 mol. %; solid line), electrolyte on a platinum large-scale electrode (10 mV.s^{-1}, 20 °C).*

Fig. 2 *(right) Cyclic voltammograms of 10^{-3} M Fc in PC (dash line) and of $2.7 \cdot 10^{-3}$ M Fc in PEMA-PC-$LiClO_4$ (38:57:5 mol. %; solid line) electrolyte on a platinum microelectrode (1 mV.s^{-1}, 20 °C); inserted – cyclic voltammogram of Fc in the same PEMA-PC electrolyte on a microelectrode at 1 V.s^{-1}.*

Also the measurements on the microelectrode were used for the apparent diffusion coefficient calculations using equation [5, 6]:

$$I = 4\, n\, F\, D_0\, c\, r\,, \qquad (3)$$

where I is the current (A), n number of transferred electrons, c concentration of the species (mol.cm^{-3}), F is the Faraday constant, r electrode radius (cm) and D_0 the apparent diffusion coefficient (cm^2.s^{-1}).

The microdisk electrode was also used for the potential step measurement. Figure 3 shows the i - t response of ferrocene, when the anodic current was recorded at the potential E_{WE} = 1.0 V vs. Cd-Cd^{2+}. From obtained experimental data, diffusion coefficients were determined by eq. (3) (see Table 1).

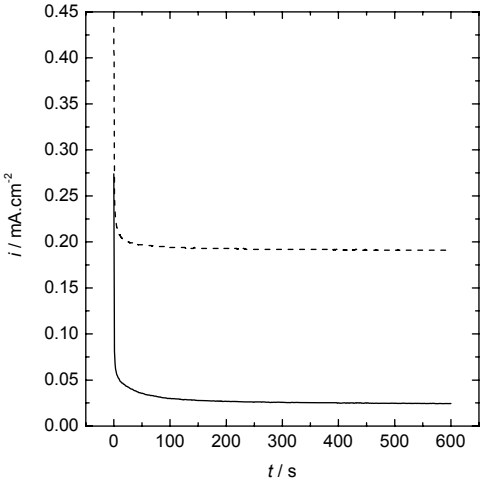

Fig. 3 *i - t plot of ferrocene oxidation on 20 μm platinum microdisk electrode (10^{-3} M Fc in PC (dash line) and 2.7 · 10^{-3} Fc in PEMA-PC-$LiClO_4$ (38:57:5 mol. %; solid line), E_{WE} = 1 V, t = 600 s).*

In the case of liquid (PC) electrolyte we also used a platinum RDE and Koutecký-Levič equation as a another method of the D_0 determination:

$$I = 0.62\, n\, F\, A\, D_0^{2/3}\, v^{-1/6}\, \omega^{1/2}\, c \quad , \qquad (4)$$

where I is the current (A), n number of transferred electrons, F is the Faraday constant, A area of the working electrode (cm^2), D_0 the apparent diffusion coefficient ($cm^2.s^{-1}$), v kinematic viscosity ($cm^2.s^{-1}$), ω angular velocity (s^{-1}) and concentration of the species ($mol.cm^{-3}$).

Table 1 *Apparent diffusion coefficients of ferrocene determined in liquid (PC) and polymer gel (PEMA-PC) electrolyte.*

Conditions	Equation	D_0(Fc) - PC ($cm^2.s^{-1}$)	D_0(Fc) – PEMA-PC ($cm^2.s^{-1}$)
CV on large-scale electrode (linear diffusion)	(2)	$7.6 \cdot 10^{-7}$	$1.5 \cdot 10^{-8}$
CV on microelectrode (spherical diffusion)	(3)	$1.5 - 2 \cdot 10^{-6}$	$0.7 - 1.0 \cdot 10^{-7}$
Fast CV on microelectrode (linear diffusion)	(2)	$1.4 \cdot 10^{-6}$	$3.1 \cdot 10^{-8}$
CV on RDE	(4)	$2.7 \cdot 10^{-6}$	–
Chronoamperometry on microelectrode	(4)	$1.5 \cdot 10^{-6}$	$8.0 \cdot 10^{-8}$

Conclusions

In our recent project we have investigated electrochemical behaviour of ferrocene in liquid and polymer aprotic electrolytes using various electrochemical methods. The apparent diffusion coefficients were determined for propylene carbonate and poly(ethyl methacrylate)-propylene carbonate medium. Thank to optimised electrolyte composition,

the polymerisation lowers the mobility of ferrocene only by 15 – 50 times contrary to previously studied PMMA-PC (Superacryl-based) electrolytes, where approx. three order decrease of diffusion coefficients was found [3].
Our further research will deal with other aprotic electrolytes prepared by direct polymerisation method, when the Superacryl resin was eliminated.

Acknowledgements

This work was supported by the Academy of Sciences (Research Plan AV0Z40320502), by the Czech Science Foundation (Grant No. 104/06/1471) and by the Ministry of Education, Youth and Sports, Czech Republic (project MSMT LC523 and project MSM 0021620857).

References

1. M. Caillon-Caravanier, B. Claude-Montigny, D. Lemordant, G. Bosser: Solid State Ionics **149** (2002) 275.
2. K.Y. Lee, W.S. Chung, N.J. Jo: Electrochim. Acta **50** (2004) 295.
3. J. Reiter, J. Vondrák, Z. Mička: Electrochim. Acta **50** (2005) 4469.
4. H. Strehlow: Electrode Potentials in Non-aqueous Solvents; in: J.J. Legowski (Ed.), The Chemistry of Non-aqueous Solvents, vol. 1, Academic Press, New York, 1966, p. 157.
5. J. Reiter, J. Vondrák, Z. Mička: Solid State Ionics **177** (2007) 3501.
6. A.J. Bard, L.R. Faulkner: Electrochemical Methods - Fundamentals and Applications, J. Wiley & Sons, New York, 2001.
7. F. Scholz (Ed.): Electroanalytical Methods, Springer, Berlin, 2002.

MICROPLASMA NOISE SOURCES IN SOLAR CELLS

Jandova K. [1], *Dolensky J.* [1], *Vanek J.* [1], *Chobola Z.* [2]

[1] *Affiliation – Department of Electrotechnology, Faculty of Electrical Engineering and Communication, Brno University of Technology, Udolni 53, 602 00 Brno, CR*
[2] *Affiliation – Department of Physics, Faculty of Civil Engineering University of Technology Brno, Zizkova 17, 602 00 Brno, CR*

Corresponding author (name underlined): Kristyna Jandova
E-mail: xkubic15@stud.feec.vutbr.cz
Tel.: +420 541146168

Abstract

Reverse biased voltage is applied to PN junction with some technological imperfections like dislocation in PN junction or crystal-grid defect causing non-homogeneity of parameters it produces in tiny areas of enhanced impact ionization called microplasma. It can leads onwards to deterioration in quality or to destruction of PN junction. Microplasma produced noise, which has random spectrum in frequency range. Microplasma noise is measurable even before the creation of light emissions.

Introduction

The continuing increases of power consumption in civilization requirements the usage of alternative electric power source. One of the sources of alternative electric power is photovoltaic system which could cover high level of demand of consumption.

The need for increasing the solar cell efficiency implies the application of selective processes within the framework of their structure preparation technology. Under the term selective processes, we understand such processes, in the course of which the solar cell structure is formed within an exactly predefined region. This process includes, as a rule, the formation of two different structure regions at the front and rear side, or, within one of the sides. In most cases, the selective processes require more sophisticated technology, which in turn implies higher costs at a time.

Microplasma noise and sources

Energy changes of the state of electron in a semiconductor are not indicated by light emission only, but are also displayed on resulting current characteristics in both time- and voltage-dependence. This fact is used by noise diagnostic methods based on the fact that owing to the microstructure of a substance material matter, all processes taking place in the substance are substance are stochastic, and are manifested by fluctuations of macroscopically measurable quantities. They can be quantitatively evaluated not only by their mean values, but also by other statistical characteristics such as the correlation

function or spectral output density. Considering the reality that the defects in silicon crystal-grid are sources of oversize noise result in degradation of physical and technical parameters, noise characteristics, can be used for evaluate the quality and service life of the watched system and its components classified.

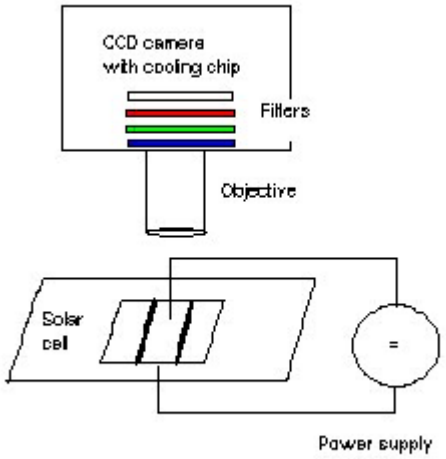

Fig. 1 *Microplasma method workplace*

By reason that microplasma emitted light in visible spectrum it is possible observed the process with a special CCD camera in a dark cryogenic box. The apparatus for the method (fig. 1.) contains highly sensitive low-noise CCD camera G2-3200 with CCD chip by Kodak KAF – 3200ME. It can be cooled up to -20° C. Camera contains set of light filters, special objectives and equipment for contacting solar cells. Solar cell is connected to reverse bias DC power source. Signal form CCD camera is analyzed by PC computer. The contact area is placed on dish with LN2. The temperature of underside area is -21° C. Due to the cooling is possible to observe the smallest defects in solar cell. The number of the visible defects in solar cell depends on connected reversed biased voltage (RBV). During increasing reverse biased voltage it is possible to observe more shining points (Fig. 2 - Fig. 7.). It was measured with exposure time 20 sec, clear light filter and the CCD chip was cooled into -20° C.

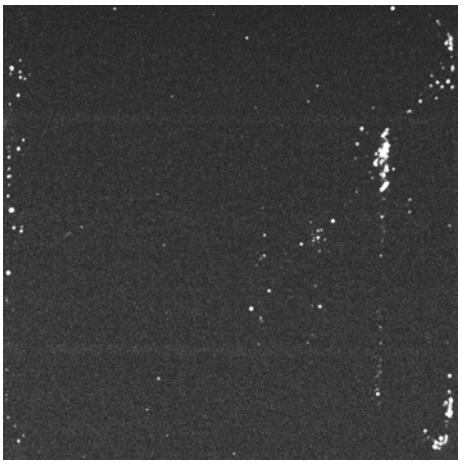

Fig. 2. *Cell type G1, RBV 4 V,*

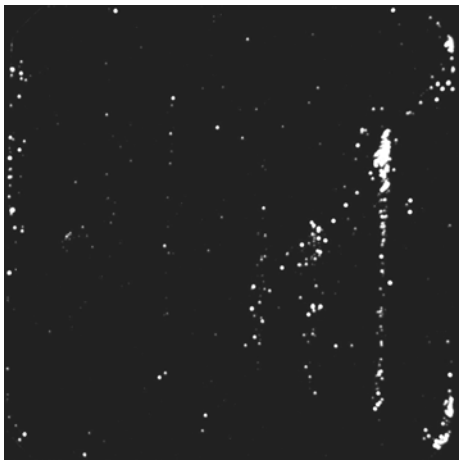

Fig. 3. *Cell type G1, RBV 8V,*

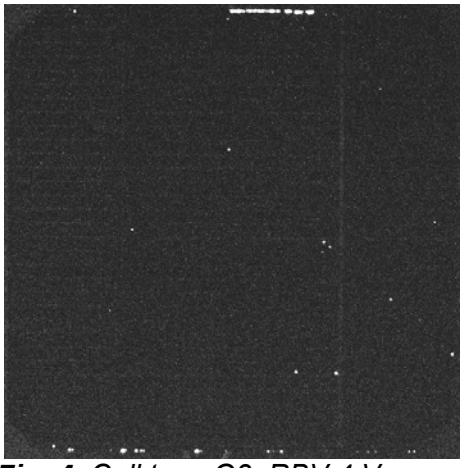

Fig. 4. *Cell type G3, RBV 4 V,*

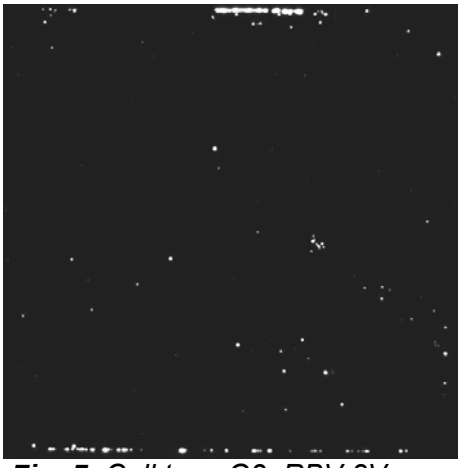

Fig. 5. *Cell type G3, RBV 8V,*

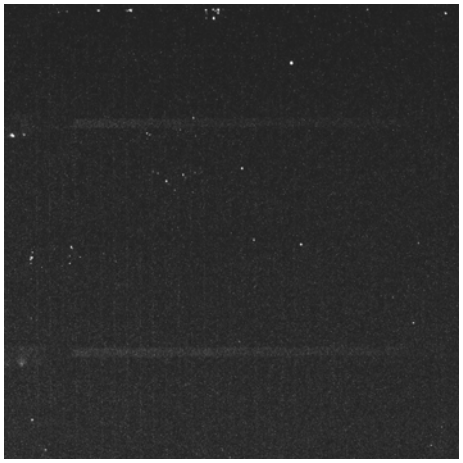

Fig. 6. *Cell type G5, RBV 4 V,*

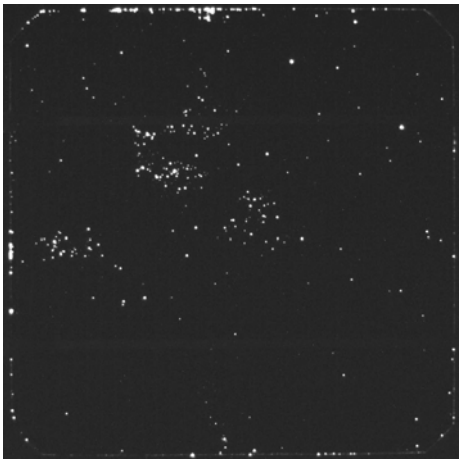

Fig. 7. *Cell type G5, RBV 8V,*

G1 type – this is a standard process. The damaged layer is removed and an alkali-etching-based double-side structuring process is carried out. A double-sided diffusion of an N+ layer follows.
ARC – silicon nitride (Si3N4), a variant employing a thin silica layer under the ARC. Finally, thick-film metal plating of both sides is performed.
G3 type – rear side etching process. The damaged layer is removed and an a alkali-etching-based double-side structuring process is carried out. A double-sided diffusion of an N+ layer follows. The rear side etching uses an acid solution. ARC – silicon nitride (Si_3N_4) or a variant employing a thin silica layer under the ARC is used. Finally, thick-film metal plating of both sides is performed.
G5 type – this is a standard process. The damaged layer is removed and an acid - etching-based double-side structuring process is carried out. A double-sided diffusion of an N+ layer follows.
ARC – silicon nitride (Si_3N_4) or a variant employing a thin silica layer under the ARC is used.
Finally, thick-film metal plating of both sides is performed.

The possibility of the use of noise measurements in analysis, diagnostics and prediction of reliability of electronic devices was studied by many researchers, namely by Van der Ziel and Tong [1], Vandamme et al. [2], Kleinpenning [3]. A new specialization Reliability Physics was created. It is concerned with identification of failure modes and mechanisms as the main sources of problems related to quality assessment and reliability prediction. It is generally supposed that reliability is determined by irreversible processes and that their time dependence is the main parameter for device lifetime prediction.

Conclusion

Counts of microplasma highly dependents on reversed biased voltage. The results from noise diagnostic shows strong correlation between used texture and noise level. The output from observed microplasma of each cell shows pointed to that the correlation between this two methods can exist. Considering that the correlation is not absolute, counts of microplasma in specimen G5 are not corresponding with noise, further investigation is needed.

According to the above described transport and noise characteristic analysis of the mentioned double-sided alkali texture silicon solar cells, it is obvious that better quality has been achieved by the structure of the groups of G3 specimens, this junction (of a thickness of about 1 um) is etched away from the rear side.

The G1 specimens in which an oxide - nitride passivation double layer has been used, show much worse noise properties. The noise parameters are likely to have deteriorated in the course of the high-temperature oxidation as a consequence of additional activation of phosphorus donors in the n^+- layer and the subsequent diffusion spreading of the doped layer (which can be recognized from the layer resistance value change). The high thermal stress the Si chips are exposed to can also reduce the minority carrier life time.

Acknowledgement

This research has been supported by the project of FRVS 1897/G1/2007 and MSM0021630516 and by the project of Ministry of Education, Youth and Sports in Research Plan 1M06031.

References

8. VAN DER ZIEL, A.H., Low frequency noise predicts when a transistor will fail, Electronics, 39(24), 95-97 (1966).
9. VANDAMME, L.K.J., ALABEDRA, R. and ZOMMITI, M., 1/f noise as a reliability estimation for solar cells, Solid-State Electron., 26, 671-674 (1983).
10. KLEINPENNING, T.G., 1/f noise in electronic devices, Proc.of Noise in Physical Systems (A. Ambrozy ed.), 443-454, Budapest (1989).
11. CHOBOLA, Z., “Noise as a tool for non-destructive testing of single-crystal silicon solar-cells”, in Microelectronics Reliability, vol. 41, no. 12,Dec. 2001, pp.1947 – 1952.
12. VANDAMME, L.K.J. “Opportunities and limitations to use low-frequency noise as a diagnostic tool for device quality”, in Proceedings of the 17th International conference ICNF 2003, Prague 2003, pp. 735 – 748.
13. CHOBOLA, Z.: Impulse noise in silicon solar cells. Microelectronics Journal, Vol.32/9 (2001), ISSN 0026-2692, pp.707-711.
14. WűRFEL, P., Physics of solar cells, Wiley-VCH verlag GMBH & Co. Kvas Weinheim (2005)

DEPOSITING OF THIN LAYERS AND POSSIBILITIES OF TESTING THE QUALITY OF THEIR SURFACE

Stejskal Petr, Barath Peter, Starý Jiří

Faculty of electrical engineering and communication, Brno University of Technology, 602 00 Brno

Corresponding author: Petr Stejskal
E-mail: xstejs08@stud.feec.vutbr.cz
Phone Number: +420 720 323 484, Fax Number: +420 317 723 092

Introduction

There are many methods how to build up the thin layers. This article treats one of them – the screen printing. Similarly to the function of the solder paste in the process of surface mount technology, the material is printed through a screen. This method guarantees the same thickness of the layer on the entire area. The quality of screen printing is provided by the three-dimensional tester. This tester evaluates the flatness and the height of printed area.

Results and Discussion

Usage Of Screen Printing For Deposition Of Thin Layers

The Most Using Methods
The most using methods of deposition of electrode material for electrochemical sources of current.

- Stencil printing
  It is a very exact method of deposition. When it is aplicated on larger area it has a problem with flatness of surface. It is caused by penetration of squeegee to volume of deposited material.

- Airbrush
  It is a good method, but it has a problems with defining and measurement of thickness of deposited material.

- Screen printing
  It has a good possibility for use in this application because it has predefined a same parameters of thickness in all area.

Screen Printing

Screen printers are available in many sizes to accommodate single aplications. They are available to be operated manually for small batches or entirely automatically for large runs. During screen printing the solder paste is forced through the exposed mesh or a patterned printing screen. The screen consists of a frame holding a mesh. The most commonly used screen mesh materials are monorilament nylon, monorilament polyester and stainless steel. For fine-line deposition the mesh is aligned with its axes at 45° to the PCB axes so that the shadowing effect of the mesh filaments is minimised and maximum line definition is available. The screen mesh count refers to the number of openings or lines per linear inch (l.p.i.); for green printing solder pastes the mesh count is usually in the range 60-200. If the solder particles are larger than the openings in the mesh they will obviously not pass through. As a general rule-of-thumb, for the free passage of the paste through the screen, the maximum particle size should be no larger than one third the mesh opening to ensure lhal the screen does not become jammed. For example, an 80 mesh screen has openings of about 224 µm. Therefore, the particle size should not exceed 75 µm, which corresponds to a -200 mesh powder size (Table 1). The parameters of some commonly used screens are given in Table 1 and defined in Figure 1.

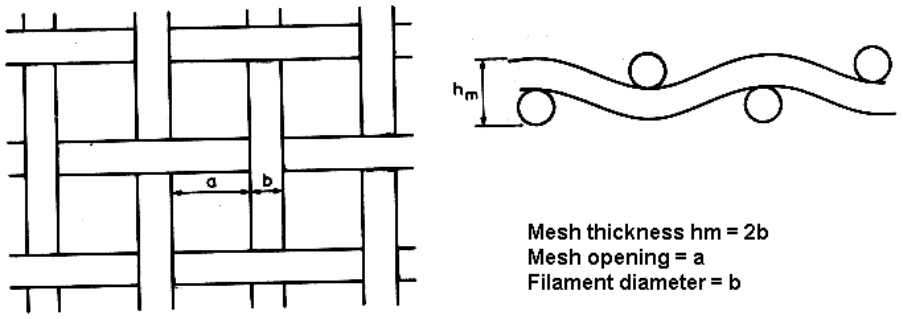

Fig. 2 *Definition of parameters of a screen for printing paste.*

Table 1 *Parameters of some commonly used screens.*

Mesh Count (l.p.i.)	Nominal Wire Diameter (µm)	Mesh Opening (a) (µm)	Open Area (%)	Nominal Mesh Thickness (µm)
60	114	310	53,5	235
80	94	224	49,5	215
105	76	165	47	175
165	51	104	45	115
180	46	97	46	100
200	41	86	46	90

The thickness of the electrode material layer is largely determined by the emulsion thickness and the screen mesh thickness, although it also depends to some extent on the pattern dimensions, the printer parameters and the solids content and rheology of the paste. In general, finer mesh screens are used for thinner deposits.
As an approximation, the wet print thickness h_w is given by

$$h_w = (h_m x A_o) + h_e \quad [1]$$

Testing of printed layer

It can be tested by three dimensional tester. Three dimensional tester can quickly detect the thickness of every place in the area. Speed of testing is about 70 cm^2 per second with 10 μm resolution. An example of testers visual output is on Fig. 2.

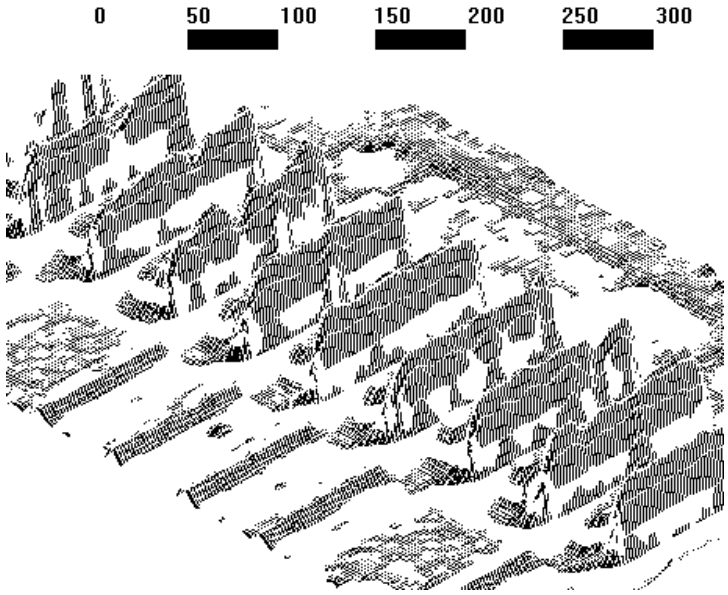

Fig. 3 *Example of testers visual output [2].*

Conclusions

Screen printing has a good possibility for use in deposition of thin layers because it has predefined a same parameters of thickness in all area. And with the proposed method of quality control the screen printing is about to become an important process in the field of deposition of electrode material for electrochemical sources of current.

References

1. Lea, C.: *A Scientific Guide to Surface Mount Technology*, Electrochemical Publications Limited 1988, Ayr, Scotland, ISBN 0 901150 22 3.
2. Stejskal, P.: Diploma Thesis*: Interoperation Check of Quality in Surface Mount Technology, Brno university of Technology, 2007,* Brno.

VOLTAMMETRY AND IMPEDANCE AS ELECTROCHEMICAL DIAGNOSIS TOOLS: WHERE DO THEY MEET AND WHERE DO THEY DIFFER.

Petr Vanýsek

Northern Illinois University, Department of Chemistry and Biochemistry, DeKalb, IL 60115, USA

Abstract

Impedance is used in many applications to supplement data from cyclic voltammetry in measuring electrochemical capacitance and charge transfer resistance. In some cases the values obtained by the two methods differ (*e.g.*, Pettit, C.M., P.C. Goonetilleke, and D. Roy, Measurement of differential capacitance for faradaic systems under potentiodynamic conditions: Considerations of Fourier transform and phase-selective techniques. Journal of Electroanalytical Chemistry, 2006. 589(2): p. 219-231.). In principle, the results from the two methods should provide identical conclusion. If there is disparity observed, then it usually originates from some improper assumption regarding one or both of the methods. We will show how one can reconcile those differences.

As an example, we will compare data collected from a capacitive system with leakage (charge transfer resistance), where the capacitance from charging current appears to be quite different from capacitance obtained from an impedance scan.

ABOUT BOCHEMIE S.R.O.

Mission

To meet the needs of its customers, in particular in the following areas: hygiene, protection of building materials, accumulation of electricity and surface finishing of metals. BOCHEMIE provides its customers with comprehensive solutions to their problems through its products, services and related equipment and user know-how.

Profile

BOCHEMIE Ltd. PERFORMS ITS BUSINESS ACTIVITIES in five primary production branches: disinfection, consumer goods, protection of building materials against biological corrosion, surface finishing of metals and production of accumulator masses and other materials for manufacturers of accumulators. Approximately half of the production is exported to foreign markets. The major sales territories include countries of Central and Western Europe, USA and Eastern Asia.
BOCHEMIE Ltd. keeps the leading position on the Czech market in the area of disinfection, which includes product lines for medicine and food industry, agriculture and institutions; the company also enjoys a significant position in Slovakia, where it is ranked third.
As for consumer goods we succeeded in keeping the leading position of SAVO product line on the Czech and Slovak market of liquid cleaners and bleaching agents.
BOCHEMIE Ltd. is a leader on the building market in Czech Republic and Slovakia with its line of fungicidal and insecticidal products for protection of wood and masonry. We are also a leading company on the market of „hobby“ fungicides in Bulgaria.
Activities connected with production of materials designed for steel treatment are of a high export potential. Progressive, environment-friendly and universal pickling technology FEROPUR is a leader on the narrow segment of the stainless steel long products market.

BOCHEMIE Ltd. is one of the world's most important suppliers of raw materials and technologies for pocket-type alkaline accumulators. Bochemie doesn't forget about developing new more effective materials designated for this segment. The company has approximately one-fifth share on the worldwide market of these commodities.
BOCHEMIE Ltd. is the holder ISO 9001:2002 certificate and Responsible Care certificate as well.
BOCHEMIE aims for the protection of environment, working environment, decreasing the release of dangerous substances and increasing the security against accidents.

ECO CHEMIE / AUTOLAB

AUTOLAB Electrochemical Instruments

ECO CHEMIE BV

Martijn van Dijk

Eco Chemie BV
Kanaalweg 29G, 3526 KM Utrecht, The Netherlands

Corresponding author: Martijn van Dijk
Phone: +31 30 2893154 Fax: +31 30 2880715
Email: martijn@ecochemie.nl
WWW: www.ecochemie.nl

Founded in 1986 and since 1999 a member of the Metrohm group of companies, Eco Chemie designs and manufactures state of the art Autolab series of instrumentation and software for electrochemistry and biochemistry. ISO 9001:2000 certified, Eco Chemie has been setting the benchmark in electrochemical research instrumentation for almost two decades. With our background and knowledge in electrochemistry and biochemistry and our worldwide distributor network, our mission is to serve the research community worldwide by supplying modern, affordable instruments, software and accessories. The Autolab instruments serve a wide range of industries and research applications.

Ever since the foundation everyone within the company has been dedicated to the development, production and testing of Autolab electrochemical instruments and their software. This focus coupled with the flexibility of the company resulted in the finest range of potentiostats/galvanostats available today.

The flexibility of Eco Chemie is reflected in the modularity of the Autolab instruments. Potentiostat range from 12 to 100 V output voltage with the possibility to add a variety of modules throughout the lifetime of the instrument.

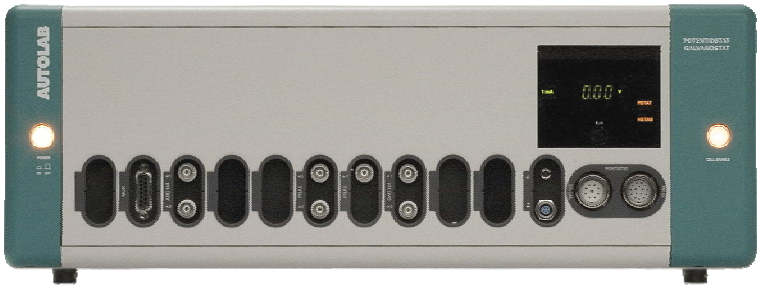

Some of the popular modules include:

FRA2 (Module for impedance spectroscopy, for battery and corrosion research)
BA (Bipoteniostat and Array, second working electrode in combination with other techniques like; Scanning Electro Chemical Microscope, Scanning Tunneling Microscope and Raman)
ADC10M (Fast sampling module, scan rates up to 250 kV/s in combination with SCAN250 true analog sweep generator)
ECD (Low current amplifier, current ranges from 10 pA to 100μA)
MUX (Multiplexing module, possibility of measuring a maximum of 96 complete electrochemical cells or 256 working electrodes in sequence)
BOOSTER 10A/20A (Current booster)

The Autolab instruments can be controlled by two different software packages:
General Purpose Electrochemical Software for all common DC electrochemical techniques and the Frequency Response Analyzer software for impedance spectroscopy (in combination with the FRA2 module)

The combination of the Autolab hard- and software gives the user an unrivalled instrument to perform a wide range of electrochemical experiments. Fundamental electrochemistry, corrosion and battery & fuel cell research are easily achieved with Autolab systems.

Rastrovací hrotové mikroskopy Agilent Technologies

Společnost H TEST a.s. rozšířila svoji nabídku testovacích systémů i o produkty divize Agilent Materials Sciences Solutions tj. AFM (Atomic Force Microscopy)/SPM (Scanning Probe Microscopy) rastrovací mikroskopy.
Zásadní výhodou technologie AFM oproti elektronovým mikroskopům je, že měřené vzorky nemusí být vodivé! S technologií AFM lze dosáhnout rozlišení až v řádu jednotek nanometrů.

Systémy Agilent se uplatní v:

- **elektrochemii**
- **nanolitografii**
- **aplikacích s polymery**
- **biotechnologiích**
- **medicíně**

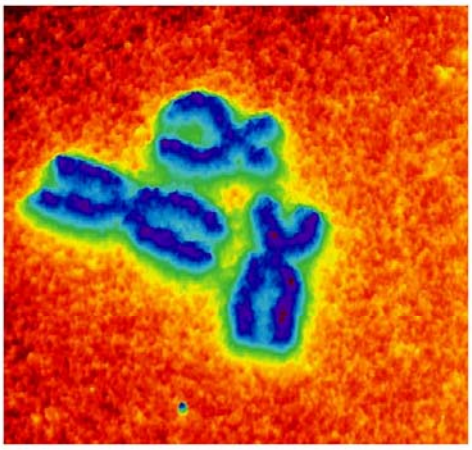

Série 5500 AFM/SPM
AFM mikroskop Agilent 5500 je vrcholný víceúčelový výzkumný mikroskopický systém pro AFM a SPM. Modulární koncepce této série dovoluje jednoduchou integraci stojanu pro velké vzorky až 150 x 200 mm (LS), invertovaného mikroskopu (ILM), scannerů pro malé i velké zobrazované plochy, adaptérů pro uchycení vzorků, soupravy pro elektrochemii nebo video mikroskopu.

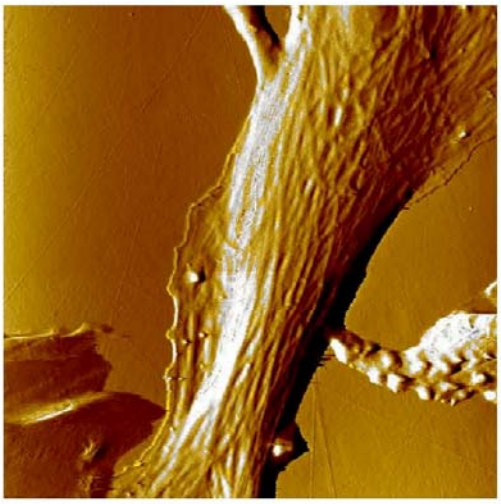

Série 5100 AFM/SPM
AFM mikroskop Agilent 5100 je vhodný pro uživatele, kteří nepotřebují plnou funkčnost vrcholného modelu Agilent 5500, a přesto vyžadují možnost plné kontroly prostředí, ve kterém se nachází měřený vzorek. Pro plnou kontrolu prostředí, ve kterém se nachází měřený vzorek, je k dispozici volitelná hermeticky uzavřená komora a teplotně regulovaný adaptér pro uchycení vzorků.

- Velikost vzorku 20 mm x 20 mm
- Kontrola teploty a prostředí

Série 5400 AFM/SPM
Nový AFM mikroskop Agilent 5400 AFM/SPM je velmi přesný, univerzální přístroj za dostupnou cenu, určený zejména pro oblast vzdělávání a výzkumu a představuje tak ideální možnost zpřístupnění AFM technologie širokému spektru potenciálních uživatelů. Mikroskop je dodáván s podklady pro výuku AFM včetně vzorků pro experimenty.

- Velikost vzorku 20 mm x 20 mm
- Kontrola teploty

Kontaktní informace:

H TEST a.s.
Na okraji 44B
16200 Praha 6
Tel: 235 365 207, 204
Fax: 235 363 893
E-mail: info@htest.cz

www.htest.cz
www.agilent.com/find/nanotech

H/test

Agilent Technologies
Authorized Distributor

Title:	Advanced Batteries and Accumulators – 9th ABA
Edited:	Jiří Vondrák Jiří Vognar
Publishing Office:	Jiří Vognar Vítězslav Novák
Deadline:	June 31th 2008
Publisher:	Brno University of Technology Faculty of Electrical Engineering and Communication Department of Electrotechnology
Press:	TIMEART Agency Jiří Vognarm Jeřábkova 6, 602 00, Brno
Year:	2008
Number of Copies:	70

The autors are fully responsible for the content and language of their contribution

ISBN 978-80-214-3659-6